CENTRE d'ETUDES et de RECHERCHES
GEODYNAMIQUES et ASTRONOMIQUES

FIFTH INTERNATIONAL WORKSHOP ON LASER RANGING INSTRUMENTATION

VOLUME I

HERSTMONCEUX CASTLE
SEPTEMBER 10–14 / 1984

PROCEEDINGS
COMPILED AND EDITED BY
J. GAIGNEBET

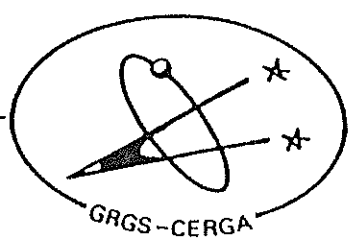

GROUPE de RECHERCHES de GEODESIE SPATIALE

produced by the Geodetic Institute,
University of Bonn, Nussallee 17,
D-5300 Bonn 1
1985

CONTENTS

ACKNOWLEDGEMENTS 1

LIST OF PARTICIPANTS 5

TABLE OF CONTENTS

1. I.I. MUELLER 10
Reference coordinate systems and frames concepts and realization

2. J.O. DICKEY, J.G. WILLIAMS, X.X. NEWHALL 19
Fifteen years of lunar laser ranging accomplishments and future challenges

3. P.L. BENDER, M.A. VINCENT 28
Effects of instrumental errors on geophysical results

4. C.S. GARDNER, J.B. ABSHIRE 29
Atmospheric refraction and target speckle effects on the accuracy of laser ranging systems

5. P.J. DUNN, D. CHRISTODOULIDIS, E.D. SMITH 42
Some Modelling requirements for precise lageos orbit analysis

6. E. VERMAAT 47
Establishing ground ties with MTLRS performance and results

7. M.R. PEARLMAN 66
Laser system characterization

8. K. HAMAL, I. PROCHAZKA, J. GAIGNEBET 85
Two wavelength picosecond ranging on ground target

9. K. HAMAL, I. PROCHAZKA, J. GAIGNEBET 92
Laser radar indoor calibration experiment

10. B.A. GREENE 98
Further development of the NLRS at orroral

11. J.J. DEGNAN 102
An overview of NASA airborne and spaceborne laser ranging development

12. W. KIELEK 112
Single-shot accuracy improvement using right filtration and fraction values in multi-photoelectron case

13. S. LESCHIUTTA, S. MARRA, R. MAZZUCCHELLI 119
Thermal effects on detectors and counters

14. B. HYDE 129
Further thoughts on a minimal transmitter for laser ranging

15. W. SIBBETT, W.E. SLEAT, W. KRAUSE 136
A picosecond streak camera for spaceborne laser ranging

16. J.J. DEGNAN, T.W. ZADWODZKI, H.E. ROWE 166
Satellite laser ranging experiments with an upgraded MOBLAS station

17. J.B. ABSHIRE, T.W. ZAGWODZKI, J.F. McGARRY, J.J. DEGNAN 178
An experimental large aperture satellite laser ranging station at GSFC

18. J. WIANT 185
Tunable etalon usage at MLRS McDonald laser ranging station

19. P. KOECKLER, I. BAUERSIMA 194
In pass calibration during laser ranging operation

20. G. BEUTLER, W. GURTNER, M. ROTHACHER 203
Real time filtering of laser ranging observations at the Zimmerwald satellite Observatory

21. K. HAMAL, H. JELINKOVA, A. NOVOTNY, I. PROCHAZKA 214
Interkosmos laser radar, version mode locked train

22. M. CECH 219
Start discriminator for mode locked train laser radar

23. J. JELINKOVA 224
Mode locked train laser transmitter

24. C. VEILLET 234
Present statutof the CERGA LLR operation

25. B.A. GREENE, H. VISSER 240
Spectral filters for laser ranging

26. B.A. GREENE 247
Epoch timing for laser ranging

27. C. WARDRIP, P. KUSHMEIDER, J. BUISSON, J. OAKS, M. LISTER, P. DACHEL, T. STALDER 251
Use of the global positioning system for the NASA transportable laser ranging network

28. D. KIRCHNER, H. RESSLER 297
A fibre optic time and frequency distribution system

29. D.R. EDGE, J.M. HEINICK 302
Recent improvements in data quality from mobile laser satellite tracking stations

30. W. SCHLUTER , G. SOLTAU, R. DASSING, R. HOPFL 313
The concept of a new wettzell laser ranging system with dual-purpose capability

31. T.S. JOHNSON, W.L. BANE, C.C. JOHNSON, A.W. MANSFIELD, P.J. DUNN 324
The transportable laser ranging system Mark III

32. P.J. DUNN, C.C. JOHNSON, A.W. MANSFIELD, T.S. JOHNSON 332
The software system for TLRS II

33. E. VERMAAT, K.H. OTTEN, M. CONRAD 342
MTLRS software and firmware

34. R.L. RICKLEFS, J.R. WIANT 361
The computer system at MLRS

35. E. KIERNAN, M.L. WHITE 371
A description of the MT. Haleakala satellite and lunar laser ranging software

36. R.J. BRYANT, J.P. GUILFOYLE 384
An overview of the NLRS ranging software

37. A. NOVOTNY, I. PROCHAZKA 396
Upgrading the computer control of the Interkosmos laser ranging station in Helwan

38. I. PROCHAZKA 401
Mode locked train YAG laser ranging data processing

39. D.R. EDGE 407
GLTN laser data products

40. Y. FUMIN, Z. YOUMING, S. XIAOLIANG, T. DETONG, X. CHIKUN, S. JINYUAN, L. JIAQIAN 414
Performance and early observation of the second-generation satellite laser ranging system at Shanghai Observatory

41. G. KIRCHNER 424
Report of the activities of the laser station Graz-Lustbuehel

42. F. PALUTAN, M. BOCCADORO, S. CASOTTO, A. CENCI, A. de AGOSTINI, A. CAPORALI 429
First results from satellite laser ranging activity at Matera

43. I. BAUERSIMA, P. KLOECKLER, W. GURTNER 448
Progress report 1984

44. P.L. BENDER, J.E. FALLER, J.L. HALL, D. HILS, M.A. VINCENT 464
Proposed one million kilometer laser gravitational antenna in space

45. J.B. ABSHIRE, J.F. McGARRY, H.E. ROWE, J.J. DEGNAN 466
Treak camera-based laser ranging receiver development

46. S.R. BOWMAN, C.O. ALLEY, J.J. Degnan, W.L. CAO, M.Z. ZHANG, N.H. WANG 480
New laser developments toward a centimeter accuracy Lunar Ranging System

47. J.D. RAYNER 484
Programming for interleaved laser ranging

48. B.E. SCHUTZ, B.D. TAPLEY, R.J. EANES 488
Performance of Satellite Laser Ranging during MERIT

49. C.A. STEGGERDA 499
Current developments in event timers at the University of Maryland

50. M.H. TORRENCE, S.M. KLOSKO, D.C. CHRISTODOULIDIS 506
The construction and testing of normal points at Goddard Space Flight Center

PROCEEDINGS OF THE LEUT MEETING 517

RESOLUTIONS 522

PREFACE

Within the progress span of Laser Ranging the Fifth International Workshop on Laser Ranging Instrumentation, held at Herstmonceux Castle in September 1984, is an interesting bench-mark.

Unfortunately the premature death of Frank ZEEMAN has hit our community. These proceedings are dedicated to his memory.

Satellite Laser Ranging achieves now a remarkable level of accuracy and operational efficiency. Measures are at the few centimeter level and are obtained regularly in such an amount that reduction to normal points is mandatory. Thes improvements are the results, to a large extent, of the fruitful cooperation between the technical and scientific communities.

This progress must be continued. It is well known that the week point of the Laser Ranging is its sensitivity to the weather. This handicap could be minimized only if the accuracy of the method were superior to other space techniques. The potentialities will achieve their full meaning only if calibrations and refraction correction are determined with a centimeter or sub-centimeter uncertainty.

Calibration is a fast moving domain. Today the necessity of cautious and frequent determination is well rekognized. For many stations, ranging on targets at known distance is still the basic method. This is progressively complemented or replaced by internal calibrations. A new concept of station construction allows a zero calibration value. Also a mobile device able to compare the various constants directly could be used.

Two-wavelenth experiments were presented for the first time at the workshop. Tested on short ranges, this technique prepares the direct

determination of the refraction correction. The preliminary results are very promising and involve the use of very impressive and accurate time measurements methods, i.e. streak cameras.

New stations will soon join the network. Some of them are highly mobile and automated. This trend allows, with reduced manpower, the development of original programs (Wegener..).

Important objectives have been achieved by Lunar Ranging people. For the first time, two stations obtained measures simultaneously and quite regularly. The accuracy of Lunar-devoted stations is following the path of satellite ones. The introduction of new sites in the network, expected soon, will enhance this evolution and will open interesting fields of research.

This brewing of ideas was made possible thanks to the organisation of the Royal Greenwich Observatory under the responsability of our host G.A. Wilkins and the participation of the Special Study Group 2.81 of the IAG. The Worshop was sponsored by the International Association of Goedesy.

Thanks are due to :

*The program committee (C.O. ALLEY USA, K. HAMAL CZ, G.A. WILKINS GB, P. WILSON FRG, J. GAIGNEBET F.) ; *The session chairman, who not only had to manage but were also given the task to collect the papers of their sessions ; *The speakers and all the participants of the workshop who have driven the meeting to a high standard ; *Pr. SEEGER from the Geodetic Institute of the University of Bonn (RFA) for the printing of the proceedings ; *M. PERRIN for her useful preparation of the edition.

J. GAIGNEBET

PREFACE

Dans l'évolution de la télémétrie laser, le cinquième "International Workshop on Laser Ranging Instrumentation" qui s'est tenu au château d'Herstmonceux en Septembre 1984, marque une étape intéressante.

En effet, la télémétrie sur satellite artificiels a atteint un degré remarquable de performances et d'efficacité opérationnelle. La précision est de l'ordre du centimètre et les mesures obtenues de façon régulière sont si nombreuses que la génération de points normaux est devenue obligatoire. Ce progrès est en grande partie dû à la bonne coopération entre le personnel responsable de la mise en oeuvre des stations et les scientifiques chargés du traitement des données.

Il est évident que cette amélioration de l'efficacité opérationnelle et de la précision doit se poursuivre. Nous savons que le point faible de la télémétrie laser est sa sensibilité à l'état du Ciel. Cet handicap ne peut être surmonté que si l'exactitude des mesures est supérieure à celle obtenue par les autres méthodes spatiales. Cet avantage potentiel ne peut acquérir sa pleine signification que si les calibrations et les corrections de réfraction sont réalisées avec une précision centimètrique.

La calibration est un domaine en pleine évolution. La nécessité de veiller au sérieux de sa détermination et à la fréquence de sa mesure est maintenant reconnue. Les tirs sur cible à distance connue restent la méthode de base pour beaucoup de stations mais sont progressivement complétés par des systèmes de calibration internes en cours de poursuite. Une nouvelle conception de stations permet d'obtenir une constante de calibration nulle de construction. Enfin, la sation de calibration LASSO permet de disposer d'un moyen de comparaison des télémètres.

Les premiers rapports sur les études de la télémétrie en deux couleurs ont été présentés au colloque. Cette technique, testée jusqu'à ce jour sur des distances faibles, doit permettre la détermination directe de la valeur de la correction de réfraction. Les résultats de ces études sont très prometteurs et actualisent des méthodes de mesure du temps impressionnantes de précision, telles les caméras à balayage de fente.

Le colloque à d'autre part permis de se rendre compte que de nouvelles stations sont bientôt entrer en activité. Par ailleurs, le développement de systèmes extrêmement mobiles et automatisés permet, d'une part de réduire le potentiel humain d'exploitation, d'autre part de développer les programmes originaux (Wegener).

La télémétrie de la Lune a atteint des objectifs importants. Pour la première fois, deux stations ont obtenu des données assez régulièrement et simultanément. La précision de ces stations suit une progression similaire à celle mentionnée plus haut. L'introduction prochaine de nouveaux sites dans le réseau va accélérer cette évolution et accroître les retombées scientifiques.

Malheureusement, cette même période a vu la disparition prématurée de Frank ZEEMAN, nous lui dédions ces quatrièmes compte-rendus.

Ces échanges d'idées ont été possibles grâce à l'organisation mise en place par le Royal Greenwich Observatory, sous la responsabilité de nôtre hôte G.A. WILKINS, avec la participation du SSG 2-81 sous les auspices de l'Association Internationale de Géodésie.

Les personnes suivantes sont également à remercier :

* Le Comité des Programmes (C.O. ALLEY USA, K. HAMAL CZ, G.A. WILKINS GB, P. WILSON RFA, J. GAIGNEBET F.) ; * Les présidents de session qui ont dû regrouper les textes présentés ; * Les conférenciers, pour le haut niveau de leurs contributions ; * Le Professeur SEEGER du Geodetic Inst. de l'Université de Bonn pour l'impression des compte-rendus ; *M. PERRIN pour sa préparation pratique de l'édition.

J. GAIGNEBET

FIFTH INTERNATIONAL WORKSHOP ON LASER RANGING INSTRUMENTATION
AT ROYAL GREENWICH OBSERVATORY ON 10-14 SEPTEMBER 1984

LIST OF PARTICIPANTS

ABSHIRE, J B
NASA/Goddard Space Flight Center
Mail Code 723
Greenbelt, MD 20771, USA (Wish Tower)

ALLEY, C O
Department of Physics & Astronomy
University of Maryland
College Park, Maryland 20742, USA (Castle)

APPLEBY, G M
Royal Greenwich Observatory
Herstmonceux Castle
Hailsham, East Sussex

BANNI, A
Stazione Astronomica
Via Ospedale 72
09100 Cagliari, Italy (Castle)

BEEK, W
Observatory for Satellite Geodesy
P O Box 581
7300 AN Apeldoorn, Holland (Castle)

BENDER, P L
Joint Inst. for Laboratory Astrophysics
University of Colorado, Campus Box 440
Boulder, CO 80309, USA (Mansion)

BERTOTTI, B
Faculty of Science
Universita Degli Studi
Corso Strada Nuova 65
I-27100 Pavia, Italy (Castle)

BOLOIX, M
Instituto y Observatorio de Marina
Observatorio de Marina
San Fernando, Cadiz Spain (Castle)

BOWMAN, S
Department of Physics and Astronomy
University of Maryland
College Park, Maryland 20742, USA (Castle)

CALAME, O
C.E.R.G.A.
Av. Copernic
F-06130 Grasse, France (Woolpack)

CAPORALI, A
Department of Physics
University of Padova
via Marzolo n. 8
I-35131 Padova, Italy (White Friars)

CECCHET, G
University of Pavia
V. Bassi 6
I-27100 Pavia, Italy (Castle)

CENCI, A
Telespazio, Via Bergamini 50,
Rome, Italy (Wish Tower)

CHEN DAONAN
North China Research Institute of
Electro-Optics
P O Box 8511, Beijing, China

COHEN, A
Atmospheric Sciences
Hebrew University
Jerusalem
Israel

CUOT, E
C.E.R.G.A.
Av Copernic
06130, Grasse, France (Albion)

DACHEL, P R
Bendix Field Engineering Corp
1 Bendix Road
Columbia MD 21045, USA (Mansion)

DASSING, R
Satellitenbeobachtungs-station Wettzel
8493 Kozting, West Germany (Mansion)

DEGNAN, J J
NASA Goddard Space Flight Center
Greenbelt, MD 20771, USA (Mansion)

DICKEY, J O
JPL/Caltech MS 264-781
Jet Propulsion Laboratory
Pasadena, CA 91109, USA (White Friars)

DUMOULIN, C
C.E.R.G.A.
Av Copernic
06130, Grasse, France (Albion)

DUNN, P J
EG/G, WASC
1707 Mitchell Road
Silver Spring, MD 20903, USA (Castle)

EANES, R
Center for Space Research
The University of Texas at Austin
W.R. Woolrich Laboratories 402
Austin, TX 78712 USA (Mansion)

ECONOMOU, G
Contraves Goerz Corporation
610 Epsilon Drive
Pittsburgh, Pennsylvania 15238, USA

EDGE, D R
Bendix Field Engineering Corporation
1 Bendix Road
Columbia, MD 21043, USA (Mansion)

FEISSEL, M
Observatoire de Paris
61 avenue de l'Observatoire
F-75014, Paris, France (Castle)

GAIGNEBET, J
C.E.R.G.A.
Av. Copernic
06130, Grasse, France (Mansion)

GAMBIS, D
Bureau International de l'Heure
61 avenue de l'Observatoire
F-75014 Paris, France (Cleavers Lyng)

GARDNER, C C
University of Illinois
Department of Electrical
& Computer Engineering
1406 W. Green Street
Urbana, IL 61801, USA (Wish Tower)

GOMEZ, F
Instituto y Observatorio de Marina
Observatorio de Marina
San Fernando, Cadiz, Spain (Castle)

GREENE, B A
Division of National Mapping
P O Box 31 Belconnen
ACT 2616, Australia (Mansion)

GRIFFIN, S G
Royal Greenwich Observatory
Herstmonceux Castle
Hailsham, East Sussex

GUISO, C
Stazione Astronomica
Via Ospedale 72
09100 Cagliari, Italy (Albion)

GU JIANGUO
North China Research Institute of
Electro-Optics
P O Box 8511, Beijing, China

HAMAL, K
Faculty of Nuclear Science
& Physical Engineering
Czech Technical University
Brehova 7, 115 19 Prague 1
Czechoslovakia (Castle)

HATAT, J L
C.E.R.G.A.
Av Copernic
06130, Grasse, France (Albion)

Hide R
Meteorological Office
London Road
Bracknell
Berkshire RG12 2SZ

HOPFL, R
Satellitenbeobachtungs-station Wettzel
8493 Kozting
West Germany (Mansion)

HYDE, R L
Ald Optics
267 Rue du Chateau du Roi
38220 Vizille
France, France

KIELEK, W
Warsaw Technical University,
Department of Electronics
Institute of Radioelectronics
Nowowiejska Street 15/19
00-665 Warsaw, Poland (Castle)

KIRCHNER, D
Observatory Graz Lustbuhel
Institute for Space Research
Lustbuhelstrasse 46
A 08042, Graz, Austria (Sussex)

KIRCHNER, G
Observatory Graz Lustbuhel
Institute for Space Research
Lustbuhelstrasse 46,
A 08042, Graz, Austria (Castle)

KLOECKLER, P
Astronomisches Institut
Sidlerstrasse 5
CH-3012 Bern (Castle)

LAPLANCHE, M
C.E.R.G.A.
Av Copernic
06130, Grasse, France (Albion)

LI, YU-HUA
Deptartment of Physics
University of Maryland
College Park, MD 20742, USA (Woolpack)

LISTER, M J
Naval Research Laboratory
4555 Over Look Ave
Code 7966
Washington, DC 20375, USA (Albion)

MANGIN, J F
C.E.R.G.A.
Av Copernic,
06130 Grasse, France (Albion)

MATTHEWS, W E
Royal Greenwich Observatory
Herstmonceux Castle
Hailsham, East Sussex

MILLER, J J
Bendix Field Engineering Corporation
1 Bendix Road
Columbia, MD 21043, USA (Mansion)

MOORE, T
Department of Civil Engineering
The University
Nottingham NG7 2RD, England (Castle)

MUELLER, I I
Department of Geodetic Science
The Ohio State University
1958 Neil Avenue
Columbus Ohio 43210, USA (White Friars)

NOVOTNY, A
Faculty of Nuclear Sciences
& Physical Engineering
Czech Technical University
Brehova 7, 115 19 Prague 1
Czechoslovakia (Castle)

OTTEN, K H O
Observatory for Satellite Geodesy
P O Box 581
7300 AN Apeldoorn, Holland (Castle)

PALUTAN, F
Telespazio
Via Bergamini 50
Italy (Wish Tower)

PAUNONEN, M V
Finnish Geodetic Institute
Ilmalankatu 1A
00240 Helsinki 24, Finland (Cleavers Lyng)

PEARLMAN, M R
Smithsonian Astrophysical Observatory
60 Garden Street
Cambridge MA 02138, USA (Mansion)

PESEC, P
Observatory Graz Lustbuhel
Institute for Space Research
Lustbuhelstrasse 46,
A-8042, Gras Austria (Castle)

PIERRON, F
C.E.R.G.A.
Av Copernic
06130, Grasse, France (Albion)

PILKINGTON, J D H
Royal Greenwich Observatory
Herstmonceux Castle
Hailsham, East Sussex

PROCHAZKA, I
Faculty of Nuclear Science
& Physical Engineering
Czech Technical University
Brehova 7, 115 19 Prague 1
Czechoslovakia (Castle)

RAYNER, J
Department of Physics & Astronomy
University of Maryland
College Park, UD 20742, USA (Castle)

SCHUTZ, B E
The University of Texas at Austin
College of Engineering
Center for Space Research
Austin, TX 78712-1085, USA (Castle)

SEEGER, H
Geodatisches Institut
Nussallee 17
D-5300 Bonn 1, West Germany (Castle)

SINCLAIR, A
Royal Greenwich Observatory
Herstmonceux Castle
Hailsham East Sussex

SMITH, D E
NASA/Goddard Space Flight Center
Code 921
Greenbelt, MD 20771, USA (White Friars)

STEGGERDA, C A
Department of Physics & Astronomy
University of Maryland
College Park, MD 20742, USA (Castle)

SU DEXING
North China Research Institute of
Electro-Optics
P O Box 8511, Beijing, China

TORRE, J M
C.E.R.G.A.
Av Copernic
06130, Grasse, France (Albion)

VEIS, G
National Technical University
K Zographou 9
Athens 624, Greece (Castle)

VERMAAT, E
Observatory for Satellite Geodesy
P O Box 581
7300 AN Apeldoorn, Holland (Castle)

VISSER, H
Observatory for Satellite Geodesy
P O Box 581
7300 AN Apeldoorn, Holland (Castle)

WANG, B C
Department of Physics & Astronomy
University of Maryland
College Park, MD 20742, USA (Woolpack)

WANNG, N H
Department of Physics & Astronomy
Unversity of Maryland
College Park MD 20742, USA (Woolpack)

WHITE, M L
University of Hawaii
P O Box 209
Kula, Hawaii 96790, USA (Mansion)

WIANT, J
University of Texas
McDonald Observatory
Fort Davis, TX 79723, USA (Albion)

WILKINS, G A
Royal Greenwich Observatory
Herstmonceux Castle
Hailsham, East Sussex

WILSON, P
Institut fur Angewandte Geodasie
Richard-Strauss-Allee 11
D-6000 Frankfurt am Main 70
Federal Republic of Germany

REFERENCE COORDINATE SYSTEMS AND FRAMES CONCEPTS AND REALIZATION

I.I. Mueller
Dept. Of Geodetic Science and Surveying
Ohio State University
Columbus, Ohio 43210-1247 USA

Telephone (614) 422 1773
TWX 810 482 1715

ABSTRACT

Geodynamics has become the subject of intensive international research during the last decade, involving plate tectonics, both on the intra-plate and inter-plate scale, i.e., the study of crustal movements, and the study of earth rotation and of other dynamic phenomena such as the tides. Interrelated are efforts improving our knowledge of the gravity and magnetics fields of the earth. A common requirement for all these investigations is the necessity for a well-defined reference coordinate system (or systems) to which all relevant observations can be referred and in which theories or models for the dynamic behavior of the earth can be formulated. In view of the unprecedented progress in the ability of geodetic observational systems to measure crustal movements and the rotation of the earth, as well as in theory and model development, there is a great need for the theoretical definition, pratical realization, and international acceptance of suitable coordinate system (s) to facilitate such work. This article deals with certain aspects of the establishment and maintenance of such a coordinate system.

IDEAL AND CONVENTIONAL REFERENCE SYSTEMS AND FRAMES

In order to clarify some of the conceptual aspects of various reference systems and frames, we propose to use specific terms proposed in [Kovalevsky and Mueller, 1981] that have been used somewhat inconsistently in the past.

The purpose of a reference frame is to provide the means to materialize a reference system so that it can be used for the quantitative description of positions and motions on the earth (terrestrial frames), or of celestial bodies, including the earth, in space (celestial frames). In both cases the definition is based on a general statement giving the rationale for an ideal case, i.e. for an *ideal reference system.* For example, one would have the concept of an ideal terrestrial system, through the statement that with respect to such a system the crust should have only deformations (i.e., no rotations or translations). The ideal concept for a celestial system is that of an inertial system so defined that in it the differential equations of motion may be written without including any rotational term. In both cases the term "ideal" indicates the conceptual definition only and that no means are proposed to actually construct the system.

The actual construction implies the choice of a physical structure whose motions in the ideal reference system can be described by physical theories. This implies that the environment that acts upon the structure is modeled by a chosen set of parameters. Such a choice is not unique: there are many ways to model the motions or the deformations of the earth; there are also many celestial bodies that may be the basis of a dynamical definition of an inertial system (moon, planets, or artificial satellites). Even if the choice is based on sound scientific principles, there remains a part of imperfection or arbitrariness. This is one of the reasons why it is suggested to use the term "conventional" to characterize this choice. The other reason is related to the means, usually conventional, by which the reference frames are defined in practice.

At this stage, there are still two steps that are necessary to achieve the final materialization of the reference system so that one can refer coordinates of objects to them. First, one has to define in detail the model that is used in the relationship between the configuration of the basic structure and its coordinates. At this point, the coordinates are fully defined, but not necessarily accessible. Such a model is called a *conventional reference system.* The term "system" thus includes the description of the physical environment as well as the theories used in the definition of the coordinates. For example, the FK4 (conventional) reference system is defined by the ecliptic as given by Newcomb's theory of the sun, the values of precession and obliquity, also given by Newcomb, and the Woolard theory of nutation. Once a reference system is chosen, it is still necessary to make it available to the users. The system usually is materialized for this purpose by a number of points, objects or coordinates to be used for referencing any other point, object or coordinate. Thus, in addition to the conventional choice of a system, it is necessary to construct a set of conventionally chosen (or arrived at) parameters (e.g., star positions or pole coordinates). The set of such parameters, materializing the system, define a *conventional reference frame.* For example, the FK4 catalogue of over 1500 star coordinates define the FK4 frame, materializing the FK4 system. Another example is the BIH Conventional Terrestrial Frame, whose

pole is the origin of the polar motion derived (and published) by the BIH, and whose longitude origin is the Greenwich Mean Astronomical Meridian, in reality the point on the equator of the above pole, used by the BIH for deriving UT1. This frame materializes the BIH Conventional Terrestrial System (CTS), which itself until recently was defined by the FK4 frame, Newcomb's constants of precession and obliquity, Woolard's series of nutation, and by all the assumptions made regarding the reference coordinates of the participating observatories and their relative weights, etc. The current BIH system is based on the IAU 1976 precession constant and the IAU 1980 (Wahr) series of nutation.

Another way of defining the CTS for the deformable earth is through the time varying positions of a number of terrestrial observatories whose coordinates are periodically reobserved by some international service. The frame of this CTS could then be derived from the changing coordinates through transformations containing rotational (and possible translational) parameters. These transformation parameters computed and published by the service would then define the frame of the system. The service, as part of the system definition, thus would have to make the assumption that the progressive changes of the reference coordinates of the observatories do not represent rotations (and translations) in the statistically significant sense. This mode seems to be the consensus for the establishment of the future CTS frame.

It is also necessary to point out that celestial reference systems may be defined *kinematically* (through the positions of extragalactic radio sources), or *dynamically* (through the geocentric or heliocentric motions of artificial satellites, moon, planets). Stellar systems, such as the FK5, are hybrid. Furthermore, approximations must be introduced in the model so that it is not true to say that these systems are realizations of an ideal inertial system. This is why it is appropriate to use the term conventional "quasi" inertial system (CIS) as a common term for all such celestial systems. The corresponding frames would be defined by either the adopted positions of a set of radio sources (kinematic frame) or the adopted geocentric or heliocentric ephemerides (dynamic frames), all serving the materialization of the CIS with greater or lesser success (accuracy).

There seems to be general agreement that only two basic coordinate systems are needed: a Conventional Inertial System (CIS), which in some "prescribed way" is attached to extragalactic celestial radio sources, to serve as a reference for the motion of a Conventional Terrestrial System (CTS), which moves and rotates in some average sense with the earth and is also attached in some "prescribed way" to a number of dedicated observatories operating on the earth's surface [Mueller, 1981]. In the latter, the geometry and dynamic behavior of the earth would be described in the relative sense, while in the former the movements of our planetary system (including the earth) and our galaxy could be monitored in the absolute sense. There also seems to be a need for certain interim systems to facilitate theoretical calculations in geodesy, astronomy, and geophysics as well as to aid the possible traditional decomposition of the transformations between the frames of the two basic systems.

As we will see later, there already seems to be understanding in principle on how the two basic reference systems should be established; certain operational details need to be worked out and an international

agreement is necesary. There are, however, a number of more or less open questions which will have to be discussed further. These include the type of interim systems needed and their connections to both CIS and CTS, the type(s) of observatories, their number and distribution, whether all instruments need to be permanently located there or only installed at suitable regular intervals to repeat the measurements; how far the model development should go so as not to become impractical and unmanageable; and how independent observations should be referenced to the CTS, i.e., what kind of services need to be established and by whom. This discussion deals only with questions related to the CTS.

CONVENTIONAL TERRESTRIAL SYSTEMS (CTS) OF REFERENCE

As mentioned, the frame of the CTS is in some "prescribed way" attached to observatories located on the surface of the earth. The connection between the CTS and CIS frames by tradition (to be preserved) is through the conventional rotations expressed as [Mueller, 1969]

$$[\ \underline{\text{CTS}}\ ] = \text{SNP}\ [\ \underline{\text{CIS}}\ ]$$

where P is the matrix of rotation for precession, N for nutation, and S for earth rotation (polar motion and sidereal time). Polar motion thus is defined as the angular separation of the third axis of the CTS, the Conventional Terrestrial Pole (CTP), and the axis of the earth for which the nutation (N) is computed (e.g., instantaneous rotation axis, Celestial Ephemeris Pole, Tisserand mean axis of the mantle (see [Mueller, 1981]).

Geodynamic requirements for a CTS may be discussed in terms of global or regional problems. The former are required for monitoring the earth's rotation, while the latter are mainly associated with crustal motion studies in which one is predominantly interested in strain or strain rate, quantities which are directly related to stress and rheology. Thus for these studies, global reference systems are not particularly important although it is desirable to relate regional studies to a global frame.

For the rotation studies one is interested in the variations of the earth's rotational rate and in the motions of the rotation axis both with respect to space (CIS) and the crust or the CTS. The problem therefore is threefold: (1) to establish a geometric description of the crust, either through the coordinates of a number of points fixed to the crust, or through polyhedron(s) connecting these points whose side lengths and angles are directly estimable from observations using the new space techniques (laser ranging or VLBI). The latter is preferred because of its geometric clarity. (2) To establish the time-dependent behavior of the polyhedron due to, for example, crustal motion, surface loading or tides. (3) To relate the polyhedron to both the CIS and the CTS. For the global tectonic problems only the first two points are relevant although these may also be resolved through point (3).

In the absence of deformation, the definition of the CTS is arbitrary. Its only requirement is that it rotates with the rigid earth, but common sense suggests that the third axis should be close to the mean position of the rotation axis and the first axis be near the origin of longitudes. An arbitrary choice, such as the one presently defined by the BIH-published polar coordinates and UT1 is appropriate.

In the presence of deformations, particularly long periodic or secular ones, the definition is more problematical, because of the inability to separate rotational (and translational) crustal motions of the crust from those of the CTS. This is why the consensus seems to be the CTS described earlier. If such a system is adapted, the secular type motions mentioned above will be absorbed in the future CTS, by definition. Residuals with respect to such a CTS will provide estimates of relative motions between stations, i.e., of the deformations.

One geophysical requirement of the reference system is that other geophysical measurements can be related to it. One example is the gravity field. The reference frame generally used when giving values of the spherical harmonic coefficients is tied to the axes of figure of the earth. This frame should be simply related with sufficient accuracy to the CTS as well as to the CIS in which, for example, satellite orbits are calculated. Another example is height measurements with respect to the geoid.

The vertical motions may require some special attention, because absolute motions with respect to the center of mass have an immediate geophysical interest and are realizable. Again, if the center of mass has significant motions with respect to the crust, such a motion will be absorbed in the future CTS, if defined as suggested above. At present there is no compelling evidence that the center of mass is displaced significantly at least at the decade time scale.

Apart from the geometrical considerations the configuration of observatories should be such that (1) there are stations on most of the major tectonic plates in sufficient number to provide the necessary statistical strength, (2) the stations lie on relatively stable parts of the plate so as to reduce the possibility that tectonic shifts in some stations will not overly influence, at least initially, the parameters defining the CTS frame.

Finally one should realize that the problem of the geometric origin of the CTS frame is linked to that of a geocentric ephemeris frame. The center of mass of the earth is directly accessible to dynamical methods and is the natural origin of a geocentric satellite-based dynamical system. But, as such, it is model dependent. And, unless the terrestrial reference frame is also constructed from the same satellites (as is the case in various earth models such as GEM, SAO, GRIM), there may be inconsistencies between the assumed origin of a kinematically obtained terrestrial system and the center of mass. A time-dependent error in the position of the center of mass, considered as the origin of a terrestrial frame, may introduce spurious apparent shifts in the position of stations that may then be interpreted as erroneous plate motions. To avoid this problem the parameters defining the CTS frame should include translational terms as suggested earlier.

Current Situation

Until 1984 the internationally accepted Woolard series of nutation was used to compute the position of the instantaneous rotation axis of the rigid earth, and the CTP was the Conventional International Origin (CIO), defined by the adopted astronomic latitudes of the five International Latitude Service (ILS) stations [Mueller, 1969].

From 1984 onward the IAU 1980 [Wahr, 1981] series of nutation for the

nonrigid earth gives the space position of the Celestial Ephemeris Pole (CEP). The CTP officially remains the same as before. Thus, conceptually, polar motion should be determined from latitude observations only at the ILS stations. This has been done for 80 years, and the results are, the best available *long-term* polar motions, properly, but not very accurately, determined. The first axis of the CTS, the Greenwich Mean Astronomical Meridian, is defined by the assigned astronomic longitudes of time observatories participating in the work of the Bureau International de l'Heure (BIH).

For reasons explained elsewhere (e.g., [Mueller, 1981]), the use of the CIO is no longer a reality. The common denominator being the series of nutation, observationally the CTP is defined by the coordinates of the pole as published by the IPMS or by the BIH. Thus it is legitimate to speak of IPMS and BIH CTP's. The situation recently has become even more complicated because Doppler and laser satellite tracking, VLBI observations, and lunar laser ranging also can determine earth rotation parameters, some of which are incorporated in the BIH computations. Further confusion arises due to the fact that the BIH has two systems: the BIH 1968 and the BIH 1979, the latter due to the incorporation of certain annual and semiannual variations of polar motion determined from the comparisons of astronomical (optical) results with those from Doppler and lunar laser observations [Feissel, 1980].

Though naturally every effort has been made to keep the IPMS and BIH pole of the CTS as close as possible to the CIO, the situation cannot be considered satisfactory from the point of view of the geodynamic accuracy requirement of a few parts in 10^8.

The Future Conventional Terrestrial Reference Frame

There seems to be general agreement that the new CTS frame conceptually be defined similarly to the CIO-BIH system [Bender and Goad, 1979; Guinot, 1979; Kovalevsky, 1979; Mueller, 1975, 1981; Kovalevsky and Mueller, 1981], i.e., it should be attached to observatories located on the surface of the earth. The main difference in concept is that these can no longer be assumed motionless with respect to each other. Also they must be equipped with advanced geodetic instrumentation like VLBI or lasers, which are no longer referenced to the local plumblines. Thus the new transformation formula may have the form

$$[\underline{OBS}]_j = \underline{L}_j + [\underline{CTS}]_j + \underline{v}_j \qquad (2)$$

where $\underline{L}_j$ is the vector of the "j" observatory's movement on the deformable earth with respect to the CTS.

The $[\underline{OBS}]_j$ is related to the observatory coordinates $(\bar{X}^\circ_j)$ determined in the terrestrial frame inherent in the observational technique (e.g., SLR) "0", through the well-known transformations involving three translation components $(\bar{\delta}^\circ)$, three (usually very small) rotations $(\bar{\beta}^\circ)$ and a differential scale factor (c):

$$[\underline{OBS}]_j = \bar{X}^\circ_j + \bar{\delta}^\circ + R_1(\beta_1)\, R_2(\beta_2)\, R_3(\beta_3)\, \bar{X}^\circ_j + c\bar{X}^\circ_j \qquad (3)$$

Naturally in case of techniques which observe directions only (e.g., astrometry), the terms containing translation and scale will be omitted. Eqs. (2) and (3) together with (4) below (and possibly others) may form the observation equations to be used when realizing the future CTS. The latter equation [Zhu and Mueller, 1983] relates an earth rotation parameter (ERP) series (x_p, y_p, and UT1) determined by the technique "O", within its own frames of reference, with the parameters of rotation above:

$$\begin{aligned} x_p - \beta_2^\circ + \alpha_1^\circ \sin\theta + \alpha_2^\circ \cos\theta &= x_p^\circ + v_{x_p} \\ y_p - \beta_1^\circ - \alpha_1^\circ \cos\theta + \alpha_2^\circ \sin\theta &= y_p^\circ + v_{y_p} \\ \omega_C\, UT1 + \beta_3^\circ - \alpha_3^\circ &= \omega_C\, UT1^\circ + v_{UT1} \end{aligned} \qquad (4)$$

where α_1, α_2, α_3 are the small rotations between the frames of the CIS of the technique "O" and that of the service, θ is the sidereal time, ω_C the conversion factor between sidereal and solar times, and v the residuals.

The unknowns in the above system of equations to be solved for, in a least squares solution minimizing the square sum of the residuals v, are $[\underline{CTS}]_j$ and $\underline{L}_j$ for the observatories; $\overline{\delta}^\circ$, $\overline{\beta}^\circ$ and c° for the terrestrial frames of the techniques; $\overline{\alpha}^\circ$ for their inertial frames; and finally, the ERP parameters (x_p, y_p and UT1) for the service. If, however, in eq. (3) the ERP's (x_p°, y_p°, $UT1^\circ$) are mean values averaged over intervals longer than a day, α_1° and α_2° cannot be determined, because the sin θ and cos θ terms average to zero in one sidereal day.

As mentioned, the parameters pertaining to the observatories ($[\underline{CTS}]_j$ and L_j) define the CTS. The others give the relationships of the CTS to the technique "O" terrestrial frame ($\overline{\delta}^\circ$, $\overline{\beta}^\circ$, c); to the CIS (x_p, y_p, UT1); and the latter's relationship to the technique "O" inertial frame ($\overline{\alpha}^\circ$).

The rotations in eq. (3) can either be determined from the Cartesian coordinates (e.g., [Moritz, 1979]) or, for possible better sensitivity, since the rotation is least sensitive to variations in height, only from those of the horizontal coordinates (geodetic latitude and longitude) (e.g., [Bender and Goad, 1979]). It is, however, unlikely that the rotations will continue to be determined (as presently) from astronomical coordinates, i.e., from the direction of the vertical, for the reasons of inadequate observational accuracy. Note that when using this method, the deformations (and the residuals) by definition cannot have common rotational (or translational) components.

As far as the origin of the CTS is concerned, it could be centered at the center of mass of the earth, and its motion with respect to the stations can be monitored either through observations to satellites or the moon, or, probably more sensitively, from continuous global gravity observations at properly selected observatories [Mather et al., 1977]. For the former method, the condition

$$\sum_D w_D\, \overline{\delta}_D^\circ = 0$$

could be imposed on the above adjustment. The summation would be

extended to all the above dynamic techniques D with given relative weights w_D. A similar condition could also be imposed on the scale extended to techniques defining the best scales (probably VLBI).

The above method of determining ERP or some variation thereof needs to be initialized in a way to provide continuity. This could be done through the IPMS or BIH poles, and the BIH zero meridian, at the selected initial epoch (or averaged over a well-defined time interval, say 1-1.2 years), uncertainties in their definition mentioned earlier mercifully ignored.

It is probably not useless to point out that if such a system is established, the most important information for the users will be the ERP and the transformation parameters, but for the scientist new knowledge about the behavior of the earth will come from the analysis of the residuals after the adjustment.

It is hoped that the IAU and IUGG will make practical recommendations on the establishment of such or a very similar Conventional Terrestrial System, including the necessary plans for supporting observatories and services. One of the recommendations ought to be that due to the fact that the ultimate goal is the determination of the total transformation between the CTS and CIS, the future service must publish not only the ERP's determined from the repeated comparisons (the situation at present), but also the models and parameters discussed above, i.e., the parameters defining the whole *system*.

In conclusion, there is little doubt that the terrestrial reference frame presently adopted is of very little practical use because of its insufficient accessibility. Further, the astronomical observations should be replaced by methods which are not tied to the direction of the vertical but rather to directions tied to the crust. Such methods are the laser observations to satellites and to the moon, and VLBI. Portable systems can establish the polyhedron(s) discussed earlier, while permanent stations at suitably chosen locations would become the observatories for the maintenance of the CTS using the method described above.

References

Bender, P. and C. Goad (1979) "Probable LAGEOS Contributions to World Wide Geodynamics Control Network," The Use of Artificial Satellites for Geodesy and Geodynamics, Vol. II, Proc. of International Symposium, Athens, May 29 - June 2, 1978, G. Veis and E. Livieratos, eds. National Technical Univ. Athens, 145-161.

Feissel, M. (1980) "Determination of the Earth Rotation Parameters by the Bureau International de l'Heure, 1962-1979," Bull. Geod., 54,1, 81-102.

Guinot, B. (1979) "Basic Problems in the Kinematics of the Rotation of the Earth," McCarthy and Pilkington, eds., Time and the Earth's Rotation, D. Reidel, Dordrecht, 7-18.

Kovalevsky, J. (1979) "The Reference Systems," McCarthy and Pilkington, eds., Time and the Earth's Rotation, D. Reidel, Dordrecht, 151-163.

Kovalesky, J. and I.I. Mueller (1981) "Comments on Conventional Terrestrial and Quasi-Inertial Reference Systems," Gaposchkin and Kolaczek eds., Reference Coordinate Systems for Earth Dynamics, D. Reidel, Dordrecht.

Mather, R.S., E.G. Masters and R. Coleman (1977) "The Role of Non-Tidal Gravity Variations in the Maintenance of Reference Systems for Secular Geodynamics," Uniserv G 26, Univ. of New South Wales, Sidney.

Moritz, H. (1979) "Concepts in Geodetic Reference Frames," Dept. of Geodetic Science and Surveying Rep. 294, Ohio State Univ., Columbus.

Mueller, I.I. (1969) Spherical and Practical Astronomy as Applied to Geodesy, Ungar Publ., New York.

Mueller, I.I. (1975) "Tracking Station Positioning from Artificial Satellite Observations," Geophys. Surveys, 2,3, 243-176.

Mueller, I.I. (1981) "Reference Coordinate Systems for Earth Dynamics: A Preview," Gaposchkin and Kolaczek, eds., Reference Coordinate Systems for Earth Dynamics, D. Reidel, Dordrecht.

Wahr, J.M. (1981) "The Forced Nutations of an Elliptical, Rotating, Elastic and Oceanless Earth," J.R. Astr. Soc., 64, 705-727.

Zhu, S.-Y. and I.I. Mueller (1983) "Effects of Adopting New Precession, Nutation and Equinox Corrections on the Terrestrial Reference Frame," Bull. Geod., 57, 29-42.

FIFTEEN YEARS OF LUNAR LASER RANGING ACCOMPLISHMENTS AND FUTURE CHALLENGES

J.O. Dickey, J.G. Williams, X.X. Newhall
Jet propulsion Laboratory
California Institute of Technology
4800 Oak Grove Drive
Pasadena, California 91 109

Telephone (818) 354 4321
TWX 910 588 3294 / 910 588 3269

ABSTRACT

The past decade and a half has been a period of achievement for Lunar Laser Ranging (LLR), having made the transition from an Apollo experiment to a program of scientific impact. Areas influenced by this technique include geodynamics, geodesy, astronomy, lunar science, and gravitational physics. Scientific results are reviewed here and are grouped by areas of impact : geophysical parameters, ephemerides, references frames, and coordinate systems and their unification. Lunar science, gravity, and relativity have been advanced by this program. Future challenges are addressed. With the reality of multi-station LLR (three sites, four systems), the future is indeed promising.

July 21 of this year marked the fifteenth anniversary of the first manned lunar landing by the Apollo 11 Mission. On the fifth day of that historic mission the lunar module Eagle touched down on the lunar surface and Man first stepped onto the Moon. The visitors stayed for less than a day, but their journey marked a new era for mankind. Included on this mission and the later Apollo flights 14 and 15 were laser reflectors that permit precise measurement of the Earth-Moon separation. In Lunar Laser Ranging (LLR), individual photons are detected. When all losses are considered, out of the $\sim 10^{19}$ photons transmitted per shot, the receiver detects only one photon every 10 or 20 shots. The three Apollo reflectors plus the French-built reflector on Lunakhod 2 create a favorable geometry for studying the rotations of the Moon and permit separation of geodynamic effects from lunar motion.

The main block of lunar range data is from McDonald Observatory (August 1969 to May 1982); the ranging system was of 10 cm accuracy during the latter half of this period. There are also less accurate data from Orroral Valley, Australia (October 1978 to October 1980), the CERGA site at Grasse, France (April 1982 to March 1984), and a few days of range data from Haleakala Observatory on Maui (in 1977). There was a hiatus in the McDonald data from May 1982 until July 1983 due to the development of a new ranging system (MLRS), which is expected to be considerably more accurate. The new system is still being optimized, and useful data were obtained last spring. April also brought an abrupt improvement in the French data to about 10 cm precision for the best ranges, as judged from our fits. The Haleakala site has also returned part of its effort to lunar ranging, after a number of years devoted to satellite ranging, and has now obtained verified lunar ranges with an improved system. These acquisitions marked a historic event for LLR; for the first time in its fifteen-year history, data were acquired at three sites with four systems (McDonald 2.7 m, MLRS, CERGA 1.5 m, and Haleakala). Multiple-station ranging is now a reality. The gap in Orroral data is due to the time required for system upgrade, and ranging will resume shortly, with improved accuracy. Research activities are also underway at the Goddard 48-inch optical facility under Carroll Alley of the University of Maryland. The future has the potential for higher accuracy and possible additional stations, such as Wettzell.

LLR has contributed much in its history. The results can be grouped and reviewed by areas of impact: geophysical parameters, ephemerides, reference frames, and coordinate systems and their unification. Lunar science, gravity and relativity have also been advanced by this technique. Reviews have addressed some of these topics: Bender *et al.* (1973) mark the transition of the LLR program from a mission experiment to a program of scientific exploration; Williams (1977) outlines the scientific accomplishments; Mulholland (1980) reviews the progress made during the first decade of LLR; and Alley (1983) discusses LLR results as a test of gravity theories.

Of importance to the geodynamics community has been the series of measurements permitting long-term studies of variations in the Earth's rotation, as well as determination of many parameters of the Earth-Moon system. The coordinates of the observatories are determined in the geocentric frame. LLR provides an accurate value of

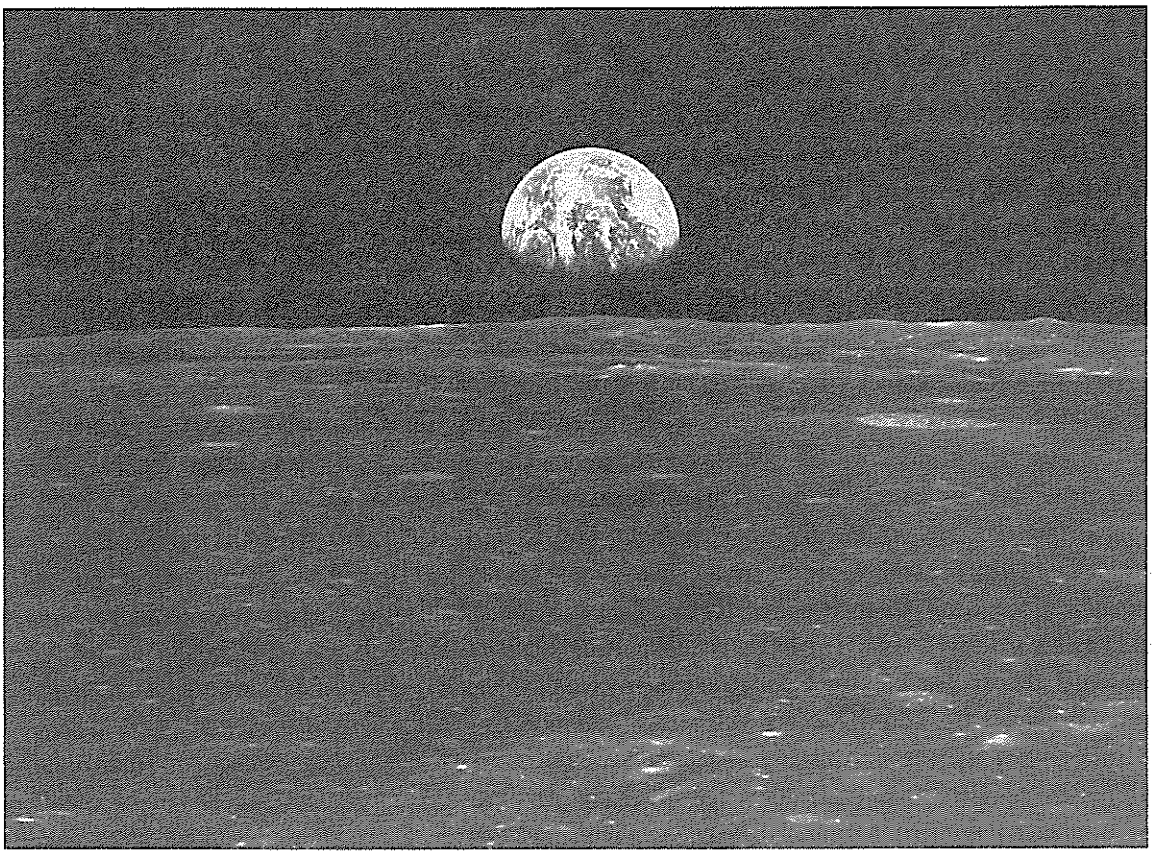

Earth Rise on the Moon

---

the principal term GM_{Earth} in the Earth's gravity field. The LLR-determined value of the secular acceleration of the Moon (-25.3 ± 1.2 arcsec/century^2, Dickey *et al.*, 1984*a*), is now significantly better than values based on conventional astrometry or inferred from artificial satellite detection of the tidal gravity field. This acceleration in longitude, which corresponds to a linear increase of 3.7 ± 0.2 cm/yr in the mean distance of the Moon, has implications for ocean tides, the decrease in spin rate of the Earth, and the evolution of the lunar orbit. LLR has contributed to determination of Universal Time (UT1) and polar motion; the long-term stability and temporal resolution of a day or less are assets of LLR data. Recent tabulations of Earth rotation from LLR data are given by Langley *et al.* (1981*a*), Calame (1982), and Dickey *et al.* (1983; 1984*b*). Earth rotation intercomparisons between LLR and other techniques (e.g. Robinson *et al.*, 1983; Dickey *et al.*, 1984*c*) are one of the principal goals of the MERIT Campaign, an effort organized by a joint working group of the International Astronomical Union and the International Union of Geodesy and Geophysics to Measure Earth Rotation and to Intercompare Techniques.

For studying the processes which underlie variations in the Earth's rotation, the long span of available LLR data is valuable. LLR has produced new information about the exchange of angular momentum between the solid Earth and atmosphere (Eubanks *et al.*, 1984 and 1985), and was instrumental in the discovery of the near

50-day oscillation in the length of day (Feissel and Gambis, 1980; Langley *et al.*, 1981*b*) and its correlation with a similar oscillation in the atmosphere. This discovery has stimulated research in the atmospheric community (Anderson and Rosen, 1983). An analysis (Yoder *et al.*, 1983) of LAGEOS satellite range data (University of Texas) with the LLR UT1 determination revealed significant nodal residual signatures, apparently arising from variations in the zonal gravitational harmonic coefficient J_2. The implied decrease of J_2 is consistent with historical observations of the nontidal acceleration of the Earth's rotation and models of postglacial viscous rebound. The determination of $\dot{J}_2$ is significant, as it constitutes the first unambiguous demonstration of a secular change in the Earth's gravity field. Tidally driven periodic terms in UT1 have been studied by Yoder *et al.* (1981*a* and *b*), who determined the response of the Earth at the fortnightly and monthly periods. Morgan *et al.* (1982) used LLR estimates of variation of latitude to derive spectra of polar motion for a shorter span of data than is possible using classical optical observations; such spectra are important for studying non-stationary mechanisms for excitation and damping of the Chandler wobble. The analysis of LLR observations has shown them to be sensitive to the nutation coefficients. Dickey *et al.* (1984*a*) reported improved upper limits for the free nutation of the Earth's core and found the amplitudes of the half-year and fortnightly nutation terms to match those of the Wahr series to within a few milliarcseconds. However, a small deviation of the annual term similar to that reported from VLBI observations (Gwinn *et al.*, 1984) appears to be present. A longer data span is needed to have a definitive separation between the precession of the Earth's equator and the 18.6-year terms.

LLR has revolutionized the lunar ephemeris, being three orders of magnitude more accurate than the classical optical data. Both JPL and MIT have produced numerically integrated lunar orbits and librations and have made solutions which include lunar and planetary data (Newhall *et al.*, 1983; King, private communication, 1984). Here, we have the best of two worlds, combining the sensitivity of the Viking ranges to Mars with the lunar ranges. The lunar and planetary ephemerides based on range data are set in a nearly inertial celestial coordinate system. LLR is sensitive to the mutual orientation of the planes of the Earth's equator, the lunar orbit, and the ecliptic; hence it locates the intersection of ecliptic and equator (the dynamical equinox) and determines the obliquity. The dynamical equinox has been used as the zero point of the right ascension system in several JPL ephemerides and has been proposed as the celestial origin for the space techniques (Williams *et al.*, 1984). Preliminary ties have been made between the quasar VLBI frame and the ephemeris frame by performing VLBI experiments between Mars- and Venus-orbiting spacecraft and quasars at small angular separation (Newhall *et al.*, 1985). The satellite systems can be linked to the dynamical equinox and the inertial frame by using colocation data with LLR and VLBI instruments; the LLR instruments which are operating or under development either have LAGEOS capability or are located near instruments which do.

Lunar laser ranging has made possible a several-order-of-magnitude improvement in measurement of the forced and free variations in the Moon's rotation—the lunar physical librations. These measurements have had two important results: the de-

tection of apparent large free librations (Calame, 1977; Cappallo *et al.*, 1982) and the detection of rotational dissipation within the Moon (Yoder *et al.*, 1978; Yoder, 1981; Ferrari *et al.*, 1980; Cappallo *et al.*, 1981). Taken together, these results place constraints on the internal structure of the Moon, particularly the size of a lunar core (Stevenson and Yoder, 1981; Yoder, 1981). In addition, LLR determines lunar gravitational harmonics, the lunar Love number k, and the fractional differences of the lunar moments of inertia. The reflector coordinates are obtained and serve as cartographic control points.

Verification of the principle of equivalence for massive bodies was achieved by seeking the Nordtvedt (1968) effect in the lunar orbit (Shapiro *et al.*, 1976; Williams *et al.*, 1976). This contribution to fundamental physics gave the first test of the nonlinear and dynamical structure of General Relativity's post-Newtonian field components (Nordtvedt, 1983).

The future is promising with the reality of multi-station LLR. Both components of polar motion will be measured; UT1 will be better determined with more continuous coverage in time. Studies by Stolz and Larden (1977) predict accuracies of 1–2 cm for polar motion and 0.02–0.04 msec for UT1 using four stations (Orroral, CERGA, Haleakala, and McDonald) operating at 3 cm accuracy; better results are expected if the goal of 1 cm range accuracy can be achieved. Baselines and corresponding plate motions can be studied using multi-station LLR results. A covariance study (Dickey *et al.*, 1984*a*) indicates that the accuracy of the nutation amplitudes and the precession constant improves substantially as the data span increases. Simulations (based on a three-station network—McDonald, Haleakala, and Orroral—with an *a priori* uncertainty of 0.5 nsec) predict an accuracy of 0.06 arcsec/century for the precession constant by the end of 1988, surpassing the standard error of 0.15 arcsec/century quoted by Fricke (1977; 1981) from analyses of optical results. The error in the 18.6-year nutation terms will be reduced to 2 milliarcseconds by the end of 1988, a level that should be useful for limiting the Earth's interior structure. Another goal is to combine LAGEOS tidal results with those from LLR (see Williams *et al.*, 1978). Artificial satellites are sensitive to many tidal terms because of their proximity to Earth. A joining of both data types can advance our understanding of the tidal processes.

In lunar science, further progress awaits only the acquisition of more accurate observations and the redundancy useful in separating signatures in the data due to (terrestrial) polar motion from those due to errors in our models of the lunar orbit and rotation. In the area of lunar interior structure, there may be range signatures having amplitudes of a few centimeters which can distinguish between solid-body and core-mantle dissipation. This discrimination requires range data having uncertainties of at most 5 cm. Another clue, advanced by Yoder (1981), to the existence of a liquid core would be the presence of irregularities or changes in the free physical librations due to turbulence at the core-mantle interface. Again, precise data are needed to detect such small effects, but a success would be scientifically valuable.

In gravitational physics, results can be improved by a factor of four by the availabil-

ity of more accurate observations. Estimates of PPN (Parametrized Post-Newtonian) quantities can be made using a combination of LLR data and planetary observations.

The past decade and a half has been productive and exciting for LLR; the technique made the transition from an Apollo experiment (LURE) to a program of scientific impact. Areas influenced are geodynamics, geodesy, astronomy, lunar science, and gravitational physics. A "giant leap" is underway with the advent of high accuracy multi-station LLR. The science of this period has been done with ranges of 10 cm or more uncertainty, heavily dominated by a single station. New insight and knowledge will be gained with 1 to 3 cm ranges from several sites. Indeed, the best is yet to come!

Acknowledgement

The work of the authors was carried out by the Jet Propulsion Laboratory, California Institute of Technology, under contract with the National Aeronautics and Space Administration.

References

Alley, C. O.: "Laser Ranging to Retro-Reflectors on the Moon as a Test of Theories of Gravity," in *Quantum Optics, Experimental Gravity, and Measurement Theory*, eds. P. Meystre and M. O. Scully, Plenum, 429–495, 1983.

Anderson, J. R. and Rosen, R. D.: "The Latitude-Height Structure of 40–50 Day Variations in Atmospheric Angular Momentum," *J. Atmos. Sci.*, **40**, 1584–1591, 1983.

Bender, P. L., Currie, D. G., Dicke, R. H., Eckhardt, D. H., Faller, J. E., Kaula, W. M., Mulholland, J. D., Plotkin, H. H., Poultney, S. K., Silverberg, E. C., Wilkinson, D. T., Williams, J. G., and Alley, C. O.: "The Lunar Ranging Experiment," *Science*, **182**, 229–238, 1973.

Calame, O.: "Earth Rotation by Lunar Distances," published in the *BIH (Bureau International de l'Heure) Annual Report for 1981*, D31–D33, 1982.

Calame, O.: "Free Librations of the Moon from Lunar Laser Ranging," in *Scientific Applications of Lunar Laser Ranging*, ed. J. D. Mulholland, Reidel, Dordrecht, 53–63, 1977.

Cappallo, R. J., Counselman, C. C., III, King, R. W., and Shapiro, I. I.: "Tidal Dissipation in the Moon," *J. Geophys. Res.*, **86**, 7180, 1981.

Cappallo, R. J., King, R. W., Counselman, C. C., III, and Shapiro, I. I.: "Evidence for Lunar Librations Near Resonance," *Celestial Mechanics*, **26**, 145, 1982.

Dickey, J. O. and Williams, J. G.: "Earth Rotation from Lunar Laser Ranging," *Astron. Astrophys. Suppl. Ser.*, **54**, 519–540, 1983.

Dickey, J. O., Williams, J. G., Newhall, X X, and Yoder, C. F.: "Geophysical Applications of Lunar Laser Ranging," *Proceedings of the International Association of Geodesy (IAG) Symposia, International Union of Geodesy and Geophysics (IUGG) XVIIIth General Assembly, Hamburg, FRG, August 15–27, 1983*, Ohio State University, Dept. of Geodetic Science and Surveying, Columbus, Ohio 43210, Vol. 2, 509–521, 1984*a*.

Dickey, J. O., Newhall, X X, and Williams, J. G.: "Earth Orientation from Lunar Laser Ranging," *BIH (Bureau International de l'Heure) Annual Report for 1983*, D31–D34, 1984*b*.

Dickey, J. O., Williams, J. G., and Eubanks, T. M.: "Earth Rotation and Polar Motion: Results from Lunar Laser Ranging Analysis and an Intercomparison Study," *Proceedings of the International Association of Geodesy (IAG) Symposia, International Union of Geodesy and Geophysics (IUGG) XVIIIth General Assembly, Hamburg, FRG, August 15–27, 1983*, Ohio State University, Dept. of Geodetic Science and Surveying, Columbus, Ohio 43210, Vol. 2, 12–27, 1984*c*).

Eubanks, T. M., Steppe, J. A., Dickey, J. O., and Callahan, P. S.: "A Spectral Analysis of the Earth's Angular Momentum Budget," accepted for publication in *J. Geophys. Res.* (Red), 1985.

Eubanks, T. M., Dickey, J. O., and Steppe, J. A.: "Geophysical Implications and Systematic Errors in the Angular Momentum Budget of the Earth," *Proceedings of the International Association of Geodesy (IAG) Symposia, International Union of Geodesy and Geophysics (IUGG) XVIIIth General Assembly, Hamburg, FRG, August 15–27, 1983*, Ohio State University, Dept. of Geodetic Science and Surveying, Columbus, Ohio 43210, Vol. 2, 122–143, 1984.

Feissel, M. and Gambis, D. C., *r. hebd. Seanc. Acad. Sci., Paris* **B291**, 271-273, 1980.

Ferrari, A. J., Sinclair, W. S., Sjogren, W. L., Williams, J. G., and Yoder, C. F.: "Geophysical Parameters of the Earth-Moon System," *J. Geophys. Res.*, **85**, 3939-3951, 1980.

Fricke, W.: "Arguments in Favor of a Change in Precession," *Astron. Astrophys.*, 54, 363–366, 1977.

Fricke, W.: "Definition and Practical Realization of the Reference Frame in the FK5—the Role of Planetary Dynamics and Stellar Kinematics in the Definition," in *Reference Coordinate Systems for Earth Dynamics*, E. M. Gaposhkin and B. Kolaczek, eds., D. Reidel, 331–340, 1981.

Gwinn, C. R., Herring, T. A., and Shapiro, I. I.: "Geodesy by Radio Interferometry: Correction to the IAU 1980 Nutation Series," *EOS*, 65, 45, 859, 1984.

Langley, R. B., King, R. W., and Shapiro, I. I.: "Earth Rotation from Lunar Laser Ranging," *J. Geophys. Res.*, 86, 11913–11918, 1981*a*.

Langley, R. B., King, R. , Shapiro, I. I., Rosen, R. D., and Salstein, D. A.: "Atmospheric Angular Momentum and the Length of Day: A Common Fluctuation with a Period Near 50 Days," *Nature*, 294, 730, 1981*b*.

Morgan, P. J., King, R. W. and Shapiro, I. I.: "Spectral Analysis of Variation of Latitude Derived from Lunar Laser Ranging and Satellite Doppler," *EOS*, **63**, 302, 1982.

Mulholland, J. D.: "Scientific Achievement from Ten Years of Lunar Laser Ranging," *Reviews of Geophysics and Space Physics*, **18**, 3, 549–564, 1980.

Newhall, X X, Preston, R. A. and Esposito, P. B.: "Relating the JPL VLBI Reference Frame and Planetary Ephemerides," to be published in the *Prodeedings of the International Astronomical Union Symposium 109: Astrometric Techniques*, Reidel, Dordrecht, Holland, 1985.

Newhall, X X, Standish, E. M., Jr., and Williams, J. G.: "DE102: a numerically integrated ephemeris of the Moon and planets spanning forty-four centuries," *Astron. Astrophys.*, **125**, 150–167, 1983.

Nordtvedt, K., Jr.: "Equivalence Principle for Massive Bodies. I. Phenomenology," *Phys. Rev.*, **169**, 1014, 1968*a*.

Nordtvedt, K., Jr.: "Testing Relativity with Laser Ranging to the Moon," *Phys. Rev.*, **170**, 1186, 1968*b*.

Nordtvedt, K., Jr.: "The Meaning of the Lunar Laser Ranging Experimintal Results for Gravitational Theory," in *Quantum Optics, Experimental Gravity, and Measurement Theory*, eds. P. Meystre and M. O. Scully, Plenum, 497–502, 1983.

Robertson, D. S., Carter, W. E., Eanes, R. J., Schutz, B. E., Tapley, B. D., King, R. W., Langley, R. B., Morgan, P. J., and Shapiro, I. I.: "Comparison of Earth Rotation as Inferred from Radio Interferometric, Laser Ranging, and Classical Observations," *Nature*, **302**, 5908, 509–511, 1983.

Shapiro, I. I., Counselman, C. C., III, and King, R. W.: "Verification of the Principle of Equivalence for Massive Bodies," *Phys. Rev. Let.*, **36**, 555, 1976.

Stevenson, D. J. and Yoder, C. F.: "A Fluid Outer Core for the Moon and its Implications for Lunar Dissipation," *Free Librations and Magnetism, LPSC XII*, Houston, 1043, 1981.

Stolz, A. and Larden, D.: "Accuracy Obtainable for Universal Time and Polar Motion During the EROLD Campaign," in *Scientific Applications of Lunar Laser Ranging*, J. D. Mulholland, ed., 201–206, D. Reidel, 1977.

Williams, J. G.: "Present Scientific Achievements from Lunar Laser Ranging," in *Scientific Applications of Lunar Laser Ranging*, J. D. Mulholland, ed., D. Reidel, 37–50, 1977.

Williams, J. G., Dicke, R. H., Bender, P. L., Alley, C. O., Carter, W. E., Currie, D. G., Eckhardt, D. H., Faller, J. E., Kaula, W. M., Mulholland, J. D., Plotkin, H. H., Poultney, S. K., Shelus, P. J., Silverberg, E. C., Sinclair, W. S., Slade, M. A., and Wilkinson, D. T.: "New test of the Equivalence Principle from Lunar Laser Ranging," *Phys. Rev. Let.*, **36**, 551–554, 1976.

Williams, J. G., Sinclair, W. S., and Yoder, C. F.: "Tidal Acceleration of the Moon," *Geophys. Res. Let.*, **5**, 943–946, 1978.

Williams, J. G., Dickey, J. O., Melbourne, W. G., and Standish, E. M., Jr.: "Unification of Celestial and Terrestrial Coordinate Systems," *Proceedings of the International Association of Geodesy (IAG) Symposia, International Union of Geodesy and Geophysics (IUGG) XVIIIth General Assembly, Hamburg, FRG, August 15–27, 1983,* Ohio State University, Dept. of Geodetic Science and Surveying, Columbus, Ohio, 43210, Vol. 2., 493–508, 1984.

Yoder, C. F., Sinclair, W. S., and Williams, J. G.: "The Effects of Dissipation in the Moon on the Lunar Physical Librations," *Lunar Science IX*, Houston, 1978.

Yoder, C. F.: "The Free Librations of a Dissipative Moon," *Phil. Trans. R. Soc. Lond. A*, **3303**, 327-338, 1981.

Yoder, C. F., Williams, J. G., and Parke, M. E.: "Tidal Variations of Earth Rotation," *J. Geophys. Res.*, **86**, 881-891, 1981*a*.

Yoder, C. F., Williams, J. G., Parke, M. E., and Dickey, J. O.: "Short Period Tidal Variations of Earth Rotation," *Les Annales de Geophysique*, **37**, 213, 1981*b*.

Yoder, C. F., Williams, J. G., Dickey, J. O., Schutz, B. E., Eanes, R. J., and Tapley, B. D.: "Secular Variation of Earth's Gravitational Harmonic J_2 from LAGEOS and the Nontidal Acceleration of Earth's Rotation," *Nature*, **303**, 5920, 757–762, 1983.

EFFECTS OF INSTRUMENTAL ERRORS ON GEOPHYSICAL RESULTS

P.L. Bender, M.A. Vinvent
Joint Institute for Laboratory Astrophysics
National Bureau of Standards and University of Colorado
Boulder, Colorado 80309, USA

Telephone (303) 492 6952
TWX 910 940 3441

ABSTRACT

A quality assurance program for satellite laser ranging data is a necessary part of trying to assess the effects of systematic instrumental errors on studies of tectonic motions and other geophysical quantities. The present informal program includes accuracy self-checks of individual stations, initial colocations of new systems, some field colocations, and analysis of residuals with respect to global orbits. Intercomparisons with results from other techniques are an essential final check, but the value of the results for each technique is enchanced if reliable confidence intervals can be obtained for each technique by itself.

As part of efforts to evaluate the level of instrumental systematic errors in data being used for tectonic studies, we have started to analyze colocation data in terms of residuals from 5 to 30 day orbits fitted elsewhere to global observations. The first case looked at was the MOB 6/ MOB 7 colocation at Goddard in October, 1982. For eight of the best passes, the rms difference of the smoothed instrumental errors for the two stations was 7.9 cm. This rms difference can be reduced to 3.4 cm by adjusting the horizontal position of MOB 6 by 13 cm, but it seems more likely that the 7.9 cm rms difference was due to the performance of MOB 6. Other colocations for wich residuals from orbits fitted to global observations are available will be analyzed also.

ATMOSPHERIC REFRACTION AND TARGET SPECKLE EFFECTS ON THE ACCURACY OF LASER RANGING SYSTEMS

C.S. Gardner
Department of Electrical and Computer Engineering
University of Illinois
Urbana, IL 61801

Telephone (217) 333 3090
TWX 910 245 2434

J.B. Abshire
NASA / Goddard Space Flight Center
Greenbelt, Maryland 20771

Telephone (301) 344 7000
TWX 710 828 9716

ABSTRACT

Atmospheric refraction and target speckle can affect significatly the accuracy of satellite laser ranging systems. The performance of the atmospheric correction formulas for both single and two color ranging systems is reviewed and the effects of target speckle on timing accuracy are discussed.

Atmospheric Effects

Pulsed laser ranging systems estimate the distance to retroreflector equipped satellites by measuring the roundtrip propagation time. The accuracy of satellite laser ranging systems is limited in part by atmospheric refraction and turbulence. Small random fluctuations in pressure and temperature due to turbulence along the propagation path will cause the path length to fluctuate. The rms path length fluctuations caused by turbulence are related to the turbulence spatial power spectrum and the refractive index structure parameter C_n^2, which varies with altitude and time of day. The mean-square path deviation calculated using the von Karmon spectrum is given by[1]

$$\langle \Delta L^2 \rangle = 3.12\ C_{no}^2\ L_o^{5/3} h_{Tur} / \cos E \qquad (1)$$

where

ΔL = path length deviation

C_{no}^2 = structure parameter value at the ranging site

L_o = outer scale of turbulence

h_{Tur} = atmospheric scale height for turbulence

E = satellite elevation angle.

For satellite ranging, L_o and h_{Tur} are on the order of 100 m and 3 km respectively. Under these conditions, the rms path deviations can be up to a few centimeters when the satellite is at low elevation angles ($\approx 10°$), and the turbulence is very strong ($C_{no}^2 \approx 10^{-13}\ m^{-2/3}$). Under most conditions C_{no}^2 will be much weaker ($< 10^{-15}\ m^{-2/3}$) so that the rms deviations will be a few millimeters or less. Two color ranging systems can partially correct for the random path fluctuations so that in most cases turbulence effects are negligible[1].

Atmospheric refraction increases the optical path length to an orbiting satellite by 2 1/2 m when the satellite is near zenith and by more

than 13 m when the satellite is at 10° elevation. Numerous formulas have been developed which can partially correct range measurements for the effects of atmospheric refraction. However, only the correction formulas derived by Saastamoinen[2], Marini and Murray[3] and Gardner[4] provide centimeter level accuracies at the lower elevation angles (10 - 20°).

Marini and Murray's[3] formula is particularly convenient for correcting satellite ranging data because it only requires measurements of atmospheric pressure, temperature and relative humidity taken at the laser site during the satellite pass. However, their formula was derived by assuming that atmospheric refraction is spherically symmetric. Because this assumption holds only approximately in the troposphere, horizontal refractivity gradients can introduce centimeter level errors into the Marini and Murray formula at low elevation angles. A correction formula that compensates for horizontal gradients was derived by Gardner[4]. The accuracies of both the Marini and Murray and Gardner formulas were evaluated by comparing them with data obtained by ray tracing through refractivity profiles calculated from radiosonde measurements of pressure, temperature and humidity. The results indicate that these correction formulas provide accuracies which vary from a few millimeters when the satellite is near zenith to a few centimeters at 10° elevation.

The range correction for atmospheric refraction can be written in the form

$$AC = SC + GC \quad . \tag{2}$$

The spherical correction term SC corresponds to a spherically symmetric atmosphere, while the gradient correction term GC includes the effects of horizontal refractivity gradients. The correction terms can be expressed as functions of meteorological parameters by evaluating the integral of the group refractivity along the propagation path. The resultant spherical and gradient correction formulas are given by[2-4]

$$SC = \frac{f(\lambda)}{F(\theta,H)} \frac{A + B}{\sin E + \dfrac{B/(A + B)}{\sin E + .01}} \tag{3}$$

$$GC = \frac{C}{\sin E \tan E} \underline{n}\cdot\nabla(P_s T_s K_s) + \frac{D(1 + 1/2 \cos^4 E)}{\sin^3 E \tan E} \underline{n}\cdot\nabla \left(\frac{P_s T_s^2 K_s^2}{2 - K_s} \right) \tag{4}$$

where

$$f(\lambda) = 0.9650 + 0.0164/\lambda^2 + 0.000228/\lambda^4 \tag{5}$$

$$F(\theta,H) = 1 + 0.0026 \cos 2\theta - 0.00031H \tag{6}$$

$$K_s = 1.163 + 0.00968 \cos 2\theta - 0.00104T_s + 0.00001435P_s \quad (7)$$

$$A = 0.002357P_s + 0.000141e_s \quad (8)$$

$$B = (1.084 \times 10^{-8})\, P_s T_s K_s + (4.734 \times 10^{-8}) \cdot (P_s^2/T_s)\, 2/(3 - 1/K_s) \quad (9)$$

$$C = 80.343 f(\lambda) \frac{R^2}{(Mg)^2} 10^{-6} = 6.915 \times 10^{-2} f(\lambda) \quad , \quad (10)$$

$$D = 80.343 f(\lambda) \frac{2}{r_o} \frac{R^3}{(Mg)^3} 10^{-6} = 6.362 \times 10^{-7}\, f(\lambda) \quad , \quad (11)$$

and

e_s = water vapor pressure at ranging site (mb)

P_s = surface pressure at ranging site (mb)

T_s = surface temperature at ranging site (K)

θ = colatitude of ranging site

H = altitude of ranging site above sea level (km)

M = 28.966 = molecular weight of dry air

R = 8314.36 J $(K)^{-1}$ $(kg\text{-}mole)^{-1}$ = universal gas constant

g = 9.784 m/sec^2 = acceleration of gravity

r_o = 6378 km = nominal earth radius

$\underline{n} = \sin \alpha \underline{x} + \cos \alpha \underline{y}$,

α = satellite azimuth angle (α = 0 = North), and

$\underline{x}$ and $\underline{y}$ are the east and north unit vectors.

Both SC and GC are given in meters when the listed values for A, B, C and D are used and the gradients are in units of m^{-1}.

The accuracy of the spherical correction formula has been extensively checked by Marini and Murray[3] by ray tracing through atmospheric refractivity profiles which were calculated from radiosonde data. The radiosonde data, which consist of pressure, temperature and humidity measurements taken at various altitudes during the balloon's ascent, were used to construct spherically symmetric refractivity profiles above the

balloon's release point. The ray trace corrections and formula showed very good agreement even at low elevation angles. Table I summarizes Marini and Murray's results for comparisons with 634 different ray traces through refractivity profiles generated from radiosonde observations taken near Dulles Airport, VA during 1967. The formula for SC is nearly an unbiased estimator of the spherically symmetric ray trace correction, RT_1.

The standard deviation of the difference between SC and RT_1 arises from two factors: modeling errors in the formula for SC and errors in the measured values of atmospheric pressure, temperature and humidity which are used to calculate SC. The dominant error source is pressure. A 1 mb pressure error introduces approximately 14 mm error in SC at 10° elevation. The effects of measurement errors can be estimated by taking the partial derivatives of SC with respect to the meteorological parameters.

TABLE I

Range error calculated by Marini and Murray[3] for a ruby laser (λ = 694 nm). RT_1 is the ray trace correction for spherically symmetric profiles.

Elevation angle	RT_1 Mean (m)	RT_1 − SC Mean (cm)	RT_1 − SC Standard deviation (cm)
80°	2.47	0.07	0.04
40°	3.69	-0.1	0.07
20°	6.91	-0.05	0.12
15°	9.08	0.05	0.19
10°	13.32	-0.08	0.49

parameters. Since the measurements of pressure, temperature and relative humidity (Rh) are statistically independent, the total rms error in SC is given by

$$\sigma_{SC} = \left[\left(\frac{\partial SC}{\partial P}\,\sigma_P\right)^2 + \left(\frac{\partial SC}{\partial T}\,\sigma_T\right)^2 + \left(\frac{\partial SC}{\partial RH}\,\sigma_{Rh}\right)^2\right]^{1/2} \tag{12}$$

where

$$\frac{\partial SC}{\partial P} \simeq \frac{f(\lambda)}{F(\theta,H)}\,\frac{2.357 \times 10^{-3}}{\sin E}\ (\mathrm{m/mb}) \tag{13}$$

$$\frac{\partial SC}{\partial T} \simeq \frac{f(\lambda)\ 1.084 \times 10^{-8}\ P_s K_s}{\sin^3 E}\ (\mathrm{m/°K}) \tag{14}$$

$$\frac{\partial SC}{\partial Rh} \simeq \frac{f(\lambda)}{F(\theta,H)} \frac{8.615 \times 10^6}{\sin E} \exp\left[\frac{17.27(T_s - 273.15)}{237.15 + (T_s - 273.15)}\right] \quad (m/\%) \qquad (15)$$

and σ_p, σ_T and σ_{Rh} denote respectively the rms errors in pressure, temperature and relative humidity. The derivatives are plotted versus elevation angle in Fig. 1. Typical measurement errors are 0.5 - 1 mb for pressure, 0.7 - 1.5 °K for temperature and 5 - 10% for relative humidity. Consequently, above 10° elevation angle, pressure errors are the dominant source of error in SC.

The gradient correction is a function of the horizontal pressure and temperature gradients and is significant only at the lower elevation angles. GC is a sinusoidal function of azimuth with a peak-to-peak value of 4 - 6 cm at 10° elevation and 1 - 1.5 cm at 20° elevation. Because surface pressure is relatively uniform, under normal conditions horizontal refractivity gradients will be predominantly a function of the temperature gradients. At a 20° elevation angle, the sea level gradient correction is approximately 1 cm peak-to-peak for a horizontal temperature gradient of 1°C/100 km. The gradient correction is more difficult to calculate than SC because the formula requires measurements of the horizontal pressure and temperature gradients at the ranging site. The horizontal gradients can be determined only by measuring pressure and temperature at three or more points surrounding the ranging site. The measurements are used to calculate the parameters of an appropriate model for the horizontal variations of P_s and T_s.

The accuracy of the GC formula was also evaluated by comparing it with ray trace corrections[5]. The results for 10° elevation are illustrated in Fig. 2. RT_3 is the correction obtained by ray tracing through a 3-D refractivity profile calculated from data obtained by radiosondes released almost simultaneously from eight locations near Leonardtown, MD during January and February 1970. RT_1 is the ray trace correction for the equivalent spherically symmetric refractivity profile. The gradient effects ($RT_3 - RT_1$) vary sinusoidally with azimuth and are predicted reasonably well by GC. The comparisons at 10°, 20°, 40° and 80° elevation are summarized in Table II. The amplitudes of the gradient correction predicted by the GC formula are within a few percent of the ray trace values ($RT_3 - RT_1$). However, the phase differs by 11°. The average ray trace correction peaks at 0° azimuth while GC peaks at 11° azimuth. Refractivity gradients have their greatest influence at the higher altitudes, where the laser beam trajectory is relatively far down range from the laser site. The correction formula attempts to predict the effects of these high altitude gradients from surface measurements of pressure and temperature. Terrain features such as mountains, large bodies of water, and ground cover probably have a greater influence on the weather near the ground than at the higher altitudes. Consequently, local geography could introduce amplitude and phase biases into the gradient correction formula.

The major error source in the gradient correction formula appears to be errors in the measured values of pressure and temperature, which are used to calculate GC, and terrain features, which distort the temperature and pressure fields near the ranging site. Both of these problems can be minimized by using many weather stations to obtain the

TABLE II

Gradient correction and ray trace comparison;
Model: $-A \cos(\alpha - \phi)$

Elevation Angle	$\overline{RT_3 - RT_1}$		$\overline{GC}$		$\overline{(RT_3 - RT_1) - GC}$	
E	A	ϕ	A	ϕ	A	ϕ
10°	2.4 cm	0°	2.2 cm	11°	0.49 cm	-66°
20°	6.5 cm	0°	6.3 mm	11°	1.2 mm	-73°
40°	1.5 mm	0°	1.5 mm	11°	0.29 mm	-75°
80°	0.15 mm	5°	0.14 mm	11°	0.041 mm	-78°

required meteorological data and distributing them over a large area. This approach has the added advantage of also improving the accuracy of spherical correction. However, there have been studies indicating the presence of relatively large temperature variations occurring over short spatial scales ($\simeq$ 10 km) which may significantly distort the calculated value of GC[6,7]. As a consequence, care must be exercised in computing the required pressure and temperature gradients. This problem becomes even more difficult in mountainous terrain where the surrounding weather stations may be at widely differing altitudes.

Two-Color Laser Ranging

Two-color laser ranging provides a very attractive alternative for determining the atmospheric correction. The difference in path length at two laser frequencies is a measure of the refractive conditions existing over the propagation path at the instant the measurements are taken and can be used to estimate the atmospheric correction[8]. Let L_1 and L_2 denote the optical path lengths measured at wavelengths λ_1 and λ_2 respectively. Let n_{g1} and n_{g2} denote the group refractive indices of air at the ranging site for wavelengths λ_1 and λ_2 respectively. Then the atmospheric correction at wavelength λ_1 is approximately

$$AC = \gamma(L_2 - L_1) \tag{16}$$

where

$$\gamma = (n_{g1} - 1)/(n_{g2} - n_{g1}) \quad . \tag{17}$$

Equation (16) is accurate at optical frequencies. However, at radio and millimeter wavelengths the water vapor content of air can introduce substantial errors into Eq. (17). If we ignore the small water vapor effects at optical frequencies, γ can be written as

$$\gamma = f(\lambda_1)/[f(\lambda_2) - f(\lambda_1)] \tag{18}$$

Because γ is on the order of ten for all wavelength pairs of the fundamental, doubled and tripled YAG laser frequencies, it is necessary to determine the differential path length $(L_2 - L_1)$ with an accuracy which is approximately ten times greater than the desired accuracy for the atmospheric correction.

The accuracy requirements on the differential path length measurement can be eased considerably if the results of numerous measurements are averaged. Since the atmospheric correction and differential path length are functions of the satellite azimuth and elevation angles, the satellite position must be taken into account when measurements are averaged. For typical refractivity profiles, the atmospheric correction given by Eqs. (2), (3) and (4) can be modeled approximately as

$$AC = \frac{\beta_1}{\sin E} + \frac{\beta_2}{\sin^3 E} + \frac{\beta_3 \cos\gamma}{\sin E \tan E} + \frac{\beta_4 \sin\gamma}{\sin E \tan E} \tag{19}$$

The model coefficients $\beta_1 - \beta_4$ can be expressed in terms of meteorological parameters using Eqs. (3) and (4). Alternatively, they can be calculated by using Eqs. (16) to compute AC from measurements of L_1 and L_2 taken during the satellite pass and using a regression analysis to fit the data to a curve of the form given by Eq. (19). A more accurate value of AC could then be obtained by evaluating the regression curve.

The performance of the regression model given by Eq. (19) has been evaluated using the parameters of Starlette Satellite passes over the Goddard Space Flight Center in Greenbelt, MD[9]. The rms error of the regression model can be written as

$$\sigma_{AC} = \frac{\gamma \sigma_{\Delta L}}{N^{1/2}} F \tag{20}$$

where $\sigma_{\Delta L}$ is the rms differential path length error at zenith, N is the number of two-color measurements made during the satellite pass and F is a dimensionless error factor which depends on azimuth and elevation angle and on the satellite pass. σ_{AC} is proportional to $N^{-1/2}$. This dependence is typical of the error reduction obtained when independent measurements are averaged. If N is large and F is small, the regression error σ_{AC} will be much smaller than the single measurement error $\gamma\sigma_{\Delta L}$.

The azimuth and elevation angle of the Starlette Satellite is plotted versus time in Fig. 3 for a typical low elevation angle pass over Greenbelt, MD. The satellite rises in the NE, reaches a maximum elevation angle of 24° and then sets in the SE. Figure 4 is a plot of the error factor F versus time for this pass. Measurements were assumed to be taken only when the satellite was above 15° elevation. At low elevation angles

the laser pulses will be attenuated more than at zenith because of the increased atmospheric extinction. This effect was taken into account in calculating the data plotted in Fig. 4 by assuming that the differential path length error was proportional to $1/(\sin E)^{\nu}$. ν was chosen so that the path length error at 20° was 1, 2, 5 and 10 times larger than the error at zenith.

The error factor is largest at the beginning and end of the pass where the satellite is at the lower elevation angles. The reason for this behavior is evident from Eq. (19). The effects of errors in the regression coefficients become more pronounced as the elevation angle decreases, particularly for errors in β_2, β_3 and β_4. Also, the error factor increases when the path length error is more severe at the lower elevation angles. However, the error factor is usually less than 10 so that if N is large, the regression model will provide a much more accurate estimate of AC than a single two-color measurement. The high elevation angle Starlette Satellite passes provide similar results[9]. Therefore, it is not unreasonable to expect a factor of 10 or more improvement in the accuracy of AC by using the regression model.

Ranging Accuracy and Laser Speckle

Mode locking and Q-switching techniques are now used routinely to generate laser pulses of a few picoseconds in duration. These short pulses can provide higher accuracies in laser ranging and altimetry. However, when the range spread of the target is larger than the transmitted pulse length, speckle can cause random small scale fluctuations within the reflected pulse which distort its shape. This effect is called time-resolved speckle and can introduce errors in laser ranging measurements.[10]

Estimation of the arrival times of laser pulses was first studied by Bar-David[11] who derived the Maximum Likelihood (ML) estimator for pulses contaminated by shot noise

$$\hat{\tau}_{SHOT} = \arg \max_{\tau} \sum_{i=1}^{n} k_i \ln \overline{k}_i(\tau) \qquad (21)$$

where

k_i = received photocount in the i^{th} time bin and

$\overline{k}_i$ = expected photocount.

The ML estimator is implemented by correlating the received pulse shape (k_i) with the logarithm of the expected pulse shape ($\overline{k}_i$). The ML estimate τ_{SHOT} is the time (τ) at which the correlation is maximum. If the expected received pulse shape is Gaussian with an RMS length of σ_R and the speckle is fully developed, the variance of the ML estimator is

$$c^2 \operatorname{Var}(\hat{\tau}_{SHOT}) = \left(\frac{1}{\langle M \rangle} + \frac{1}{K_s} \right) \sigma_R^2 \qquad (22)$$

where

$\langle M \rangle$ = expected received photocount/pulse

K_s = speckle signal-to-noise ratio.

K_s is related to the target geometry and the laser cross-section and has a minimum value of 1. In general, K_s is small ($\sim$ 1) whenever the target is small. The RMS ranging error using the ML estimator is plotted versus photocount ($\langle M \rangle$) in Fig. 5 for the case of an infinitely large flat diffuse target. Results are plotted for laser incidence angles of 5, 10 and 20°. Initially, in the shot noise dominated regime, the ranging error decreases ($\sim \langle M \rangle^{-1/2}$) as the photocount increases. But the error then reaches a limiting value in the speckle noise dominated regime. Similar results would be expected for partially developed speckle of the type generated by reflections from retro-reflector arrays used in satellite ranging. Most laser ranging receivers use constant fraction discriminator (CFD) timers. The timing error for the CFD is larger than the error for the ML estimator. As a consequence, speckle establishes a fundamental limit in ranging accuracy and its effects should be considered when using short pulse lasers.

References

1. C. S. Gardner, "Effects of random path fluctuations on the accuracy of laser ranging systems," Applied Optics, 15, 2539-2545, Oct. 1976.

2. J. Saastamoinen, "Introduction to practical computation of astronomical refraction," Bull. Geod., 107, 383-397, 1972.

3. J. W. Marini and C. W. Murray, Jr., "Correction of laser range tracking data for atmospheric refraction at elevation angles above 10 degrees," NASA Tech. Rep., X-591-73-351, Goddard Space Flight Center, Greenbelt, MD, 1973.

4. C. S. Gardner, "Correction of laser tracking data for the effects of horizontal refractivity gradients," Applied Optics, 16, 2427-2432, Sept. 1977.

5. C. S. Gardner, J. R. Rowlett and B. E. Hendrickson, "Ray tracing evaluation of a technique for correcting the refraction errors in satellite tracking data," Applied Optics, 17, 3143-3145, Oct. 1, 1978.

6. B. P. Gibbs and V. Majer, "Accuracy assessment of the atmospheric correction used in the NASA laser ranging program," Business & Techn. Sys. Tech. Rep., BTS-FR-81-166, Seabrook, MD (Sept. 1981).

7. P. Dunn, W. Pearce, K. Borman, "The effects of atmospheric refraction in laser ranging measurements," Proceeding, General Meeting of the International Assoc. Geodesy, May 7-15, 1982, Tokyo.

8. P. L. Bender and J. L. Owens, J. Geophys. Res., 70, 2461 (1965).

9. C. S. Gardner and R. A. Axford, Jr., "Regression models for multicolor satellite laser ranging," Radio Research Lab Tech. Rep. 505, University of Illinois (Urbana), March 1980.

10. B. M. Tsai and C. S. Gardner, "Theoretical and experimental analysis of laser altimeters for barometric measurements over the ocean," Radio Research Lab. Tech. Rep. 527, University of Illinois (Urbana), March 1984.

11. I. Bar-David, "Communication under the Poisson regime," IEEE Trans. Inform. Theory, IT-15, 31 (1969).

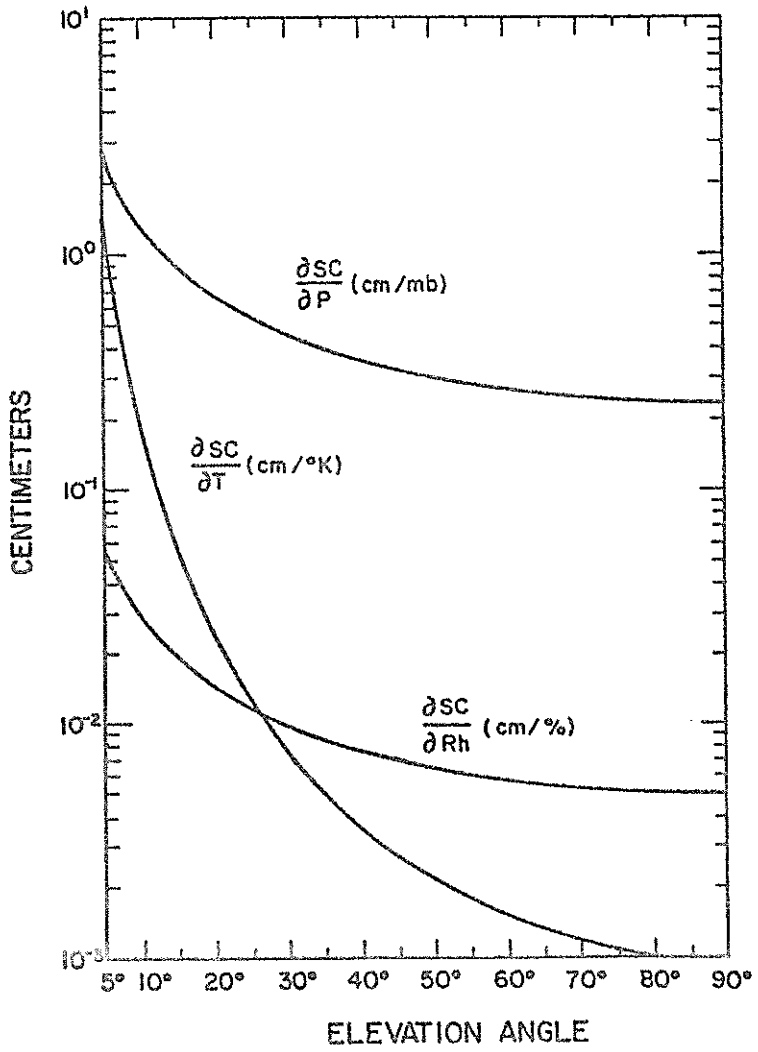

Figure 1. Variation of the spherical correction formula (Equation (3)) with respect to pressure, temperature and relative humidity.

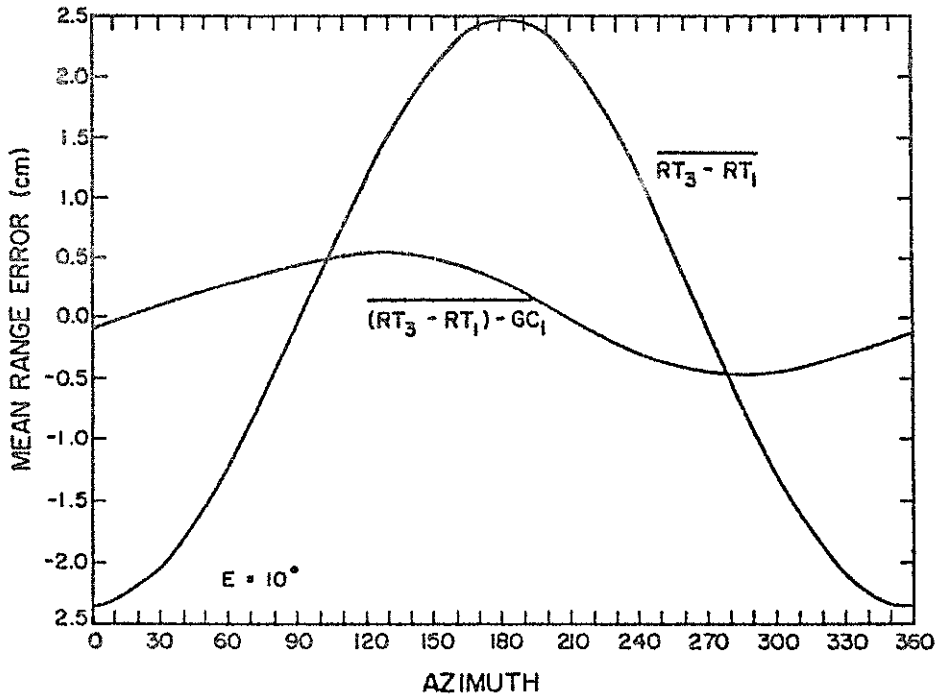

Figure 2. Mean of the uncorrected ($RT_3 - RT_1$) and corrected ($RT_3 - RT_1 - GC_1$) gradient error versus azimuth. The elevation angle is 10°.

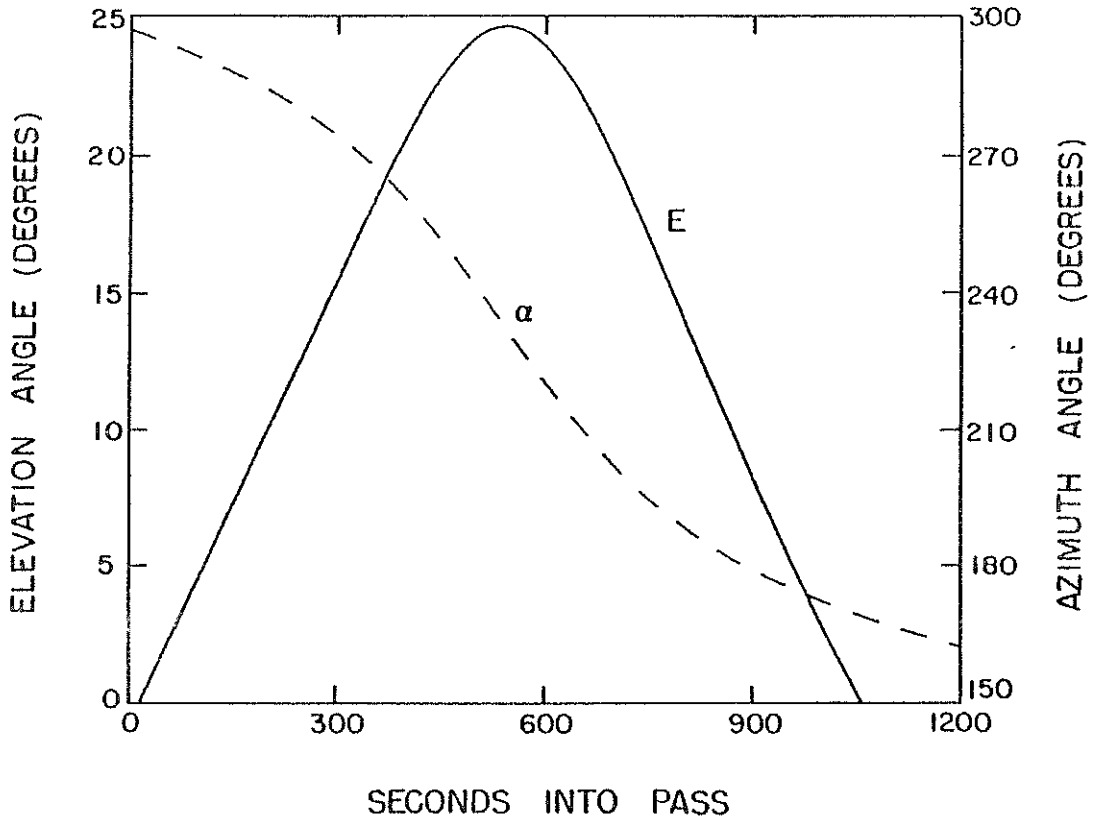

Figure 3. Azimuth and elevation angle of the Starlette Satellite as seen from the Goddard Space Flight Center in Greenbelt, MD on July 5, 1979. Zero seconds into the pass is 03:47 GMT.

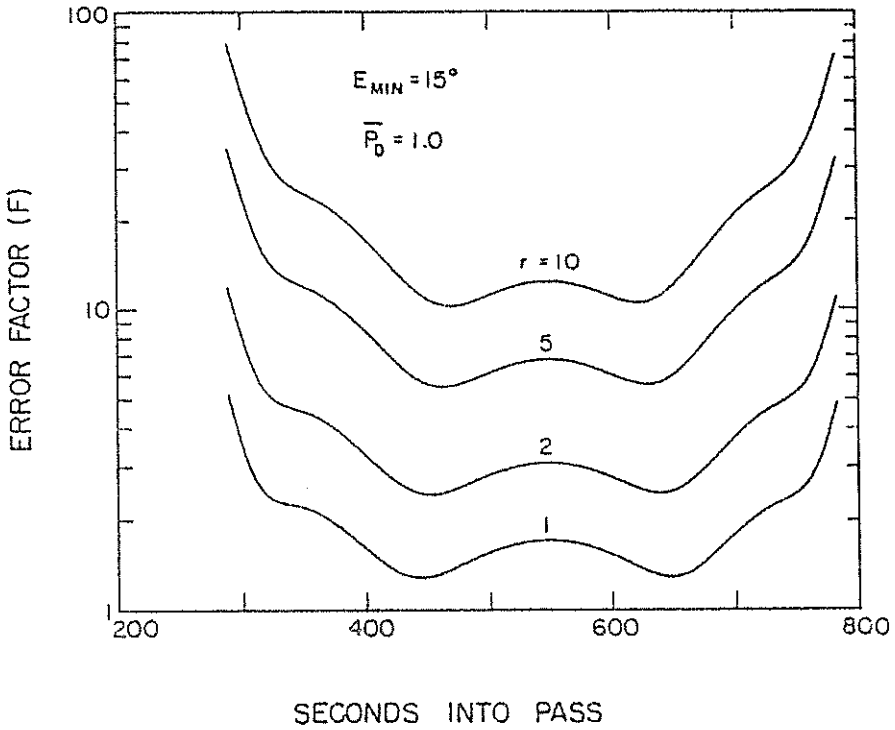

Figure 4. Error factor for the atmospheric correction model of Eq. (19) and the low elevation angle Starlette pass plotted in Figure 1. The detection probability is one and the minimum elevation angle is 15°. r is the ratio of the differential pathlength error at 20° elevation to the error at zenith.

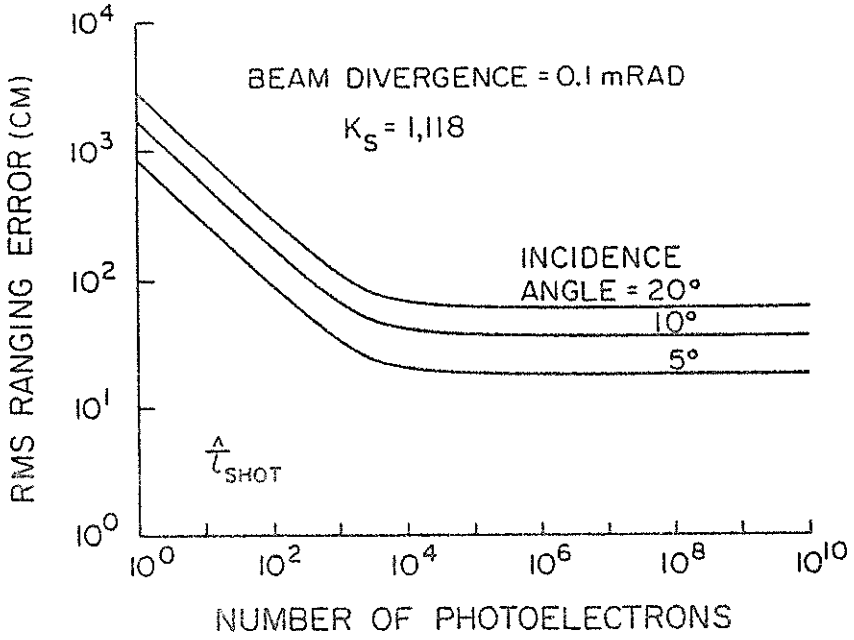

Figure 5. RMS ranging error using $\hat{\tau}_{SHOT}$ for non-normal incidence on an infinite flat diffuse target. (Target distance = 500 km, Transmitted pulse length = 0.5 cm, Receiver area = 100 cm^2, λ = 1 μm)

SOME MODELLING REQUIREMENTS FOR PRECISE LAGEOS ORBIT ANALYSIS

P.J. Dunn, EG. G. Wasc
6801 Kenilworth Avenue,
Riverdale, Maryland 20737

Telephone (301) 779 2800
Telex 590613

D. Christodoulidis, E.D. Smith,
Geodynamics Branch
NASA / Goddard Space Flight Center,
Greenbelt, Maryland 20771

Telephone (301) 344 7000
TWX 710 828 9716

ABSTRACT

The potential accuracy of LAGEOS observations from the worldwide laser network can only be realized if relatively subtle effects in the station and satellite force model are considered. In this report, the effects on station position predicted by recent models for the Earth and ocean tides are described. The perturbations on the LAGEOS orbit due to tidal effects must also be modelled as well as along-track variations which have been ascribed to the effect of charged particle drag.

SOME MODELLING REQUIREMENTS FOR PRECISE LAGEOS ORBIT ANALYSIS

In order to use the capability of LAGEOS observations to monitor crustal deformation and tectonic plate motion at the centimeter level, tidal influences on the tracking stations must be modelled to a similar level of precision. The tidal model adopted for the MERIT Project (USNO, 1983) includes the solid earth response due to Wahr (1981). Wahr considers an elliptical, rotating, elastic and oceanless earth, and this model yields station motion which differs from the decimeter variation predicted by Love's simpler spherically symmetric model at the K_1 tidal frequency. The differential effect amounts to about one centimeter in the radial direction and is a maximum at 45° latitude. A thorough mathematical treatment is given in the MERIT Standards document (op. cit.) which also alerts the user of laser observations to the need for a consistent treatment of a zero frequency station displacement which may be included in nominal station coordinates.

The ocean tidal model currently adopted for LAGEOS analysis is that due to Schwiderski (1980). Goad (1980) has developed a technique using integrated Green's functions which defines tidal loading height displacement amplitude and phase values for important laser sites. The vertical displacement can amount to several centimeters at coastal locations and should be included in a precise station position analysis.

The ocean tidal model is however more critical in its long period effect on the orbital behaviour of LAGEOS. Eanes et al. (1981) have shown that effective modelling of the

ocean tides can improve our determination of the inclination and node of the orbit at the meter level. The period of these effects ranges from 14 days (M2) to 1050 days (K1) and influence the definition of the inertial reference system as well as the resolution of earth rotation rate. The much larger effects on the orbit due to the solid earth tides (see, for example, Smith and Dunn, 1980) can be accommodated with more certainty that the ocean tidal perturbations, which will require refinement from analyses of LAGEOS and other laser satellite observations.

A very long period effect has also been observed in the nodal evolution of the LAGEOS orbit by Yoder et al. (1983). It has been ascribed to the viscous rebound of the solid Earth from the decrease in load due to the last glaciation, and appears as an apparent secular decrease of the second zonal harmonic. This subtle perturbation is unlikely to warrant inclusion in most geodynamic studies.

A much larger secular variation has been observed in the along-track component of the orbit (Smith, 1983). Rubincam (1982) concluded that charged particle drag could account for the effect, but Anselmo et al. (1983) have suggested that the Earth's albedo could also contribute significant periodic terms. An empirical model for the along-track variation must be used to accommodate the effect in orbital analyses based on continuous orbits of more than a few days. Data reduced in shorter arc lengths allow the perturbation to be absorbed into an estimate of the orbital semi-major axis, and the size of the orbit must be continuously monitored to provide a measure of the variation.

E M P T Y P A G E

References

USNO Circular No. 167, "Project Merit Standards," December 27, 1983.

Wahr, J.M., "Body Tides on an Elliptical, Rotating, Elastic and Oceanless Earth," Geophys. J. Roy. Astr. Soc., 64, 677-703, 1981.

Schwiderski, E.W., "On Charting Global Ocean Tides," Reviews of Geophysics and Space Physics, Vol. 18, No. 1, 243-268, 1980.

Goad, C.C., "Gravimetric Tidal Loading Computed from Integrated Green's Functions," J. Geophys. Res., 85, 1679-2683, May 10, 1980.

Eanes, R., B. Schutz and B. Tapley, "Earth and Ocean Tide Effects on Lageos and Starlette," Proc. 9th Int. Symp. on Earth Tides, (ed., Kuo. J.T.) E. Schweit. Verlags. (in press).

Smith, D.E. and P.J. Dunn, "Long Term Evolution of the Lageos Orbit," Geophys. Res. Letters, Vol. 7, No. 6, 437-440, June 1980.

Yoder, C.F., J.G. Williams, J.O. Dickey, B.E. Schutz, R.J. Eanes and B.D. Tapley, "Secular Variation of Earth's Gravitational Harmonic J_2 Coefficient from Lageos and Nontidal Acceleration of Earth Rotation," Nature, Vol. 303, No. 5920, 757-762, June 30, 1983.

Smith, D.E., "Acceleration on Lageos Spacecraft," Nature, Vol. 304, p. 15, July 7, 1983.

Anselmo, L., P. Farinella, A. Milani and A.M. Nobili, "Effects of Earth-Reflected Sunlight on the Orbit of the Lageos Satellite," Astr. Astrophys., Vol. 117, No. 3, 1983.

ESTABLISHING GROUND TIES WITH MTLRS
PERFORMANCE AND RESULTS

E. Vermaat
Delft University of Technology
Observatory for Satellite Geodesy
P.O. Box 581
NL - 7300 AN APELDOORN The Netherlands

Telephone 057 69 341
Telex 36442

ABSTRACT

The method employed to position the Modular Transportable Laser Ranging System (MTLRS) with respect to ground markers has been optimized to produce ground ties with optimal precision and reliability.

This paper describes the practical application of this method and summarizes numerical results obtained during the testing phase of MTLRS1 at the Kootwijk Observatory in the period April-July 1984

1. Introduction

Laser ranging to satellites utilising mobile ranging equipment requires the realisation of a geometric connection between an operationally well defined reference point S in the ranging system and an equally well defined reference point P for the site (figure 1).

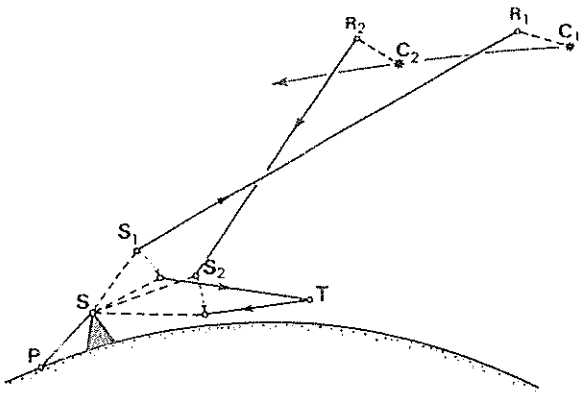

figure 1. Earth-fixed geometry of laser ranging to satellite C and to calibration target T. The observed ranges are referred to the instrumental center S. Coordinate solutions must be referred to marker P in case of mobile satellite laser ranging.

Once this connection has been established, the latter point serves as the terminal point of the baseline which can be solved for in the data reduction of the observed satellite ranges. If this geometric tie is not available or erroneous it will be impossible to relate baseline solutions from different site occupations, since a proper common reference for the baseline terminal points does not exist. Therefore a scrupulous approach to the determination of this geometric connection is a necessity.

For the Modular Transportable Laser Ranging System (MTLRS) a special positioning device has been constructed which can be attached to the front end of the telescope tube and with which markers in the immediate vicinity of the telescope mount can be observed in 3 dimensions. The method of data reduction employed to obtain the ground tie, has been designed to minimise the influence of undetected errors in the observations i.e. to maximise the reliability of this determination.

In the period of April-July 1984 MTLRS1* has been stationed at the Kootwijk Observatory for final testing and performance validation. Also the positioning method has been tested in this period and the results clearly indicate the excellent precision and

* The first one of two identical systems to be constructed

reliability of the obtained ground tie, in spite of the remarkable simplicity of the observational technique. Essential to the approach is the use of a number of markers more or less symmetrically arranged around the telescope mount.

2. The Technique

2.1 The positioning device

The positioning device (figure 2) comprises a standard He-Ne laser together with a simple 3 meter spring-rule, housed in a framework which can be firmly attached to the front end of the telescope tube. The He-Ne laserbeam points downward and passes through a prism which allows for small corrections to the direction of the beam. The tape of the spring-rule, once pulled out (figure 3) will be immediately adjacent to the laserbeam and thus directions and slant range can be observed simultaneously.

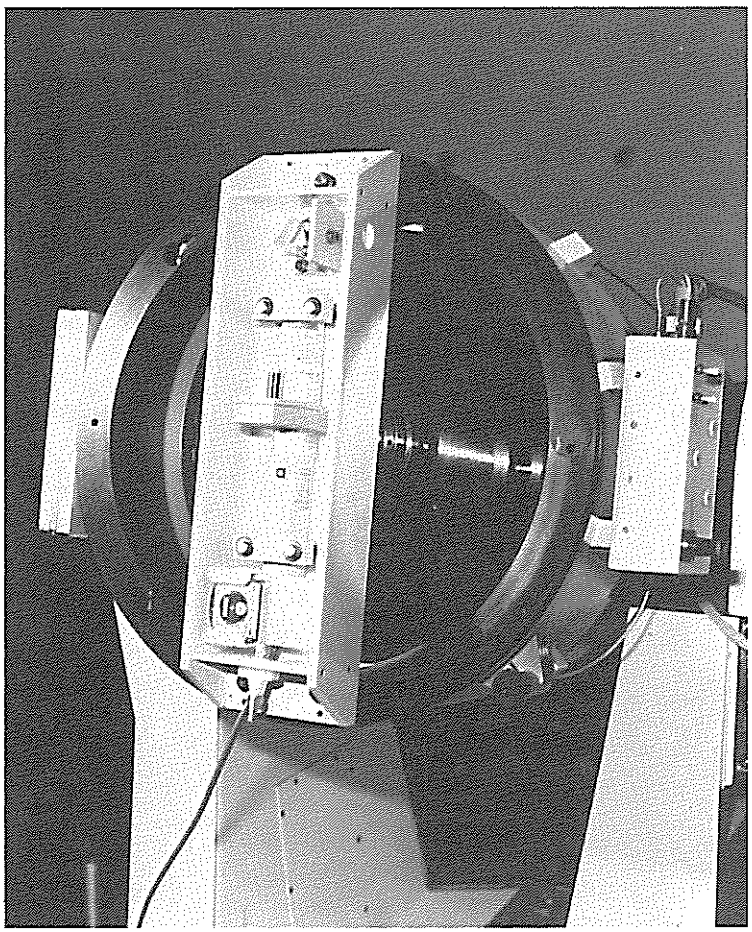

Figure 2 The positioning device attached to the front end of the telescope of MTLRS. The device is made up of a He-Ne laser for pointing at the marker and of a spring rule for ranging to the marker.

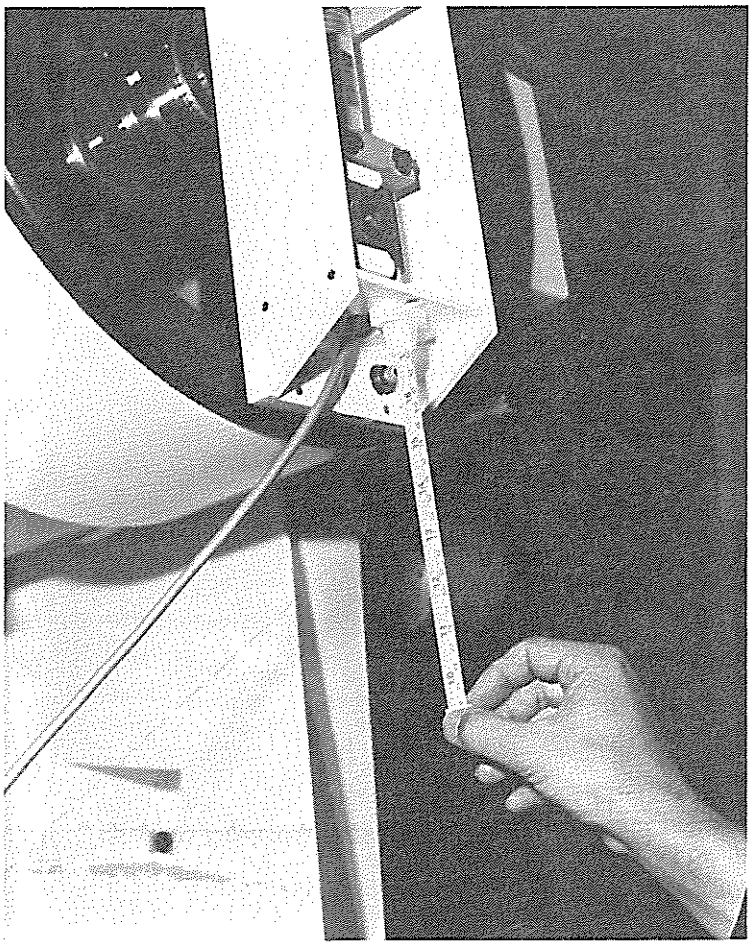

Figure 3 Close-up of the spring rule device.

During installation of MTLRS at a site, the mutual orthogonality of the telescope axis, the azimuth- and elevation axis will be checked and the index error of the elevation circle will be eliminated utilising standard techniques, involving stars and other remote targets. Subsequently, after attaching the positioning device to the front end of the telescope tube the He-Ne laserbeam will be adjusted to be orthogonal to the telescope axis and parallel to the azimuth axis, employing a simple auto-collimation technique illustrated in figure 4. Salad oil turned out to be a liquid that excellently reflects the laser beam. After this calibration procedure accurate directions can be obtained by simply pointing the He-Ne laserbeam at markers utilising the mount positioning system. The slant ranges can be obtained by pulling out the tape and reading the tape at a mark in the positioning device.

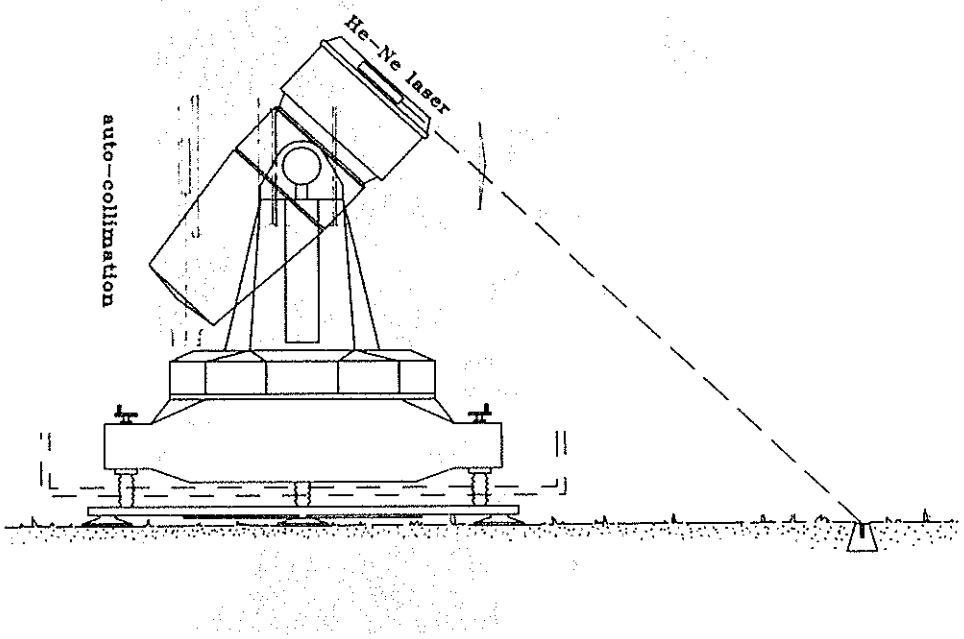

figure 4. Observing a marker utilising the positioning device. Prior to the observations the laser beam is properly adjusted, employing a simple technique of auto-collimation.

2.2 The markers

The markers must be designed to allow for precise pointing with the He-Ne laser beam and for observing the slant range with the spring rule. An engraved circle of about 9 mm diameter turned out to be optimal for centering the oval shaped reflection of the laser beam at a distance of 2 to 3 meters. A central pinhole in the circle defines the actual point of reference and facilitates the taking of the slant range.

The bronze marker must have a slightly curved topsurface to enable precise 3-dimensional surveying. These markers must be carefully installed at the site, firmly attached to the subsurface soil and properly isolated from surface soil or site pad. (figure 5). Installation in vertical constructions like a stable wall or the side of a pier is also possible. The topsurface of the marker should then preferably be tilted to have a similar angle of incidence of the laserbeam as for ground based markers (figure 6).

Especially if more than one marker is available at a site, a clearly readable letter or other character must be engraved in each marker for reliable identification.

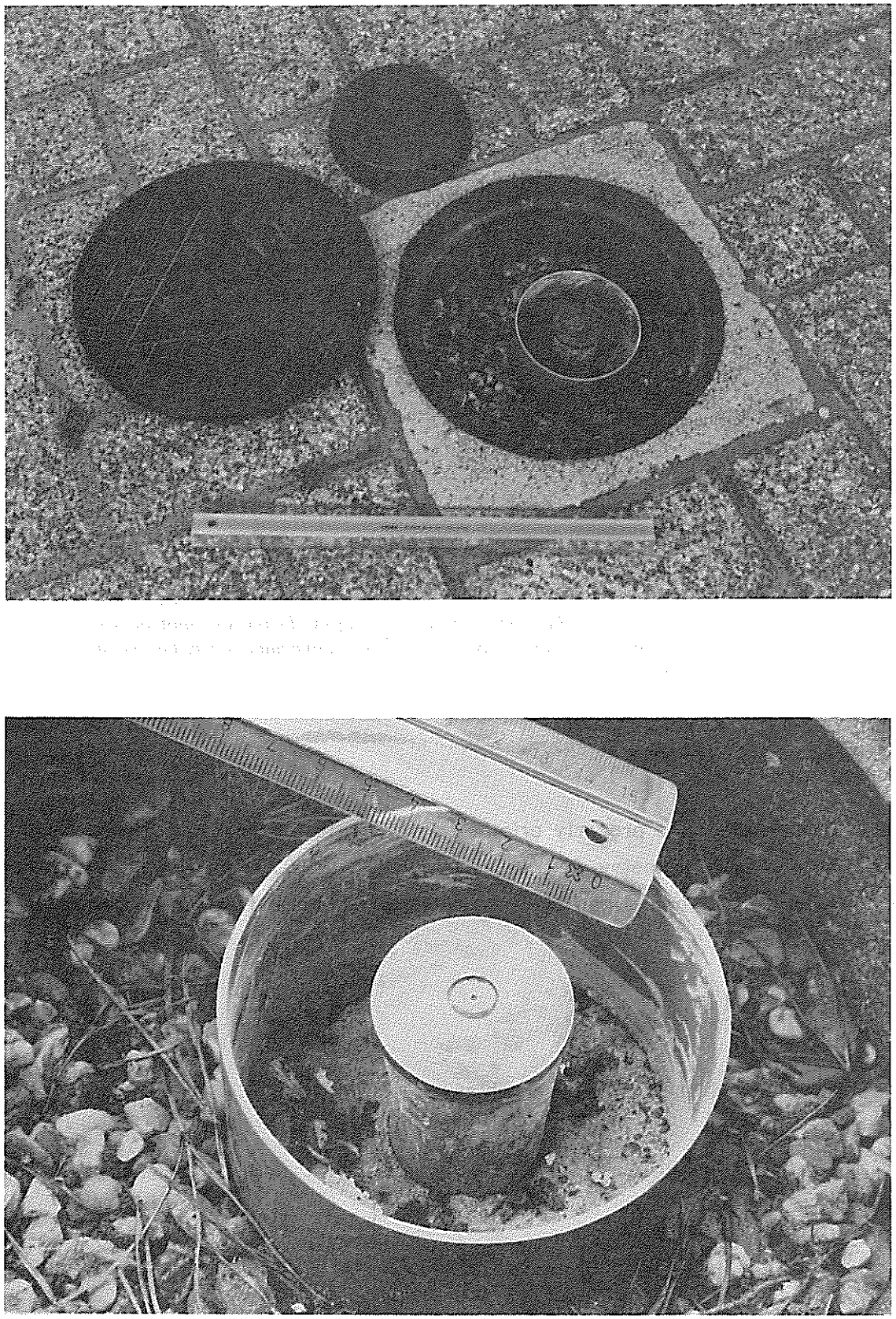

Figure 5 The markers must be properly isolated from the surfac soil or side pad.

Figure 6 A marker attached to a vertical wall. An engraved circle of 9 mm diameter facilitates pointing the laser beam. The pinhole materializes the actual reference point.

2.3 The redundant approach

If the telescope mount is properly oriented in azimuth, the required ground tie can be deduced from simple geometry. If the vector $\mathbf{SP}_i$ in figure 7 is expressed in components on the reference system defined by the telescope mount and scaled by the spring rule (the S-system) as:

$$\mathbf{SP}_i = ({}^{s}X_i^1, {}^{s}X_i^2, {}^{s}X_i^3) \tag{2.1}$$

this vector can be related to the observables as:

$$\left.\begin{aligned} E_i &= \tfrac{1}{2}\pi - \operatorname{atan}\left(\frac{{}^{s}\lambda_o a}{R_i}\right) - \operatorname{atan}\frac{C\,S}{C\,P_i} \\ A_i &= \operatorname{atan}\left(\frac{{}^{s}X_i^2}{{}^{s}X_i^1}\right) \\ R_i &= (S\,P_i^2 - ({}^{s}\lambda_o a)^2)^{\frac{1}{2}} \end{aligned}\right\} \tag{2.2}$$

where $C\,S = X_i^{s3}$

$$C\,P_i = ((X_i^{s1})^2 + (X_i^{s2})^2)^{\frac{1}{2}}$$

$$S\,P_i = ((X_i^{s1})^2 + (X_i^{s2})^2 + (X_i^{s3})^2)^{\frac{1}{2}}$$

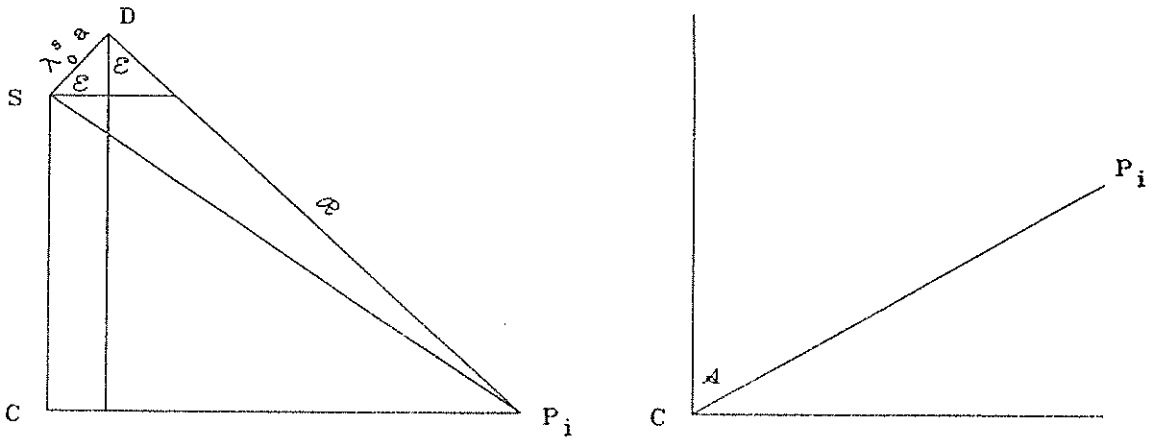

figure 7. The geometry of observing elevation, azimuth and range to a marker P_i. The observations determine the vector SP_i in the instrumental reference system S.

in which the distance $\lambda_o^s a$ is a calibrated instrumental constant. If only one marker is observed, these observations would be sufficient to uniquely define the ground tie vector. However, there would be no way of checking the occurrence of errors in pointing, reading or recording. Realizing the vital importance of a proper ground tie for relating baselines obtained from different site occupations, it would be extremely hazardous to suffice with observations to only one marker. Moreover, in view of the relative low cost of installing several markers at a site and the ease of observing them, it must at least be considered careless not to adopt a redundant approach to the ground tie problem.

The method employed for MTLRS not only requires redundancy, but also seeks optimal reliability in the ground tie vector. (Vermaat and Van Gelder, 1983) studies the effect of number and distribution of markers on the precision and reliability of this determination. This study reveals that a minimum of four or five markers, more or less symmetrically arranged about the site center is an optimum. It is required that from a previous, precise survey, relative positions of the markers are available in a cartesian and right-handed, but otherwise arbitrary coordinate system (0-system).

The software installed in MTLRS then solves for a seven parameter similarity transformation between the instrumentally defined S-system in which the observations are taken and the O-system in which the marker coordinates are given (figure 8):

$$X_i^S = \lambda_O^S (R_O^S)(X_i^O - X_S^O) \qquad (2.3)$$

where X_i^S is the observed position vector of marker i in the S-system

X_i^O is the vector of given coordinates of marker i in the O-system

λ_O^S is the ratio of scale factors of O- and S-system

(R_O^S) is the 3-dimensional rotation from O- to S-system i.e.

$$(R_O^S) = R_1(\gamma)\, R_2(\beta)\, R_3(\alpha)$$

X_S^O is the position vector of point S in the O-system.

In the satellite range data reduction a baseline will be solved for, terminating at point S, the center of the S-system. This baseline must be corrected for the eccentricity vector X_O^S to obtain the baseline terminating in point O. (figure 8). This vector can be obtained from the transformation parameters solved for:

$$X_O^S = \lambda_O^S (R_O^S)(-X_S^O) \qquad (2.4)$$

It is recommendable to maintain the length scale as implied in the marker coordinates in the O-system, instead of the scale of the S-system being determined by a bending and temperature dependent spring rule, thus:

$$X_O^{S'} = (R_O^S)(-X_S^O) \qquad (2.5)$$

This correction can be best applied in a global reference system, requiring astronomical latitude (Φ) and longitude Λ, so the baseline correction can be obtained from:

$$X_O^g = R_3(-\Lambda)\, R_2(90^o + \Phi)(R_O^S)(-X_S^O) \qquad (2.6)$$

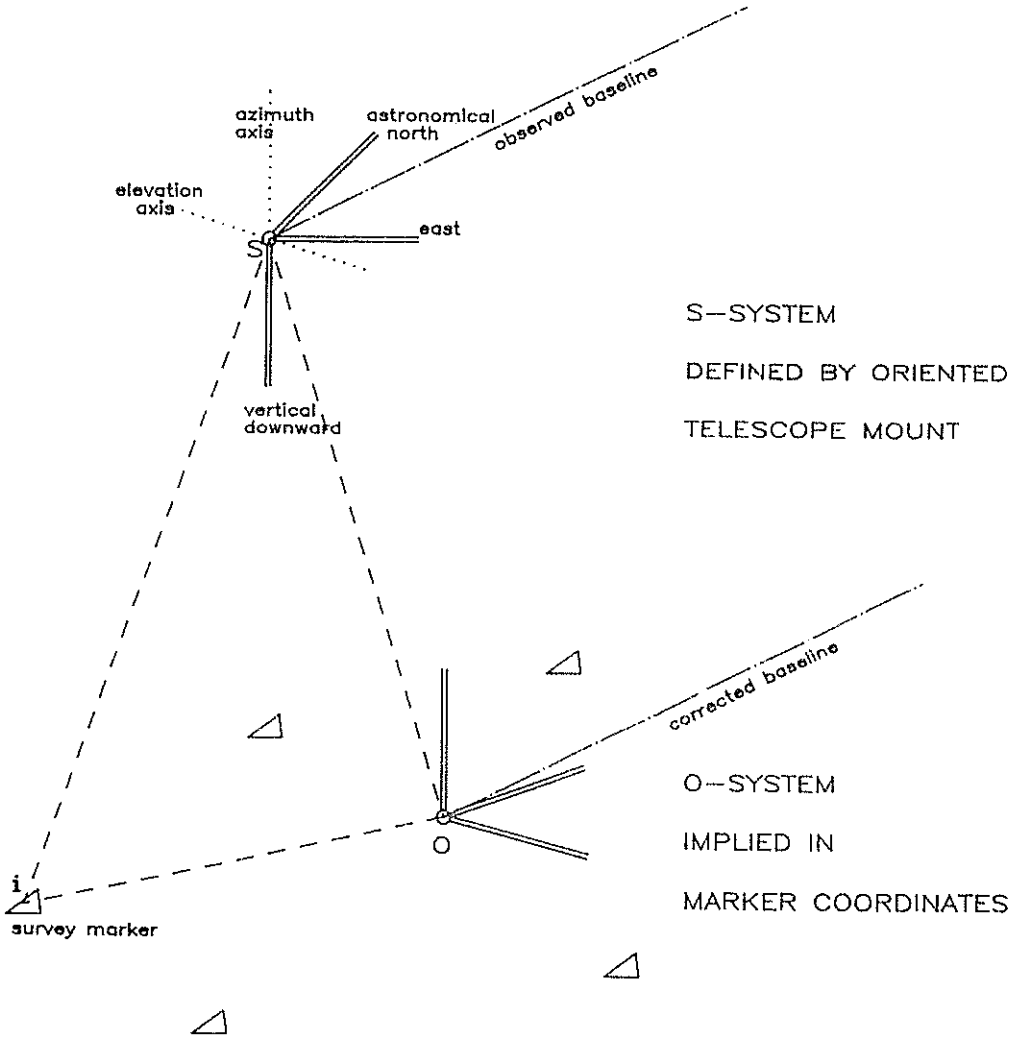

TRANSFORMATION:

$$X_i^s = \lambda_o^s \left(R_o^s\right)\left(X_i^o - X_s^o\right)$$

figure 8. The similarity transformation between S-system and O-system.

3. Numerical results

During the test-period for MTLRS1 at Kootwijk, various ground tie determinations were performed employing the method outlined above. At the observatory two different sites are available for MTLRS. The so-called astronomical platform (figure 9) can accommodate MTLRS in a semi-stationary position when actual satellite observations are to be performed. The second site is at the parking lot where five positioning markers are arranged just as suggested for international site pads where MTLRS is to be expected (figure 10). This site is primarily meant for testing purposes. Both sites have been occupied in the testing period and the numerical results obtained with the positioning device are presented in tables 1 and 2.
The upper part of each table displays the seven estimated similarity transformation parameters, their formal precision (σ) as well as their worst-case reliability (∇) i.e. the upper bound influence of marginally detectable errors in any of the observations. The lower part of each table contains the residuals of the observations together with their test-variates i.e. the squared normalised residuals. These test variates are used for testing against a critical value of 10.80 resulting from an adopted significance level of 0.1% and a power of the test of 80%. An asterisk indicates rejected observations.

3.1 The site at the astronomical platform

Table 1a presents the results of the first positioning attempt at this site. Obviously this solution cannot be accepted since the test rejects all but one of the observations. Inspecting the magnitude of the normalised residuals it becomes apparent that the range to marker A is suspected most, because the magnitude of its test variate is about ten times higher than any other one. Due to correlation between the residuals most observations will be rejected in case of one large error. After re-measurement it became clear that in the range to marker A, a 30 cm error had occurred. A "9" had been replaced by a "6" probably because the range at the spring-rule had been read in an upside-down position. The new results after re-measurement are presented in table 1b. The residuals and the test-variates are very small and the observations obviously fit the adjustment very well. The precision of the translation parameters is about half a mm and their reliability about 2 mm. The latter means that a marginally detectable error in any one of the observations (in this case producing a test variate value of about 10.8) can only have a maximum influence on these parameters of about 2 mm. These very satisfactory results are a consequence of the utilisation of five markers, about symmetrically arranged around the ranging system, and are in agreement with the expectations arrived at in the

figure 9.

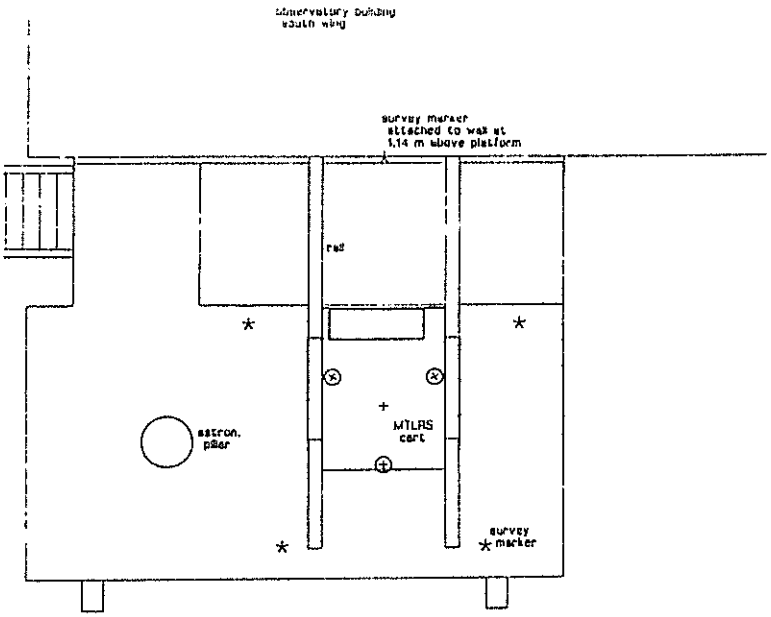

figure 10.

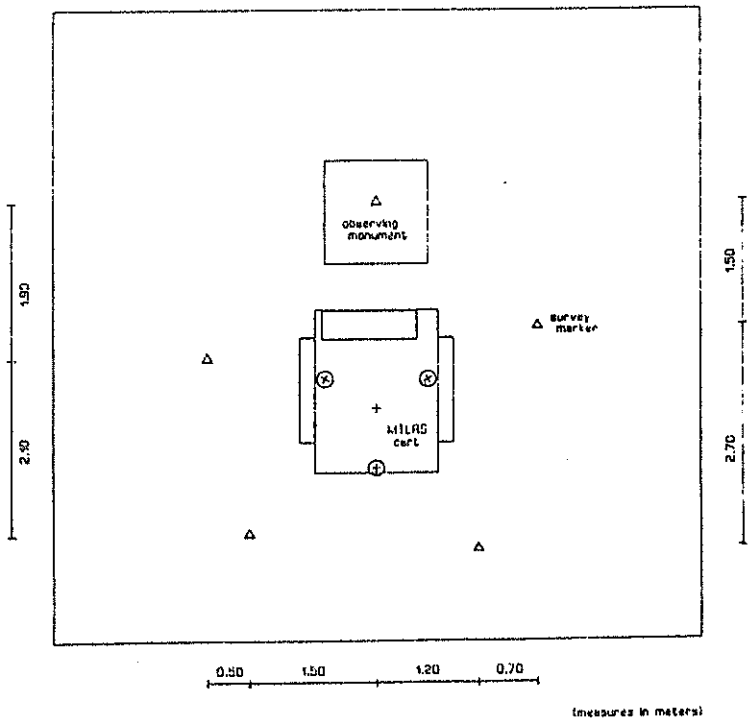

Footprint of MTLRS.
Figure 9 depicts the accomodation for MTLRS at the Kootwijk observatory.
Figure 10 displays the optimal configuration of five markers as suggested for international site pads.

	param.	σ	∇	
X_s^{O1} m	-.0080	.6	2.0	mm
X_s^{O2} m	.0520	.5	1.7	mm
X_s^{O3} m	.0288	.4	1.4	mm
α_O^S degr	90.3592	27.5	86.6	arcsec
β_O^S degr	.4204	50.5	228.0	arcsec
γ_O^S degr	180.0217	65.0	175.9	arcsec
λ_O^S	.9713	.4	1.0	1E-3

	observation	res. degr/m	test	
marker "A"	elevation	.1710	303.74	*
	azimuth	.0073	.40	
	range	.1966	14795.50	*
marker "B"	elevation	-.1148	101.55	*
	azimuth	.2595	571.20	*
	range	-.0698	1552.46	*
marker "C"	elevation	-.2300	463.73	*
	azimuth	-.1629	215.43	*
	range	-.0526	940.01	*
marker "D"	elevation	-.2419	512.02	*
	azimuth	-.1565	200.69	*
	range	-.0529	951.37	*
marker "E"	elevation	-.1170	105.88	*
	azimuth	-.2731	641.05	*
	range	-.0701	1563.03	*

table 1a

	param.	σ	∇	
X_s^{O1} m	-.0078	.6	1.9	mm
X_s^{O2} m	.0323	.5	1.7	mm
X^{O3} m	.0203	.4	1.4	mm
α_O^S degr	90.3589	27.4	86.2	arcsec
β_O^S degr	-.0012	50.3	225.8	arcsec
γ_O^S degr	180.0210	64.7	176.0	arcsec
λ_O^S	1.0006	.4	1.0	1E-3

	observation	res. degr/m	test
marker "A"	elevation	-.0080	.66
	azimuth	.0067	.33
	range	.0011	.49
marker "B"	elevation	.0058	.26
	azimuth	-.0041	.14
	range	-.0005	.08
marker "C"	elevation	.0030	.08
	azimuth	.0058	.28
	range	.0006	.11
marker "D"	elevation	-.0103	.92
	azimuth	-.0008	.01
	range	-.0003	.03
marker "E"	elevation	.0068	.36
	azimuth	-.0076	.50
	range	-.0013	.52

table 1b

table 1. Positioning results at the site at the astronomical platform.

design study (Vermaat and Van Gelder, 1983). The size of the translation parameters is only a few cm due to the fact that the origin of the 0-system has been chosen at the site center at an elevation of 1.3 m above the pad, thus very close to the expected location of the instrumental center S. This results in an only marginal influence of the rotation parameters on the baseline correction derived from formula (2.6).

3.2 The site at the parking lot

The results of the first positioning attempt at this site are presented in table 2a, which indicates the rejection of one observation: the elevation of marker E. Closer inspection reveals that some other observations have rather large test-variate values as well (e.g. the elevation to marker A and D). This rather puzzling situation could not be improved after re-measurement. The next step was to leave out any one suspected marker from the solution (e.g. marker E, D or A) but not any of these attempts gave acceptable results. Ultimately it could only be concluded that a rather complicated distortion had occurred at this site, after the survey and prior to the occupation by MTLRS, affecting the position of the majority of the markers. Thus these markers were re-surveyed and the coordinate differences obtained are presented in table 3. These figures fully support the assumption of a complicated distortion of a magnitude of 0.5 to 6.0 mm. Subsequently the positioning procedure was repeated utilising the new marker coordinates and table 2b presents the results, which are very acceptable. As could be expected, the precision and reliability is very similar to the results obtained at the astronomical platform.

It must be clear that a problem of disturbed markers never may occur in practical situations. Especially in a situation without evidence that only one particular marker has been disturbed, the reference point of the site has been irrecoverably lost and no accurate relation to baseline solutions obtained from previous site occupations will be possible. The site at the parking lot is only intended for testing purposes and for training crews in manoeuvring, packing and unpacking of the system. Although some care has been taken to isolate the markers from the pavement (figure 5) it is obvious that this has not been very successful, mainly due to the type of pavement, the instability of the subsurface soil and the sometimes heavy traffic to be expected at this location.

Sites meant for satellite observations have to be selected with extreme care and special attention has to be paid to the installation of the markers.

	param.	σ	V	
X_S^{O1} m	.0053	.7	1.9	mm
X_S^{O2} m	.0863	.6	1.8	mm
X_S^{O3} m	.0656	.5	1.5	mm
α_O^S degr	90.3343	26.9	82.0	arcsec
β_O^S degr	-.0760	61.5	234.8	arcsec
γ_O^S degr	180.0109	66.9	198.2	arcsec
λ_O^S	1.0003	.4	.9	1E-3

	observation	res. degr/m	test	
marker "A"	elevation	.0326	9.44	
	azimuth	.0202	2.82	
	range	.0017	1.03	
marker "B"	elevation	-.0087	.63	
	azimuth	-.0113	1.05	
	range	.0009	.27	
marker "C"	elevation	-.0169	2.78	
	azimuth	.0087	.68	
	range	-.0029	2.95	
marker "D"	elevation	.0346	9.56	
	azimuth	-.0018	.02	
	range	-.0004	.05	
marker "E"	elevation	-.0407	13.28	*
	azimuth	-.0157	1.95	
	range	.0005	.10	

table 2a

	param.	σ	V	
X_S^{O1} m	.0066	.7	1.9	mm
X_S^{O2} m	.0890	.6	1.8	mm
X_S^{O3} m	.0631	.5	1.5	mm
α_O^S degr	90.3486	26.9	82.0	arcsec
β_O^S degr	-.0064	61.5	234.6	arcsec
γ_O^S degr	180.0065	66.9	198.2	arcsec
λ_O^S	1.0005	.4	.9	1E-3

	observation	res. degr/m	test
marker "A"	elevation	.0101	.91
	azimuth	-.0005	.00
	range	.0014	.70
marker "B"	elevation	-.0142	1.65
	azimuth	.0125	1.29
	range	-.0012	.52
marker "C"	elevation	.0096	.89
	azimuth	-.0171	2.64
	range	-.0002	.02
marker "D"	elevation	-.0066	.35
	azimuth	.0164	2.02
	range	-.0002	.01
marker "E"	elevation	.0007	.00
	azimuth	-.0114	1.02
	range	.0000	.00

table 2b

table 2. Positioning results at the site at the parking lot.

	ΔX	ΔY	ΔZ	
marker "A"	0.5	-1.0	-6.0	mm
"B"	0.5	-0.9	-2.0	
"C"	4.6	-0.5	-1.0	
"D"	2.8	1.4	-2.0	
"E"	1.8	0.1	-1.0	

table 3. Coordinate differences at the site at the parking lot due to local deformation.

4. Concluding remarks

From tests at two different sites, it can be concluded that the method designed for MTLRS of determining the ground tie vector, not only easily discovers observational errors, but also detects relatively small local disturbances in the immediate site area.
In addition it has become evident that the precision of the estimated parameters is very satisfactory, especially the translation can be obtained to sub-millimeter precision, in spite of the rather simple surveying technique employed.
The necessary requirement for accurate ground tie vector determination is the availability of a sufficient number of markers in an optimal configuration. These markers must be accurately surveyed prior to site occupation.
Another feature of the method employed for MTLRS, which already has proven its value, is the fact that the data analysis is performed on-site, immediately after obtaining the observations. Thus the operators are able to identify problems of observational errors or local site deformations immediately, and take measures accordingly.

Reference

Vermaat, E. and B.H.W. van Gelder, 1983. "On the eccentricity of MTLRS". Delft University of Technology. Reports of the Department of Geodesy, Mathematical and Physical Geodesy, No. 83.4.

Acknowledgement

The software utilised, could be scrupulously tested with laboratory measurements made by Leendert van Dijk and Ayse Açikel. They also surveyed the markers at Kootwijk assisted by Danny van Loon who, subsequently supervised the positioning procedures with MTLRS. Joop Bodde manufactured and installed the markers and last but not least an unknown truck-driver disturbed the site at the parking lot.

LASER SYSTEM CHARACTERIZATION

M.R. Pearlman
Smithsonian Astrophysical Observatory
60 Garden St.
Cambridge, MA 02138

Telephone (617) 495 7481
Telex 92148

ABSTRACT

A model is provided to standardize the evaluation of laser ranging system perfomance in terms of ranging accuracy. The model deals with the magnitude and temporal nature of the known data error sources and aggregates them in terms of Ranging Machine Errors, Epoch (Timing) Errors, and Modelling (Environmental) Errors. The model is provided to characterize and verify system performance for engineering operations and data analysis requirements. It is anticipated that this model will be dynamic, evolving with our understanding and needs. An application of the model to the Arequipa station is included as an example.

LASER SYSTEM CHARACTERIZATION

1. REQUIREMENT AND METHODOLOGY

The Laser System Characterization is intended to provide a "Standard Error Model" to: 1) verify system performance; 2) verify system upgrading; 3) compare systems, and 4) establish and adopt constants and models for intercomparisons and data analysis. The model is not a substitute for collocation tests which evaluate the total aggregated error budget of the systems under study, but rather is designed to support collocation and other system performance tests by providing the basis upon which different systems utilizing different philosophies and techniques may compare error budgets. In addition, total model specification is considered essential for accurate preprocessing and optimal weighting of network observations in any least squares adjustment process.

The model characterizes each system, including local site dependent variables, under normal operating conditions of a given epoch. That is, the model parameters are tabulated for each system and site as a function of time, being updated on a regular basis or whenever maintenance or modification effecting the measurement occurs. The model also provides a format to characterize system performance under malfunctioning conditions, but its application to such a situation would have to be considered on a case by case basis. It may be more practical to disregard certain data than try to characterize data under conditions of equipment malfunctions or operator error.

In organizing this model, we placed requirements that it should:

1. Focus on the systematic error sources.
2. Specify the statistical means of characterizing each component (1 sigma, peak-to-peak, etc.)
3. Specify relevant time period or periods for each component.
4. Define a means of measuring and specifying each error component.
5. Specify a means of aggregating the error components.
6. Be practicable.

This model does not include the averaging effect derived through orbital geometry. Such averaging depends upon the method of analyses, the station configuration, and the geophysical parameters being sought. This model is intended to provide the analyst with the input required to test error sensitivity in his own application of data.

For convenience, we have divided the error components into three categories corresponding to the nature of the errors.

1. Ranging machine errors are those associated with the laser hardware and its calibration.

2. Epoch or timing errors are those associated with the station clock, or time and frequency transfer.

3. Modelling or environmental errors are those associated with data compensation for effects outside the ranging and timing system.

In order to provide a firm basis for evaluation of total system performance, this specification aggregates hardware related effects independently from environmental effects. This has the advantage of allowing the user to focus on his area of immediate interest. It is common practice in laser ranging for the observing station to provide estimates for ranging machine and timing errors but not for modelling and environmental errors. In addition, traditional parametric data describing the atmosphere is usually supplied by the station without precision estimates. Since corrections for all three types of errors are applied or furnished for all range observations, and an accurate a-priori estimate of the precision of this corrected range is needed, it is necessary to state all corrections with precision estimates.

The "Standard Model" should evolve and improve with our knowledge of the error sources. In particular, it is assumed that the models and techniques used to characterize the environmental effects will be replaced by new models as they are developed and accepted. It is also anticipated that archived data will be periodically reanalyzed as major improvements are introduced.

2. CLASSIFICATION OF ERROR SOURCES

The model components are divided into categories:

1. Ranging Machine Errors

    a. Wavefront distortion (Spatial Errors)
    b. Uncorrected System Drift (Temporal Errors)
    c. Uncorrected Variation in system delay with Signal Strength
    d. Errors in target range or calibration path length
    e. Error in calibration due to uncertainties in meteorological conditions along the calibration path
    f. Variation in system calibration with background noise level
    g. Mount eccentricities

2. Epoch (Timing) Errors

   a. Portable Clock Set
   b. Broadcast Monitoring

3. Modelling (Environmental) Errors

   a. Atmospheric Propagation (Model)
   b. Atmospheric Propagation (Meteorological Measurements)
   c. Spacecraft Center-of-Mass
   d. Ground Survey of Laser Position
   e. Data Aggregation

The user must be aware of the nature of each of the error sources, otherwise, he runs the risk of confusing an error source with a geophysical observable. This means that the operators of each laser ranging system must provide a determination of each error source (size and time constant) on a routine basis and make the full characterization schedule available to the users.

A comprehensive system evaluation must be made at least every six months and before and after each major modification to the hardware data flow path.

3. CHARACTERIZATION OF ERRORS

Each error source for each participating laser system must be characterized by its size and temporal nature. For simplicity, we use a one sigma representation for those components that appear random (such as wavefront) and one-half peak-to-peak for those effects that appear to have well defined trends (such as uncorrected variation with signal strength). This gives strong incentive to make analytic a posteriori corrections where possible.

Each error component has a characteristic signature in the pattern of residuals from a perfect orbit. In this model, the temporal nature of the error sources are quantified by time constants (decorrelation time) after which the pattern of residuals would change appreciably; it is assumed that the influence of error sources average out over 4-6 time constants. A specific component of error may decorrelate in steps owing to the various contributing activities.

In this model we characterize the error sources by their influence over specific integration periods which span the range of geophysical interest and operational constraints. In particular, we have chosen periods of a pass, a day (several passes), a month, a year, and several years (indefinite or trends). Many of the error sources, especially those in the environmental category, are much better understood over short periods and hence semi-annual, annual and decade fluctuations still need to be defined or improved.

4. RANGING MACHINE ERRORS

The known ranging machine errors are summarized in Figure 1.

4.1 Spatial Variations

Spatial variations in time of arrival (or wavefront distortion) are the result of mode structure in the laser. Patterns in the far field tend to change appreciably over periods of a few hours or less, and hence the effect which can give a strong residual signature (depending upon mode pattern and satellite path within the laser beam) can vary from pass to pass. The effect tends to vary with pulse width and laser configuration.

Spatial variations are measured by mapping the wavefront with a fixed ground-based retroreflector. The effect would be characterized by the r.m.s. variation over the wavefront. Sufficient data must be taken to assure that range noise is negligible and there must be enough redundancy in the data taking sequence to verify the pattern (and avoid temporal effects).

4.2 Temporal Variations

Temporal variations refer to uncompensated system drift (change in internal delay) during ranging operations. These would be due to changes in temperature, cycling of fans and compressors, changes in line voltage, etc. The potential for a problem is exacerbated by increased time intervals between calibrations; systems that are calibrated on a pulse by pulse basis avoid the problem, whereas those that rely on pre-and-post pass calibrations must be very carefully monitored.

Temporal variations are evaluated on an r.m.s. basis by monitoring and analyzing pre-minus-post calibration differences over an extended period of time (at least one month). The pre-minus-post calibration is not unambiguously separable from meteorological fluctuations along the calibration path, (see below) but the method is simple and will give an upper bound to the effect.

Temporal variations can also be monitored by ranging to a close ground target (to minimize propagation effects) over a period of several hours.

SOURCE	DEPENDENCE	MEASUREMENTS	RELEVANT TIME PERIOD	COMMENTS
SPATIAL VARIATIONS (WAVEFRONT DISTORTION)	PROPORTIONAL TO PULSE WIDTH	MAP WAVEFRONT WITH CORNER CUBE	PASS OR SEVERAL HOURS	SYSTEMATIC RESIDUAL SIGNATURE (PASS); MAY AVERAGE OUT OVER SEVERAL PASSES
TEMPORAL VARIATION (UNCORRECTED SYSTEM DRIFT)	SYSTEM STABILITY INTERVAL BETWEEN CALIBRATIONS	STABILITY TEST RUN PRE-POST CALIBRATIONS	PASS (BETWEEN CALIBRATIONS)	REAPPEARING SYSTEMATIC TREND: TENDS TO AVERAGE OUT WITH TIME
SIGNAL STRENGTH VARIATION (UNCORRECTED VARIATION IN SYSTEM DELAY WITH SIGNAL STRENGTH)	PMT, PULSE AMPLITUDE AND WIDTH	CALIBRATE OVER FULL DYNAMIC RANGE	INDEFINITE (LONG TERM)	RANGE ERROR CORRELATED WITH SIGNAL STRENGTH (RANGE)
ERROR IN CALIBRATION TARGET DISTANCE (EXCLUSIVE OF METEOROLOGICAL EFFECTS)	SURVEY MEASUREMENT	SURVEY	INDEFINITE (LONG TERM)	FIXED BIAS
ERROR IN CALIBRATION MEASUREMENT	METEOROLOGY	P.T.%R.H.	DAY, ANNUAL	BIAS WITH DIURNAL CYCLE AND SLOWER VARIATIONS
VARIATION WITH BACKGROUND LEVEL	PMT	CALIBRATE OVER RANGE OF ANTICIPATED CONDITIONS	DIURNAL	DIURNAL VARIATION
MOUNT ECCENTRICITY	TRACKING ANGLES	STELLAR CALIBRATION, SURVEY	INDEFINITE	SYSTEMATIC RESIDUAL SIGNATURE OVER A PASS; VARIATION IN INFLUENCE WITH SATELLITE ORBITAL GEOMETRY

FIGURE 1
SATELLITE LASER RANGING SYSTEMS
RANGING MACHINE ERROR SOURCES

4.3 Signal Strength Variations

Variations in system delay with signal strength arise because performance of devices within the system including PMTs are amplitude and/or pulse-width dependent. Those systems that are calibrated and intended to operate at the single photoelectron level only would have very minimum degradation due to this effect. This, of course, presumes that there is proper discrimination against occasional multiple photon returns (with different system propagation times) which would degrade range accuracy.

The variations with signal strength, which are measured by detailed target calibrations over the full dynamic range of the system, tend to have a systematic trend which may lend itself to a posteriori analytic correction. Since this error source is dependent upon signal strength and hence range, it can give systematic residual patterns. As such, the effect is long term. As an incentive to consider analytic corrections, this model uses a one-half peak-to-peak representation (over the pertinent dynamic range) to characterize this effect.

4.4 Calibration Target Distance

4.4.1 Measurement Techniques (Exclusive of Meteorological Correction)

Error in calibration target distance includes both ground targets and internal calibration paths. This is essentially how well a path can be measured by ground survey or tape measure. Each station must provide an estimate of target range accuracy which is based on the measurement technique. This error is a fixed long term bias.

In addition, as mentioned in 6.3 below, each station may have significant diurnal and annual signatures in the distance between the laser and the ground target. Ideally, target distance should be measured at several times during the day as well as a number of times during different seasons to determine: (1) if such a variation exists; (2) if it is significant and reproducible, and, (3) if a useable model can be developed.

4.4.2 Meteorological Correction to Calibration

In those systems that use ground targets for calibration, corrections must be made for horizontal propagation delay. The technique for computing this correction should be standardized to the group refractivity (Ng) derived from the Barrel and Sears formula adopted by the IAG in 1963.

$$Ng = N - \lambda \frac{dN}{d\lambda} = 80.343 \quad f(\lambda) \frac{P}{T} - 11.3 \frac{e}{T}$$

where:

$$f(\lambda) \equiv 0.9650 + \frac{0.0164}{\lambda^2} + \frac{0.000228}{\lambda^4}$$

which has been normalized to 1 for λ = 6943Å (ruby laser wavelength)

and where:

λ = wavelength in microns

P = total air pressure (mb)

e = partial pressure of water vapor (mb)

T = temperature (degrees Kelvin)

The refractive correction must be based on measurements of P, T, and e (or %R.H.) at both ends of the calibration path or in the very least, an extrapolation based on the slope of the calibration path. No curvature corrections need be applied if the line is shorter than 10 km.

The total effect of the atmosphere is about 270 parts in 10^6 at sea level. The major uncertainties in making this correction are temperature and pressure variations along the path. This effect probably includes short period terms which average out over time spans of a day plus longer term biases which may include seasonal and even annual effects. Fluctuations of several degrees, which are not uncommon over a 1 km path can lead to an error in the refraction correction of as much as 1% (3mm). The size of the annual component is not clear, but it may be significant.

Instrument and procedural errors in the reading of pressure and temperature also add uncertainties to the refraction correction. A reading error of 1 mb in pressure or 0.5 C in temperature will introduce a bias error of .1% in the refraction correction (or about .3 mm for a 1 km calibration path).

The value of the error (r.m.s.) in the meteorological correction must be determined by each station based on local measurements, topography, and instrument calibration.

4.5 Mount Eccentricities

Laser range measurements must be referred to an "invariant" (fixed) reference point (usually termed the "intersection of the axes") on the laser mount. This point must be specified along with the associated path offset. In reality, however, these "invariant" points may not be fixed in space and the resulting "mount eccentricities" can produce pass-dependent systematic range errors. The pertinent eccentricities must be measured and/or modelled with appropriate range error characteristics. The influence of this effect is of particular importance with large instruments and with X-Y mounts. Since mount eccentricities produce reproducible, systematic components, the unmodelled (uncompensated) effects should be estimated on a half peak to peak basis.

4.6 Variation with Background Noise Level

There is some speculation that system delay may be a function of background noise level. However, to date there has been no verification of this effect.

5. TIMING ERRORS

The standard epoch reference used for laser ranging is UTC (BIH) or its close proximity UTC (USNO). The accuracy to which epoch is maintained is station dependent and must be furnished by each operating station. In practice, all station clocks are checked periodically with a portable clock and monitored at least once per day using LORAN, GPS, TV Reception, VLF or some other broadcast source. On a single pass basis with Lageos, a 1 microsec epoch error will introduce an error in station position of about 4 mm.

5.1 Portable Clock Check

Portable clock checks are typically of .1-1.0 microsec quality depending upon the portable clock, the length of the clock trip, and the station clock. An error in the portable clock set introduces a fixed bias component (long term) until a subsequent clock trip takes place.

5.2 Time Broadcast Monitoring

Epoch and/or frequency broadcasts are monitored at least daily by most operating stations. Those that receive TV line signals, or ground wave LORAN should be able to monitor epoch to 1 microsec; GPS reception should be considerably better. The daily values are independent determinations of station clock offset and hence the time constant for this component of epoch error is one day. For those using skywave LORAN or VLF, daily fluctuations of several microseconds due to propagation effects are common. In this case, averaging over several days is required to smooth out the data. The time constant in this case is 3-5 days. Routine monitoring of VLF propagation by the U.S. Coast Guard indicates that long term (even annual) variations measured during periods of stable propagation during the day are typically 1 microsecond or less.

It should be pointed out that historically long term timing errors have been notorious at the field stations. For the most part however, these have been the result of hardware and/or operational difficulties which should be documented as malfunctions.

6. MODELLING ERRORS

A summary of the modelling errors appears in Figure 2, with notation whether they are determined (measured) on a site by site basis or estimated from general models in use.

CORRECTION	METHOD	ESTIMATED ACCURACY	TIME PERIOD	NATURE
ATMOSPHERIC PROPAGATION (MODEL)	MARINI AND MURRAY MODEL	0.5 CM (AT 45 ALT)	DAY; PROBABLY ANNUAL	BIAS (P.T.%R.H.): VARIES WITH AZIMUTH AND ALTITUDE
ATMOSPHERIC PROPAGATION (MEASUREMENT)	MEASUREMENT OF P, T, H	DETERMINED	LONG TERM	OFFSET INCREASES WITH RANGE
S/C CENTER OF MASS (MODELS)	GSFC MODELS ARNOLD MODELS	2 MM	INDEFINITE (LONG TERM)	FIXED BIAS
GROUND SURVEY OF LASER POSITION (MEASUREMENT)	SURVEY MEASUREMENT	DETERMINED	INDEFINITE; PROBABLY ANNUAL	STATION POSITION ERROR
DATA AGGREGATION	AVERAGING 1-3 MINUTE DATA SEGMENTS	DETERMINED	PASS	DEPENDS ON DATA YIELD AND DISTRIBUTION

FIGURE 2
SATELLITE LASER RANGING SYSTEMS
MODELLING ERROR SOURCES

6.1 Atmospheric Propagation Model

6.1.1 Model

The recommended model for columnar refraction between ground station and satellite is the model by Marini and Murray (1973) based on the Barrel and Sears model for atmospheric refractivity and a standard exponential atmosphere. (The use of this model should be standardized and changed only with the organized consensus of the community.) Although this model does not include the effects of horizontal gradients in atmospheric density and temperature, it is believed to be accurate to within 1-2 centimeters of ray tracing results performed on radiosonde data (Marini and Murray, 1973, Gardner 1976).

It must be recognized, however, that this model does not include the effects of horizontal gradients in atmospheric density. At low elevation angles, the laser beam may be passing through pressure fields that vary by a few millibars at ground level. This alone could introduce uncertainties as large as 1 cm or more. Even with no surface pressure changes with position, horizontal gradients in temperature can influence the model error for slant ranges by making the scale height depend on position. Gardner (1976) and Dunn et. al. (1982), have studied this effect and find typical errors of 1.5 and 2 cm (r.m.s.) respectively at 20 degrees elevation if no correction for horizontal gradient is made.

Since observations are taken over all accessible elevation angles (usually above 20 degrees), and since the effects of horizontal gradients fall off rapidly with elevation angle, the average effect is about 0.5 cm. In lieu of more definitive data at the moment, we have characterized the refraction error as 0.5 cm at 45 degrees elevation. Since atmospheric conditions typically change on both diurnal and longer time scales, we anticipate that the size of this error source would decrease slowly with observing time. In addition, there is probably an uncorrected annual variation, but as yet this is unquantified.

6.1.2 Meteorological Measurement Error

The most significant term in the Marini and Murray model is proportional to pressure (p) and inversely proportional to elevation angle (E):

$$\delta\Delta R(m) = \frac{0.0024}{\sin E} \quad \delta p(mb)$$

The dependance on temperature change (δT) of this model can be expressed as:

$$\delta\Delta R(m) = \frac{1 \times 10^{-5}}{\sin^3 E} \quad \delta T(^{o}C)$$

A measurement error of 1 mb in pressure and 1 C in temperature, which are common in todays field operations, will introduce errors of about 7 mm and 0.3 mm respectively at 20 degrees altitude. However, it is quite feasible with available instrumentation to measure barometric pressure at field

stations to 0.3 mb. To the extent that errors in pressure and temperature readings are due to instrument calibration or reading procedure, the influence of these components would be long term range biases which increase with zenith angle and hence range. These errors should be estimated on a site by site basis by comparison with calibrated instrumentation.

6.2 Spacecraft Center of Mass

The range correction to spacecraft center-of-mass for Lageos has been calculated analytically (Fitzmaurice et. al. 1978; Arnold 1978) and measured in the laboratory prior to launch (Fitzmaurice et. al. 1978). The analytical models show a dependence of range correction on pulse width and pulse detection scheme. For those situations in common the differences between the analyses by Fitzmaurice et. al. and Arnold is less than 1 mm. Our estimate for the error in range correction to Lageos is taken from the experimental measurement uncertainty which was about 2 mm (Fitzmaurice et. al. 1978). This value, of course, assumes that the correction made is appropriate for the laser pulse width and detection scheme. Otherwise, an error as large as 1 cm is possible. This error would be a long term fixed range bias.

6.3 Ground Survey of Laser Position

Lasers that reoccupy a site can not be placed in exactly the same position each time. As such the system reference point must be surveyed to the local geodetic reference marker. The error in this measurement will constitute a fixed offset in station position for the period of one site occupation. These estimates of measurement accuracy must be furnished by each laser ranging group for each occupation by a mobile laser system. In the case of fixed laser systems, the local survey errors are important from the standpoint of interconnecting datum, however, they do not effect direct measurement of station position or crustal motion. It should also be recognized that many ground sites have significant annual signatures due to changes in ground water. At some point, this issue must be systematically addressed.

6.4 Data Aggregation

No specification is recommended at this stage as there is at yet no agreed "best" method. Several methods based on 1-3 minutes of ranging data are being used to produce normal points with errors less than 1 mm are currently under intensive study. Once these are concluded we expect standardization to occur.

7. AGGREGATION OF ERRORS

Since the nature and representation of the separate error sources is quite varied a rigorous aggregation of the error sources would be quite difficult. However, a simplified approach to data aggregation is to assume that the individual components of error are uncorrelated and that an r.s.s.

of all pertinent error sources is sufficient to give an overall estimate of total ranging error. For this, we would form separate estimates of range error for each integration (averaging) time of (1) a pass, (2) a day, (3) a month, and (4) an indefinite period (long term).

As pointed out earlier, once the annual components are better understood, they should be tabulated separately. An example of how the data could be presented and aggregated is shown in Figure 3. An example using the SAO laser in Arequipa is shown in Figure 4.

8. AN EXAMPLE: THE AREQUIPA LASER

The "Standard Error" Model for the Arequipa Laser appears in figure 4.

8.1 Environmental Errors

8.1.1 Atmospheric Propagation Model

We use the Marini and Murray Model for the atmospheric propagation correction to satellite ranges. We estimate the refraction error to be 0.5 cm (see above). With our ground based meteorological instruments we read barometric pressure with a mercury column to an estimated accuracy of ± 1 mbar based on a comparison among instruments. Temperature is measured to ± 1 degree Celsius with a mercury thermometer and relative humidity to $\pm 10\%$ with a sling psychrometer.

8.1.2 Spacecraft Center-of-Mass

SAO uses the Arnold Models for its spacecraft center-of-mass corrections. The correction used for Lageos on the Arequipa data is 24.3 cm. This is appropriate for a 3 nsec pulse and a centroid (center of gravity) detector. The estimated error is 2 mm (r.m.s.).

8.1.3 Ground Survey of Laser Position

Since the Arequipa laser is a fixed system, no error for ground survey of laser position is included.

8.1.4 Data Aggregation

We do no aggregation on the quick-look or final data.

8.1.5 Summary of Environmental Errors

The aggregated environmental contribution is estimated at 1.6 cm over the short term (a day or less) and 1.2 cm for longer periods.

RANGING ERRORS (CM)

	PASS	DAY	MONTH	INDEF.
MODELLING ENVIRONMENTAL ERRORS				
ATMOSPHERIC PROPAGATION (MODEL)				
ATMOSPHERIC PROPAGATION (METEOROLOGICAL MEASUREMENTS				
SPACECRAFT CENTER OF MASS				
GROUND SURVEY OF LASER POSITION				
DATA AGGREGATION				
R.S.S.				
RANGING MACHINE ERRORS				
SPATIAL VARIATION				
TEMPORAL VARIATION				
SIGNAL STRENGTH VARIATION				
CALIBRATION PATH (SURVEY)				
CALIBRATION PATH (METEOROLOGICAL CONDITIONS)				
MOUNT ECCENTRICITIES				
R.S.S.				

RANGING ERRORS (CM)
TIMING ERRORS (MICROSEC)

PORTABLE CLOCK SET				
BROADCAST MONITORING				
R.S.S.				

FIGURE 3
ESTIMATED RANGING ERRORS FOR SATELLITE LASER RANGING SYSTEM

RANGING ERRORS (CM)

	PASS	DAY	MONTH	INDEF.
MODELLING (ENVIRONMENTAL ERRORS)				
ATMOSPHERIC PROPAGATION (MODEL)	0.5	0.5	0.5	0.5
ATMOSPHERIC PROPAGATION (METEOROLOGICAL MEASUREMENTS	0.5	0.5	0.5	0.5
SPACECRAFT CENTER OF MASS	0.2	0.2	0.2	0.2
GROUND SURVEY OF LASER POSITION	-	-	-	-
DATA AGGREGATION	-	-	-	-
R.S.S.	0.7	0.7	0.7	0.7
RANGING MACHINE ERRORS				
SPATIAL VARIATION	3.0	2.0	1.0	1.0
TEMPORAL VARIATION	2.0	1.0	1.0	1.0
SIGNAL STRENGTH VARIATION	3.0	3.0	3.0	3.0
CALIBRATION PATH (SURVEY)	1.0	1.0	1.0	1.0
CALIBRATION PATH (METEOROLOGICAL CONDITIONS)	0.4	0.4	0.4	0.4
MOUNT ECCENTRICITIES	0.1	0.1	0.1	0.1
R.S.S.	4.8	4.0	3.5	3.5

RANGING ERRORS (CM)
TIMING ERRORS (MICROSEC)

PORTABLE CLOCK SET	1.0	1.0	1.0	1.0
BROADCAST MONITORING	4.0	4.0	1.0	1.0
R.S.S.	4.2	4.2	1.4	1.4

FIGURE 4
ESTIMATED MEASUREMENT ERRORS FOR THE AREQUIPA SATELLITE LASER RANGING SYSTEM

8.2 Ranging Machine Errors

8.2.1 Spatial Variations

Spatial variations are measured in Arequipa by ranging on a ground-based corner cube at a distance of about 1 km. Range measurements are made in sets of 50-100 laser shots at return signal strengths in the range of 5-20 photoelectrons. Measurement sets are taken over a matrix with 20 arcsec spacings over the 2 arcmin wide laser output beam. The sets are taken in random order around the matrix with scheduled returns to the central "reference" position to check for temporal drift. The mean values of the sets are used to map the wavefront contours and to calculate the r.m.s. wavefront variation.

The r.m.s. spatial variation in Arequipa is typically in the range of 2-3 cm. Experience has shown that the wavefront pattern changes appreciably over a period of a day. We use a value of 2 cm for the daily average to accommodate the fact that the acquired Lageos pass in a given day may come within a few hours of each other. Examination of wavefront data over extended periods of time indicates that over the long term, the effect averages to zero for this ranging system. However, since the resolution of the Arequipa system is about 1 cm, we use this value (1 cm) for our long term estimate of error.

8.2.2 Temporal Variations

An upper bound for the temporal variations have been estimated from the historical pre- and post-calibrations (which are taken on the billboard target before and after each pass). In pre- and post-calibrations at least 50 laser measurements are taken to the ground target in the return signal strength range of 5-25 photoelectrons. Mean values for each are calculated; the pre-post difference for each pass is used to bound the system drift over the pass time duration. These differences, which have typical r.m.s. values of 2 cm, show no systematic trend over a period of several months, indicating that temporal variations (if they are at all significant) average out very quickly. Once again, due to the limitation in system resolution, we estimate the long term error component for temporal variations at 1.0 cm.

8.2.3 Signal Strength Variations

In Arequipa, the system delay variation with signal strength is measured routinely with extended calibrations on the billboard target. Measurements are taken over the range of 1 to 100 photoelectrons by adjusting neutral density filters in the photoreceiver. Sufficient data are taken to ensure that at least a hundred returns are received at the single photoelectron level and at least 25-50 returns are received in each half decade interval over the return energy range (the actual set size is made sufficiently large to reduce the statistical errors (1 sigma) to about 1 cm). The data are aggregated in corresponding signal strengths sets to examine system performance. Typical variations over the full dynamic range are 3 cm or less (half peak-to-peak). As a rule, system calibration value

increases with signal strength, but point by point fluctuations make it difficult to model and correct.

8.2.4 Calibration Target Distance

The target distance in Arequipa is about 1 km along a nearly horizontal path. The target distance is measured with a laser geodimeter (Hewlett Packard Model 3808A) which has an accuracy of about 1 cm. The distance is measured repeatedly over the period of a day to average out statistical errors. Propagation corrections are made using the Barrel and Sears formula. At the moment we measure temperature and pressure only at the ranging site. We anticipate fluctuations of a few degrees (Celsius) along the path giving an uncertainty of about 1% or 3 mm. It is not clear how much of this is short term and how much is seasonal. At the moment we assume that this is a long period effect. We use a Mercury column to measure pressure and a standard mercury thermometer to measure temperature. In addition, a reading error of 1 mb and 1.0^{o}C which could add another mm in long term bias error.

8.2.5 Mount Eccentricities

The eccentricity of the mount in Arequipa has not been measured but on the basis of the compact design of the Azimuth-Altitude Mount and the separated laser and photoreceiver we estimate the eccentricity at 1 mm or less.

8.2.6 Summary of the Ranging Machine Errors

The aggregated ranging machine errors amount to about 5 cm on a single pass basis, and about 3.5 cm over the long term.

8.3 Timing Errors

The timing system at the Arequipa station uses redundant clocks (with Cesium and Rubidium Standards), VLF, Omega and portable clock checks. The accuracy of portable clock sets as determined from closure is typically 1 microsecond (r.m.s.) or better. The portable clock readings indicate that station time continuity over the short term (single pass) as maintained by VLF phase reading to be better than $\pm$4.0 microseconds. Based on our experience and that of the U.S. Coast Guard in monitoring VLF, it appears that data smoothing reduces this error considerably over a few days.

The long term bias is assumed to be 1 microsecond which is typical of U.S. Coast Guard measurements.

References

Arnold, D. A., Optical and Infrared Transfer Function of the Lageos Retroreflector Array, NASA Grant NGR 09-015-002, May 1978.

Dunn, P. J., W. A. Pearce, and T. S. Johnson, Studies of Atmospheric Refraction Effects on Laser Data, Final Report, NASA Contract No. NAS 5-25884, June 1982.

Fitzmaurice, M. W., P. O. Minott, J. B. Abshire, and H. E. Rowe, Prelaunch Testing of the Laser Geodynamic Satellite (Lageos), Technical Paper #TP-1062 for Goddard Space Flight Center, October 1977.

Gardner, C. S., Effects of Horizontal Refractivity Gradients on the Accuracy of Laser Ranging to Satellites, Radio Science, 11, 1037-1044, 1976.

Marini, J. W. and C. W. Murray, Jr., Correction of Laser Range Tracking Data for Atmospheric Refraction at Elevations Above 10 Degrees, Preprint #X-591-73-351 for Goddard Space Flight Center, November 1973.

Contributors and Reviewers

Peter Bender/UColorado
John Bosworth/GSFC
Robert Coates/GSFC
Steve Cohen/GSFC
Dave Edge/Bendix
Charles Finley/NASA
Tom Fischetti/NASA
Ben Greene/NATMAP Australia
Wayne Hughes/GSFC
Tom Johnson/GSFC
Henry Linder/GSFC/DIS
Lou Macknik/UHawaii Hollas
James Maddox/SAO
Peter Morgan/NATMAP Australia
Hays Penfield/SAO
Randy Ricklefs/UTex/TLRS-1 MLRS
Robert Schutz/UTexas
David Smith/GSFC
Chris Stephanides/GSFC
Byron Tapley/UTexas
David Townley/NASA
John Thorp/SAO
Peter Wilson/IFAG Germany

TWO WAVELENGTH PICOSECOND RANGING ON GROUND TARGET

K. Hamal, I. Prochazka
Faculty of Nuclear Science and Physical Engineering
Brehova 7, 11519 Prague 1 Czechoslovakia

Telephone (2) 84 8840
Telex 121254

J. Gaignebet
C.E.R.G.A.
Avenue Nicolas Copernic 06130 Grasse France

Telephone (93) 36 58 49
Telex 470865

ABSTRACT

One of the limiting factors to decrease the systematic error of laser ranging is the influence of the atmospheric refraction. Two colour ranging may contribute useful information for more precise refraction factor modelling and calculation. We describe two wavelength experiment using linear sweep streak camera for ground target distance measurement. The flight time difference 16 psec corresponding to 100 m horizontal pass was measured with RMS = 5 psec.

TWO WAVELENGTH PICOSECOND RANGING ON GROUND TARGET

The third generation of the satellite laser ranging was/1/ characterised by RMS less than 3cm, RMS below 1cm may be accepted for 4-th generation. The error budget consists in principle of the instrumental error (including timing), target error contribution and the enviromental errors.

One of the possibility to verify the existing atmospheric models, the multiwavelength laser ranging experiment, may be accomplished. The time diference (TD) in the flying time is increasing with increasing ratio of the wavelengths to be used. For this reason, the harmonic generation will be the natural choise for such an experiment. To be able to model the atmospheric refraction index with accuracy required on the basis of the TD, the TD must be measured with the accuracy of 3-7psec /2/.

Assuming the existing photocathode materials and their quantum efficiencies, two wavelength laser ranging experiment may be carried out using high power laser pulses. The available choise is ruby (1HG/2HG), Nd YAG (2HG/3HG), Alexandrite /3/ (1HG/2HG) and Emerald (1HG/2HG). Several kinds of photoreceivers may be adopted. A considerable effort was put to exploit two photomultipliers for 1km target ranging and the circular scan streak tube has been proposed /2/.

In our experiment we are using linear streak camera as a photoreceiver for ranging the 100meter target. The block scheme is on fig.1. The Nd YAG laser /4/ is used to generate the mode locked train of picosecond pulses. The Nd YAG rod 70mm/7mm is cut at 1° near the 100% mirror. The perpendicular surface on the opposite side acts as the output coupler. The saturable dye ML51 /5/ is in 2mm thin cell in contact with the 100% mirror. One milimeter apperture restrictes the laser to single transversal mode operation. The reprate is 1pps. The concentration of the dye is set to generate short train of pulses consisting of 2 or 3 pulses at FWHM of the envelope, the time interval between the pulses is 2.nsec. The output beam passes the second harmonic generator (2HG) and the third harmonic generator (3HG) using TypeII/TypeII KDP crystals. The output beam is reflected by the corner reflector at the distance 100m. The reflected light passes the ND

filters and the dispersion prism and illuminates the photocathode of the streak camera (Hammamatsu C979 /7/). The streak image is recorded by the SIT TV camera and processed in the Temporal Analyser Hammamatsu C1098. The digitalised data from the Temporal analyser are on-line transfered to the HP65 calculator (one streak window/15 seconds) for processing, statistical treatment, display, plot and storing. The data may be off-line processed on the HP1000 computer.

During the initial stage, the indoor experiment was carried out. The statistical treatment of the laser pulse length gives the value 34+/-4.5 psec at 0.53um (raw data). The histogram of pulse length is on fig.2. Assuming the 30um slit width and 4psec/channel, the deconvoluted value of the typical pulse length is 30 psec. The measured pulse length at 0.35 um is 20psec.

To obtain a smooth streak record of a pulse and hence the required time resolution, several hundreds photons are necessary. This value is consistent with the value of 570 photons published in /6/. The streak readout system permits to process two windows of one streak image simultaneously. This way, both pulses at different wavelength are recorded at the same time and thus we eleiminated the streak trigger jitter. The cross sweep streak image distorsion was testet and found to be below resclution limit. On fig.3 there is a record of the 0.53 and 0.35um signals. The time delay of in the indoor pass 6+-2psec was determined on the basis of 8 measurements (the histogram of measured values is on fig.4).

During the ground target ranging stage the corner cube retroreflector has been placed at 100 meter distance. The typical streak record at 0.53/0.35um is on fig.5. Due to a complex far field pattern structure of the 2-nd/3-rd harmonics, the two colours were not fully spatialy resolved on the streak input apperture. Totaly, 23 strak measurements were made during 20 minutes. The histogram of the measurements is on fig.6. The mean of the delay is 22psec, the RMS is 4.5psec. Refering to the indoor experiment (0.53/0.35um, TD=6+-2psec), the corrected outdoor two wavelength time delay is therefore 16psec, RMS=5psec. Taking into account the atmospheric conditions of that day, the calculated value /7/ of the 0.53/0.35um TD is 16psec. To increase the confidence of our results, more data would be perhaps necessary to obtain.

L i t e r a t u r e

1/ The Second Workshop on the Laser Tracking Instrumentation, edited by.J.Weifenbach and K.Hamal,Prague,1975

2/ J.B.Abshire, Applied Optics 19,No20,1980,3436-3440.

3/ V.N.Lisitsin et. all, Quantum Electronics,9,198, p 609,(in russian)

4/ H.Jelinkova, Mode Locked Train YAG Laser Contact Cell Preprint Series FJFI No. /64

5/ K.Hamal, to be published

6/ Picosecond Streak Camera and its Aplications, Picosecod, Vol 14, June 1983, published by Hamamatsu Corp., Japan
7/ J.W.Marini, C.W.Murray, "Correction of Laser Tracking Data for Atmospheric Refraction at Elevations Above 10 Degrees" GSFC X-591-73-351, November 1973

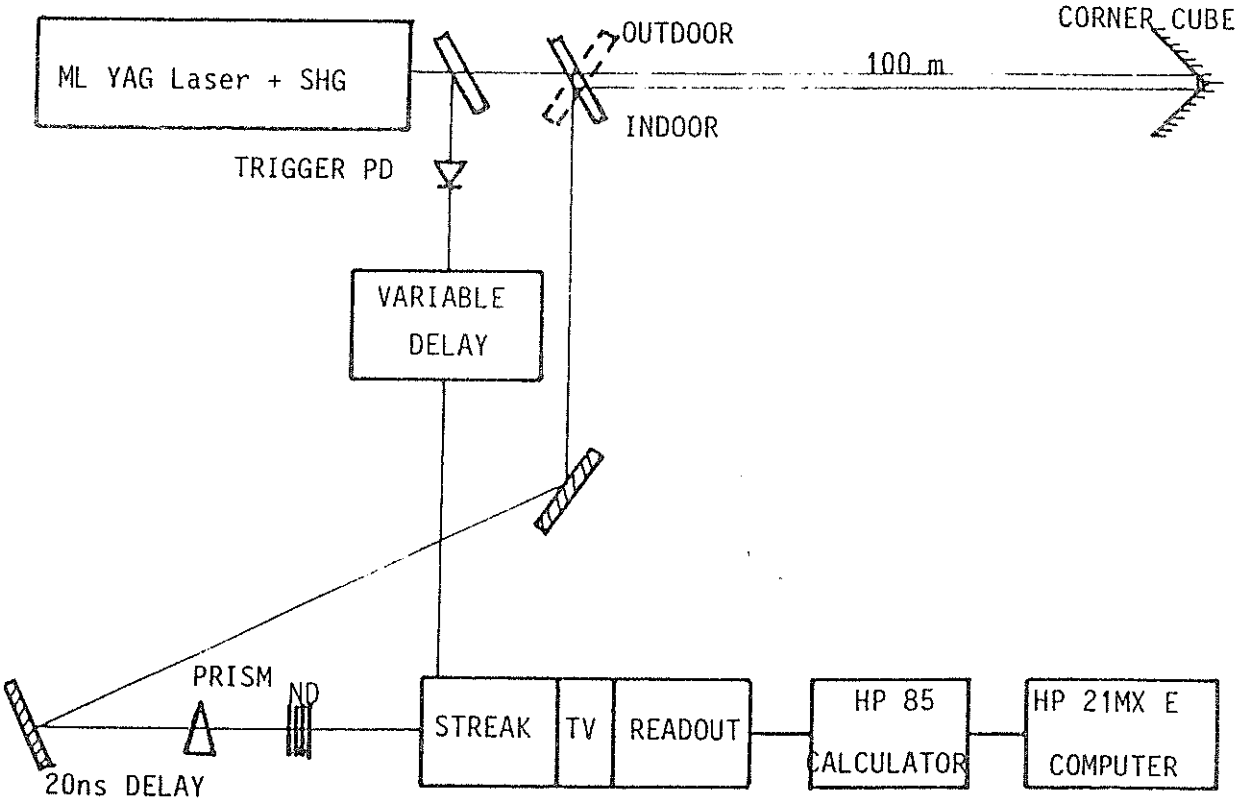

BLOCK SCHEME OF THE TWO WAVELENGTH PICOSECOND RANGING EXPERIMENT

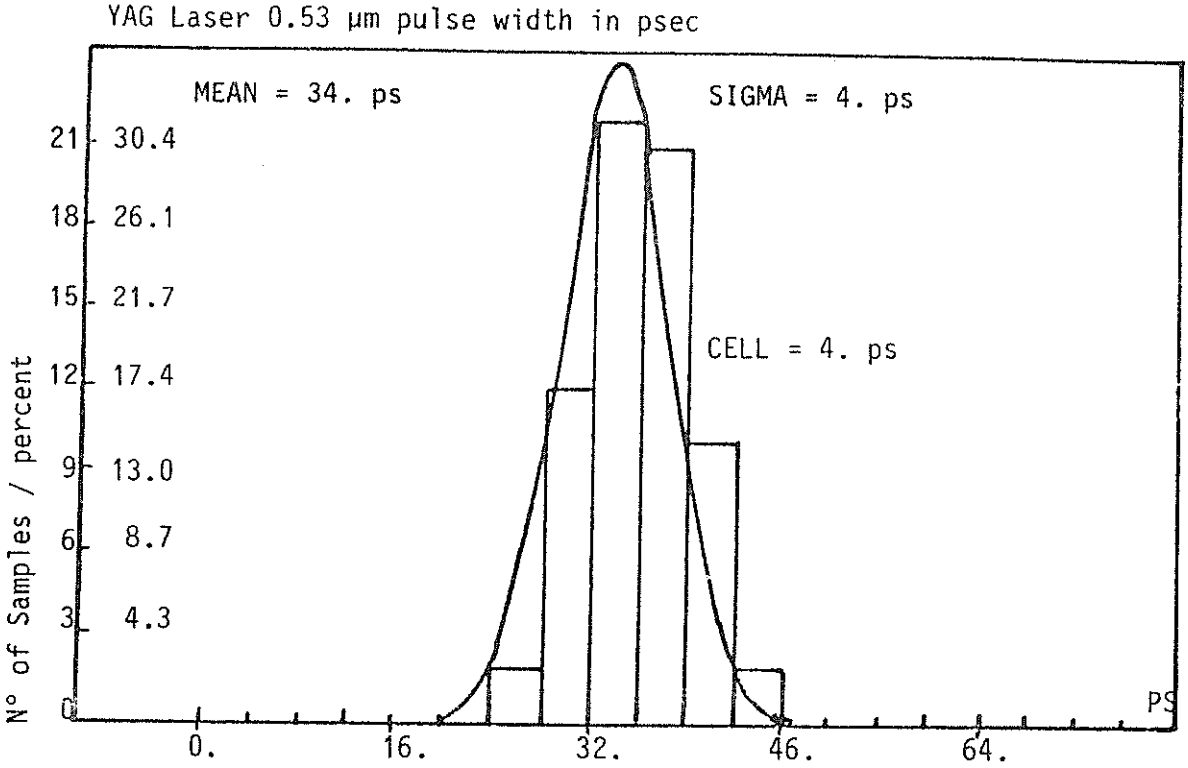

HISTOGRAM OF THE LASER 0.53 µm PULSE LENTH

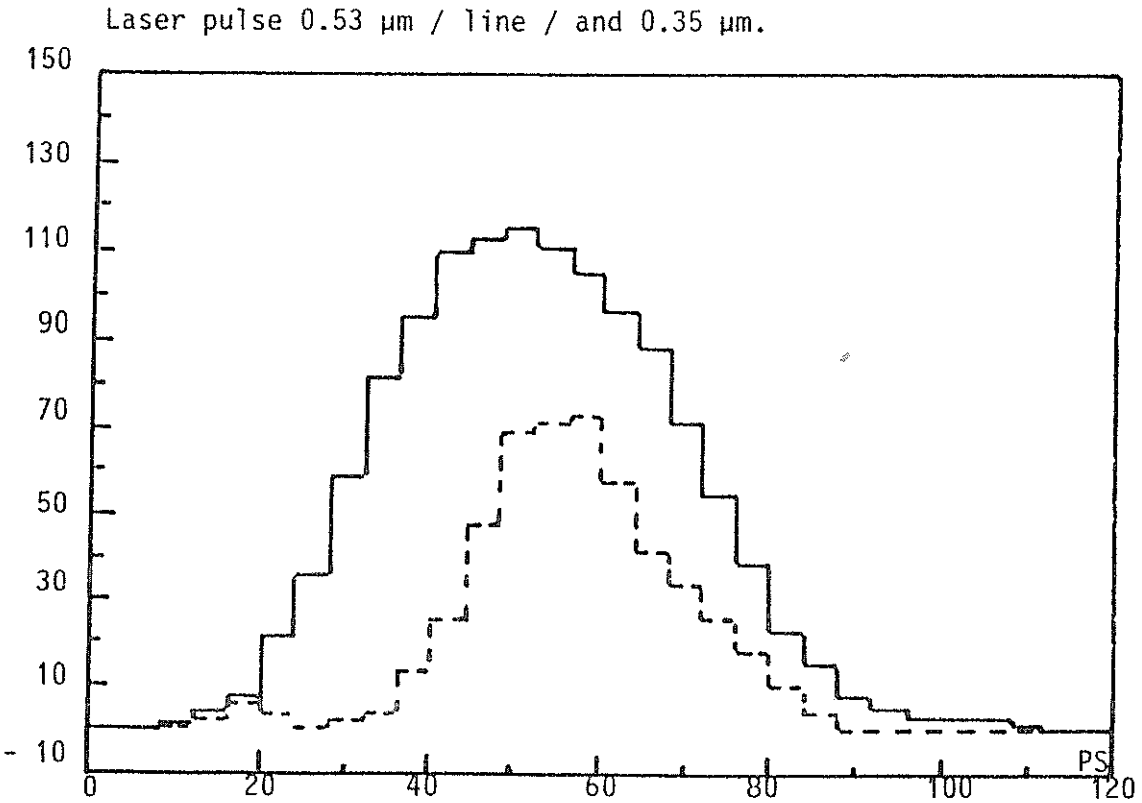

STREK RECORDS OF THE 0.53 AND 0.35 µm PULSES

Indoor 0.53/0.35 μm time delay / two windows /

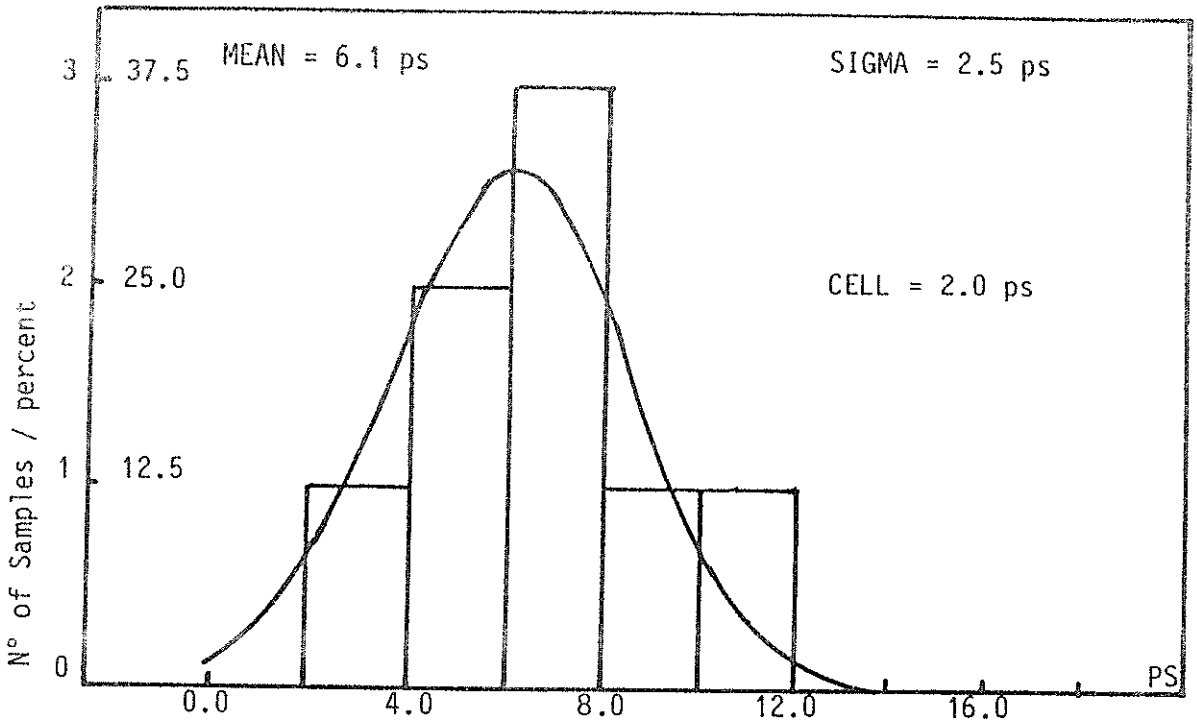

HISTOGRAM OF 0.53/0.35 μm TIME DELAY / INDOOR /

Green + Blue ext. target (106 m) ranging

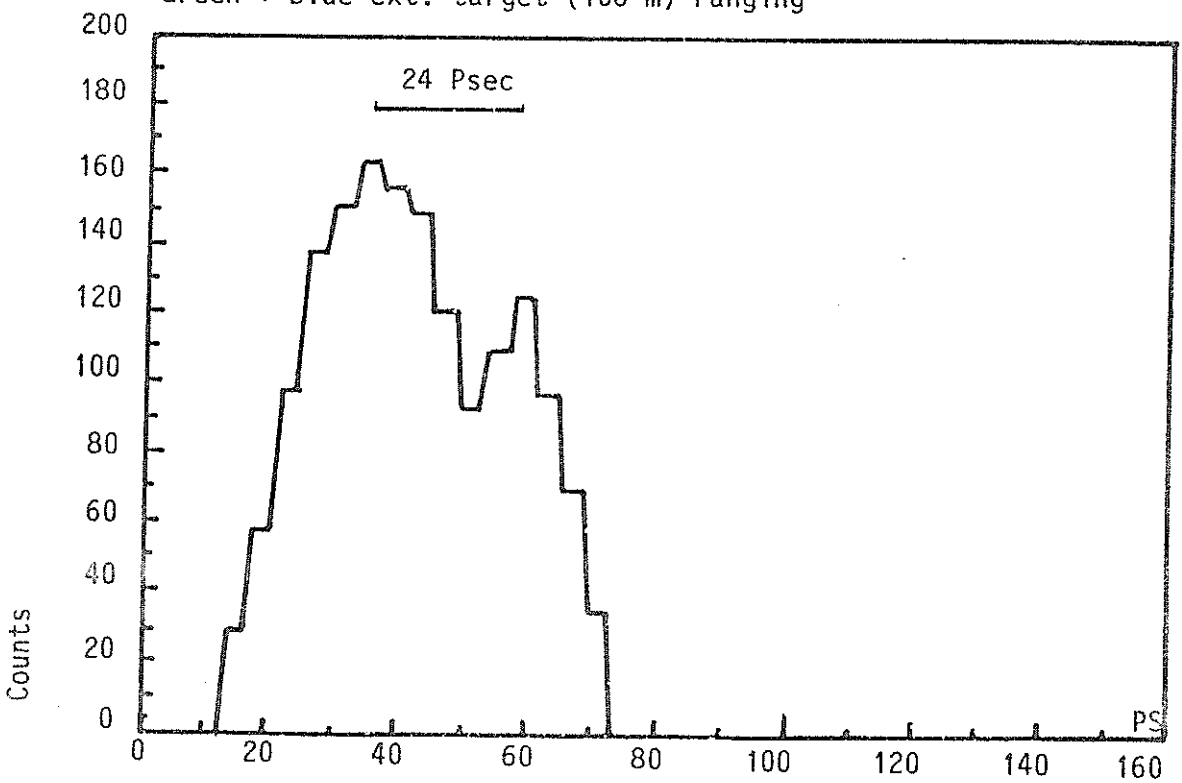

STREAK RECORD OF GROUND TARGET 0.53/0.35 μm RANGING

Ground target 0.53 /0.35 µm time delay (17.4.1984)

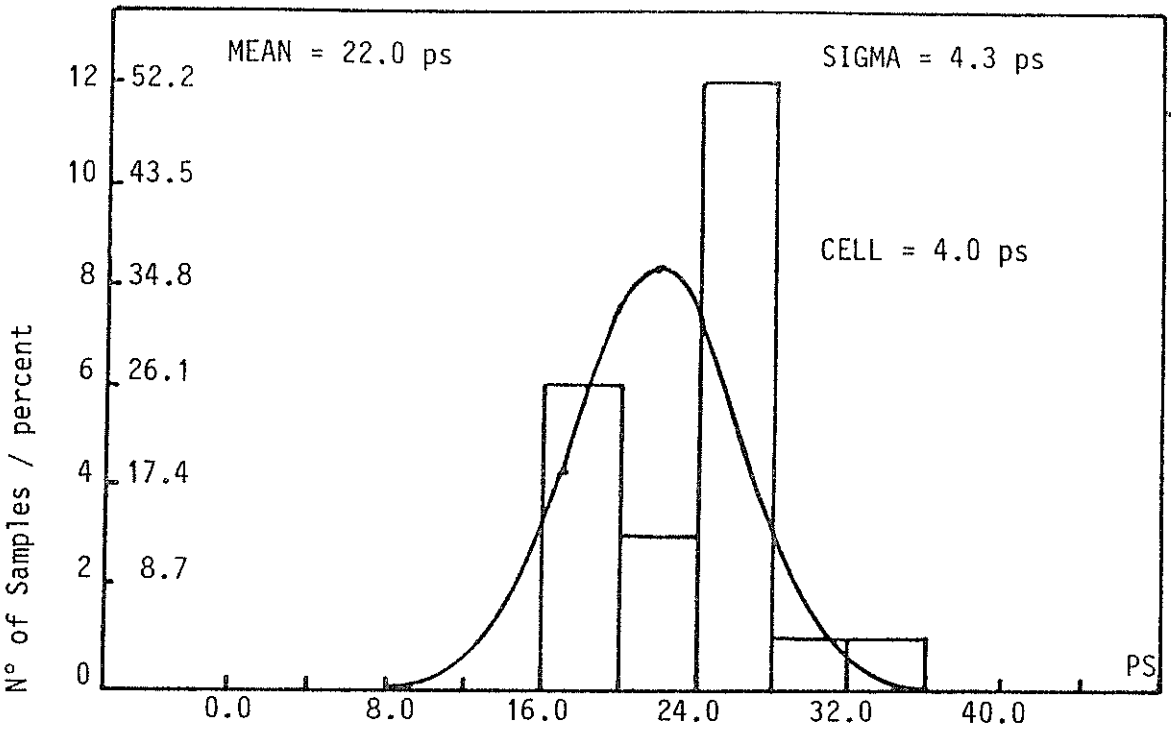

HISTOGRAM OF 0.53/0.35 µm DELAY / GROUND TARGET /

LASER RADAR INDOOR CALIBRATION EXPERIMENT

K. Hamal, I. Prochazka
INTERKOSMOS
Faculty of Nuclear Science and Physical Engineering
Czech Technical University
Brehova 7, 115 19 Prague 1 Czechoslovakia

Telephone (2) 84 8840
Telex 12 1254

J. Gaignebet
C.E.R.G.A.
Avenue Nicolas Copernic 06130 Grasse France

Telephone (93) 36 58 49
Telex 470 865

ABSTRACT

To range the satellites, we are using the train of picosecond pulses generated by Nd YAG oscillato/amplifier/second harmonic generator laser system. To establish an optimum discriminator/timing system, the indoor calibration experiment was carried out. The results indicate a limit single shot uncertainty 6cm RMS.

LASER RADAR INDOOR CALIBRATION EXPERIMENT

To obtain the system internal noise level below 10cm at the Interkosmos laser radar in Helwan /1/, the picosecond laser was implemented. To establish the optimal detector/discriminator/timing configuration, to decrease the ranging chain jitter and to increase the system stability, the extensive set of calibration experiments was completed. The aim of the calibrations was to measure the timing jitters of the most critical parts of the ranging chain.

The scheme of the calibration set up is on fig.1. The passively mode locked YAG laser /2/ generating a train of pulses was used. The resonator round trip time was 1.6nsec, The idividual pulse width 70 psec. Most of the energy was contained in 2-3 pulses. The laser output was frequency doubled to 0.53um. As the high resolution timing system, the Tranzient Digitizer Tektronix 7912AD, together with the appropriate software package, is used. The bandwidth of the system is 500MHz, its resolution is 512x1024 (time x amplitude) ,the fastest sweep is 1upsec/channel. The Tranzient is interfaced via HP85 to the master computer HP21MX with a 50MByte disc storage. The image data are recorded on line on the disc file with the repiate 0.3 frames/second. Completing the measurement series (100-500 events), the measured data are processed off line. A powerfull software package for data processing was prepared. It enables: smoothing the recorded images, pulse processing for radar purposes, modelling of various types of discriminators, computing the pulse amplitude, risetime, energy, etc. The triggering jitter of the Tranzient together with the proper function of the software were tested by the series of tests, using uniform calibration pulses. The measured trigger jitter was 25psec.

The START detector jitter calibration

To proceed the mode locked train of pulses properly, the special type photodiode/discriminator scheme is used /4/. The Tranzient is externaly triggered by the output signal of the START detector under test. The laser output signal, monitored by the fast photodiode, is displayed (the switch in a/ position). The time spread of the recorded pulses determines the detector jitter, its mesured RMS is 150psec. Simultaneously, processing the set of laser output records, the useful

information about the laser output stability, train length, etc. may be obtained /3/. The measured value of the START detector jitter is in table 1.

Single photoelectron PMT jitter calibration

The block scheme is on fig.1, the switch in position b/. The Tranzient was externaly triggered by the START discriminator pulse, the laser output pulse was attenuated and reflected to the PMT (RCA8852) input. The light was focused to the small area near the photocathode center. The PMT output signal was amplified by the 26dB/1200MHz amplifier and fed to the Tranzient. Using the ND filters, the received signal intensity was adjusted to single PE level (typically 100 echo PE from 1000-3000 laser shots). The no detected PE images were omitted, the recorded ones were processed by a program, which converts the data into the range values. Processing one image, four different range values are available, each one corresponding to one ideal discriminator of the type:

1. fixed threshold
2. constant fraction
3. centroid
4. maximum.

These range values were processed by the mode locked train YAG laser ranging data processing software package /5/. The resulting values of signle PE photomultiplier jitter are summarised in table 1. The lowest jitter was measured for an ideal constant fraction discriminator type (340psec).

PMT/discriminator jitter measurement

To determine the optimal PMT/discriminator (RCA8852/Ortec473A) configuration, the special experiment was carried out. Using the Tranzient digitizer the mutual position of the PMT output pulse and the discriminator output was measured. The PMT output pulse was devided, one part was fed to the discriminator input, the other was delayed and fed to the Tranzient input. The Tranzient was triggered by the discriminator output. The PMT dark noise signal was used for this test. The measured data were converted into the rangig data form using the software described above (constant fraction discriminator). Then, the jitter could be evaluated. This way, the deviation of the real constant fraction discriminator from the ideal one was determined.

Conclusion

The error budget of the laser radar ranging electronics was measured to be 0.41nsec (6cm). The main contribution to this value is due to the PMT RCA8852 single PE transit time jitter. To compare the indoor/outdoor measurements, the histogram of laser calibration series measured at the laser station in Helwan (July 1984) is shown on Fig.2. (In fact, the RCA31034A PMT is used on this station, but according to /7/,/8/ and our experience, their timing performance is the same.)

Literature

1/ K.Hamal,H.Jelinkova,A.Novotny,I.Prochazka,M.Fahim B.Baghos,A.G.Massevich,S.K.Tatevian, Interkosmos Laser Radar, Version Mode Locked Train, in this Proceedings
2/ K.Hamal, I.Prochazka,M.Cech,P.Hirsl,H.Jelinkova,A.Novotny, 2.Generation Laser Radar /INSATLAS2.2./ Mode Locked Train Experiment No.1 /indoor/, FJFI Preprint Series 191/83
3/ K.Hamal,I.Prochazka,M.Cech,P.Hirsl,H.Jelinkova,A.Novotny 2.Generation Laser Radar /Insatlas 2.2./ Mode Locked Train Experiment No. 2, FJFI Preprint Series No. 195/83
4/ M.Cech, Start Discriminator for the Mode Locked Train Laser Radar, in this Proceedings
5/ I.Prochazka, Mode Locked Train Laser Ranging Data Processing in this Proceedings
6/ EG&G Ortec 473a Constant Fraction Discriminator,Operating and Service Manual,USA
7/ R.W.Engstrom, RCA Photomultiplier Handbook published by RCA Solid State Division,Lancaster,USA,1980
8/ S.K.Poultney, Single Photon Detection and Timing: experiments and Techniques, Advaces in Electronics and Electron Physics, Vol.31, Academic Press, New York 1972

START detector		150 psec	/4/
PMT (RCA8652)	fixed threshold	(350 psec)	
	constant fraction	340 psec	applied
	centroid	(350 psec)	
	maximum	(470 psec)	
STOP dicriminator (Ortec 473A)		100 psec	/6/
flying time counter (HP5360)		150 psec	
Ranging electronics error budget		410 psec (6cm)	
		**********	

Table 1.

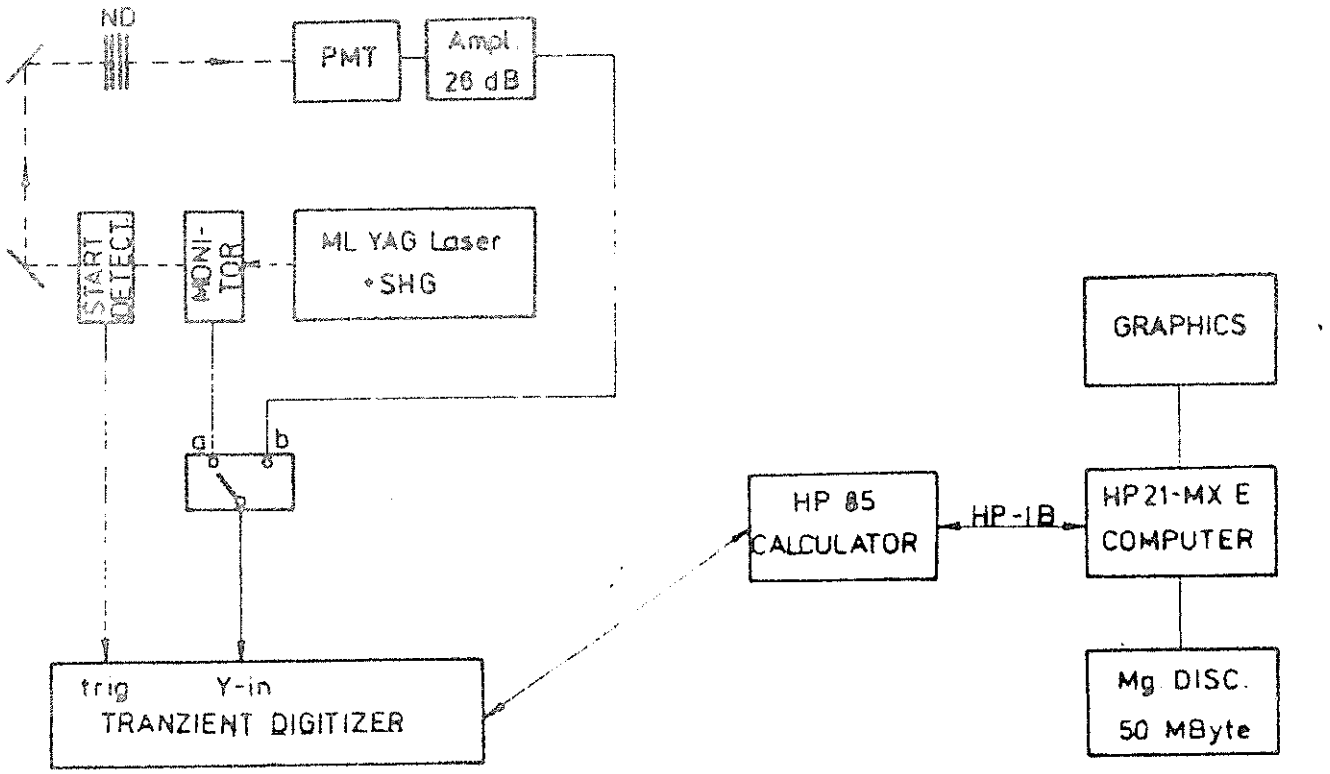

Indoor calibration experiment block scheme.

Fig. 1.

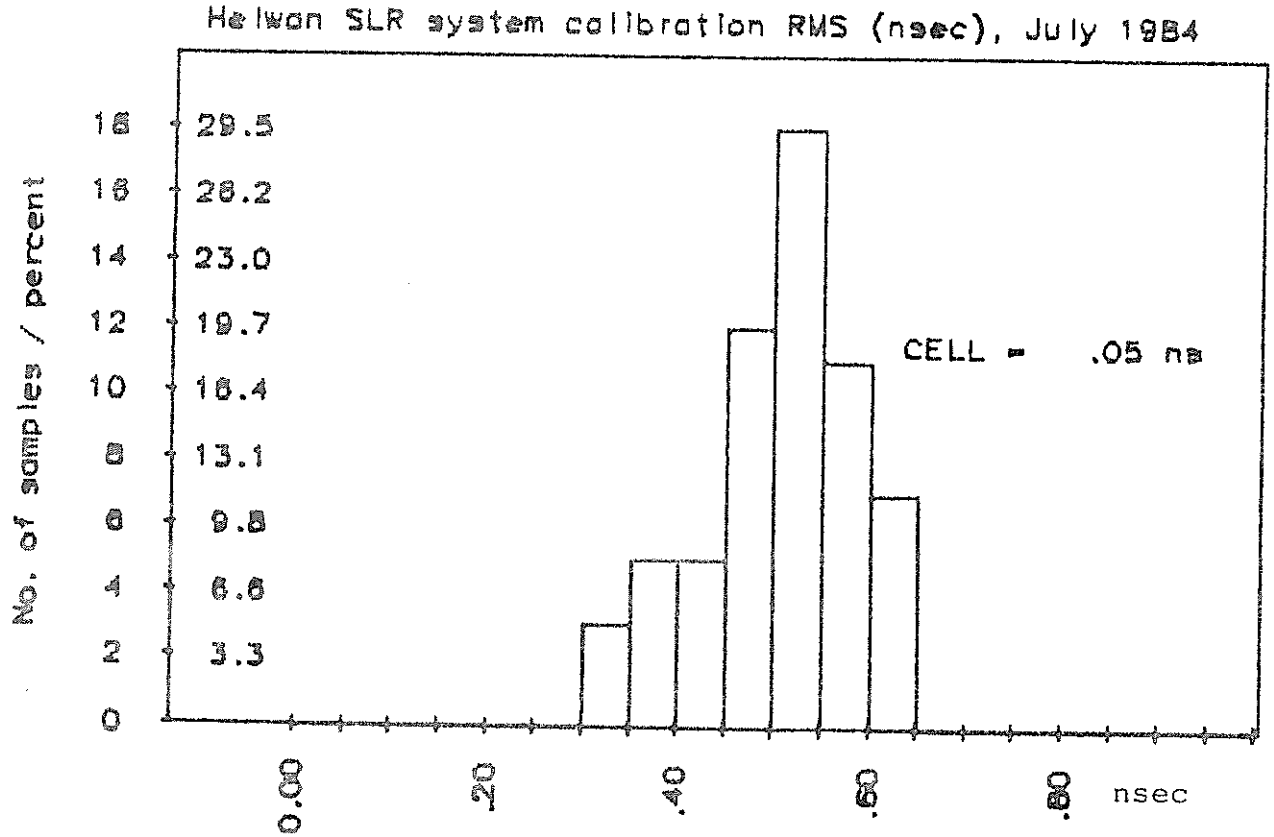

Histogram of SLR system calibration /internal pass/ RMS, station Helwan, period July 1984.

Fig. 2.

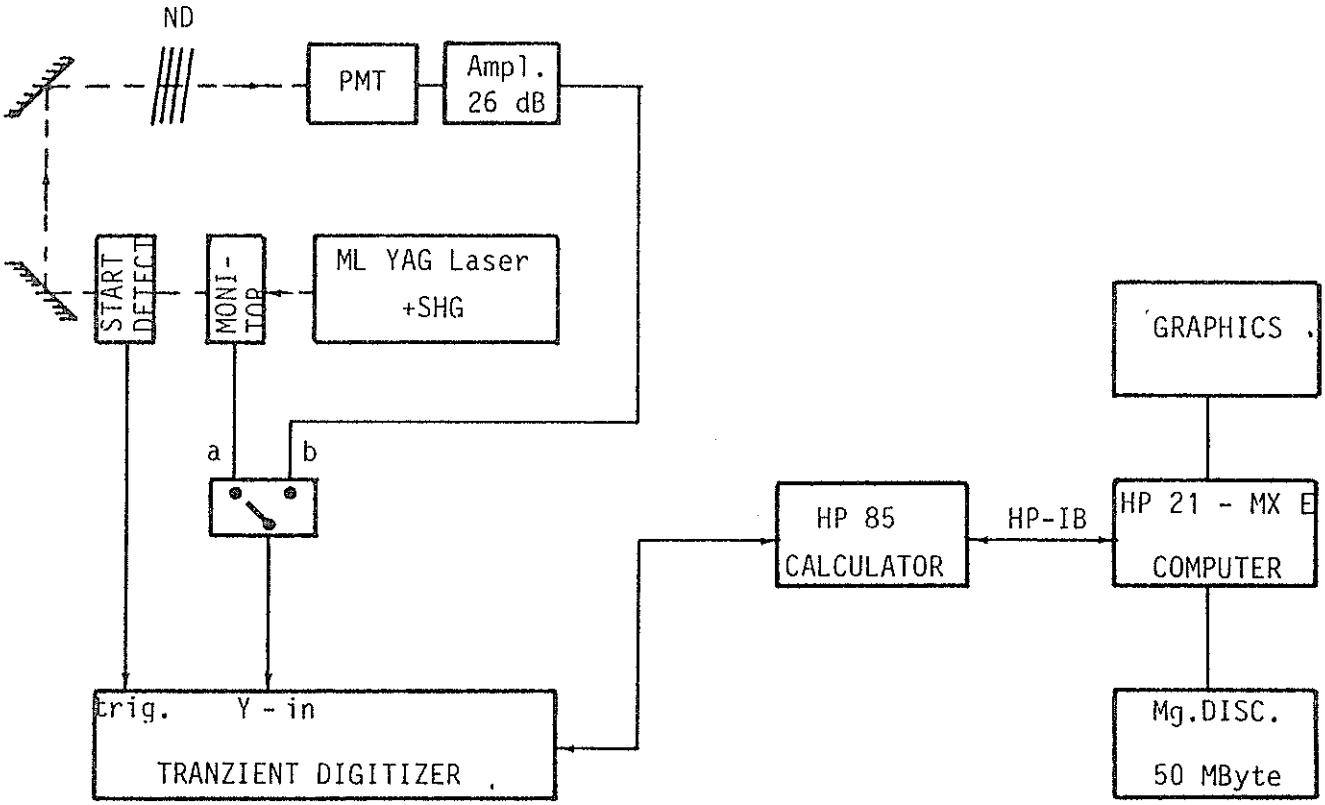

INDOOR CALIBRATION EXPERIMENT BLOCK SCHEME

- FIG. I -

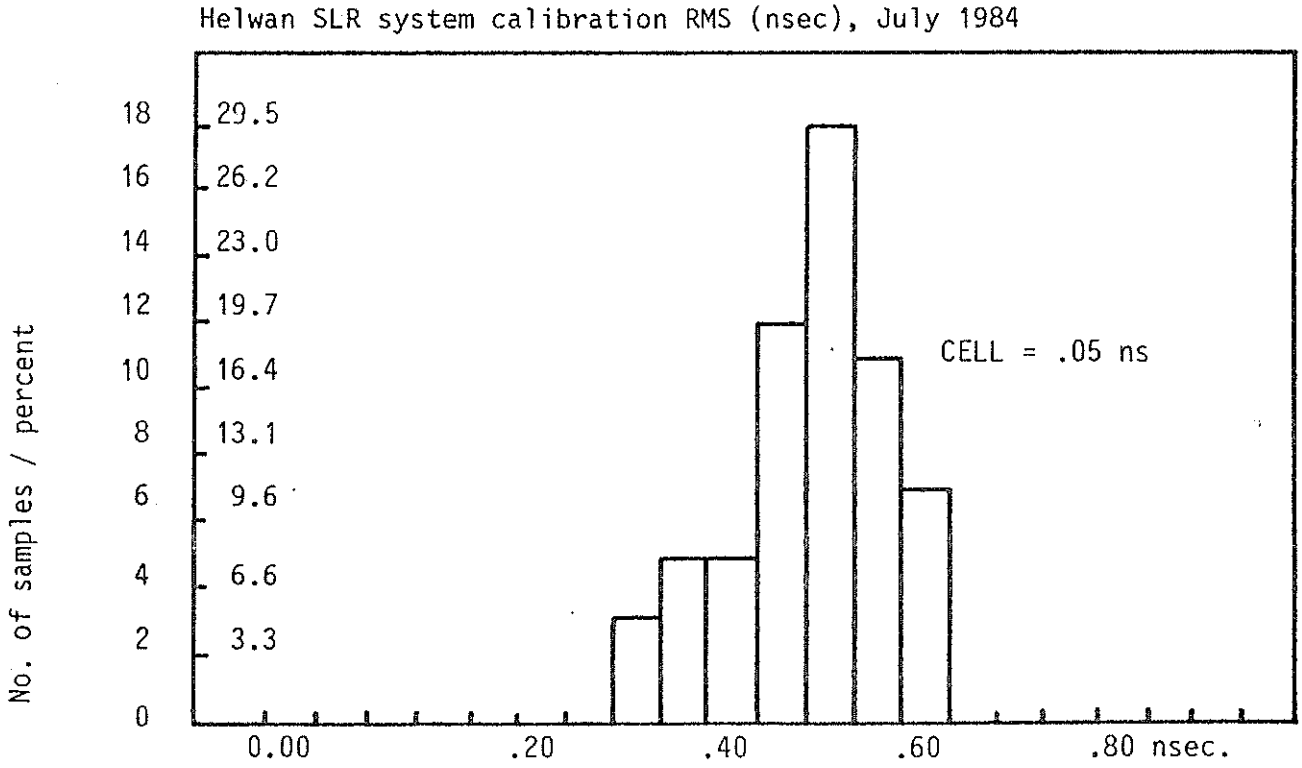

HISTOGRAM OF SLR SYSTEM CALIBRATION /INTERNAL PASS/ RMS, STATION HELWAN, PERIOD JULY 1984.

- FIG. II -

FURTHER DEVELOPMENT OF THE NLRS AT ORRORAL

B.A. Greene
Division of National Mapping
PO Box 31
Belconnen ACT 2616 Australia

Telephone 062 525095
Telex 62230

ABSTRACT

The recently commissioned Natmap Laser Ranging System is described and some initial performance figures given. The development program for the system is briefly outlined. The fundamental goals of the program are to maximise precision, accuracy, and efficiency in SLR and LLR modes. From an initial capability near the state of the art, developments are outlined which will produce sub-centimetre SLE precision to any satellite within 10 seconds under even marginal meteorological conditions over the next 12 months. Preliminary considerations of multi-Gigawatt LLR lasers and multi-wavelength SLR are given.

FURTHER DEVELOPMENT OF THE NLRS AT ORRORAL

1. Current Status

The Natmap Laser Ranging System (NLRS) is now fully operational to LAGEOS, and is under development for Lunar ranging operations in late 1984. The principal characteristics of the NLRS can be given as:

Telescope aperture	:	1.5 metre
Pointing accuracy	:	3 arc seconds
Laser	:	QUANTEL YG402-AP
Computer System	:	HP A700
Receiver	:	RCA 31034A
Single shot precision	:	7 cm
10 second precision	:	1 cm (LAGEOS)

The NLRS is currently performing adequately to LAGEOS, obtaining 5-15000 hits/pass, depending on conditions. It has a day/night capability.

2. Short Term Developments

The random current errors of the NLRS are due to:

Laser pulse width	:	300 ps
PMT/Receiver	:	400 ps
Timing	:	200 ps

These represent the NLRS at initial configuration, which will be altered for the first 4-5 months of operation.

Commencing early in 1985, several changes will be made to the system which will improve performance. The laser pulse width selected will be reduced to 50 ps for all SLR operations. The PMT will be replaced by a new Microchannel Plate PMT with a Transit-Time jitter specification of 100 ps (max), and a rise time of 30 ps (max).

These modifications alone should reduce the single shot uncertainty to better than 4 cm, and the 10 second normal point precision to 6 mm (for LAGEOS).

Other significant improvements planned for 1985 are in the AUTOTRACK capabilities of the system. Currently, a significant proportion of the LAGEOS data is obtained without any operator assistance in guiding (i.e. absolute pointing to LAGEOS). It is expected that as the station coordinates of the site become better defined and our in-house ability to 'improve' our predictions using previously observed data improves, the dependence upon an operator will diminish significantly. The goal is to obtain 100% of LAGEOS observations without operator intervention in the long term.

The AUTOTRACK developments extend also to LLR observations. Since the mount model for the 1.5m telescope can be better than 3 arc seconds on any night (it is not stable at this level for more than 1 night), absolute pointing and guiding seems feasible, perhaps with some minimal search pattern capability added.

3. Long Term Developments

3.1 SLR Precision

The single largest error in the ranging system after the laser and receiver have been modified (above) will be the timing system (200 ps/event). An improvement in this area to 50 ps would give 2 cm single-shot precision immediately. A multi-stop, 50 ps precision timing system is under development.

If the laser is tuned to 30 ps pulse width, the system error budget becomes:

Laser	:	30 ps
Timing	:	50 ps
PMT/Receiver	:	100 ps
RSS		116 ps or 1.8 cm

Theoretical studies are currently being undertaken into the viability of using a streak camera as an additional vernier for the timing system to give 10 ps precision. Preliminary work indicates that the total random error budget for such a system could be 50 ps, resulting in sub-centimetre single shot precision.

3.2 LLR Data Density

The single most effective way of improving LLR system performance is to increase the laser power. Such a development is being considered for Orroral. The objection is to obtain 300 mJ in a single 100 ps pulse, or 800 mJ in a train of four 100 ps pulses, at 10 Hz. Alternatives to slab laser configurations are being actively pursued, and some feasible designs have been put forward which would reach the performance goal without the need for a slab. However, very significant performance improvements for Nd:YAG lasers will come from solid state pumping systems now under

development in other laboratories. If adequate performance can be maintained in the short term using the existing laser, then it is likely that further development of the laser will await developments in solid-state pumping.

3.3 Multiple Wavelength Ranging

Even preliminary examination of the two wavelength technique reveals the considerable difficulties inherent in the technique. However, if SLR ranging will be, from 1985, of 1 cm precision (normal point) for a large proportion of the ranging stations in operation, then it may be necessary for one or two stations to acquire a data base of two colour ranging data for purposes of 'calibrating' the atmospheric correction formulae. The Orroral system has some unique advantages for performing this experiment.

1. large telescope with very precise pointing and high quality Coude optics

2. extensive computing facilities on site

3. extensive optical and electronic facilities

4. colocation with a national time and frequency calibration laboratory

5. site weather characteristics much like most of the rest of the network.

For these reasons the topic is kept under review, so that when the accuracy requirement for SLR exceeds 1 cm, a decision could be made to attempt to range at more than one wavelength.

The streak camera which can operate as a 10 ps timing vernier can be adapted to determine the differential return epoch of the two returns with 10 ps (possibly even better) precision.

AN OVERVIEW OF NASA AIRBORNE AND SPACEBORNE LASER RANGING DEVELOPMENT

J.J. Degnan
Instrument Electro-Optics Branch, code 723
NASA Goddard Space Flight Center
Greenbelt, MD 20771 USA

Telephone (301) 344 7000
TWX 710 828 9716

ABSTRACT

Beginning in the mid-Seventies, there was a great deal of scientific and technical interest in the development of a Spaceborne Geodynamics Ranging System (SGRS) which would be capable of making global geodesy measurements to a dense network of relatively inexpensive, passive, ground-based retroreflectors. It was argued that such a system would provide a vastly larger and more timely data set for the study of tectonic plate motion and regional crustal deformation relative to what could reasonably be achieved with ground-based satellite laser ranging (SLR) systems. The data could be further augmented and densified through the development and use of relatively low cost aircraft-based systems. Modest funding during the period from 1975 to 1983 permitted the completion of various fundamental engineering, scientific, and simulation studies and the development of several prototype hardware components and software packages. The present article gives a brief history of NASA and recent European efforts in airborne and spaceborne laser ranging, summarizes the scientific ans technological achievements, provides a bibliography which permits readers to obtain more detailed information, and speculates on possible future development activities.

AN OVERVIEW OF NASA AIRBORNE AND SPACEBORNE LASER RANGING DEVELOPMENT

Beginning in the mid-Seventies, there was a great deal of scientific and technical interest in the development of a Spaceborne Geodynamics Ranging System (SGRS) which would be capable of making global geodesy measurements to a dense network of relatively inexpensive, passive, ground-based retroreflectors. It was argued that such a system would provide a vastly larger and more timely data set for the study of tectonic plate motion and regional crustal deformation relative to what could reasonably be achieved with ground-based satellite laser ranging (SLR) systems. Furthermore, it would accomplish this feat at a greatly reduced cost. Modest funding during the period from 1975 to 1983 permitted the completion of various fundamental engineering, scientific, and simulation studies and the development of several prototype hardware components and software packages.

The original system concept assumed a Space Shuttle-Borne system which utilized a frequency-doubled, Q-switched Nd:YAG laser with a seven nanosecond pulsewidth as the source. This concept was driven, to a very large extent, by the availability of relatively compact, hardened military lasers which had flown and operated successfully in rather hostile, high altitude, fighter aircraft environments. A reasonably concise account of the spaceborne concept and simulations of system performance can be found in references 1 and 2. A detailed engineering analysis is available in reference 3 and a summary of the proposed science applications can be found in reference 4.

It soon became apparent, however, that the anticipated 10 to 20 cm accuracy of the system was not going to satisfy the rapidly burgeoning number of science applications which were now demanding accuracies on the order of one to two centimeters. This fact spurred NASA to develop space-qualifiable prototype components which would permit ranging from a space platform to ground-based retroreflectors with centimeter accuracy. These included: (1) a compact, 10 mJ (green), 200 picosecond pulse, modelocked Nd:YAG laser transmitter[5,6]; (2) a low time walk constant fraction discriminator[7]; (3) a 19.7 picosecond resolution event timer (ET)[8]; (4) a 9.7 picosecond resolution time interval unit[9,10]; (5) a high-speed, arcsecond accuracy pointing mount and all-digital controller[11,12]; and (6) large cross-section, ground reflectors. In addition, developmental work began on a circularly scanned streak tube (CSST) receiver intended to improve the receiver impulse response by almost two orders of magnitude[13]. The latter acts as a vernier on the "coarse" receiver which primarily consists of a high-speed photomultiplier (e.g., the ITT 4129 microchannel plate photomultiplier having a 450 picosecond impulse response), a low time walk discriminator, and a high-resolution time interval unit.

The transmitter/ "coarse" range receiver combination typically yields 5 millimeter one sigma precisions in horizontal range experiments over kilometer long paths. Bias errors in the range map to a fixed retro-reflector are at the subcentimeter level as reported previously[14]. The limiting resolution of the prototype CSST receiver (when the program was terminated due to funding cuts) was about 33 picoseconds and was due to an inability to focus the electron beam image adequately within the tube.

The SGRS pointing system requirements were rather unique in that, in addition to being able to track with arcsecond precision at rates up to two degrees per second, the system required a slew velocity of 200°/sec and a maximum angular acceleration of 500°/sec^2 in order to acquire and track multiple ground based targets. The final engineering prototype met all of the SGRS requirements. The tracking mount supports a 32cm by 19cm elliptical mirror constructed of lightweight beryllium. Sixteen-bit incremental optical encoders, augmented by precision measurements of the phase of the quadrature detector outputs, yield an effective 23-bit resolution angular position in each of the two axes. The optical mount is driven by a "smart" all-digital, microprocessor-based controller. This frees up the main driving computer by requiring tracking updates only once a second consisting of a position, angular velocity, and angular acceleration. The microprocessor interpolates between updates using the resulting second order polynomial in the time variable at a rate of 512 times per second for each axis. Math models for system dynamics, bearing friction, stiction, etc., are used in Kalman Filtering algorithms to maintain system pointing and tracking accuracies. A plot of the measured RMS tracking jitter versus tracking rate is shown in Figure 1. Except near the maximum tracking rates, the tracking jitter is at the subarcsecond level. A more complete written description of the full range of pointing system tests and results is in preparation.

In 1979, the original SGRS hardware was upgraded to a subnanosecond system based on the previously mentioned hardware prototypes and renamed the Global Geodynamics Ranging System (GGRS). The GGRS was reconfigured as a free flyer instrument compatible with the Multimission Modular Spacecraft (MMS)[15]. The latter spacecraft can be launched from either Shuttle or NASA's Delta Rocket. The proposed GGRS package included two modelocked transmitter heads with a single power supply in order to extend the mission life to approximately 3 years for a combined geo-dynamics and ice altimetry mission. The GGRS concept did not incorporate the CSST receiver since the latter was still undergoing development.

Unfortunately, the funding necessary to begin development of a fully space-qualified system never materialized. Thus, in 1980, a concept for a six beam Airborne Laser Ranging System (ALRS) was developed[16,17] as an intermediate, low-cost, alternative which would simultaneously provide useful geophysical data on a regional scale and demonstrate the technical feasibility of the global spaceborne system. In these earlier versions of the ALRS, we planned to use a LORAN C navigator and a pressure altimeter to provide navigational updates to the aircraft to aid in acquisition and tracking of the ground retroreflectors. In the most recent version, however, we propose to use a GPS receiver to update the three position

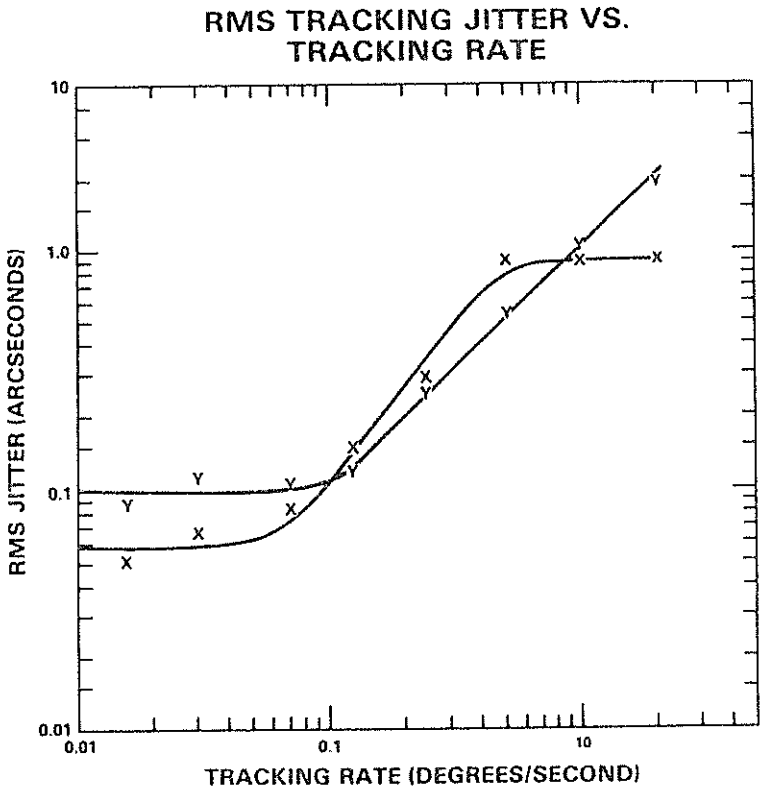

FIGURE 1: ROLL (X) AND PITCH (Y) TRACKING JITTER

coordinates since the GPS system is now nearing operational status. A block diagram of the current scheme is shown in Figure 2. From 1980 to 1982, the ALRS was actively studied and simulated. The NASA Lockheed Orion was chosen as the host aircraft. From this aircraft, baseline precisions of 1 cm per 30 Km of baseline could be achieved. High flying aircraft, such as NASA's ER-2 research aircraft, would yield the same precision over 100 Km baselines. Optomechanical designs for the ALRS were generated, components were procured, and assembly of selected subsystems was begun. The development of operational, navigational, and data analysis software packages was well underway. Target sites in the area of Shenandoah, Virginia, were chosen for the initial test flight. The Shenadoah area is convenient to the Goddard Space Flight Center and to the aircraft's home field at Goddard's Wallops Flight Station, has a terrain which varies widely in altitude above sea level thereby simulating most of the interesting fault regions, and contains approximately 17 first order survey monuments providing excellent ground truth information. Funding cuts brought all ALRS hardware work to a halt in 1982 but system simulations continued into 1983.

In an attempt to salvage the program, a concept for a greatly simplified (and even less expensive) airborne system was developed and named the Broadbeam Laser Surveyor (BLS)[18]. A block diagram of the system is shown in Figure 3. It uses a 100 mJ (green) modelocked laser such as the Quantel YG402 DP and distributes the energy over a 70 degree half-angle cone via an axicon. A matching, wide field-of-view receiver collects returns from any retroreflectors lying within the transmitter field-of-view and focuses them onto a single, high-speed photomultiplier. The system uses a multiple-stop time interval unit to record the multiple times-of-flight and contains no moving parts.

Operation of the BLS would be limited to low altitudes (less than 4 km) and to night flights due to the high daytime background noise resulting from the wide instrument field-of-view. The principal technology barrier to this instrument was the development of a practical receiver collecting lens which would simultaneously provide the ±70 degree field-of-view and an effective aperture on the order of two inches. Recent in-house studies have resulted in a realistic lens design. It is hoped that our basic advanced laser ranging funds will permit us to build and flight test a breadboard of this very simple system by 1986.

At the present time, NASA has no active program in the area of airborne or spaceborne laser ranging. However, during the past year, some discussions were held between the United States and Italy for a possible joint program to develop first the airborne and then a spaceborne system, but, to my knowledge, no agreement has yet been reached between the two countries. NASA/Goddard has recently proposed the single-color GGRS as an instrument on the Earth Observation System platform. The latter is a proposed experimental platform to be placed in an approximate polar orbit in the 1993 time frame and periodically visited and maintained, probably on a biannual basis, by crews from Space Station. The ability to refurbish the package on a periodic basis removes one of the major obstacles to the free flyer concept, i.e., the limited operating lifetime of the laser as

AIRBORNE LASER RANGING SYSTEM

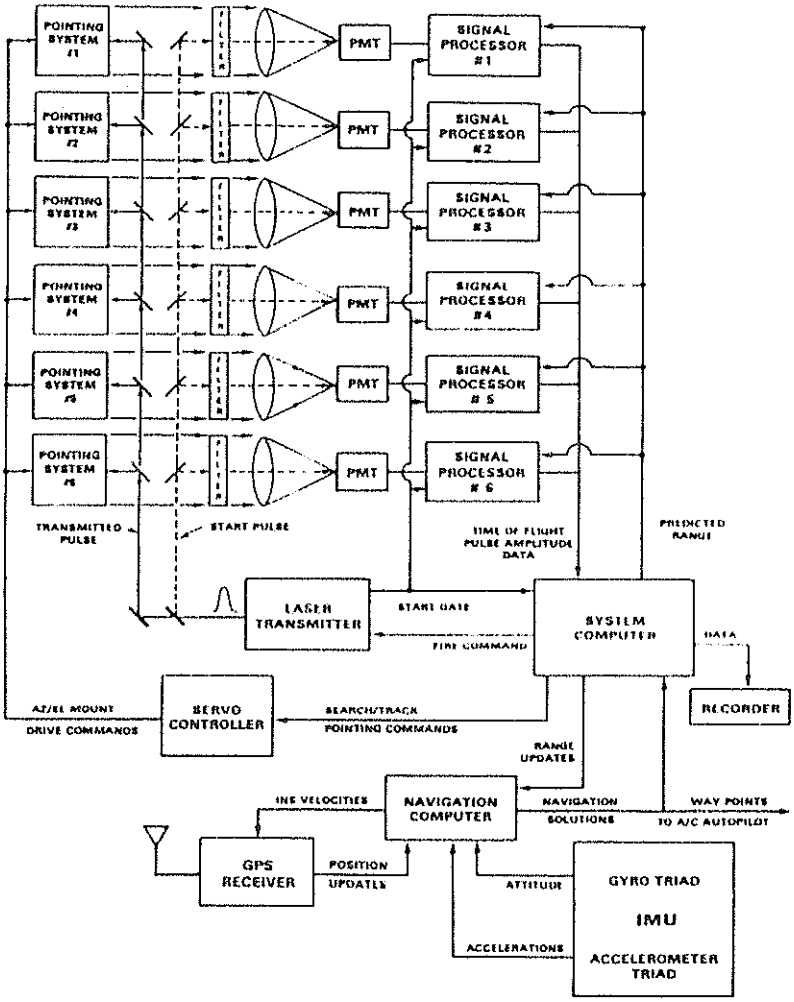

FIGURE 2

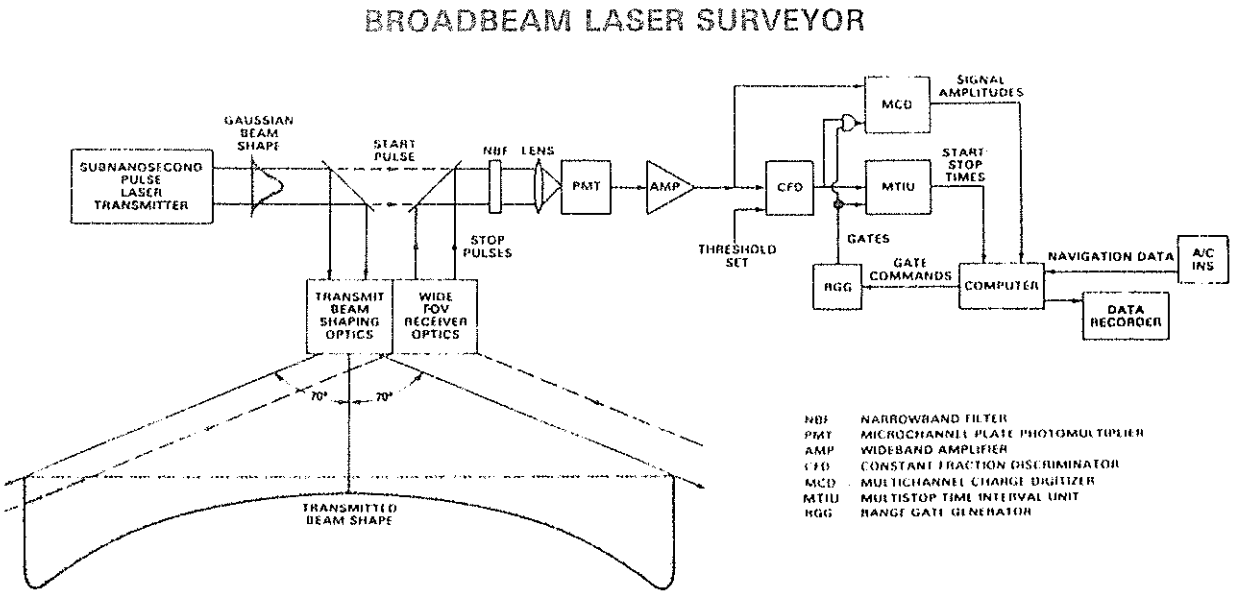
BROADBEAM LASER SURVEYOR
SUBNANOSECOND PULSE LASER TRANSMITTER
GAUSSIAN BEAM SHAPE
START PULSE
NBF
LENS
PMT
AMP
CFD
MCD
SIGNAL AMPLITUDES
MTIU
START STOP TIMES
THRESHOLD SET
GATES
RGG
GATE COMMANDS
COMPUTER
NAVIGATION DATA
A/C INS
DATA RECORDER
STOP PULSES
TRANSMIT BEAM SHAPING OPTICS
WIDE FOV RECEIVER OPTICS
70°
70°
TRANSMITTED BEAM SHAPE
NBF NARROWBAND FILTER
PMT MICROCHANNEL PLATE PHOTOMULTIPLIER
AMP WIDEBAND AMPLIFIER
CFD CONSTANT FRACTION DISCRIMINATOR
MCD MULTICHANNEL CHARGE DIGITIZER
MTIU MULTISTOP TIME INTERVAL UNIT
RGG RANGE GATE GENERATOR

FIGURE 3

determined by the flashlamp life (typically 10^7 shots). Alternate laser pumping schemes, however, such as pumping the Nd:YAG laser material with arrays of AlGaAs diode lasers may ultimately lead to a system with an operational lifetime two orders of magnitude longer.

Recently, a European group has studied a spaceborne laser ranging system which utilizes a two-color, picosecond pulse Alexandrite laser[19,20] and a second system which uses a CO_2 laser and superheterodyne transceiver[21]. NASA/Goddard also plans to explore mode- locked Alexandrite beginning in 1985. We have believed for some time that the fundamental and second harmonic frequencies of Alexandrite at 760 and 380 nm are near ideal for the two-color application because of their good atmospheric transmission, excellent detector quantum efficiencies, and good relative dispersion by the atmosphere. The wide gain bandwidth also permits the generation of pulsewidths on the order of a few picoseconds. One also eliminates the need for the relatively inefficient nonlinear generation of the third harmonic of Nd:YAG. The Alexandrite laser medium has a higher pump threshold than Nd:YAG, however, and therefore would require significantly more spacecraft prime power.

Spaceborne laser ranging faces stiff competition from proponents of the Global Positioning System (GPS) geodetic receiver approach who believe that their systems are also capable of yielding one centimeter accuracies in spite of a difficult water vapor calibration problem. The Global Positioning System satellite constellation is already partially in place and will almost certainly be completed. It therefore becomes a relatively inexpensive proposition to build and test geodetic receivers which make use of a system whose existence is a foregone conclusion even though the eventual operational costs of a global geodetic program might be prohibitively high. Furthermore, the GPS receivers have the decided political advantage that they are technically similar to devices already fielded by various user agencies and hence are a more "familiar" technology to those users.

A recent study[22] carried out by ORI, Inc., under contract to NASA Headquarters, compared the relative costs of a ten-year, global, geodetic campaign using on the one hand, GPS receiver techniques and, on the other, a spaceborne laser ranging system launched and periodically refurbished by the Space Shuttle. The study concluded that, within the probable error bounds (which in the present author's opinion are quite high), the ten-year costs of the GPS and GGRS approaches are comparable. The study did not attempt to address the relative quality of the data from a scientific standpoint.

REFERENCES

1. M. W. Fitzmaurice, P. O. Minott, and W. D. Kahn, "Development and Testing of a Spaceborne Laser Ranging System Engineering Model," NASA TM X-723-75-307, NASA/Goddard Space Flight Center, Greenbelt, MD 20771, USA, November 1975.

2. F. O. Vonbun, W. D. Kahn, P. D. Argentiero, D. W. Koch, and K. J. Eng, "Spaceborne Earth Applications Ranging System," NASA TM X-71035, NASA/Goddard Space Flight Center, Greenbelt, MD 20771, USA, December 1975.

3. E. A. Paddon, "Synthesis and Analysis of Precise Spaceborne Laser Ranging Systems," Final Report, McDonnell Douglas Astronautics Company-East, St. Louis, MO 63166, USA, Volumes 1 and 2 (MDC E1729), August 1977.

4. "The Report from the Workshop on the Spaceborne Geodynamics Ranging System," Institute for Advanced Study in Orbital Mechanics, The University of Texas at Austin, Austin, Texas, USA, IASOM TR79-2, March 1979.

5. R. H. Williams, L. L. Harper, and J. J. Degnan, "Ultrashort Pulse Solid-State Laser Development," presented at Laser '78, Orlando, Florida, USA, December 1978.

6. "Nd"YAG Laser Development for Spaceborne Laser Ranging System," International Laser Systems, Inc., Orlando, FL 32804, USA, NASA/GSFC Contract NAS5-22916, Phase I Final Report (February 1979), Phase II Final Report (December 1981).

7. B. Leskovar, C. C. Lo, and G. Zizka, "Optical Timing Receiver for the NASA Spaceborne Ranging System Part I: Dual Peak-Sensing Timing Discriminator, Lawrence Berkeley Laboratories. LBL-7274, NASA/Goddard Space Flight Center Contract NDPR S-40220B, January 1978.

8. B. Leskovar and B. Turko, "Optical Timing Receiver for the NASA Laser Ranging System Part II: High Precision Event-Timing Digitizer," Lawrence Berkeley Laboratories, LBL-6133, Lawrence Berkeley Laboratories, Berkeley, CA 94720, USA, LBL-8129, August 1978.

9. B. Turko, "A Picosecond Resolution Time Digitizer for Laser Ranging," IEEE Trans. Nucl. Sci., MS-25, No. 1, pp. 75-80, February 1978.

10. T. Zagwodzki, "Testing and Evaluation of a State-of-the-Art Time Interval Unit," NASA/Goddard Space Flight Center, Greenbelt, MD 20771, USA, TP-1051, September 1977.

11. "Final Technical Report: SGRS Pointing System Study, Volumes I and II," TRW Defense and Space Systems Group, Redondo Beach, CA 90278, NASA/GSFC Contract NAS5-23454, November 1978.

12. R. J. Brown, "Digital Control for the SGRS Mirror," Navtrol Company, Dallas TX 75243, USA, NASA/GSFC Contract NASA5-26891, January 1983.

13. C. B. Johnson, S. Nevin, J. Bebris, and J. B. Abshire, "Circular Scan Streak Tube with Solid-State Readout," Applied Optics, Vol. 19, pp. 3491-3495, October 1980.

14. J. J. Degnan and T. W. Zagwodzki, "A Comparative Study of Several Transmitter Types for Precise Laser Ranging," Proceedings of the Fourth International Workshop on Laser Ranging Instrumentation, Austin, TX, USA, pp. 241-250, October 1981.

15. "Global Geodynamics Ranging System (GGRS) Feasibility Study," General Electric Company Space Division, Valley Forge, PA, USA, GE Document No. 79SDS4245, NASA/GSFC Contract NAS5-23412, Mod. 175, August 1979.

16. J. Degnan, "Airborne Laser Ranging System for Rapid Large Area Geodetic Surveys," Proceedings of the Fourth International Workshop on Laser Ranging Instrumentation, Vol. II, Austin, Texas, USA, pp. 447-454, October 1981.

17. J. Degnan, W. Kahn, and T. Englar, "Centimeter Precision Airborne Laser Ranging System," J. Surveying Engineering, Vol. 109, No. 2, pp. 99-115, August, 1983.

18. J. Degnan, "Airborne Laser Ranging System for Precise Geodetic Surveys and Land Control," Proceedings of the International Symposium on Land Information at the Local Level, Orano, Maine, USA, August 9-12, 1982.

19. H. Lutz, W. Krause, and G. Barthel, "High Precision Two-Color Spaceborne Laser Ranging System for Monitoring Geodynamic Processes," Space 2000, pp. 236-254, 1983.

20. "Assessment of Technology Requirements Associated with Spaceborne Laser Ranging: SPALT Task 1 Final Report," Deutsches Geodätisches Forschungsinstitut, Munich, Germany, ESA Contract 4405/80/NL/HP(SC), DGFI Project No. 1/80/SPALT, June 1981.

21. "Study of Spaceborne Laser Range and range Rate Finder," Messerschmitt-Bolkow-Blohm GMBH, Space Division, RX12, Ottobrunn, Munich, Germany, ESTEC Contract No. 3883/79/NL/HP(SC), MBB Contact No. R 3700/2773 R, March, 1980.

22. E. Eller, N. Roman, and A. Wellen, "Life Cycle Cost Comparison of Four Space Technologies for Crustal Motion Measurement," ORI, Inc., Silver Spring, MD 20910, USA, May 1984 (draft), to be published.

SINGLE-SHOT ACCURACY IMPROVEMENT USING RIGHT FILTRATION AND FRACTION VALUES IN MULTI-PHOTOELECTRON CASE

W. Kielek
Faculty of Electronics
Technical University of Warsaw
00 665 Nowowiejska street 15 19 Warsaw Poland

Telphone 48 22 21007653 / 48 22 253929
Telex 813307

ABSTRACT

The approximate analytical formulas for the errors due to discrete generation and gain of photoelectrons and due to delay jitter in photomultiplier tube for the fixed threshold and constant fraction of the current and charge are given. The error is dependent on the filtration and fraction value. Also some simulation and experimental results are given, of reasonable agreement with the theory. Existing stations can be somewhat improved in some cases, using proper filtration and fraction values following the results presented.

SINGLE - SHOT ACCURACY IMPROVEMENT USING RIGHT FILTRATION AND FRACTION VALUES IN MULTI-PHOTOELECTRON CASE

1. Introduction

The signal at the anode of real PMT with the delay jitter is the same as in the case of ideal PMT without jitter, whose photocathode is illuminated by the equivalent signal pulse of the same energy, whose shape is the convolution of the signal pulse shape and the delay density curve of the real PMT. In the case of very short signal pulse, this equivalent shape is the shape of the PMT delay density curve only. Single - shot accuracy is dependent on the width of this equivalent shape. For the realisations of the received signal of more than single photoelectron, there exists the possibility to improve this accuracy using some processing of the signal, for example linear filtering before applying a constant or proportional threshold for the PMT current or charge. The part of the linear filter is the PMT itself, whose single photoelectron response curve convoluted with the pulse response of the eventual electric filter after PMT gives the response of the overall linear filtering. Author obtained the approximate analytical solutions for the error dependence on the filtration and threshold value, confirmed by simulation and experiment.

2. Results

Using some results of the inhomogeneous filtered Poisson process theory, one can obtain the formula for the normalised random time interval error, valid for all pulse signal shapes and all pulse responses of the filter in the limit case of sufficiently high number of photoelectrons in the signal:

$$\sigma_\Delta / T = g \alpha^{1/2} N^{-1/2} \qquad (1)$$

where: T is the measure of the equivalent signal pulse width, equal of the σ parameter of the gaussian equivalent signal pulse, or equal to the half of the width of equivalent signal pulse for the other shapes; α is the mean square of the normalised to 1 gain of the PMT tube; N is the mean photoelectron number in the signal; g - coefficient dependent on the shape of the equivalent signal, overall filter response shape and width, and on the threshold (fraction) value.

For the gaussian equivalent signal and filter response, g coefficient values vs fraction and filtration values are given by formulas (2), (3) and (4), and at the Fig. 1, 2, and 6, for the fixed threshold of the current, constant fraction of the current and constant fraction of the charge, respectively. Filtration parameter F at the Figs 1 and 2 is the filter res-

ponse width divided by σ parameter of the equivalent signal, when the z parameter in formulas is the square of the relation of σ parameter of the signal to σ parameter of the filter. Fraction f in the case of c.f. it is the fraction of the peak value in each realisation, when in the case of fixed threshold, it is the threshold value divided by the expectation of the peak value.

$$g^2 = \frac{(1+z)^2}{z \cdot \sqrt{2z+1}\; 2 f^2 \ln \frac{1}{f}} \cdot \exp\left(-2\,\frac{z+1}{2z+1}\ln\frac{1}{f}\right) \quad \ldots(2)$$

$$g^2 = \frac{(1+z)^2}{z \cdot \sqrt{2z+1} \cdot f^2 \ln \frac{1}{f}} \cdot \qquad (3)$$

$$\cdot\left\{\frac{1}{2}\exp\left[-2\,\frac{z+1}{2z+1}\ln\frac{1}{f}\right] - f\cdot\exp\left[-\left(\frac{z^2}{2z+1}+1\right)\ln\frac{1}{f}\right] + \frac{f^2}{2}\right\}$$

$$g = \left[2\pi f(1-f)\right]^{1/2}\left\{\exp\left[-(\text{inv erf}_* f)^2/2\right]\right\}^{-1} \qquad (4)$$

where $\text{erf}_* x = (1/\sqrt{2\pi})\int_{-\infty}^{x}\exp(-y^2/2)\,dy$

3. Comments

The results for the fixed threshold case are comparably poor (Fig 1); the best value of g is about 1.5. For the c.f. of charge, the results obtained for no additional filtration before integration of the current [formula (4)] are given at Fig. 6. The optimum fraction is 0.5, which holds also for any symmetric bell-shaped, triangular and other with distinct peak, shape of the equivalent signal. Using some linear filtration before the integration one can obtain g smaller than 1 (simulation results of Ojanen [1] and Kiełek). Bias changes with energy exist for the unsymmetric in time filter response only but are small (Fig. 5, simulations). For the fraction 0.5, this method is sometimes called as median, or half-area detection. The results for c.f. of the current are mostly surprising. The g coefficient improves and approaches 1, the value for some optimum estimation methods as conditional mean [2] and max. likelihood [3], when the filtration value F increases (Fig. 2). The optimum fraction value changes from 0.26 for small F values to 1 for $F > 2$ (Fig. 3). The dependency of g vs fraction f is small when F exceeds 4 (Fig. 2). The g coeff. is also energy dependent (Fig. 4, simulations), but for $F > 2$ the dependency is small for $N \geqslant 10$. Mean value of the result change vs energy are smaller when increasing F and f (Fig 7, simulations, filter response $\exp[-t/(5\tau)] - \exp(-t/\tau)$, and experiment).

4. Importance of the results obtained for the laser ranging

In the analogue signal processing case, use of the very high filtration F can be risky due to the threshold instability and electric noise. The F value of 4 ÷ 7 is recommended by author for the constant fraction of the current case, and also for the approximate max. likelihood implementation using the detection of position of the maximum of filtered signal [4]. This last case is also included in author's results (Fig 2), as the case of f ≅ 1. In the range of the width of laser pulse 2 ÷ 20 ns, this F value leads to the necessity to include some electrical filter after the PMT tube. Internal F value of PMT tube itself is 6 ÷ 12 for the RCA 8852, and 1.5 for new microchannel plate units. To set F at the proper value one can use approximate formula for the response width w_f of the additional electrical filter, at least 2-pole:

$$w_f = \left[\frac{F^2}{8\ln 2} \left(w_s^2 + w_j^2 \right) - w_p^2 \right]^{1/2} \quad \ldots\ldots\ldots \quad (5)$$

where w_s, w_p, w_j are the widths of: laser pulse, single photoelectron response of PMT, and PMT jitter density full width at half max , respectively. The need of additional filter exists when the right-hand side of (5) squared gives the value greater than zero. The need of the additional filter is strongest for the stations using wide laser pulses, but when using new microchannel plate PMT's, this need exists for all pulse widths used, also the smallest. The additional filter is not necessary in case of using the amplifier or other circuitry with the 3 db cut-off frequency $0.312/w_f$ or smaller.
The fraction value should be set as high as possible. The value f = 1 can be set using the differentiation, 35-40 db amplification, and zero-crossing detection.
Peak detection types of c.f. discriminators are preferable, but there is the lack of this type instruments at the market. In case of using c.f. discriminator used in scintillation-counter technique, for instance ORTEC 473 or similar, there is the need to lengthen the delay line to the value of delay

$$t_d = \frac{1}{2} \sqrt{\frac{w_p^2 + w_f^2}{\ln 2} \ln \frac{1}{f}} \quad \ldots\ldots\ldots \quad (6)$$

5. Conclusion

Existing stations having multi - photoelectron returns and using MCP type of PMT's, or in case of other PMT's, using pulse widths greater than 2 ns, can be somewhat improved by using enough analog filtration (Fig. 2).
Above holds for the stations using c.f. discriminators and approximate max. likelihood estimation as well. For the fixed threshold, use of Fig. 1 can decrease the error.

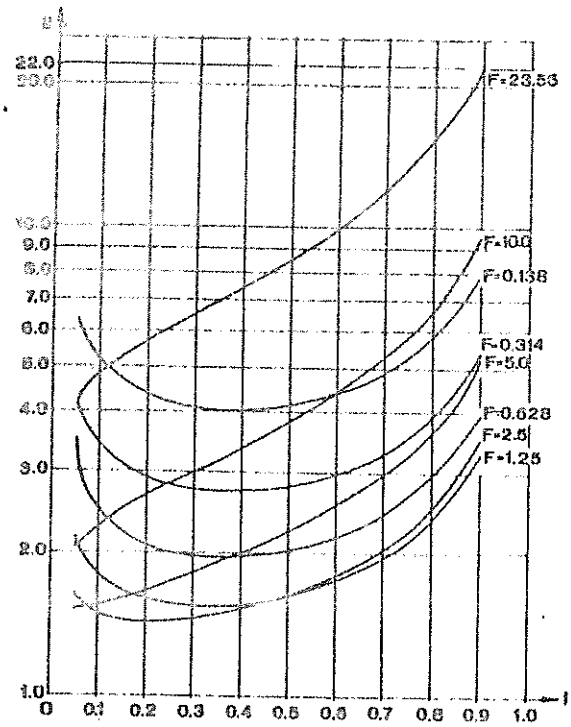

Fig.1. g coeff./form.2/

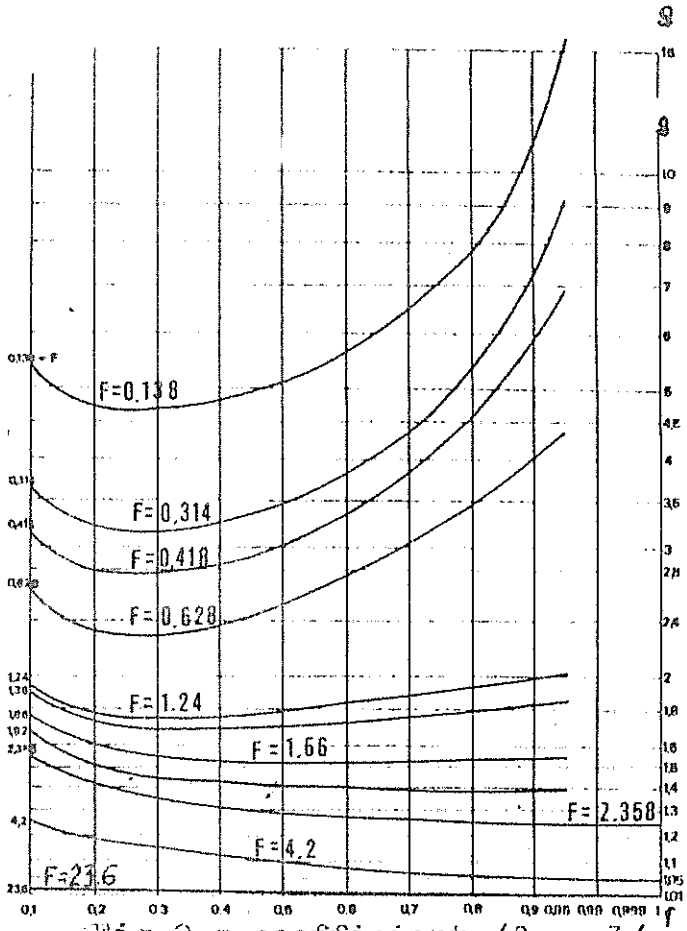

Fig.2. g coefficient /form.3/

Fig.4. g coeff.vs energy

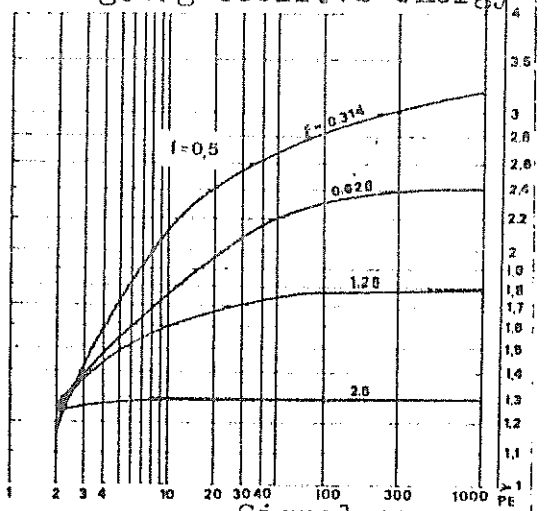

Signal energy

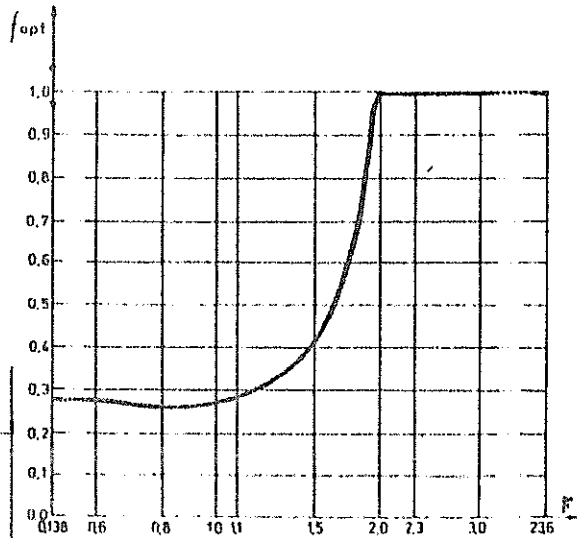

Fig.3 Optimum fraction $f_{opt.}$ vs.filtration F for c.f. of current

FIG.6

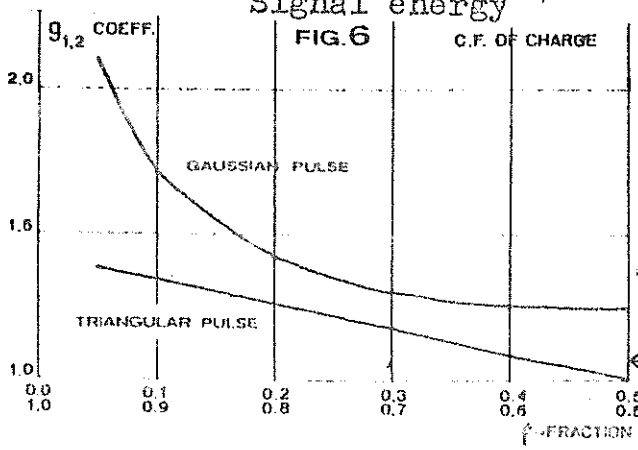

←Fig.6. g coeff./form.4/

REFERENCES

1. O.Ojanen, Reports of the Finnish Geodetic Institute No.79: 1,1979
2. I.Bar-David, IEEE Transactions on IT, May, 1975, pp.326-330.
3. I.Bar-David, IEEE Transactions on IT, vol.IT-15, No1, Jan. 1969, pp.31-37.
4. J.B. Abshire. IV-th Laser Workshop Proceedings, Vol.II. p.339.

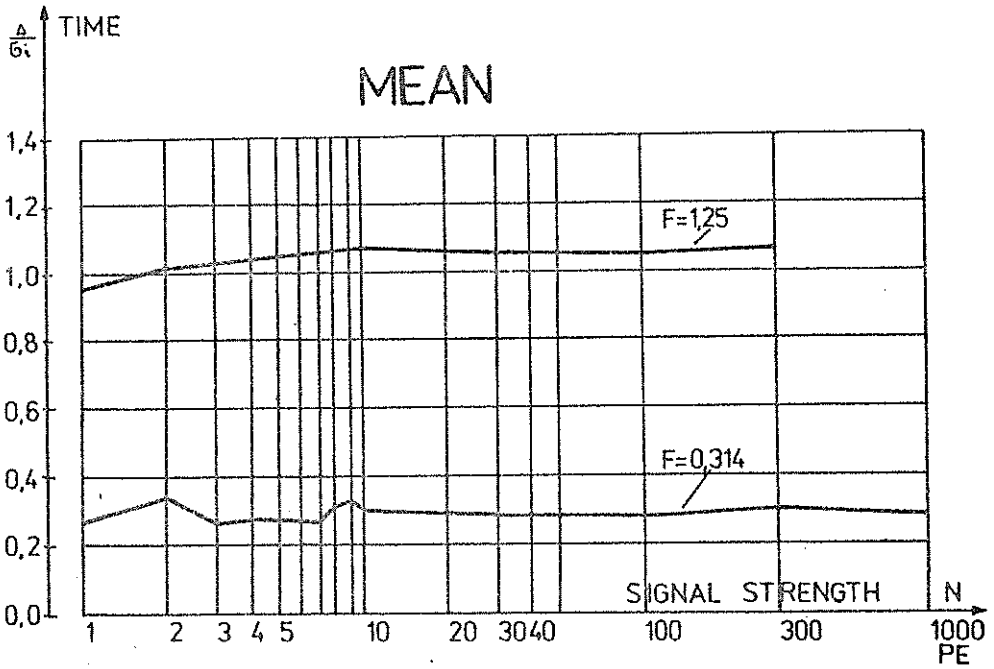

Fig.5. Mean value of result vs energy-half area case

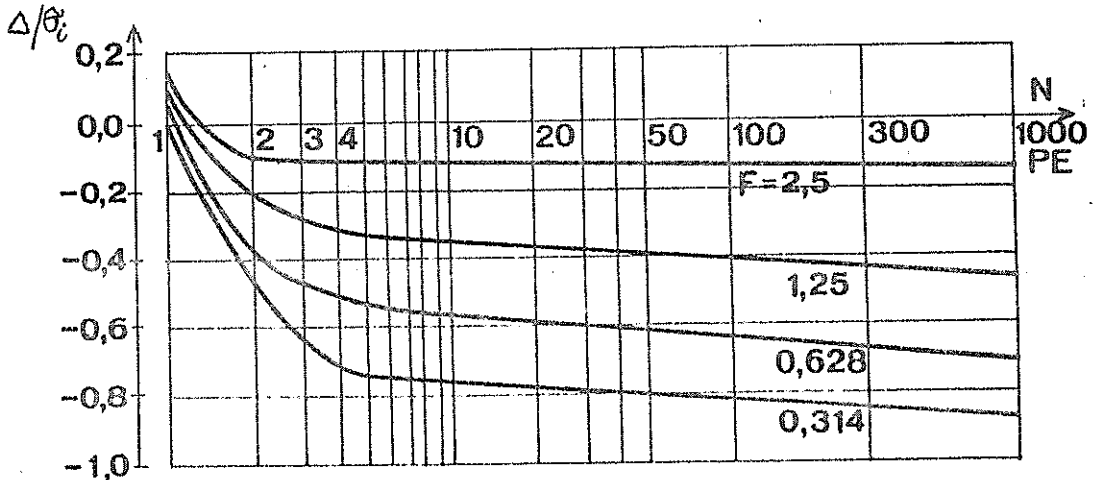

Fig.7. Mean value of result vs energy - c.f. case, f=0.5

TABLE 1

g coefficients, obtained experimentally

Fraction	Filter \ Signal energy /PE/	6	10	20	310
f=0.5	TF	1,61 /80/	1,45 /80/	1,27 /80/	1,34 /100/
	3PF , F=1.25	1,59 /180/	1,86 /220/	1,57 /260/	1,26 /100/
	3PF , F=2.5			1,32 /80/	
	3PF , F=3.75			1,20 /40/	
f≈1	TF	1,52 /40/	1,30 /40/	1,38 /240/	
	3PF , F=1.25	1,41 /60/	1,85 /100/	1,85 /300/	

g values

Filters: TF-11-section transversal filter matched to the logarithm of the signal shape.

3PF-3-pole RC filter of different filtration coefficients F.

Fraction f≈1 was obtained via zero-crossing detection in filtered and differentiated signal

Sample sizes are given in parentheses.

THERMAL EFFECTS ON DETECTORS AND COUNTERS

S. Leschiutta, S. Marra, R. Mazzucchelli,
Politecnico di Torino
Dipartimento di Electronica
Corso Duca degli Abruzzi, 24
10123 Torino Italie

Telephone 11 539 162
Telex 220646

ABSTRACT

With the centimeter accuracy approaching, also the minor uncertainty sources, such as the thermal effects on time discriminators and counters must be investigated. The behaviour of some of these devices is investigated experimentally and some results are presented.

THERMAL EFFECTS ON DETECTORS AND COUNTERS

1 Introduction

The laser ranging technique is now approaching the subcentimeter accuracy level and conseguently also the minor delay sources must be investigated.

This paper aims mainly to the thermal effects encountered in timers and time discriminators.

For the counters, the investigation was perfermed on the HP5370A device, that finds widespead use in laser ranging stations for its truly remarcable resolution of 20 ps. As time discriminators, a number of circuits were investigated, the final choice being the so called "centroid" type. In the following section the technical set up will be briefly described, while the third is devoted to the results. During these investigations also some amplitude effects and noise levels were measured and some relevant results are pointed in the fourth section. In the last, some conclusions are presented, along the planned future measurements.

2 Measurement system

The set up is depicted in Fig. 1; for the time discriminators, that can be operating outside of a building, the temperature range was -20 to +50°C; for the counter, that usually is kept in a shelter, the range was +12 to +30°C.

The temperature gradient was particulary controlled in the case of the counter, being of about 1°C/20 min, in order to allow a smooth variation of the temperature inside the device. The instrument was kept in the middle of the thermostatic chamber and a baffle was provided to shield the device from drafts coming via the conditioning system. The room in wich the testing equipment was operating, remained +1°C during the operations; sufficient time was allotted in order to reach a thermal equilibrium for all the instrumentation.

3 Results

3.1 Measurements on the counter

Two HP5370A (serial 1848A00413 and 2213A01367) were tested, with similar results; the reader is anyway warned not to extend the hereinbelow given results to other instruments of the same model, also if it seems that similar behaviours were encountered in other laboratories(1).

Since the "start" and "stop" levels can be set indipendentty via the computer, a number of measurement runs were performed at each temperature, changing the levels by steps of 50 mV, in the range 0.2 - 0.4V. The test pulse used was of 0.5V amplitude with a risetime of 2V/ns.

As a general rule, at any start and stop level, (also if different for the two channels), the counter readings increase with the temperature; this variation is roughly proportional to the temperature. There is additional evidence that, in the two instruments inspected, both levels rise with the temperature, albeit with a slight different slope.

In the particular case of same start and stop levels, the results are given in Fig. 2. The slope increases regulary with the level, and at 0.4V, shows a value of about +10ps/C°.

For any combination of trigger voltages and counter temperatures, no significant variations were observed in the fluctuation of the results, being the one-signa value around 20-25ps.

3.2 Measurement on a "centroid" time discriminator.

The time discriminator used for the temperature effect

measurements is a centroid device (2) that was presented at the 4th Workshop on laser ranging istrumentation. The circuit, with its delay line (a length of coaxial cable), was inserted in the chamber, mounted in a box, with the lid closen or open. The results are given in Fig.3; the delay slope, in the region from -20°C to +50°C, is of about -10ps/°C. In the range +15 to +25°C, the variation amounts to 120ps. With open or closed box the slope is the same, with a difference of some 150ps (Fig. 3).

It must be stressed that no particular selection or ageing of the components was previously performed.

Also in this case no significant variations were found in the fluctuations, as can be seen in table 1, in wich the absolute delay and the one-sigma standard deviation are given versus temperature; for each value, 10^3 measurements were averaged.

TABLE I

DELAY AND FLUCTUATIONS VERSUS TEMPERATURE
CENTROID DETECTOR

TEMPERATURE °C	-20	-10	0	+10	+20	+30	+40	+50
DELAY ns	6.387	6.222	6.130	6.047	5.986	5.801	5.791	5.698
STANDARD DEV. ps	27	26	25	24	25	26	25	22

4 Noise and amplitude effects on time discriminators

Three time discriminators were investigate a commercial constant level (not constant fraction) circuit, an "integrator" detector (3,4) and the abovementioned centroid device.

All the discriminators, were fed by an avalanche diode, illuminated by a laser diode pulse generator (5) sending 1000 pulses per second.

Tests on counters

The short term stability of the counters was tested with measurements lasting from 10ms to 10s.Fixed settings (1.5V) were used both for start and stop channels, that were driven via fixed delay lines from the same TTL pulse. The results for the fluctuations (one sigma values) and the relevant standard deviations (again one sigma) are given in table II.

TABLE II

COUNTER TIME STABILITY
duration of measurements seconds

	0.01	0.1	1	10
fluctuations ps	19.5	19.3	19.3	19.4
stand. dev. ps	1.35	0.47	0.1	0.1

No apparent drift is evident and the steady reduction of the standard deviation with the square rooth of time between 0.01 and 1s means that in this region we are confronted with a whithe noise process.

As regards the average fluctuations versus the pulse amplitude, the time proven rule to use settings just above half of the pulse amplitude was generally confirmed. For instance, with a trigger level of 1.5 V, the fluctuation drops sharply from 30-40ps to about 20ps, when the pulse amplitude crosses 3V.

A closer look to this behaviour has shown that, with fixed pulses and variable start and stop settings, the delay fluctuation is a non-monotonic function of the settings. This pattern depends from the pulse shape and from the individual counter and it is fairly constant. To quote some figures, with a 5V pulse and the stop level at 2.5V, the variation of the delay (one sigma value) ranges from 18 to 35ps, when the start level is changed from 1 to 4.5V. Conseguently it can be recommended to investigate for each individual counter, the "best" combination of pulse amplitudes and trigger settings.

As previously mentioned, the time discriminators were driven by an avalanche photo detector,illuminated by a solid state laser. Three devices were tested: A, fixed level discriminator; B, integrator; C "centroid", with a fixed delay line. The delay of each circuit, in nanoseconds, and the fluctuations (one sigma) in picoseconds are given in table III, for measurement durations from 0,1 to 100s.

The absolute values of the delays are of no concern, since they depend from the specific values of the circuitry; the attention is called on the variations, with time, of the delay, that anyway can be disregarded for all three circuits. The performances of the circuit A (fixed trigger levels) is remarcable,

but this solution is quite sensitive to signal amplitude variations.

Changing the slope of the electrical pulse driving the laser from 1.8 to 3.1ns and keeping constant the energy, the variations in fluctuation for circuits A and C, are less of 1ps and for circuit B of about 6ps. Conseguently discriminator B is more sensitive to e shape of the pulse.

TABLE III

TIME STABILITY
Duration of measurements-seconds

CIRCUIT		0,1	1	10	100
A	ns	5.428	5.428	5.428	5.428
	ps	16.8	16.7	16.9	17
B	ns	1.842	1.848	1.852	1.846
	ps	28.5	29.7	29.4	29.2
C	ns	6.116	6.120	6.125	6.130
	ps	23.4	24.8	24.6	24.1

5 Conclusions and programs

From the above given results it seems that the "centroid" time discriminator is well adapted for the timetagging of the departing pulse in laser telemetry stations.

The time walk can be disregarded for calibration intervals up one hour, but the temperature of the time discriminators and counters must be kept under strict control if the 100ps accuracy region must be reached, since some of these devices are affected by temperature effects of 10ps/°C.

As regards the future developments, similar tests will be performed on preamplifiers and on commercial "constant fraction" discriminators.

Torino, November 1984

References:

1) Dr. D. Kirchner, Graz Technical University, private communication.

2) J.F. MANGIN: The laser and the calibration of the CERGA lunar ranging system. 4th Int. Workshop on laser ranging intrumentation, vol. 2, p. 162-165, 1982.

3) A.B. SHARMA, S.J. HALME. Receiver for laser ranging to satellites IEEE. Trans. Instrum. and Measur., vol IM 30, p. 3-7, 1981

4) A.B. SHARMA: An Integrating, Centroid Timing Receiver for Satellite Ranging, Reports of the Finnish Geodetic Institute 75:10.

5) Y. TSUCHIYA, A. TAKESHIWA, M. HOSODA: Stable ultrashort laser diode pulse generator. Rev. Sci. Instr., vol. 52, p. 579-581,1981.

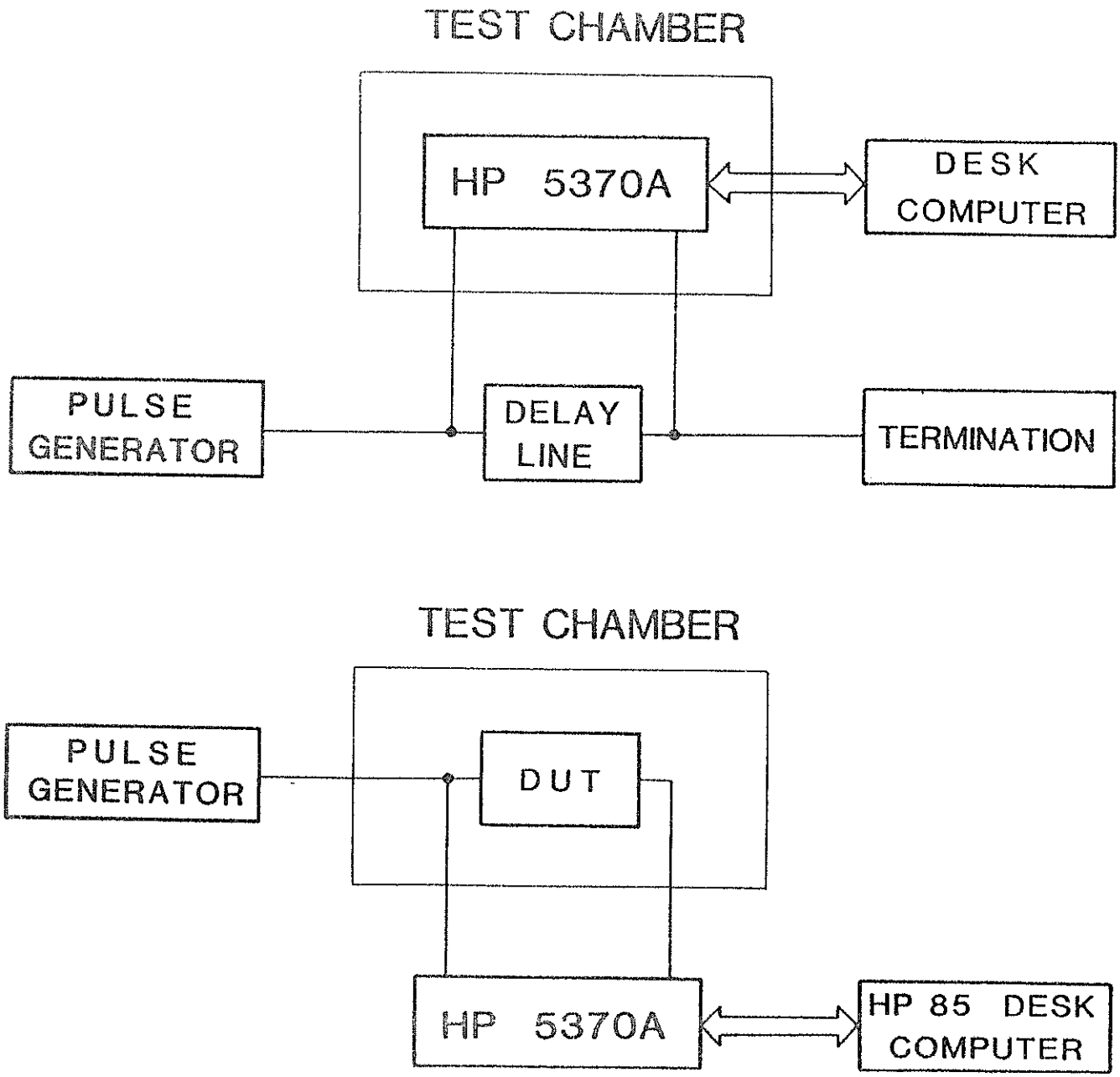
TEST CHAMBER
HP 5370A
DESK COMPUTER
PULSE GENERATOR
DELAY LINE
TERMINATION
TEST CHAMBER
PULSE GENERATOR
DUT
HP 5370A
HP 85 DESK COMPUTER

FIG.1

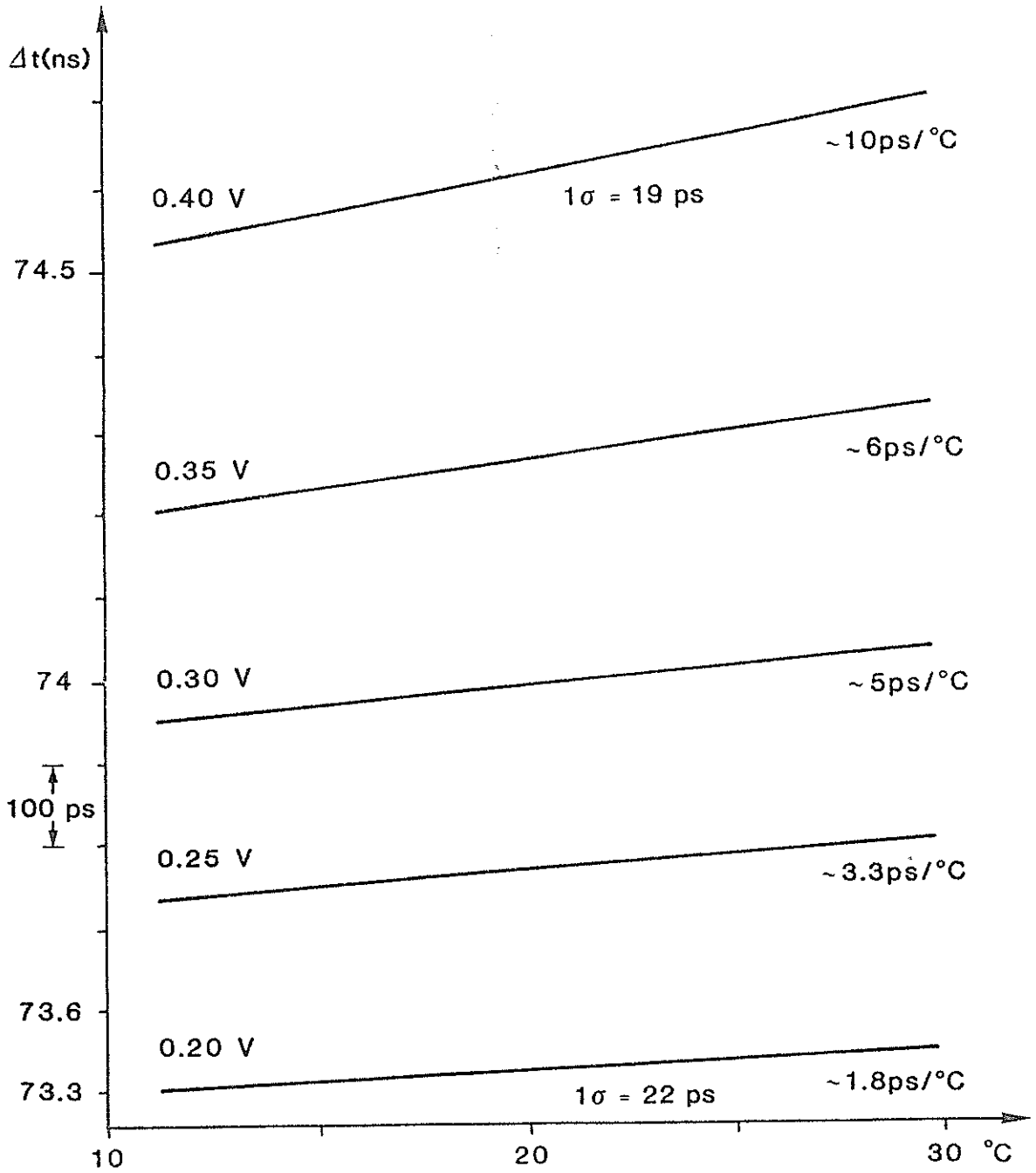

SAME START AND STOP LEVELS

FIG. 2

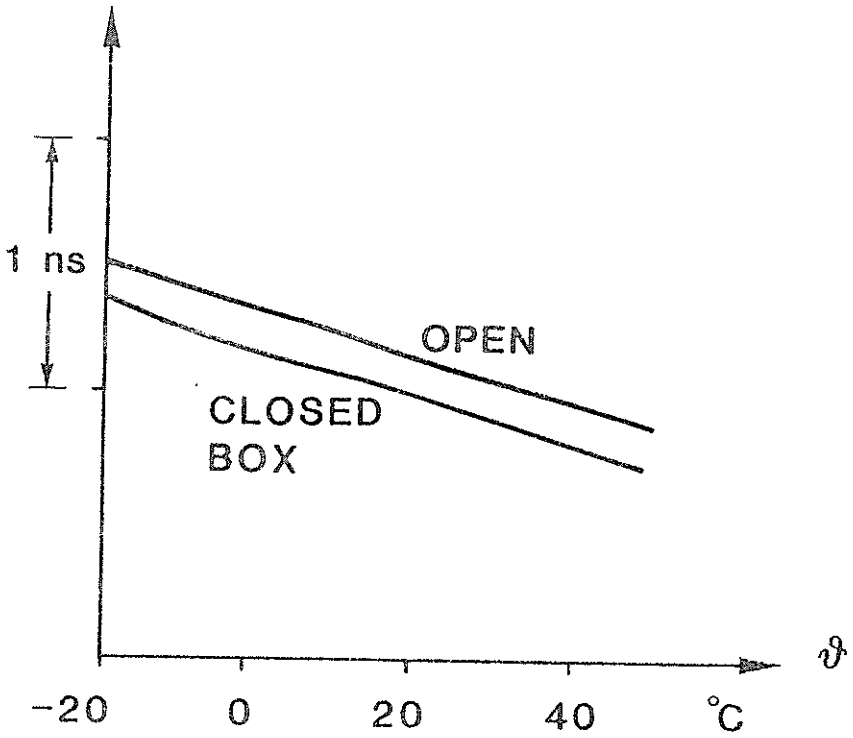

FIG. 3

FURTHER THOUGHTS ON A MINIMAL TRANSMITTER FOR LASER RANGING

B. Hyde
Alp Optics
267. Rue du Château du Roi
38220 Vizille France

Telephone (76) 68 24 05

ABSTRACT

It has been suggested that it is advantageous to utilise the fundamental wavelength for satellite (or lunar) laser ranging. This has the merit of better atmospheric transmission etc.. and consequently a simpler laser system. A major objection was the P.M.T. required. In this paper, we exploit the high quantum efficiency of the triggered avalanche detector (TAD), which appears to answer this critisism, and using the more rigorous approach, recalculate the minimal transmitter requirements for, for example, LAGEOS at 1,06 µm. To further the raliability of the laser, we also introduce an automatic peak power limiter of simple form.

Further Thoughts on a Minimal Transmitter for Laser Ranging.

Introduction.

As third generation systems reach maturity and become widespread,it is instructive to review their fundamental design, with new technology in mind,and make recommendations for future Instruments and updates of existing ones.

A third generation system as implemented at present, has,typically,an emitter producing a single pulse of 30mJ,100pS, at 532nM and 10Hz,with a receiver which detects single photo-electrons.(P.Sharman,SLR Technical Note No. 1,MAY 1982, Roval Greenwich Observatory)

These systems are sub- optimum,as discussed at Lagonissi and there would seem to advantages in reviewing the suggestions presented there.(Proc. of the Third & Fourth Int. Workshop, 1978 & 1981).

Recapping,these were;

a) Detection by single photo-electron counting.
b) Using the mode- locked train of pulses.
c) Transmitting the fundamental wavelength(1064nM).

The first recommendation is now in common use.The second idea is sound but has not been popular or necessary given the large laser pulse energy available. The final idea was impractical for lack of a suitable photon counter in the near infra-red.

Our purpose in this paper is to quantify these advantages of using the intrinsic properties of the laser,and by means of a solid-state photon detector of high quantum efficiency,indicate how this may be done.

Advantages.

A quantitative 'feel'for the benefits of the aforementioned suggestions can be gleaned from a system budget. (figure.1)
Here we present the maximum and typical performance of a current system,relative to that of a proposed system emitting and receiving photons as a mode-locked train of pulses. An Instrument can be improved in this way by up to two orders of magnitude,dispencing with two lossy laser components and introducing a solid-state detector.There is also a gain in atmospheric transmission at the longer wavelength,dependant upon local visibility,elevation angle and station altitude. (R.I.HYDE,D.G.WHITEHEAD,Proc. of the Fourth Int. Workshop, Vol.1 pg. 251).

On the debit side the noise count increases due to dark noise of the detector and one should note the increase in the diffraction limited beam divergance.These are not normally limiting factors of an instrument.

There is a tacit assumption that the radar cross-section of the cube- corners is similar at both wavelengths.

On balance the gain of two to three orders of magnitude will manifest themselves in reliability, transportability and cost.Instrument downtime is normally dominated by laser reliability.

Implementation.

Photon counting is a well established and precise detection technique when one ensures 'singles' so avoiding discriminator non-linearity.To date it has been limited to the visible and ultra- violet wavelengths,so necessitating second harmonic generation.

Detection ,with internal gain,in the near infra-red is limited by 'excess noise'. The recent use of such detectors in a pulsed mode demonstratedthat they could detect single photons for a small but acceptable period of a duty cycle.

The identification of a return from a train of pulses requires a decoding procedure,but given the precise interval between each pulse, it is possible and has been used by E.C.Silverberg et al on TLRS-1.

FIG.2 Minimal Laser Energy versus Solid Angle.

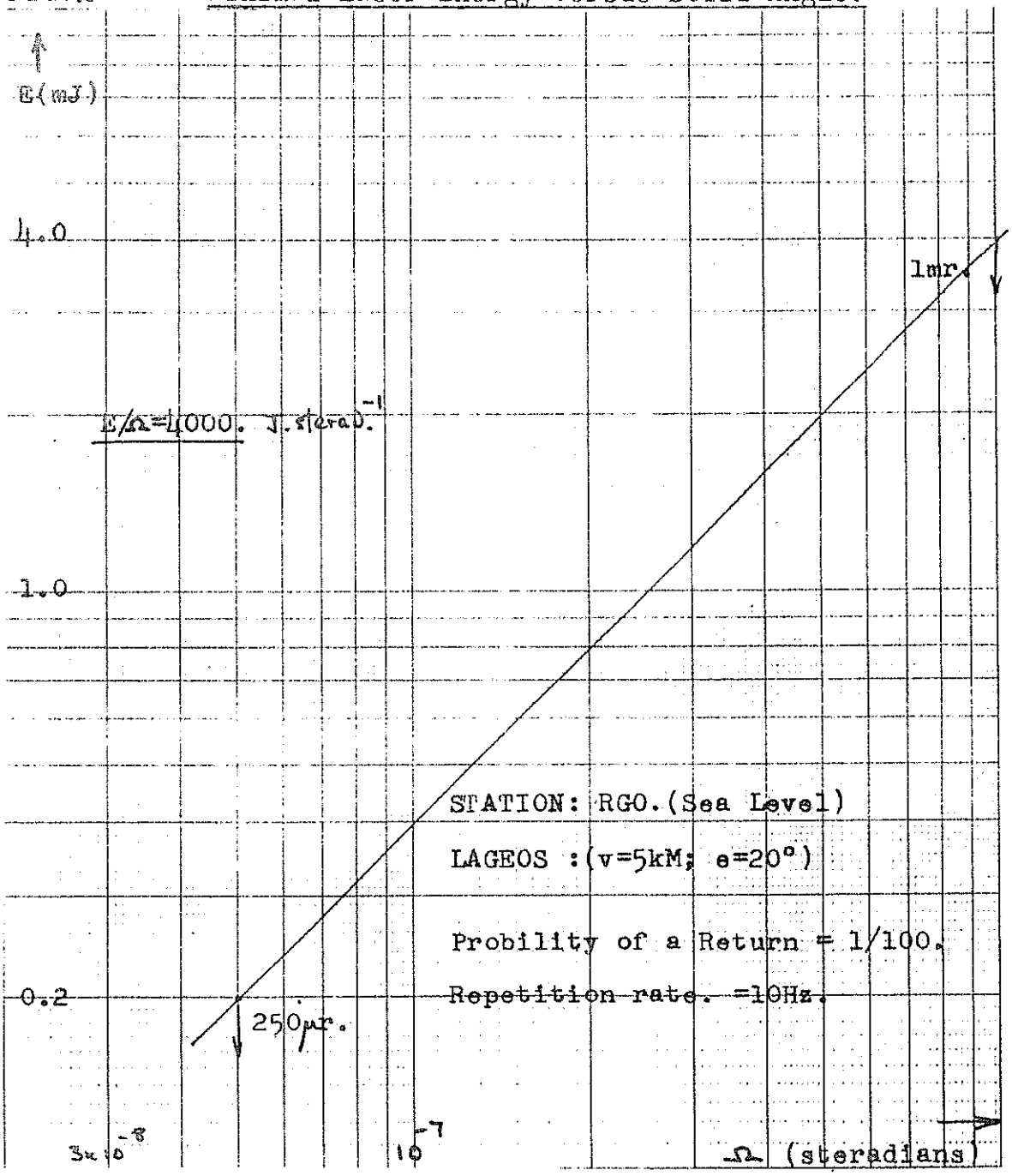

The Triggered Avalanche Detector.

In its continuous mode the avalanche photo-diode is unable to detect signals of less than 100pe. Recently a regular APD was operated in a pulsed mode and was able to detect single photo-electrons,during part of its duty cycle.

This work was reported by P.A.Ekstrom,J.App.Phys. 52(11),Nov.1981,pg.2013, and was followed up by work done by T.E.Ingerson et al ,App.Optics,vol.22, No.13, Silicon devices are now available commercially.

Our interest,here,is in the near infra-red,and therefore with a germanium device.Although germanium is not conducive to avalanche detection 'TAD operation is favoured by large and equal ionisation rates.' Ekstrom concludes his paper thus.'germanium should be an excellent material for TAD fabrication extending the ability to count photons to 1.5micro-meters.'

With such a device the following specification would be expected.

Quantum efficiency.	0.5
Gain.	1.exp(9)
Response time.	0.1nS
Enable period.	0.1S
Turn on delay.	200nS
Dark noise.	1.exp(5)/S at 77°K.

Minimal Energy Required.

It is instructive to estimate the minimal laser energy for the SLR system proposed.Using the parameters of the RGO instrument we determine that the minimum radiance of 4000Joules/steradian is required to range to Lageos in marginal conditions.
Figure 2. is a plot of minimal energy againstthe emitted beam solid angle.We see,for example,that with a beam divergence of 1mradian the minimal laser energy is 4mJ. i.e.within the compass of an unamplified oscillator. (Extrapolation to Lunar operation with a 30microradian beam at 10° above the horizon indicates a minimal of o.1J).'

Conclusion.

The intrinsic properties of the laser and in particular the mode-locked laser may be utilised more effectively.

To summarize,these properties are;

The near infra-red wavelength.

The mode-locked output format.

A unique polarisation.(e.g.see D.Curry et al, Proc. of the Third Laser Workshop.)

A 'clean' wavefront.(to avoid wavefront noise in the latter pulses of a train,see Spectroscopy Letts.8(5),329-340, 1975.R.B.Weisman etal.)

Finally,to implement them,to use the germanium TAD.

The advantages may be as much as three orders of magnitude,enabling one to operate without YAG amplifiers and a pulse switch out unit.

A retrospective update can be carried out during a regular service interval.Reliability and financial advantages follow.Other positive factors are eye-safe operation and mobility.Lunar systems can also benefit.

Clearly it is necessary to prove the germanium TAD but lasers of Ruby or Alexandrite can use the silicon device.

'.....you have nothing to lose but your chains'. (Marx.K.)

System Budget

FIG.1

STAGE	MAX.	TYP.	PROP.	COMMENTS.
0.Oscillator.	1	1	1	-
1.Swich-out.	1/3	1/10	1	transmit whole train.
2.Ampl.gain.	G	G	g	
3.Harmonic genr.	1/4	1/6	1	no photon conversion.
4.Detector q.e.	2/3	1/5	1	germanium TAD.
	G/18	G/300	g	factor 18 to 300.
Atmos. Trans.				
5a).v=25kM. e=90°.	2/3	2/3	1	
5b).v= 5kM. e=20°.	2/35	2/35	1	factor of 5000 max.
Noise.				
6a).Backgrnd.	2/3	1/5	1	high q.e. of TAD.
6b).Dark noise.	1/2	1/2	1	

A PICOSECOND STREAK CAMERA FOR SPACEBORNE LASER RANGING

W. SIBBETT, W.E. SLEAT
Blackett Laboratory, Imperial College
Prince Consort road, London SW7 2BZ ENGLAND

Telephone 01 589 5111
Telex 261503

W. KRAUSE
Messerschmitt-Bolkow-Blohm GMBH,
Postfach 801169
D-8000 München 80, WEST GERMANY

Telephone 089 6000 4093
Telex 5287370

ABSTRACT

Pertinent details relating to the design, construction and preliminary evaluation of an experimental circular-scan streak camera are presented. This "Photochron IIC" picosecond camera is intended as a major subcomponent of a spaceborne laser ranging instrument. Experimental data are included which confirm that an instrumental function of less than 6 ps can be achieved in both single-shot and repetitive modes of streak operation

A PICOSECOND STREAK CAMERA FOR SPACEBORNE LASER RANGING

1. INTRODUCTION

A spaceborne ultrashort-pulse laser ranging system may be employed to determine with high accuracy the distance from an artificial earth satellite to ground-based retroreflector targets. (1, 2) The laser ranging instrument essentially comprises a laser which emits picosecond pulses at a repetition frequency of 10-20 Hz, transmitting and receiving optics, a detector and some means of measuring the round-trip time between the satellite and retroreflector. Provided a correction is made by which the pulse retardation arising from atmospheric refraction is taken into account, then this round-trip time can be translated into a measurement of the straight-line distance. However, this atmospheric correction is computed from a theoretical model of the atmosphere that requires knowledge of the atmospheric surface pressure at each target site. An elegant method of obtaining such surface pressure data consists of deriving them from differential pathlength measurements carried out simultaneously at two or more laser wavelengths (3).

The general concepts for a modern two-colour spaceborne laser ranging system have been reviewed by Lutz and coworkers. (2) In this, the time-interval measurement unit is based on a circular-scan streak tube (4,5) operating in a "vernier" mode. This means that in order to measure the round-trip transit time, complete periods at the scan frequency that elapse between the start and stop pulse registrations are counted by a "coarse" counter and the fractional period is recorded with high precision at the output screen of the streak tube. (2,6) An experimental "Photochron IIC" streak camera is being developed for such a spaceborne differential ranging application in conjunction with fundamental (λ750nm) and second harmonic (λ375nm) picosecond pulses from a vibronic (eg alexandrite) solid-state laser. The specialised features of the Photochron IIC will be described and data will be included which relate to preliminary evaluations of its temporal resolution capability when incorporated in an experimental camera format.

2. CIRCULAR-SCAN STREAK CAMERA PRINCIPLE

The basic component of any electron-optical streak camera is the image tube and although several tube configurations exist the general principles of their operation have a lot in common. Before discussing the circular-scan version it is perhaps worthwhile reviewing the concept and operation of linear-scan, single-shot and repetitively-operating modes.

2.1 Single-Shot Operation

A conventional single-shot modular camera system which comprises a Photochron II (7) streak tube is illustrated schematically in figure 1. For the sake of clarity, suppose

that two temporally separated reflections of a single ultrashort pulse are produced by a glass disc of known thickness. These illuminate a slit which is imaged onto the photocathode by an appropriate input relay lens. The length of the slit image is typically a few mm at the cathode where its height is arranged to be less than the width of one spatial resolution element. A photoelectron replica of each incident transient slit image is then produced promptly ($<10^{-13}$s) at the cathode. However, it is at this initial stage that one of the primary contributions to the limiting time resolution of the streak tube becomes evident. This is that the electrons are liberated from the cathode with a distribution of energies and angles. Consequently, the spatial and temporal confinement of the electron image very near the cathode surface would rapidly degenerate with propagation and in the time dimension this is usually referred to as photoelectron transit time dispersion. The energy spread of the photoelectrons is a function of both the wavelength of the incident radiation and the cathode spectral response characteristic and therefore when these parameters are preselected it is then necessary to ensure that the transit time dispersion is minimised. To do this, a mesh electrode is placed close to the photocathode so that a high "extraction" electric field can be applied to enable the low energy (usually < 1eV) emitted electrons to rapidly reach relatively high energies (> 1keV) such that they achieve high velocity before significant spatial separation has occurred. Appropriate voltage applied to suitably shaped cone and anode electrodes complete the focussing electron-optical lens which constrain the photoelectronic signal to pass through a small anode aperture. This geometry thus effectively decouples the electron-lens from the deflection and subsequent field-free (or drift) sections of the streak tube. (The accelerating potential maintained on the anode and phosphor screen (or equivalent) is generally 15 - 20KV for this type of arrangement). When no electrostatic deflection is applied, then the two ultrashort electron slit images would be

focussed onto the phosphor screen where they would be super-imposed with the so-called "static" (or "focus") spatial resolution of the image tube.

Temporal resolution is afforded in a single-shot "streak" (or "dynamic") mode of operation. To achieve this, a bias voltage is applied to the deflectors so that the electron signal is prevented from reaching the screen within a prescribed detection area. An appropriately synchronized linear, time-varying voltage differential is then applied to the deflectors (either symmetrically, ie + V to one plate, - V to the other, or asymmetrically) so that the electron packets experience a deflecting electric field as they travel through the deflection region. The transient and temporally separated replicas of the incident optical slit images are thus displayed on the screen with a displacement separation that depends on the rate of change of applied voltage. A time-to-space transformation has therefore been accomplished in the streak image tube.

In the example which is depicted in figure 1, the streak image has in inbuilt time calibration because the glass disc was of known thickness. It follows, therefore, that when the width (FWHM) of the intensity profiles of the streaks is determined (directly from photoelectronic recording) this can be related to the temporal separation to provide the so-called recorded streak duration, δT_R. When gaussian pulse shapes are assumed then the relationship connecting δT_R and the incident pulse widths δT_p is given by:

$$\delta T_R = \{(\delta T_p)^2 + (\delta T_{phys})^2 + (\delta T_{tech})^2\}^{\frac{1}{2}} \quad (1)$$

δT_{phys} and δT_{tech} are the main contributing factors that determine the limiting time resolution (often referred to as instrumental function) of the streak tube and refer

respectively to the transit time dispersion of the photoelectrons in travelling from the cathode to the deflectors and the streak limited time taken for the electrons to be swept across one resolution element at the screen. These so called physical and technical contributions can be expressed in the form given in equations (2) and (3)

$$\delta T_{phys}\ (ps) = \frac{23.4(\delta\varepsilon)^{\frac{1}{2}}}{E} \qquad (2)$$

where $\delta\varepsilon$ is the FWHM (eV) of the energy distribution of the initial photoelectrons emitted from the cathode and E (in KV/cm) is the applied electric field strength close to the cathode. (Other factors which contribute towards δT_{phys}, for example pixel aperture size effects, are excluded in this context. Information is considered only as far as the screen of the sheet image tube).

$$\delta T_{tech}\ (ps) = \frac{10^{11}}{v\delta} \qquad (3)$$

where v is the streak velocity (cm/s) at the screen and δ (line pairs/mm) is the estimated spatial resolution under streak conditions. (It has been recently shown in theoretical studies (8, 9) of Photochron streak tubes that the evaluation of the instrumental function according to equations (1)-(3) is rather too simplistic. δT_{phys}, as given, really only refers to the photo-electron transit time dispersion in the cathode-to-mesh region whereas a proper treatment includes all the regions between the cathode and deflectors. Moreover, a better method (9) for estimating the overall camera resolution which involves a temporal modulation transfer function has been suggested. In this more physically realistic approach, account is taken of the interactive aspects of acceleration, focus and deflection. However, in the context of the present consideration, where

an instrumental function of several picoseconds is involved, then the approximate estimates deduced from equation (1) - (3) are adequate).

It must also be pointed out that it is usually not possible to draw sufficient photocurrents in picosecond streak tubes to provide streak intensities at a recordable level in single-shot operation. This arises because space charge effects give rise to severe degradation in both spatial and temporal performance (8). As a result it is commonplace to employ externally (or internally, see section 3.2) coupled high-gain intensifiers. The fact that the temporally dispersed data are displayed on the streak tube as a spatio-intensity variation, determines the requirements of the intensifier to be (i) high signal gain and (ii) good spatial resolution with minimal image distortion. The intensified output is then generally recorded photoelectronically or photographically.

It has already been demonstrated experimentally that an S20 Photochron II single-shot streak camera having a lens-coupled, magnetically focussed intensifier can have a limiting time resolution of just less than 1ps at a wavelength of 735nm (10). Also, an S20 Photochron II camera which incorporated a fibre-optically coupled channel-plate intensifier has been demonstrated to have an instrumental function <2ps for an incident wavelength of 605nm (11).

2.2 Repetitive (or Synchroscan) Streak Operation

When the incoming luminous information has a moderately high repetition rate (>MHz) then a synchronous streak operation can be exploited (12). The basic concept is indicated in figure 2 where it can be seen that the applied sinusoidal waveform provides a synchronised repetitive electrostatic deflection. The central half amplitude of the sinusoid is linear to within 5% and provided there is little or no

relative jitter between the incident light signals and the deflection voltage waveform, then all of the streak images can be superposed on the streak tube screen. A direct result of this scheme is that many weak individual streaks can be integrated in intensity to achieve a recordable output signal level without the need for an image intensifier while still avoiding space charge effects. The streak images, however, have a recorded width which also includes any jitter component and so the instrumental function must be expressed as:

$$\delta T_{instru} = \{ (T_{phys})^2 + (T_{tech})^2 + (T_{jitt})^2 \}^{\frac{1}{2}}$$

where δT_{phys}, δT_{tech} are as explained in section 2.1 and δT_{jitt} is the additional limitation arising through jitter.

Photochron I, II streak cameras operating synchronously at repetition rates of 140MHz and 165MHz have been demonstrated to have time resolutions < 10ps (13 - 15). More recently, an improved design of the Photochron II which has been designated as the "Photochron IIA" has been operated in the synchroscan mode and the results show that the instrumental function is 1ps (16), which implies that the jitter contribution is relatively small.

2.3 Circular-Scan streak Operation

For the purposes of laser ranging it is convenient to have a circular-scan streak (4 - 6) of constant period so that no synchronization requirements arise. The basic operation is single-shot in nature but the electrostatic time-varying deflection is established by the application of two RF sinusoidal voltages in phase quadrature and so this scheme combines many of the features mentioned in the two previous subsections. It is distinct in that the voltage sinusoids are supplied to two sets of deflectors which produce

orthogonal electric fields with a $\pi/2$ phase difference so that a circular trace is produced at the screen or equivalent plane. When the period of this continous scan is T(in ns) then the technical resolution limit may be expressed as:

$$\delta T_{tech}\ (ps) = \frac{100T}{\pi d S}$$

where d is the diameter of the circle (in cm) and S is the spatial resolution (in lp/mm) under the streak conditions. The expression for the photoelectron transit time dispersion (δT_{phys}) remains the same as that already given in equation (2).

Clearly it is necessary in this approach to use a point image on the photocathode rather than an extended slit format and since a single picosecond pulse is selected from the laser at a low repetition rate (~20Hz) then image intensification must be retained. The experimental circular-scan Photochron IIC streak camera which has been designed specifically for this type of operation is described in the following section.

3. CIRCULAR-SCAN "PHOTOCHRON IIC" STREAK TUBE

The design of the circular scan streak image tube, designated as "Photochron IIC" is shown schematically in figure 3. The defining areas of electron manipulations are; (a) the electron-optical lens constituted by the photocathode K, mesh M, focussing cone C and anode A, (b) the deflection section comprising orthogonally oriented pairs of deflectors placed on each side of a "screening" aperture plate; and (c) a field-free drift section terminated by a proximity-focussed high gain microchannel plate (MCP) intensifier where the electron image is directed onto a phosphor screen (S) deposited on a fibre-optic faceplate (F).

3.1 Electron-Optical Lens Section

A semitransparent S20-type (Na-K-Cs-Sb) photocathode was processed on a specially profiled substrate such that a usable diameter of 10 mm was provided. The available spectral ranges of sensitivity extend over the 300 - 900 nm region and easily accommodates the 760 nm, 380 nm optical pulse wavelengths to be used in ranging systems. When illuminated by pulses at these wavelengths, the photoelectrons emitted from the cathode have an associated energy distribution. As already pointed out in subsection 2.1 it is necessary to minimise the transit time dispersion that accrues as the electron packet travels towards the deflectors, so a planar mesh electrode is placed 0.5 mm from the cathode such that the electrons rapidly reach an energy of approximately 1KeV. This is arranged by maintaining a dc EHT voltage of -15kV on the cathode and -14kV on the mesh. The mesh to which is applied this so-called "extraction" potential is fabricated in thin copper from which a high density of "cells" or windows have been etched. (The cell density is 300 cells/cm and the transparency is 50%). It is ensured during construction that good surface contours exist in this region of high electric field (20kV / cm) so that the incidence of "field emission" is eliminated.

The imparted energy of 1KeV to the electrons transmitted through the mesh electrode is sufficiently low that a photoelectronic image can be focussed in the plane of the input face of the microchannel plate using the "singlet" electron-lens obtained by supplying an appropriate combination of voltages to the mesh M, cone C and anode A electrodes. (The anode and the input of the microchannel plate are maintained at the same potential). For the voltages already mentioned for the cathode and mesh, the typical operating potentials for the cone and anode electrodes are 13.45KV, 4.5KV respectively. Under these operating conditions the electron-optical magnification is

-1.8 (-ve signifies image inversion) and the limiting spatial resolution at the photocathode is in excess of 35 lp/mm. Although this spatial resolution can be retained in the sweep direction under conditions of repetitive or "synchroscan" streak operation (see section 2.2) the elevated current densities that arise in the single-shot streak mode lead to substantial reductions in this value. In fact, a typical estimate is 20 lp/mm at the photocathode.

The basic feature of this type of tube is that the electron lens provides moderate spatial resolution (in two dimensions) together with reasonably good retention of the temporal fidelity of a "transient" photoelectron slit object. The Photochron II (7) and Photochron IIA (16) version have achieved subpicosecond resolution (10,17) and therefore have adequate performance characteristics for the purposes of laser ranging applications.

3.2 Proximity-Focussed Intensifier Section

It has already been explained that an image intensification stage is necessary in a single-shot streak camera so that recordable image intensity levels can be produced without compromising the image tube performance through the space charge effects arising from enhanced photocurrent densities. An alternative to coupling an external image intensifier module is to incorporate an intensification stage within the structure of the streak tube. This is the design concept of the Photochron IIA tube where a high electron gain is offered by a proximity-focussed microchannel plate-to-phosphor section. The micro-channel plate comprises a matrix of 12.5μm diameter ratio of 80: 1 on a 15μm centre-centre spacing. The activated inside walls of the hollow channels have a suitably high secondary emission coefficient for the incident 10.5 KeV primary electrons and a cascade of secondaries is ensured by the multiple collisions within the confines of the microchannel plate (MCP). Forward momentum

of these secondaries is provided by the positive voltage bias (>1.5kV) applied between the output and input MCP faces. A gain 10^3 can be obtained in such a MCP which has a limiting spatial resolution of more than 25 lp/mm. In this type of intensifier, the creation of +ve gas ions can be a problem because their feedback, which is encouraged by favourable potential gradients, gives rise to serious induced "noise" levels. This shortcoming is alleviated by having a 15^o bias angle on the channels and a 20 nm aluminium oxide (Al_2O_3) layer on the input MCP face so that the penetration by primary electrons is permitted by the feedback of slow positive ions is suppressed.

There are advantages in this internal proximity-focussed intensifier scheme compared to the optically-coupled external intensifier arrangement that relates to the modular approach outlined earlier in section 2.1. For instance, the electron lens aberrations such as off-axis image distortions that exist in many "inverting" direct-viewing intensifiers are eliminated and inherent photocathode background noise associated with a separate intensifier tube is avoided. One possible disadvantage is, however, that picosecond electron signals are amplified in the internally intensified version in contrast to microsecond electron images (arising from the screen phosphorescence timescale) for the externally coupled counterpart and consequently gains saturation problems (18) may be exacerbated. Notwithstanding, subpicosecond resolution in single-shot operations has been measured for a Photochron IIA type camera (17). Another problem, arises from the feature that the open area ratio of the microchannel plates is 66% and the resultant loss of signal photoelectrons is damaging to the overall signal-to-noise ratio.

The intensified electronic image is proximity-focussed onto a suitable phosphor screen which is deposited on a fibreoptic output faceplate. For this purpose an accelerating potential of 3-5KV is applied between the exit face of the MCP and the

screen which have a separation of 0.8 mm. It is important that the properties of the phosphor screen are designed to be compatible with both the image tube and the read-out device employed.

To facilitate a spatial resolution parameter which does not limit the performance of the streak tube a fine grain phosphor power is a prerequisite where the grain size should be 1 - 2μm (19). The method of deposition onto the fibre-optic faceplate (6μm cores) is chosen so that a uniform layer thickness and packing density is obtained.

In the case of the CSST where the read-out device is a self-scanned photodiode array (RETICON) or CCD which have a peak detection efficiency at 800 nm, it is clear that a red phosphor should offer the best spectral match. However, it must be remembered that a high efficiency and good spatial resolution are needed to ensure an overall detection efficiency comparable with the alternative yellow-green (P20) phosphor screens that are presently available on commercial intensifiers.

The forward transfer of the luminescence towards the detector is enchanced by depositing a backing layer (50 nm thick) of aluminium onto the phosphor screen. This is arranged so that it can withstand the application of electric fields in excess of 40KV/cm in the proximity section. (The screen is generally maintained at earth potential).

3.3 Deflection section

To produce the desired circular sweep in the streak tube, two pairs of orthogonally oriented deflection plates are arranged as illustrated in figure 3. The design of the deflector assembly in the Photochron IIC lends itself to efficient coupling of power via metal-ceramic electrical feedthroughs which exhibit acceptably low RF losses. The dimensions and

separations of the deflectors have been chosen to provide equal deflection sensitivities and it turned out in practice that due to tube manufacturing tolerances the set nearer the anode required 211V for 1 cm deflection while the orthogonally oriented set had the slightly reduced sensitivity of 226V/cm. It is necessary therefore, to differentially adjust the suppplied RF power because of the importance of providing equal deflection amplitudes in phase quadrature. Failure to ensure this leads to ellipticity in the scan as illustrated in figure 4 where one amplitude is allowed to exceed the other by 2%, 4% and 6%. (Dotted outline of ideal circle is included for comparison).

The effect of any departures from precise phase quadrature is also indicated in figure 4 where the induced distortion in the scan is clearly evident for phases differences that are 2^{o}, 4^{o} and 6^{o} larger than the required $\pi/2$. The overall distortion in the circular scan that results from combined amplitude and phase drifts are also included in figure 4 and the correspondingly computed amplitude and phase errors are presented for a total scan rotation in figure 5. Both of these figures vividly confirm that the fidelity of the circular scan relies critically on keeping the amplitude and phase errors to a minimum during the operational period of the camera.

Our first practical attempt to satisfy the stringent deflection requirements for the Photochron IIC involved the use of an effective half wavelength of transmission line with the deflectors located at points of equal signal amplitude but $\pi/2$ out of phase. Unfortunately, the deflector capacitance was sufficiently dominant that this scheme behaved as two tightly-coupled tuned circuits with inevitable multiple resonances. Consequently, the simultaneous adjustment of resonance and phase proved to be impractical without the use of excessive power.

In the alternative approach, that is being used at present, a single amplifier is used to provide two independent drive signals. The two sets of deflection plates are coupled to the 50 ohm impedance signal lines by suitable coupling loops which are adjusted to provide a matched load. To minimise the influence of phase drift resulting from induced thermal effects, the two circuits are appropriately damped and phase adjustment is made by slight alterations to the cable lengths. As mentioned earlier, our experimental streak tube has sets of deflectors that differ by approximately 7% in sensitivity but this was overcome by a suitable amount of resistive damping.

The sinusoidal deflection voltages are produced by a 300 MHz crystal controlled oscillator, figure 6 or for synchroscan operation a laser driven tunnel-diode oscillator. The signal is further amplified by a wide band amplifier (Model TRW-CA2820) to give an output of 400 mw into a 50Ω load. For practical demonstration of a 3 cm diameter circular scan further amplification is required. An appropriate amplifier module was obtained (Microwave Modules Ltd) which is capable of continuously delivering 30 watts of RF power without requiring a precisely matched load.

The actual power used in experiments to date is approximately 15 watts total. This power and damping has proved to give satisfactory stability to enable mutual evaluation of the CSST time resolution (20) to proceed and produced a circular scan having a diamter of 30mm at the phosphor screen. A photograph of such sweep, for a continuous light surce, is reproduced in figure 7.

As well as amplitude variations on the circular scan it must be remembered that an absolute ranging measurement relies critically on exacting frequency stability. In fact, if a loss of 1 ps time resolution is to be avoided then the frequency stability should be better than one part in 1.5 x

10^{10} during the 15ms double-transit time. This could be satisfied by basing the 300 MHz oscillator on a Rubidium clock frequency standard rather than the quartz crystal specified for this study. An additional constraint is that the circular orbit of the electron beam must remain centred at the same point to ensure appropriate detection and so it follows that influences such as stray magnetic fields must be avoided.

4. THE PHOTOCHRON IIC CAMERA AND ITS DYNAMIC PERFORMANCE

In our laboratory camera arrangement the input optics to the streak tube comprised a 20 μm diameter pinhole which was imaged, with a X2 demagnification by a relay lens on to the photocathode. The streaked output images were recorded photographically on Ilford HP5 film using an f/1.5 lens operating at a magnification of unity. A crystal-controlled oscillator/multiplier network (21) produced a power of 400 mW at 300 MHz which was subsequently amplified to approximately 15 W before being appropriately shared in phase-quadrature between the sets of deflectors. This was accomplished by supplying the RF signals to the tube via $\lambda/4$ matching transformer and two 50 ohm impedance coaxial cables that differed in length by one quarter of a wavelength. These cable outputs were then loop-coupled to the deflection plates, the loops being adjusted to give matched loads. Although we have already demonstrated that a 30 mm diameter scan can be obtained with as little as 2.5 W of power in each feed channel (21) we chose to supply higher power levels, in this instance typically 5 - 10 W per channel, to lower Q tuned circuitry. By this means it was possible to reduce drifts in signal phase and hence maintain the fidelity of the scan and also have a better mechanical arrangement for the resonant circuits. (The importance of maintaining relative phase together with the necessary avoidance of appreciable amplitude variations to the orthogonally oriented pairs of deflectors has already been alluded to (section 3.3).

As has been stated earlier, an estimate of the instrumental function of this Photochron IIC camera can be inferred from the Gaussian approximation involving the technical time resolution limit (δT_1) and the inherent photoelectron transit time dispersion (δT_2). Associated with the circular scan operation.

$$\delta T_1 \text{ (ps)} = \frac{100T}{\pi D \delta}$$

where T is the scan period (ns), D is the diameter (cm) of the circle and δ (lp/cm) is the dynamic spatial resolution. Substituting the values T = 3.3ns, D = 3cm and a realistic value of δ = 70 lp/cm under single-shot conditions, then δT_2 is 5ps. When a value of 2 - 3ps is taken for δT_1 for wavelengths somewhat away from the vicinity of the photosensitivity threshold of the cathode) then the instrumental function becomes approximately 6ps.

To check this prediction under experimental conditions, the camera was illuminated with pulses produced by a mode-locked, flashlamp-pumped rhodamine 700 dye laser. As can be seen from schematic of figure 8, seven pulses were selected from the 1us laser output train using a Pockels cell switch. As each pulse passed through the calibrated optical delay, two subpulses having a temporal separation of 66ps could be conveniently directed into the camera.

The pulse repetition period of just less than 3.3ns also meant that all seven streaked sub-pulse pairs could be recorded simultaneously. To ensure recordable intensity levels for these streaks while avoiding undue space charge effects (8), the gain of the microchannel plate intensifier was set to 10^4. At this level of gain, the background noise signal accumulated during the 10ms photographic recording exposure times was sufficiently low that it was not necessary to gate the forward bias voltage on to the

microchannel plate.

The disposition of the streaked laser pulses (without the optical calibration) on the circular scan is illustrated in figure 9(a) where the pulse selection has been deliberately timed during the evolutionary phase of the mode-locked train. To obtain more quantitative time resolution data, shorter pulses were selected later in the train where the steady-state had been established and a representative microdensitometer trace for one of the image pairs is included as figure 9(b). When the laser pulse durations which are typically 3 - 5ps at the operating wavelength of 760nm (22), are deconvolved from recorded streak duration of 5.7ps then the camera resolution is deduced to be 5ps. This is in good agreement with the predicted value for the instrumental function and clearly confirms that the Photochron IIC can perform to the required time resolution specification.

In addition to these single-shot streak tests, the camera was operated repetitively in conjunction with a mode-locked CW laser so that short-term phase stability could be assessed. Subpicosecond pulses (615nm) were produced at a 100 MHz repetition frequency by a passively mode-locked CW ring, rhodamine 6G dye laser (23). One of the two output beams was directed to the camera by way of a calibration glass disc as illustrated in figure 10 while the other triggered a tunnel-diode oscillator. This electrical output was then frequency tripled, filtered and amplified to provide the synchronised RF drive deflection to the streak tube. Because of the superpositioning of the streak images on the phosphor screen for this "Synchroscan" operation (12), there is no requirement for high electron gain in the intensifier section of the tube so a low gain setting 100 was selected.

For the purposes of providing an illustration of the circular scan and the display of streaked images, a small intensity

component of the pump argon ion laser as well as the dye subpulses were directed on to the input pinhole of the camera. A photographic recording of the resulting image is reproduced in figure 11(a) where the calibration delay between the ultrashort dye pulses is 57ps. The microdensitometer trace for such a pair of streak images in the absence of the background continuous illumination is included as figure 11(b) where it can be seen that the recorded streak duration is 4.7ps. Bearing in mind that subpicosecond pulsewidths are available from this test laser source (23), the main contribution to the recorded duration arises from the technical time resolution limit and to a lesser extent the photoelectron transit time dispersion and integrated jitter between the deflection voltage and the incidence of the laser pulses. Clearly this latter effect cannot be too significant because when account is taken of the expected photoelectron transit time dispersion (~2ps for 615nm wavelength and S20 photocathode) the implied technical time resolution limit is approximately 4ps. This is consistent with the expectation that under the conditions of repetitive streaking, the dynamic spatial resolution should exceed the corresponding value for single-shot operation.

It may therefore be concluded that phase drifts occurring during the recording periods (generally 1 - 5 seconds) are small and likely to be substantially less than 4ps for total supply RF powers of 15W. This result complements those of the single-shot experiement in that an instrumental time resolution of less than 6ps can be sustained over short term periods of several seconds.

5. CONCLUSION

The experimental data presented here confirm that the circular-scan Photochron IIC streak camera has a temporal resolution of better than 6ps and possesses good short term

stability of operation. For future applications, particularly those involving laser ranging, an electronic readout will be developed for full compatibility with telemetry.

It is envisaged that this readout will initially be a CCD camera placed external to the tube body and optically contacted to the existing faceplate via a fibre optic reducer. Although a circular array would appear to be the obvious form for the electronic readout it will probably turn out to be an impractical solution due to the difficulty involved in establishing optimum tube focus and scan characteristics. When in operation, a circular array would probably impose too severe a restraint on scan accuracy and alignment. The current development of large area two dimensional CCD arrays would appear in the future to offer the best solution to the problem. The placing of the electronic readout internally, as an integral part of the image tube, would appear to offer optimum performance by removing some of the loss coupling elements and some experiments will be carried out to ascertain the feasibility of this approach.

The detection of extremely low light-level signals involve a study of the various ways of improving the overall signal to noise ratio of the image tube. The usee of, for example, cooling of the photocathode and signal gating techniques will be investigated.

It has been demonstrated that a CSST can be constructed using metal and ceramic technology which should prove to be sufficiently rugged for spaceborne applications.

ACKNOWLEDGEMENT

The support of this work by ESTEC/ESA on Contract No. 5159/82/NL/HP(SC) is gratefully acknowledged.

6 REFERENCES

Abbreviations: ICHSP (P) - International Congress on High-Speed Photography (and Photonics)

(1) D E Smith, "Spaceborne Ranging System", Proc, 9th GEOP Conference, an International Symposium on the Application of Geodesy to Geodynamics, Dept of Geodetic Science, the Ohio State University, Report No 280, pp 59 - 64 (1978).

(2) H Lutz, W Krause and G Barthel, "High-Precision Two-Colour Spaceborne Laser Ranging System for Monitoring of Geodynamic Processes", Space 2000 (Edit: L G Napolitano) Amer Inst of Aeronautics and Astronautics, New York, p 236, 1983.

(3) C S Gardner, "Technique for Remotely Measuring Surface Pressure from a Satellite Using a Multicolour Laser Ranging System", Appl Opt Vol 18, pp 3184 - 3189, 1979.

(4) E K Zavoisky and S D Fanchenko, "Image-Convertor High-Speed Photography with 10^{-9} - 10^{-14}s Time Resolution", Appl Opt Vol 4, pp 1155 - 1167, 1965.

(5) R Hadland, K Helbrough and A E Huston, "Synchroscan - A Technique for the Photography of Repetitive Picosecond Pulses", Proc 11th ICHSP pp 107- 111, 1974.

(6) C E Johnson, S Nevin, J Bebris and J B Abshire, "Circular-Scan Streak Tube with Solid-State Readout", Appl Opt Vol 19, pp 3491 - 3495, 1980.

(7) P R Bird, D J Bradley and W Sibbett, "The Photochron II Streak Camera", Proc. 11th ICHSP, (London, Sept 1974) p 112.

(8) H Niu and W Sibbett "Theoretical Analysis of Space - Charge Effects in Photochron Streak Cameras", Rev Sci Instrum 52 (12), 1830 (1981).

(9) H Niu, W Sibbett and M R Baggs, "Theoretical Evaluation of the Temporal and Spatial Resolutions of Photochron Streak Image Tubes", Rev Sci Instrum, 53(5), 563 (1982).

(10) D J Bradley and W Sibbett, "Subpicosecond Chronoscopy", Appl Phys Lett, 27, 382 (1975).

(11) D J Bradley, S F Bryant, W Sibbett and J R Taylor, "Intensity-Dependent Time Resolution and Dynamic Range of Photochron Picosecond Streak Cameras", Rev Sci Instrum, 49 219 (1978).

(12) W Sibbett, "Synchroscan Streak Camera Systems", Proc 15th ICHSPP, SPIE 348 (San Diego 1982), p 15.

(13) M C Adams, W Sibbett and D J Bradley, "Linear Picosecond Electron-Optical Chronscopy at a Repetition Rate of 140 MHz", Opt Commun, 26 273 (1978).

(14) M C Adams, W Sibbett and D J Bradley "Electron-Optical Picosecond Streak Camera Operating at 140 MHz and 165 MHz Repetition Rates", Advances in Electronics and Electron Physics, 52, 265 (1979)

(15) P G May, W Sibbett, W E Sleat, J R Taylor and J P Willson, "Mode-Locked Ring C W Dye Laser Systems", Quantum Electronics and Electro-Optics, Edit P L Knight (John Wiley, 1983), p 33.

(16) W Sibbett, W E Sleat, J R Taylor and J P Willson, "Internally-Intensified Photochron II Streak Tube", Proc 15th ICHSPP (San Diego, August 1982) SPIE, 348, 217.

(17) P G May and W Sibbett, "Transient Stimulated Raman scattering of Femtosecond Laser Pulses", Appl Phys Lett 43, 624 (1983)

(18) D J Bradley, S F Bryant and W Sibbett, "Intensity-Dependent Time Resolution and Dynamic Range of Photochron Picosecond Streak Cameras - II, Linear Photoelectric Recording", Rev Sci Instrum, 51, 824 (1980).

(19) M Aslam, "An Investigation into Phosphor-Photocathode Cascade Screens for Use in Image Intensifiers", PhD Thesis, University of London, 1965.

(20) W Sibbett, W E Sleat and W Krause "Photochron Streak Tube for 300 MHz Circular Scan Operation", Proc 16th ICHSPP, Strasbourg 1984.

(21) W Sibbett, W E Sleat and W Krause, "Circular-scan Photochron Streak Camera for Spaceborne Laser Ranging Applications", Proc ESA Workshop on Space Laser Applications and Technology - ESA sp - 202, P171, 1984.

(22) W Sibbett and J R Taylor, "Passive Mode-locking in the Near Infrared", IEEE Quantum Electron, QE-20, 108, 1984.

(23) J P Willson, W Sibbett and W E Sleat, "Pulsewidth and Interpulse Jitter Measurement of a Passively Mode Locked ring C W Dye Laser", Opt Commun, 42, 208, 1982.

FIGURE CAPTIONS AND FIGURES

(1) Schematic of modular, externally-intensified single-shot streak camera.

(2) Comparison of deflection voltage profiles applied to single-shot and repetitively-operating (Synchroscan) streak cameras.

(3) Schematic of circular-scan Photochron IIA streak image tube.

(4) Scan distortion induced by amplitude and phase variations.

(5) Amplitude and Phase errors during one scan rotation.

(6) Circuit Diagram for 300 MHz oscillator.

(7) Photograph of Circular Sweep having 30 mm diameter.

(8) Experimental Set-up used in evaluation studies of single shot streak performance.

(9a) Uncalibrated streak images of seven "evolving" mode-locked dye laser pulses.

(9b) Microdensitometer trace for two "calibrated" streak images (reproduced in inset) of "steady state" dye laser pulses.

(10) Experimental set-up used for streak evaluation of repetively-operating camera.

(11a) Photograph of streak recording showing circular scan with superimposed ultra short laser pulse images.

(11b) Microdensitometer trace for two streaked images (reproduced in inset) associated with mode locked pulses

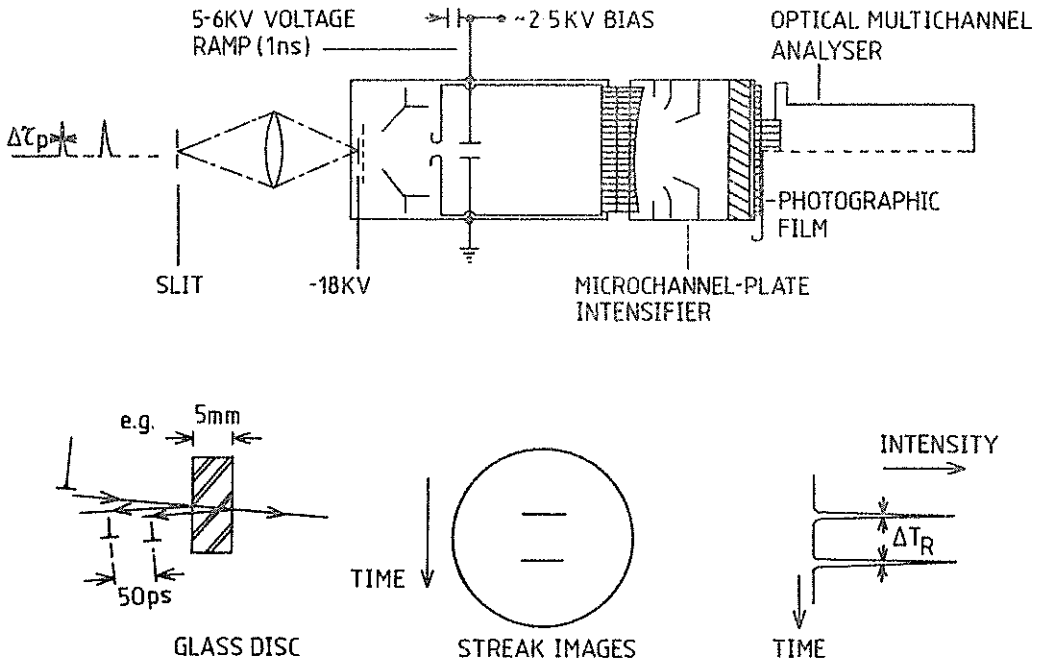

Figure (1)

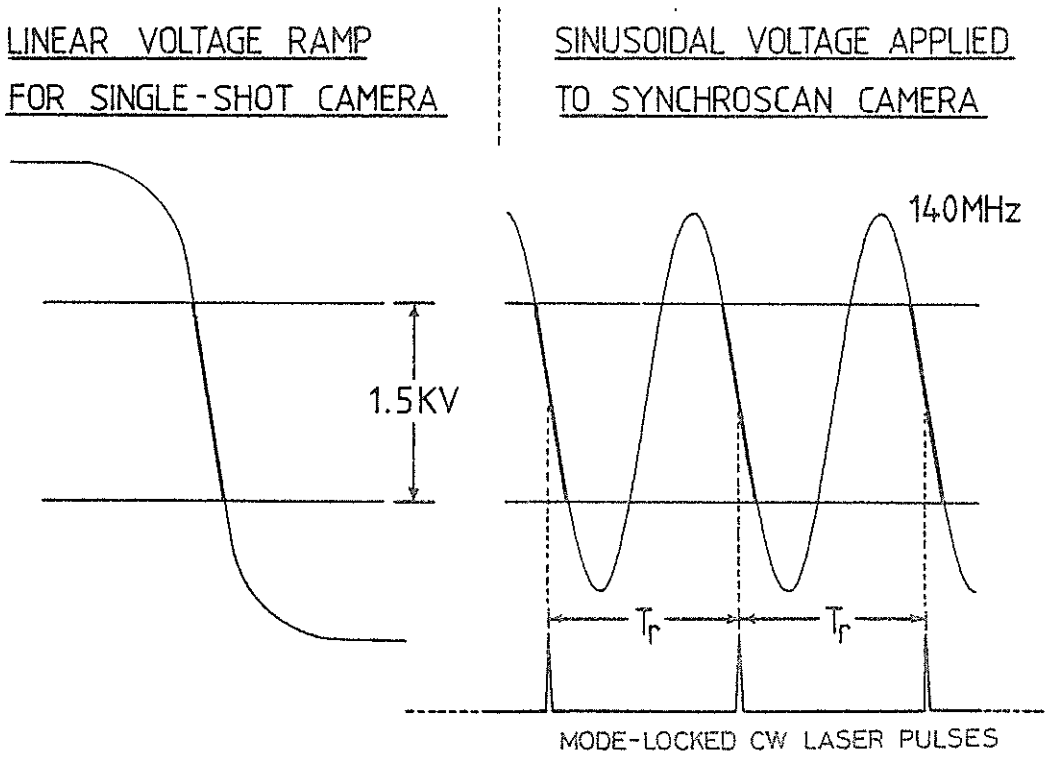

Figure (2)

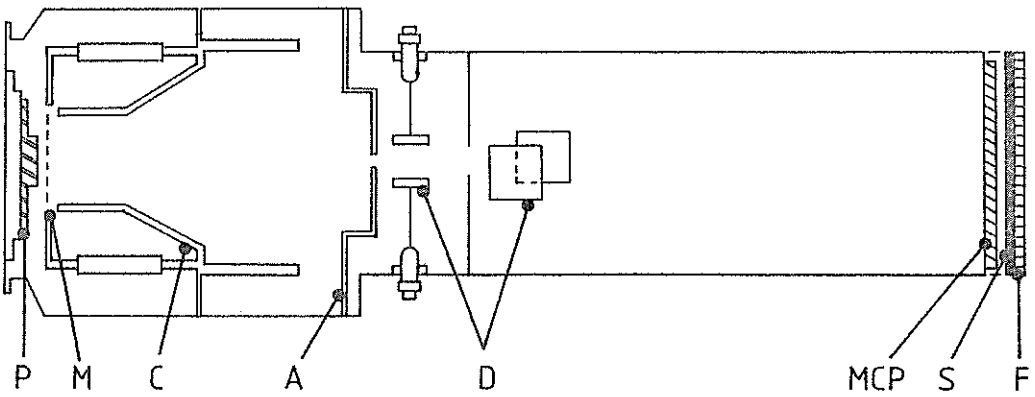

Figure (3)

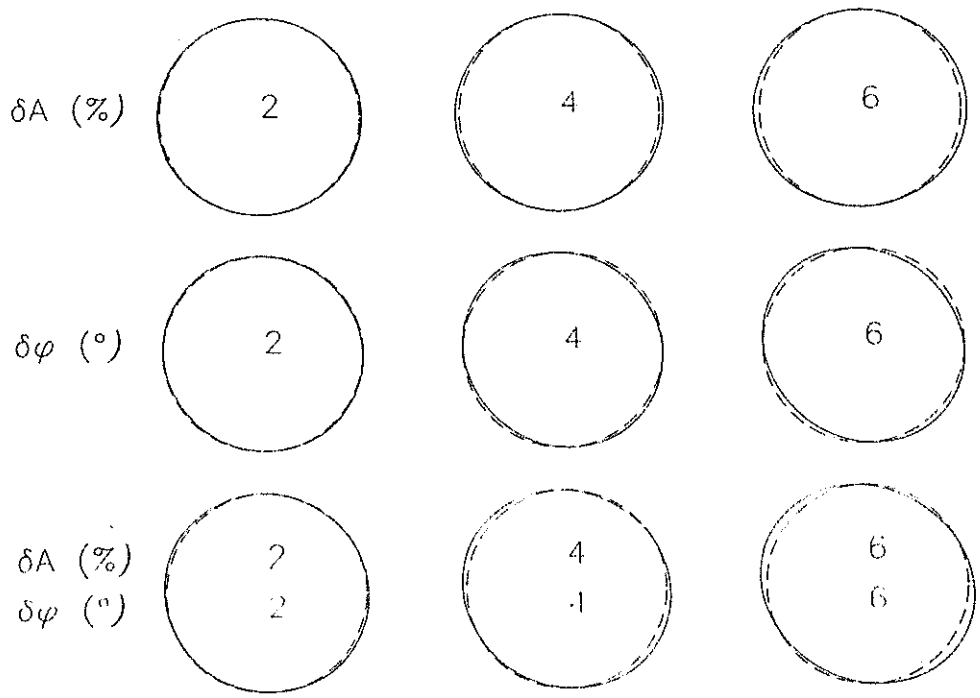

Figure (4)

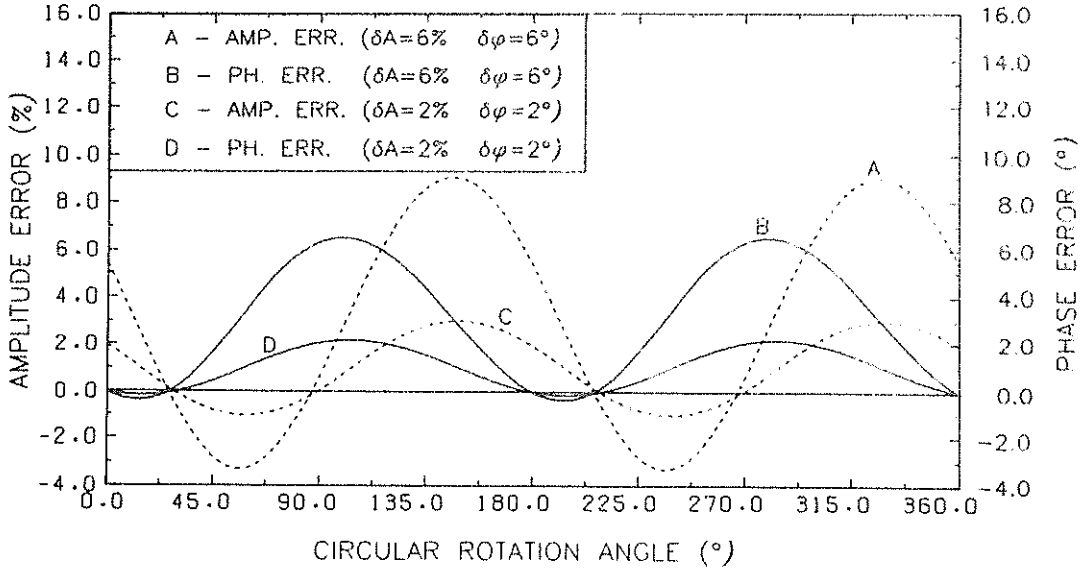

Figure (5)

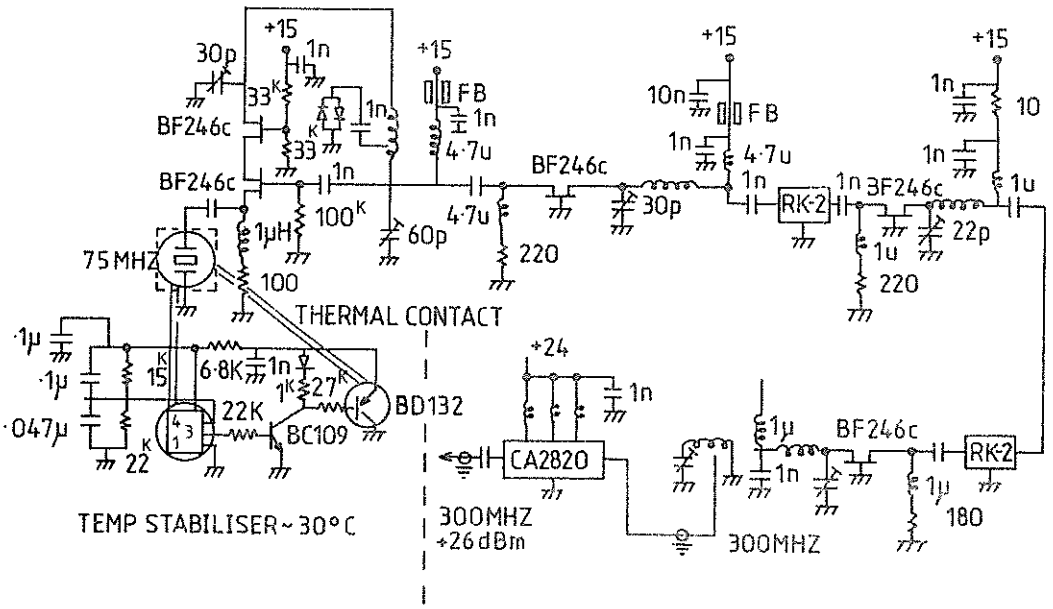

Figure (6)

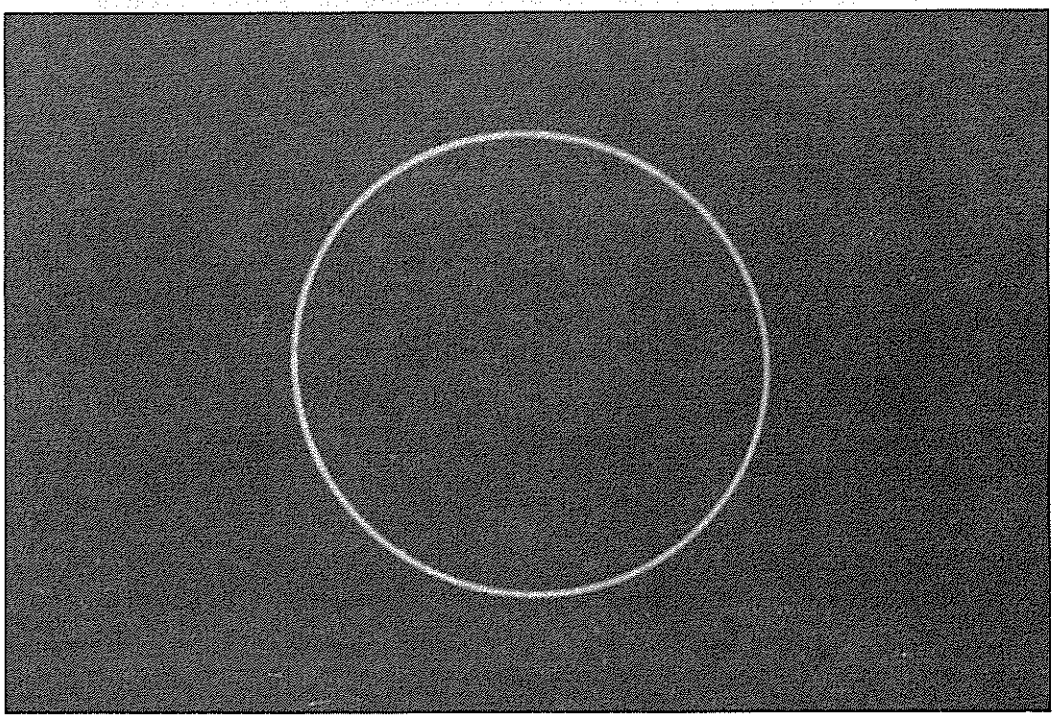

Figure 7

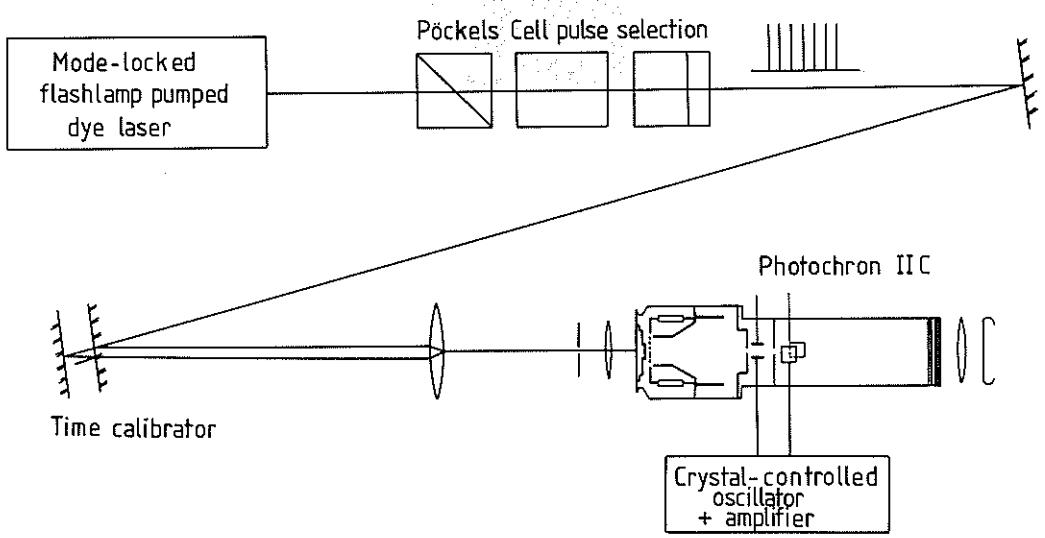

Figure 8

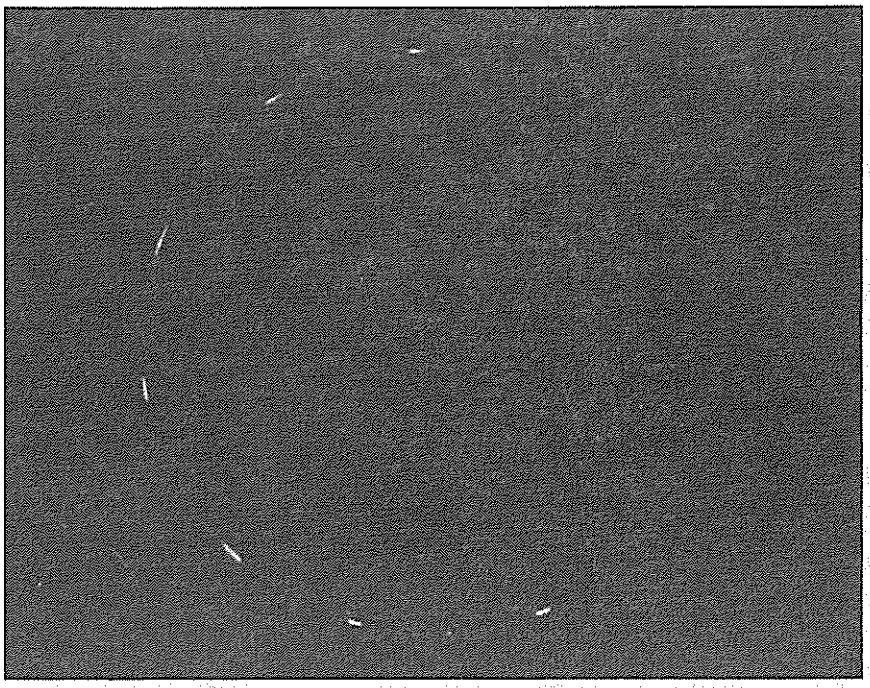

Figure 9a

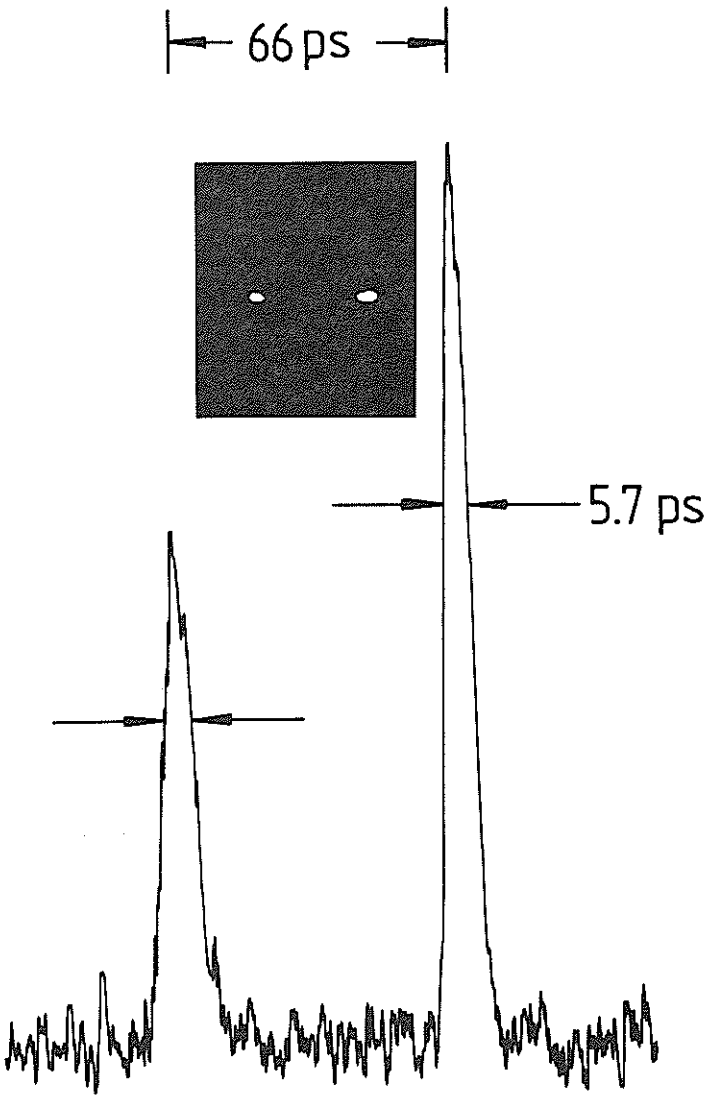

Figure 9b

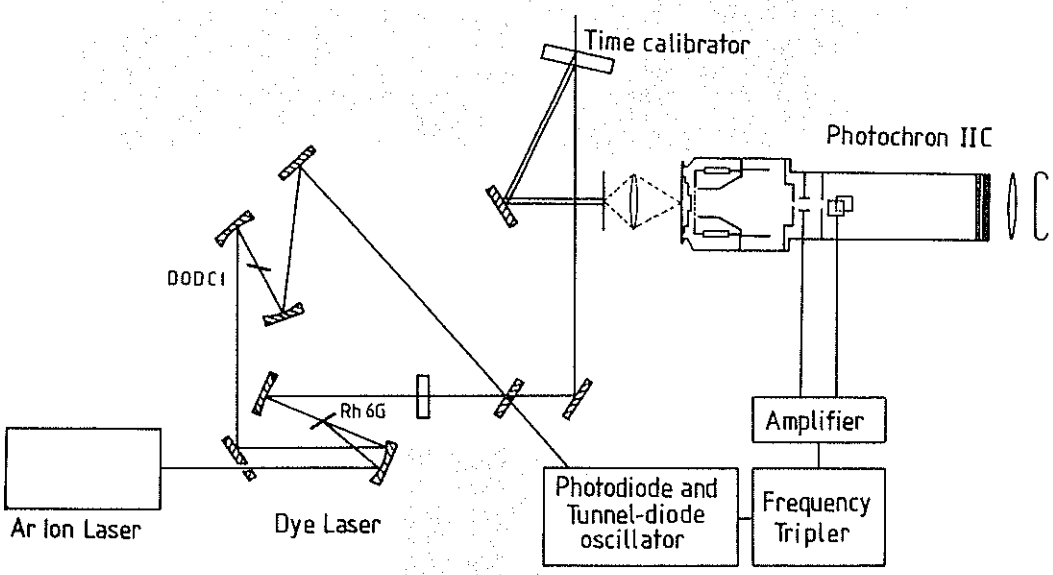
Time calibrator
Photochron IIC
DODCI
Rh 6G
Amplifier
Photodiode and
Tunnel-diode
oscillator
Frequency
Tripler
Ar Ion Laser
Dye Laser

Figure (10)

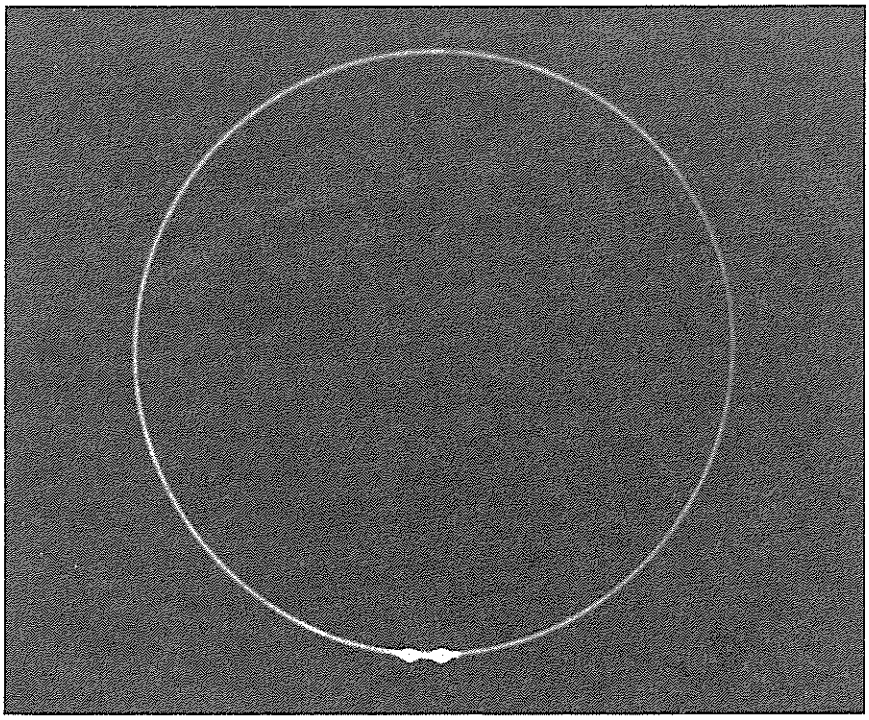

Figure 11a

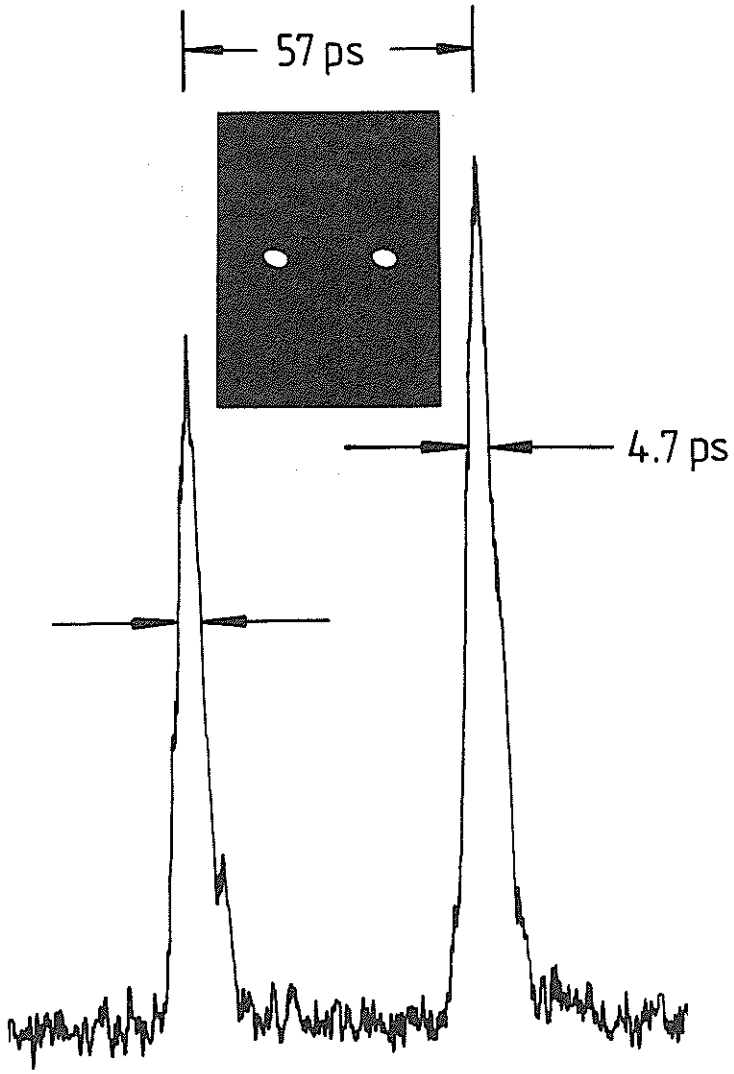

Figure 11b

SATELLITE LASER RANGING EXPERIMENTS WITH AN UPGRADED MOBLAS STATION

J.J. Degnan, T.W. Zadwodzki, H.E. Rowe
Instrument Electro-Optics Branch, code 723
NASA Goddard Space Flight Center
Greenbelt, MD 20771 USA

Telephone (301) 344 7000
TWX 710 828 9716

ABSTRACT

In the present article, we summarized the results of ranging receiver component tests which have been carried out at the NASA/ Goddard Space Flight Center since the last workshop. Based on these experiments, we have recommended a new range receiver configuration to the MOBLAS network consisting of an ITT 4128 microchannel plate (MCP) photomultiplier (PMT), a 1 GHz bandwidth ENI amplifier, a gatable Tennelec TC454 constant fraction discriminator (CFD), and Hewlett Packard HP5370A time interval unit (TIU). The ITT MCP PMT has a 450 picosecond impulse response, a 2 cm RMS transit time jitter for single photoelectron inputs, a subcentimeter RMS jitter for signal levels greater than eight photoelectrons, and millimeter level biases resulting from image motion on the photocathode surface. It is far superior to the current MOBLAS network standard, the Amperex 2233B. Similarly, the Tennelec TC454 gatable four channel constant fraction discriminator has a much flatter time walk characteristic than the ORTEC 934 CFD currently used by the network. The RMS deviation of the TC454 from the nominal zero point is about 0.20 cm over the full dynamic range compared to 1.5 cms for the ORTEC device. After substituting the MCP photomultiplier for the Amperex 2233B in a 1981 version MOBLAS receiver, the single shot range residuals and normal point residuals were reduced by roughly a factor of three in ranging experiments to the LAGEOS satellite. The one sigma scatter of the MCP normal points was consistently subcentimeter with 0.3 cm being a typical value. The one sigma single shot scatter of 1.5 cms obtained with the MCP was largely limited by the resolution of the older HP5360 TIU.

SATELLITE LASER RANGING EXPERIMENTS WITH AN UPGRADED MOBLAS STATION

1. INTRODUCTION

During the past several years, the Advanced Electro-Optical Instrument Section at the Goddard Space Flight Center has conducted a series of experiments, in support of NASA's mobile laser (MOBLAS) ranging network, to determine the "optimum" commercial laser ranging components. At the last workshop, we reported on a comprehensive laboratory study of a variety of laser transmitters and demonstrated the performance superiority of modelocked transmitters, of both the active and passive variety, over Q-switched and cavity-dumped systems[1]. In a second paper, we discussed our plans for a general upgrade of the MOBLAS systems based on the ranging hardware available in the fall of 1981[2]. We also discussed some preliminary satellite laser ranging results obtained with a passively modelocked laser built by Quantel International. Since that time, a number of attractive new receiver components have appeared on the commercial market including a microchannel plate photomultiplier (MCP/PMT) built by ITT and a new low time-walk constant fraction discriminator (CFD) offered by Tennelec. In this paper, we compare the performance of these new devices to that of their component counterparts in the operational MOBLAS stations and suggest an "optimal" dual channel receiver configuration for a MOBLAS-like station. We also report on the results of satellite laser ranging tests with a partially upgraded MOBLAS test station.

2. COMPONENT TEST RESULTS

In our previously reported tests of three different modelocked laser transmitters[1], we demonstrated that the bias errors introduced by the laser were consistently less than one centimeter. The pulsewidths of these lasers varied between 60 and 150 picoseconds. Because of the relatively simple nature of passively-modelocked Nd:YAG transmitters, a commercial transmitter built by Quantel was recommended to the NASA Laser Tracking Network. Following successful field tests in the Fall of 1981[2], all of the active MOBLAS stations have since been upgraded to include a 150 picosecond pulse transmitter consisting of a combined actively-passively modelocked Nd:YAG laser oscillator, one double-pass amplifier, a single pass amplifier, and a KD*P doubling crystal. The use of an active acousto-optic Bragg cell modulator in conjunction with a passive modelocking dye cell increases the stability of the laser output energy and reduces the number of missed pulses as compared to a totally passive device. The maximum total output energy of the system is about 200 millijoules at 1.06 microns with about 50 percent conversion to the .53 micron green radiation.

The four nanosecond impulse response of the Amperex 2233B photomultiplier used in the current MOBLAS receiver is a poor match to the new 150 picosecond transmitter. Our choice for a photomultiplier tube in the upgraded MOBLAS receiver was a microchannel plate built by ITT which has an impulse response of about 450 picoseconds. Earlier photomultipliers, such as the electrostatic and static crossed field devices built by Varian, also had impulse responses on the order of a few hundred picoseconds but are no longer available at a reasonable cost. Furthermore, recent experiments have shown that image motion on the photocathode in conventional photomultipliers can result in a greatly varying transit time for the electrons propagating down the amplifying dynode chain, and this, in turn, can lead to substantial time biases on the order of a nanosecond (15 cms)[3]. In MCP tubes, the length of the electron propagation path does not vary greatly with image position since the electrons are confined by the microchannel itself, and preliminary experiments[3] suggest that the potential biases are at the few millimeter level[3].

Figure 1 compares the performance of the ITT 4128 MCP PMT with that of the Amperex 2233B currently used in the MOBLAS network. The one sigma transit time jitter for an ungated MCP tube is about two centimeters for single photoelectron inputs compared to 10 centimeters in the 2233B. For input signal levels of eight photoelectrons or more, the jitter is subcentimeter in the MCP/PMT. The jitter increases between 10 percent and 25 percent, depending on signal level, for one particular gating configuration developed at Goddard. The ITT 4128 is a photomultiplier containing two internal MCP amplifier stages and has an electron gain of 2×10^5. In our upgrade recommendations to the network, the 4128 was chosen over the higher gain 4129 model (3×10^6), with three stages, because of the former's greater tolerance for the higher background radiation levels expected in daylight tracking experiments although a prototype of the 4129 was the first to be used in actual satellite laser ranging tests to be described later. The lesser gain is compensated for by the inclusion of a 1 GHz bandwidth amplifier available from ENI. A 1 GHz amplifier is an adequate match for the system considering the bandwidth limitations imposed by long receiver cables in typical field systems.

The output from the photomultiplier/amplifier is input to a discriminator. The latter unit generates a logic pulse which, in turn, starts or stops the time interval unit. Extensive discriminator testing has shown the constant fraction discriminator (CFD) to be the logical choice for a ranging system[4]. Other discriminator types such as fixed threshold, rise time compensated, and hybrids typically display time biases on the order of half the input pulsewidth due to input signal amplitude effects. Constant fraction discriminators include circuitry which attempts to compensate for a varying signal level. A plot of time bias versus signal amplitude is a measure of the degree to which the aforementioned compensation circuitry has been successfully implemented. In-house studies further show that discriminator time biases are very repeatable in both short term and long term operation and can be corrected for via a combination of auxiliary hardwired circuitry and appropriate software models. In fact, this approach has been utilized to elevate the performance of threshold and hybrid discriminators to that of the constant fraction

PHOTOMULTIPLIER PERFORMANCE

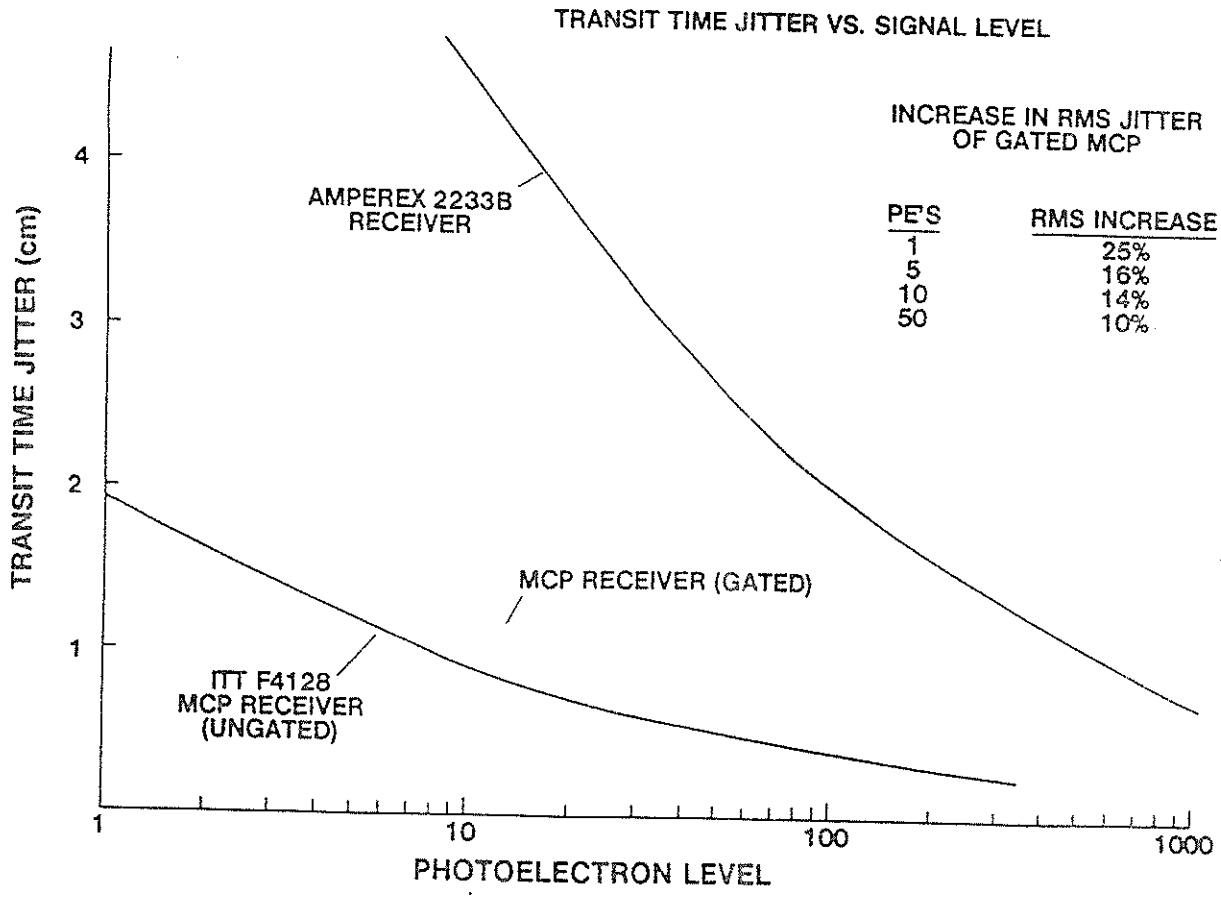

FIGURE 1

discriminator. Furthermore, the performance of constant fraction discriminators can be further improved through careful measurements of the time walk characteristic and signal amplitudes and the use of software corrections.

Figure 2 displays the time walk characteristics for the ORTEC 934 constant fraction discriminator, currently used in the MOBLAS network, and a new CFD, the Tennelec TC453. No software correction has been applied in generating these curves. Both discriminators were adjusted for minimum time walk with a one nanosecond full width half maximum input pulsewidth. Each point on the curve represents a mean of 100 time interval measurements at a fixed electronic start and stop signal amplitude. The vertical dashed lines represent the specified dynamic range of the ORTEC unit. As one can easily see from the figure, the TC453 has a much flatter time walk characteristic. The RMS deviation from the nominal zero point is about 0.20 cms over the full dynamic range compared to 1.5 cms for the ORTEC 934. Tennelec also offers a gateable four channel version of their basic CFD, the TC454.

Our 1981 recommendation to the NASA network to upgrade the time interval unit from the 100 picosecond resolution Hewlett-Packard HP5360 to the 20 picosecond resolution HP5370A has now been implemented in all of NASA's operational MOBLAS stations. We are not presently aware of any new commercial products with performance specifications superior to the HP5370A although specialized units with a factor of two better resolution have been successfully built and tested[4].

To summarize, Figure 3 is a block diagram of the upgraded MOBLAS receiver which we have recommended to the network. In addition to the usual ranging components previously described, we recommended the inclusion of two ORTEC 227 integrators for the precise determination of signal amplitude. At this time, all of the MOBLAS stations have installed a Quantel YG402DP modelocked transmitter, a HP5370A time Interval Unit, and the ORTEC 227 integrators. However, the Amperex 2233B PMT and the ORTEC 934 CFD are still the standard equipment in the operational stations. To date, no MOBLAS station has ever been fully upgraded. The change in operational performance of the MOBLAS network as individual components were upgraded is the subject of another paper at this conference[5]. In the next section, we present the results of earlier engineering test measurements to the LAGEOS satellite using prototypes of the Quantel YG402DP laser and the ITT 4129 MCP/PMT to illustrate the marked improvement to be expected when the relatively slow Amperex 2233B photomultiplier tubes are replaced by microchannel devices.

3. LAGEOS Ranging Results

In the summer of 1981, a prototype of Quantel's YG402DP laser was installed in the MOBLAS 4 station at the Goddard Optical Research Facility in Greenbelt, Maryland. The transmitter was passively modelocked and did not include the acousto-optic modelocker supplied to the present MOBLAS network. For these engineering tests, the repetition rate of the system

DISCRIMINATOR TIME WALK CHARACTERISTICS

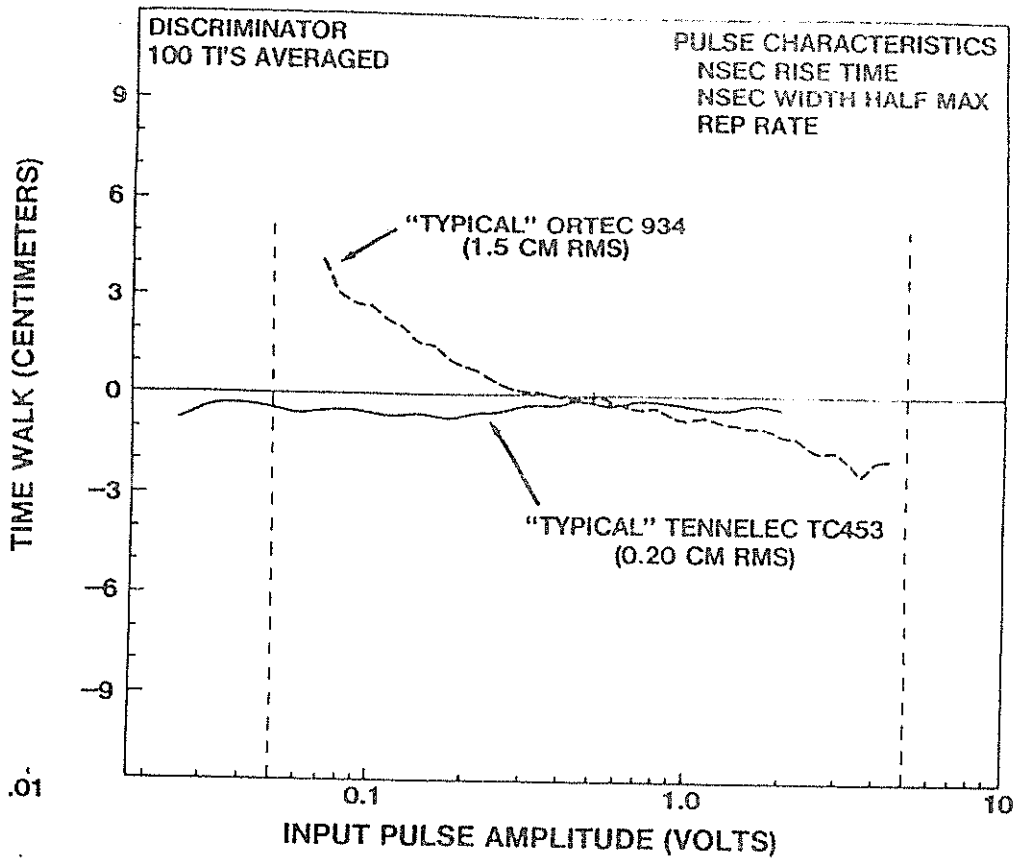

FIGURE 2

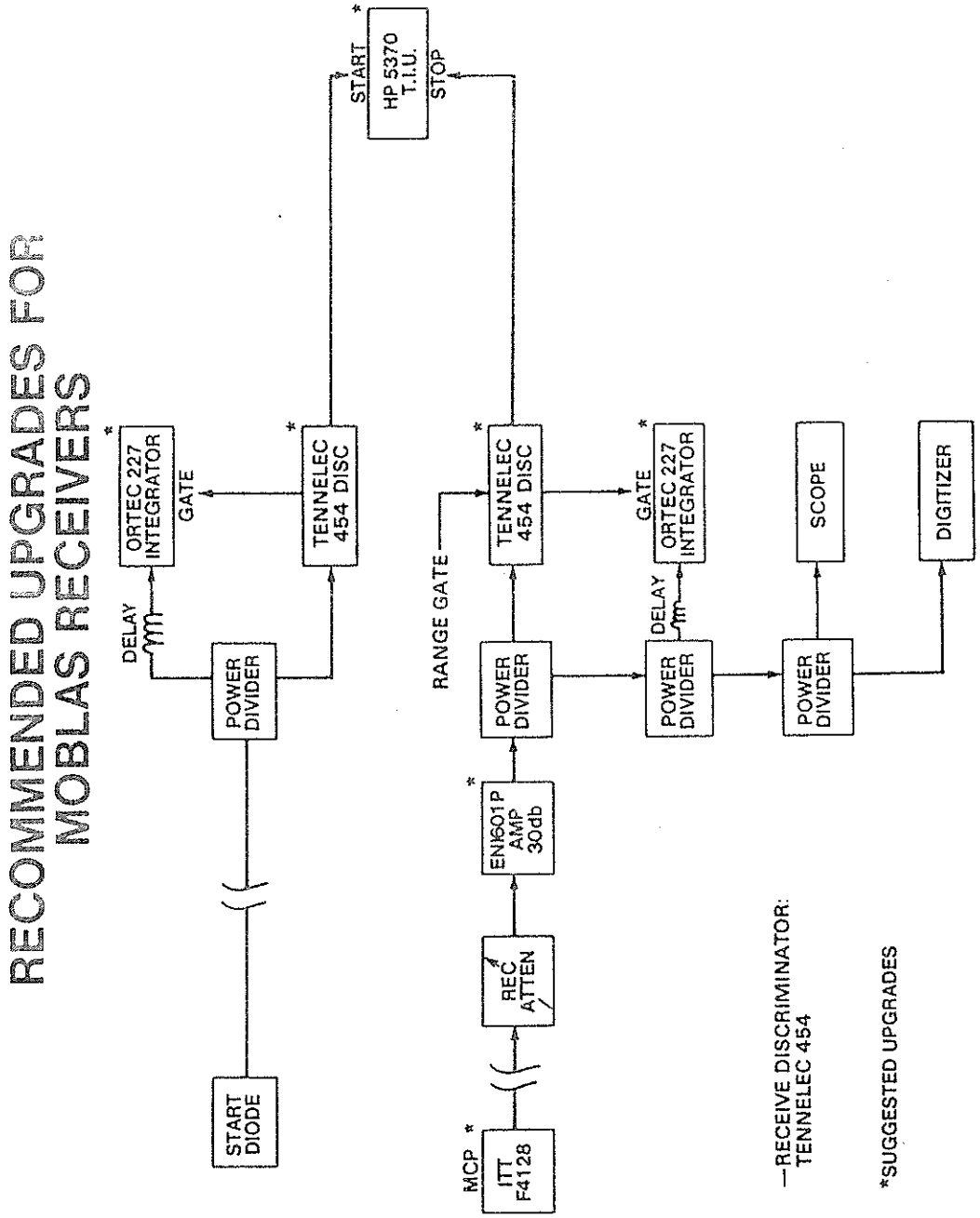
RECOMMENDED UPGRADES FOR
MOBLAS RECEIVERS
START DIODE
POWER DIVIDER
DELAY
ORTEC 227 INTEGRATOR
GATE
TENNELEC 454 DISC
START
HP 5370 T.I.U.
STOP
MCP
ITT F4128
REC ATTEN
ENI601P AMP 30db
POWER DIVIDER
RANGE GATE
TENNELEC 454 DISC
POWER DIVIDER
DELAY
GATE
ORTEC 227 INTEGRATOR
POWER DIVIDER
SCOPE
DIGITIZER
—RECEIVE DISCRIMINATOR: TENNELEC 454
*SUGGESTED UPGRADES

FIGURE 3

was also increased from the then standard 1 pps rate to 5 pps which resulted in a substantial increase in data yield and greatly simplified satellite acquisition. The 5 pps rate has since become the standard for the network. Satellite tracking tests were initially performed using the standard operational receiver of the period which consisted of the Amperex 2233B photomultiplier, the ORTEC 934 constant fraction discriminator, and the HP5360 time interval unit. After taking three LAGEOS and one BEC pass with the standard receiver, the 2233B photomultiplier was replaced by a prototype of the ITT F4129 microchannel plate PMT. The latter had only a 5 percent quantum efficiency compared to current commercial devices which have a 12 to 15 percent efficiency. Because of the shorter pulsewidth out of the MCP/PMT, it was necessary to adjust the ORTEC 934 CFD for short pulse operation. The ranging performance of both systems was evaluated using the software package LASPREP which fits the measured range data to an orbit (J2 term only) using best least square estimates of range and time bias, applies a three sigma filter to the data, and repeats the procedure until there is no further improvement in the RMS of the orbital fit. The software also computes running normal points which are obtained by averaging 50 returns and then dropping the first data point in the subset and adding the subsequent data point to compute the next normal point.

Table 1 summarizes the results of the field experiments. Using the Amperex 2233B PMT with the ultrashort pulse laser resulted in single shot RMS precisions to LAGEOS between 2.5 and 4.2 cms, as determined by the LASPREP processor, for three separate passes in September, 1981. The RMS precision of the normal points was between 0.8 and 1.2 cms. In these runs, anywhere from 3 to 8 percent of the raw data was edited out by the iterative processor. Interestingly, the satellite data was better than the ground data, i.e. the tower system calibration data or the pre-and-post calibration agreement. This apparent inconsistency was later traced to the support pole behind the calibration target which reflected spurious pulses into the receiver resulting in a double-peaked range calibration histogram.

After painting the offending pole black and installing the microchannel plate PMT, agreement between the pre-and-post calibrations was typically subcentimeter with only one exception (1.97 cms) for the nine LAGEOS passes. The single shot RMS for the system calibration runs fell between 1.1 and 2.3 cms. The single shot RMS for the orbital data sets was only slightly higher than for the calibration data sets, i.e., typically between 1.5 and 2.5 cms for large data sets. Only 1 to 6 percent of the raw data was edited by the processor in obtaining these results. Extensive laboratory tests have suggested that 1.5 cms is about the limit of precision achievable with the HP 5360 TIU and that the latter was the limiting error source in the field receiver. Nevertheless, the normal point RMS was impressive, varying between 0.05 and 0.83 cms over the nine pass data set. Figure 4 displays a LAGEOS data set taken on October 20, 1981, with the MCP/PMT installed. Figure 4a is a graph of the raw data set totalling 3707 measurements of which approximately 101 were rejected following 10 iterations through the LASPREP processor. The single shot RMS of the edited data was 1.68 cms. Figure 4b is a plot of the resulting normal

SATELLITE PASS SUMMARY

BEC PASSES

DATE	RETURNS	POINTS REJECTED	SINGLE SHOT RMS SYS CAL	SINGLE SHOT RMS PASS	NORMAL PNT. RMS (50 AV)	PRE/POST	NOTES
10/8/81	450	16.8%	2.7CM	2.7CM	.5CM	0.0CM	2233PMT
10/9/81	287	10.1%	1.3	2.67	.4	.4	MCPPMT

LAGEOS PASSES

9/25/81	2420	3.5%	5.6	3.7	.8	0.0	2233PMT
9/26/81	3717	3.0%	3.6	4.2	1.2	-8.1	2233PMT
9/29/81	3510	8.0%	5.5	2.5	1.0	-25.8	2233PMT
10/9/81	86	17.%	1.41	1.68	.05	1.97	MCPPMT
10/14/81	2594	6.7%	1.18	1.77	.27	0.0	MCPPMT
10/15/81	5286	4.7%	1.62	2.56	.83	.66	MCPPMT
10/17/81	1877	3.3%	1.15	1.51	.24	.39	MCPPMT
10/20/81	3803	2.6%	1.28	1.68	.30	.88	MCPPMT
10/20/81	2963	1.7%	2.3	2.2/2.0	.4	0.0	MCPPMT
10/21/81	315	24%	2.24	4.1	.79	-.63	MCPPMT
11/3/81	594	4.3%	1.4	2.1	.37	-.58	MCPPMT

TABLE 1

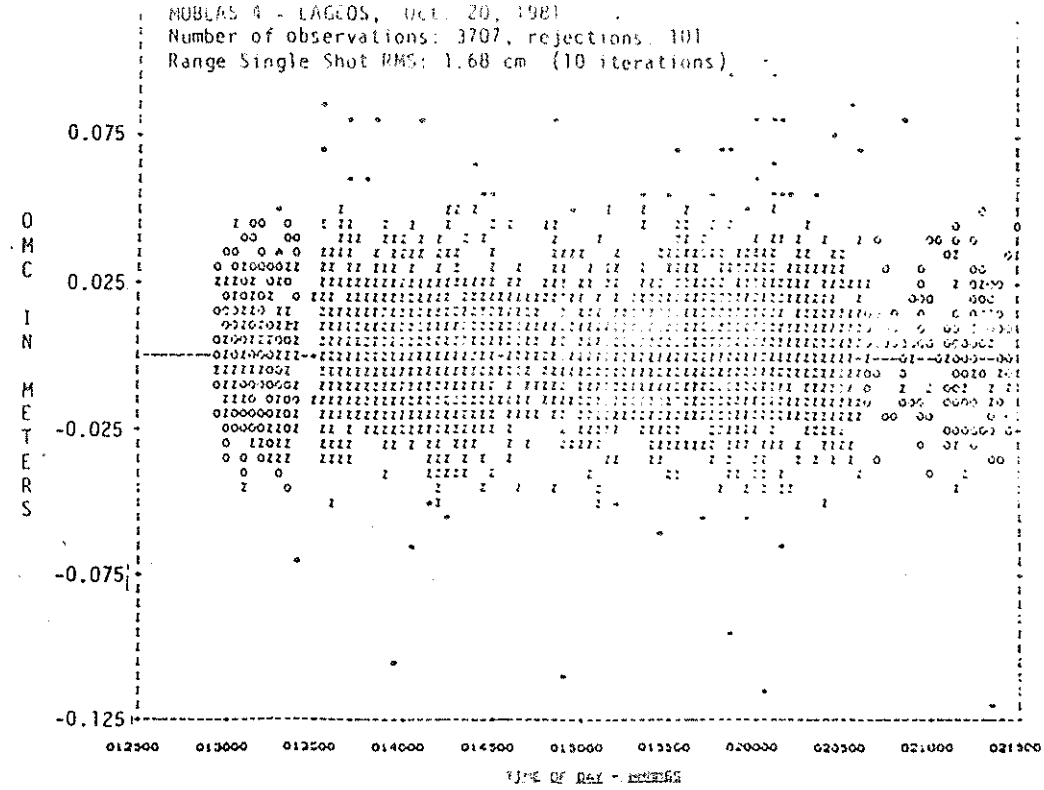

FIGURE 4(a): SINGLE SHOT DATA FROM LAGEOS

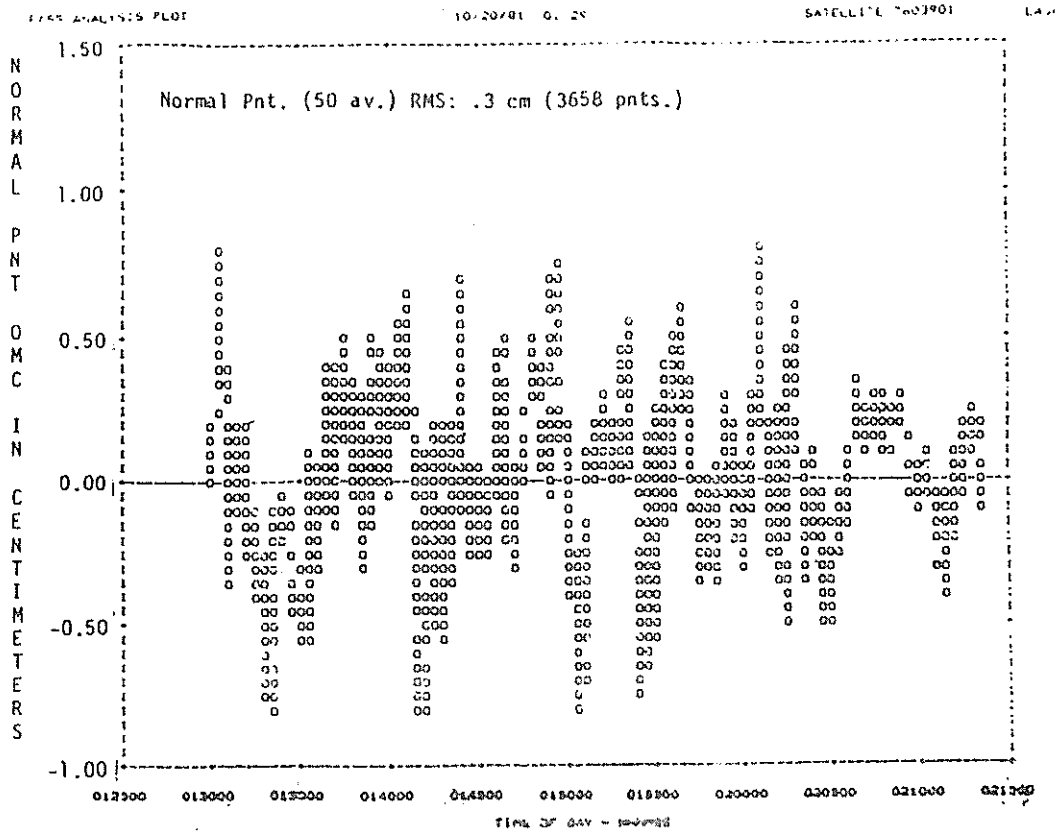

FIGURE 4(b): NORMAL POINTS FOR LAGEOS

points which have an RMS of only 0.3 cms which is only slightly higher than what would be expected for a totally random error, i.e., $1.68/\sqrt{50} = 0.25$ cms. The peak-to-peak variation in the normal points was about ±0.8 cms. Based on tests performed on LAGEOS prior to launch[7], variation in the center of mass correction as a function of satellite aspect angle is not expected to exceed ±0.3 cms.

4. CONCLUDING REMARKS

In this paper, we have suggested a dual channel range receiver configuration, based totally on commercially available parts, which is capable of providing subcentimeter precision single shot laser ranging to LAGEOS for high signal levels (tens of photoelectrons). Laboratory tests over kilometer horizontal range paths have yielded subcentimeter long term (one hour) stabilities in the mean range measurement and range uncertainties as small as 0.5 cms (one sigma). Impressive preliminary results with a partially upgraded MOBLAS field receiver have bolstered our belief that subcentimeter single shot range precisions are achievable from MOBLAS in the very near future with the installation of the microchannel plate photomultipliers and the new low time walk discriminators. So far, our efforts to implement a fully upgraded receiver in an operational field system have been severely hampered by the heavy work schedules of the MOBLAS stations and the resulting inability to schedule adequate engineering modification and test time with the Network. Consequently, we have recently established an independent Experimental Satellite Laser Ranging Station at Goddard to permit the rapid evaluation of new technology in the field independent of Crustal Dynamics Project schedules[8]. Most recently, our attention has been focused on the achievement of subcentimeter absolute range accuracies (as opposed to precisions) through the development of single channel, zero system delay ranging configurations[8]. A streak camera-based two color system is under final development and should reduce the uncertainties associated with the refractive atmospheric delay to about 5 millimeters[9].

REFERENCES

1. J. J. Degnan and T. W. Zagwodzki, "A Comparative Study of Several Transmitter Types for Precise Laser Ranging," Proceedings of the Fourth International Workshop on Laser Ranging Instrumentation, pp. 251-250, Austin, Texas USA, October 1981.
2. J. J. Degnan and A. Adelman, "Upgrade and Integration of the NASA Laser Tracking Network," Proceedings of the Fourth International Workshop on Laser Ranging Instrumentation, pp. 2-11, Austin, Texas USA, October, 1981.
3. J. B. Abshire, NASA/Goddard Space Flight Center, unpublished.
4. T. W. Zagwodzki, "Test Techniques for Determining Laser Ranging System Performance," NASA/GSFC TM-82061, January 1981.
5. D. R. Edge, "Recent Improvements in Data Quality From Mobile Satellite Laser Tracking Stations," these Proceedings.

6. B. Leskovar and B. Turko, "Optical Timing Receiver for the NASA Laser Ranging System Part II: High Precision Time Interval Digitizer," Lawrence Berkeley Laboratories Report LBL-6133, February 1977.
7. M. W. Fitzmaurice, P. O. Minott, J. B. Abshire, and H. E. Rowe, "Prelaunch Testing of the Laser Geodynamic Satellite (LAGEOS)," NASA Technical Paper 1062, October 1977.
8. T. W. Zagwodzki, J. F. McGarry, J. J. Degnan, R. S. Chabot, J. G. Lessner, and J. B. Abshire, "Experimental Large Aperture Satellite Laser Ranging System at GSFC," these Proceedings.
9. J. B. Abshire, J. F. McGarry, H. E. Rowe and J. J. Degnan, "Streak Camera-Based Laser Ranging Receiver Development," these Proceedings.

AN EXPERIMENTAL LARGE APERTURE SATELLITE LASER RANGING STATION AT GSFC

T.W. Zagwodzki, J.F. McGarry, J.J. Degnan, J.B. Abshire
Instrument Electro-Optics Branch
NASA Goddard Space Flight Center
Greenbelt, MD 20771 USA

Telephone (301) 344 7000
TWX 710 828 9716

R.S. Chabot
Bendix Field Engineering Corporation
Goddard Optical Site
Route 2, Box 274
Laurel, MD 20708

Telephone (301) 964 7000
Telex 197700

J.G. Lessner
Formerly of GSFC
Now with XEBEC
5565 Sterrett Place
Clark Blvd., Suite 501
Columbia, MD 21054

ABSTRACT

An Experimental Satellite Laser Ranging System has recently been installed at the Optical Research Facility of the Goddard Space Flight Center. The facility utilizes Goddard's multiuser 1.2 Meter Diameter Tracking Telescope. The purpose of the system is to facilitate the rapid and timely implementation of advanced laser ranging components and techniques in the field following fundamental laboratory tests. At present, we are also experimenting with a "zero delay" range receiver configuration which dictates that both start and stop pulses follow precisely the same optical and electronic paths in the receiver which, except for calibratable amplitude dependent effects, results in zero system delay. The present paper describes the current experimental configuration and summarizes ground tests and preliminary measurements to the LAGEOS satellite.

Introduction

To facilitate the transition from experimental laboratory laser ranging systems to field operable satellite laser tracking systems an engineering test facility has been incorporated into the 1.2 meter tracking telescope at the Optical Research Facility at the Goddard Space Flight Center (GSFC). The system was built to support the testing and field evaluation of advanced instrumentation, ideas and philosophies in a satellite tracking system. Use of this facility frees the experimenter from operational and scheduling constraints dictated by NASA's Crustal Dynamics Project. Having system control allows experimenters to make timely component and configuration changes to optimize system performance. Interesting problems may also be studied in detail. This effort is a continuation of laboratory work at the GSFC in which subcentimeter single shot RMS range measurements to fixed ground targets have been made. This engineering test facility will allow for the monitoring of instrument performance levels which should result in satellite tracking accuracies approaching that of laboratory systems.

System Description

Shown in Figure 1 is a block diagram of the Experimental Satellite Laser Ranging Station (ESLRS). The ELRS consists of commercially available, specially ordered, and custom built in-house instrumentation, the majority of which has come from other laser ranging programs within the GSFC. The two computer system approach was determined by the availability of existing hardware and cost constraints.

The laser ranging system is physically housed in several different work locations. The 1.2 meter diameter telescope is situated in a dome building with the controlling Honeywell tracking computer in an adjoining room. At the base of the telescope, near the system focal plane, is the receiver package and Transmit/Receive (T/R) switch. The laser transmitter is housed in a clean room adjacent to the rack mounted PDP 11/23 computer and ranging electronics. System timing is maintained at a separate building with precision 1 pps, 1 MHz, 5 MHz, and NASA 36-bit time code brought in on coaxial cables.

The Honeywell 716 (H716) computer is responsible for the pointing and tracking operation of the 1.2 meter coude focus telescope. The H716 also calculates azimuth, elevation, and range data required for the Digital 11/23 Ranging System Computer. Satellite acquisition data is input in the form of an Inter-Range Vector (IRV) which gives the position and velocity of the satellite at a specific time. A simplified model of the earth's gravity field (J2 term only) is used to compute satellite acceleration. The simplified gravity model and the initial position and velocity from the IRV are used to produce position and velocity at points one second apart along the orbit by using a fourth order Runge-Kutta numerical integrator. IRV's must be supplied for each pass since the gravity model and numerical integrator are not accurate enough to integrate orbits around the earth from one pass to the next.

To maintain smooth tracking the servo system requires pointing updates at a 20 Hz rate. The numerical integrator supplies the pointing angles and range data at one second intervals. A second order polynomial is used to interpolate between one second points to obtain data at the required 20 Hz rate.

In order to attain the required pointing accuracy for satellite ranging the telescope pointing errors must be modelled. The mount modeling coefficients are determined periodically by recording angle biases required to boresight the telescope onto predetermined stars in a grid. Absolute pointing at or near the arcsecond level is possible with this mount error modeling technique.

The range data is sent from the H716 to the Ranging Computer (Digital 11/23) at a 5 Hz rate. Each range is sent 150 milliseconds before the corresponding laser fire. This allows the ranging computer time to input, decode, and output the data to the range gate generators before laser fire.

Along with the ranging data, the H716 also sends current pointing angles, time-bias and system mode to the ranging computer to be recorded on magnetic tape. Every 200 milliseconds a record is made of the predicted angles and range, the observed range, time bias, cross track bias and other pertinent data corresponding to the current laser fire. This data is analyzed after the pass to determine data quality.

The Ranging System Computer provides for operator interface by displaying on the CRT the observed minus calculated (O-C) plot of satellite range data and indicates signal strength of either transmit or satellite return with an audible tone. The ranging computer is responsible for recording all pass data on the log tape and controls all the I/O and electronic functions required to operate the ranging system.

The transmitter is a Quantel passively mode locked Neodymium YAG laser model YG402 DP. Laser output is 100 millijoules (mj) at 5320Å with a pulsewidth less than 200 picoseconds. Laser repetition rate is 5 pulses per second. The beam exits the laser with a diameter of about 7/16 inch. Approximately 10 meters away at the coupling lens the beam diameter has grown to about 5/8 inch. The negative coupling lens is positioned at its focal length inside of the telescope's focus, matching the cone angle of the F29 system. The whole primary mirror is illuminated resulting in a final transmitted beam diameter of 1.2 meters and a beam divergence of about 10 arcseconds.

The laser ranging system incorporates a common optics, common channel range receiver. The system transmits and receives through the same telescope optics and uses one common detector, amplifier, and discriminator chain for both outgoing and return pulse measurements. This configuration has proven to be the most accurate with single shot RMS accuracies approaching 5mm in horizontal range tests over kilometer distances. Single channel receivers, although simple in theory, are more difficult to implement than the more common dual channel approach. The range receiver must view through the telescope optics as the 100mj pulse

exits the system. Near perfect isolation is required to prevent receiver saturation from backscatter of the outgoing pulse. The single channel approach requires that a small portion of the outgoing laser pulse be sampled as it leaves the telescope. This has been done with a rather unique Transmit/ Receive switch. Shown in Figure 2 is the configuration used in the T/R switch to permit single channel operation. The glass disk in the T/R switch is geared to a synchronous motor and is matched to the laser repetition rate of 5 Hz. The laser fire circuitry is enabled only during a short period of time in which a Hall Effect pick-off is properly aligned with a small magnet mounted in the disk hub. This insures that the laser fires only through the windowed portion of the glass disk. This window is an anti-reflective (AR) coated 24° sector of the disk. The remaining disk surface is coated for maximum reflectivity at 5320Å. To further protect the range receiver from a laser misfire, the non- windowed back surface of the disk is covered with an opaque absorber.

Normal T/R switch operation permits passage of the outgoing laser pulse into the telescope while controlling the optical level into the receiver. Disk rotation during satellite round trip time provides for the high reflectivity mirrored surface required to complete the T/R sequence efficiently. By transmitting through a window rather than a hole in the rotating disk a start pulse may be derived from any point beyond the T/R switch. This is done by placing a cube corner reflector in the outgoing beam facing back toward the laser transmitter and receiver. As the laser pulse exits the system, the small portion intercepted by the cube corner is reflected back on axis towards the source. Over 99 percent of the start cube return is transmitted through the AR coated window in the T/R switch. The remaining fractional percent is reflected into the range receiver. This start pulse requires an additional attenuation of 3 to 4 Neutral Densities (ND's) to maintain the proper start signal level. The ND's are held in a small hub mounted holder which rotates with the glass disk. These ND filters protect the receiver from the outgoing backscatter, and then rotate from view for the satellite return. The key for reliable operation is to maintain a start cube corner signal level well above backscatter.

All range measurements are made relative to a start cube corner mounted in the system reference plane in the telescope. Optical and electrical path lengths are identical for both start pulse and satellite return from the point of the apex of the cube corner. This unique feature means the system is self calibrated and has zero system delay.

System calibration is a serious problem with current ranging systems in NASA's Laser Tracking Network (LTN). These systems generally require calibration procedures which rely on geodimeter ground surveys over several kilometers. It appears that the upgraded short pulse laser ranging systems in use in the LTN are actually more accurate than current ground survey techniques used to establish system delay. The latter techniques appear to be accurate only to a few centimeters which in turn limits the absolute accuracy of LTN systems such as NASA's Mobile Laser Ranging Systems (MOBLAS). This inconsistency in calibration is eliminated in the Experimental Satellite Laser Ranging System by designing a system with no system delay.

The range receiver consists of a microchannel plate (MCP) photomultiplier tube (PMT), amplifier, constant fraction discriminator, and choice of time interval units. The photomultiplier tube is an ITT model F4128 two-stage MCP. This PMT has a full width at half maximum impulse response of 450 picoseconds and a gain of approximately $2X10^5$. Tube transit time for the MCP PMT is 3 to 4 nanoseconds with a single photoelectron transit time jitter of 100 picoseconds. The system is capable of single photoelectron detection with the 1 GHz amplifier and Tennelec TC454 Constant Fraction Discriminator. A choice of three time interval units are available for system use. They include a 20 picosecond resolution Hewlett-Packard HP5370 time interval unit and two developmental units built for NASA by Lawrence Berkeley Laboratory (LBL), i.e., a 19.5 picosecond resolution event time and a 9.7 picosecond resolution time interval unit.

Results

Although system configuration has not reached the final goal as shown in Figure 2, preliminary results of the Experimental Satellite Laser Ranging System are very encouraging. Start cube corner placement in the telescope was temporarily moved 26.075 inches forward to prevent self shadowing on the primary mirror. Satellite tracks taken early as proof-of-concepts of the common optics approach, and common receiver approach were convincing enough to proceed without hesitation. The system presently derives the start pulse from within the T/R switch and uses common transmit/receive optics and common MCP range receiver. Cube corner placement in the telescope will be finalized upon fabrication of a non-shadowing holding fixture which assures reliable operation in all telescope azimuth positions.

Ground ranging tests to a fixed cube corner over a 3.4 kilometer horizontal path repeatedly show the system capable of single shot RMS accuracies of 1 centimeter or less. System stability over a 1 hour period is typically a few millimeters for 100 point averages.

LAGEOS satellite passes taken in late August and early September 1984 show the system is now comparable to NASA's best tracking MOBLAS systems. The ELRS has achieved a 60 to 80 percent data return rate from the LAGEOS satellite on a single pass with typically 8000 to 10000 range measurements. Early analysis of pass data using a 15th order polynomial fit appears inadequate for centimeter range data. The polynomial fit used by the LTN appears to introduce a modeling error which limits system performance to approximately 3 centimeters, while rejecting good data. Other methods of actually fitting the data to an orbit as in the GSFC's LASPREP program are being investigated. Absolute system accuracy at the moment may be known only to a few centimeters but as the final system configuration is implemented this accuracy should approach one centimeter. Work will continue on this system to better characterize new instrumentation, techniques and procedures required to achieve one centimeter satellite laser ranging accuracies.

Future plans for the 1.2 meter ESLRS include single photoelectron versus multiphotoelectron studies, daytime tracking, simulated synchronous satellite range measurements for time transfer experiments, lunar range measurements and multiwavelength range measurements.

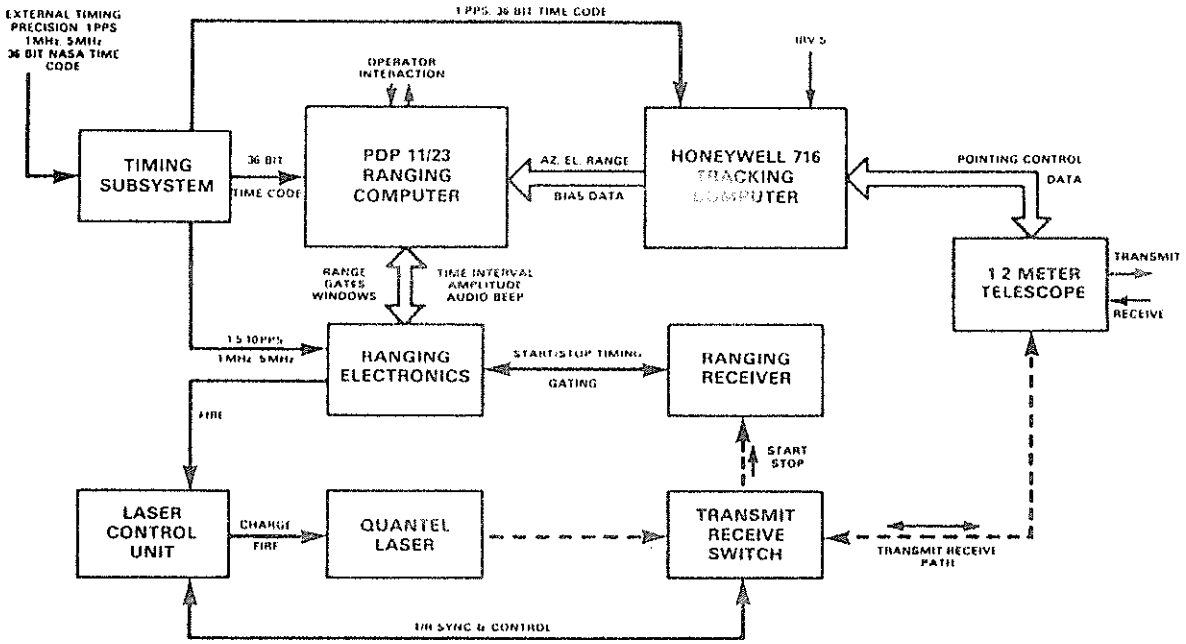

SIMPLIFIED BLOCK DIAGRAM OF
EXPERIMENTAL SATELLITE LASER RANGING SYSTEM

FIGURE 1

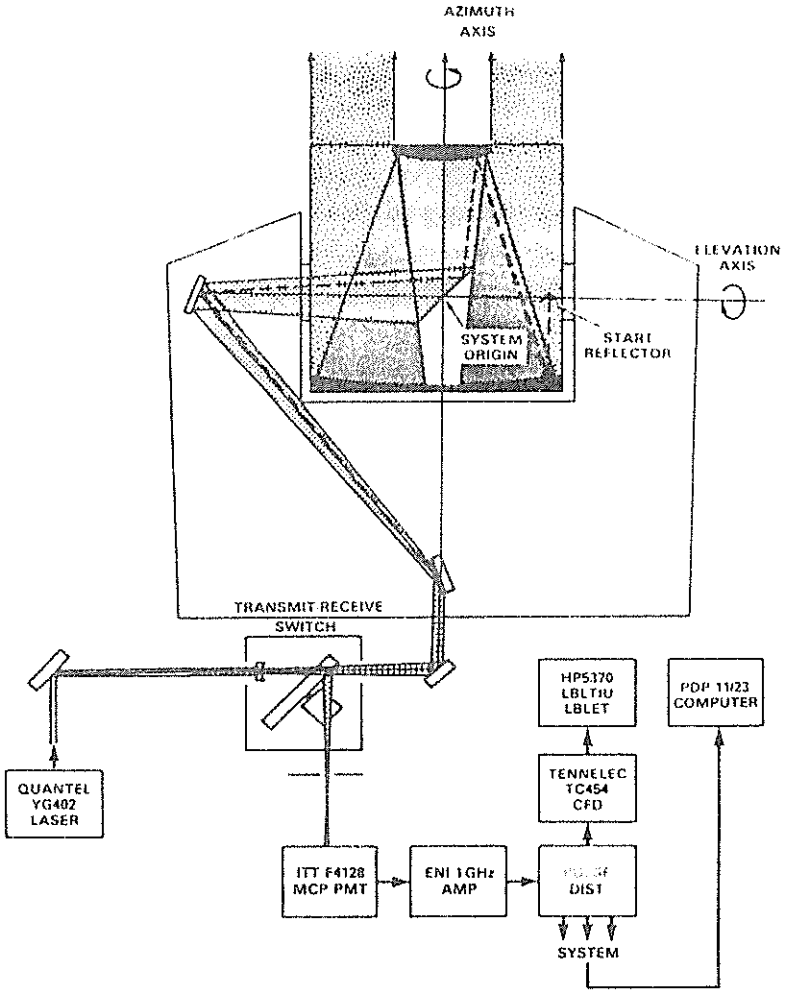

COMMON OPTICS, SINGLE CHANNEL
RANGE RECEIVER

FIGURE 2

TUNABLE ETALON USAGE AT MLRS
McDOANLD LASER RANGING STATION

J. Wiant
University of Texas
McDonald Observatory
Fort Davis, Texas 79734 USA

Telephone (915) 426 3263
TWX 910 874 1351

ABSTRACT

A tunable etalon is tried as a spectral filter in the signal return path of the McDonald Observatory Laser Ranging Station (MLRS). The piezoelectric elements of the etalon are actively tuned for 532 nanomenters by sensing a helium neon laser passing through the etalon at an angle.

Goal: To use the spectrally tunable etalon to reduce background optical noise during,

a) daylight Lageos and lunar ranging, and
b) near full moon lunar ranging.

Advantages: This etalon has a narrow bandpass (≈1Å). Because this etalon is piezoelectrically driven, using active feedback circuits, it is thermally and mechanically stable.

Restrictions: Used with a 76 cm telescope, the effective aperture of this etalon is ≈4 arcsecond.

Results: The calculated normalized throughput of 0.8 units has not been reached. The maximum throughput obtained is 0.5 units. This lower than expected throughput is disappointingly low. Therefore, the Burleigh etalon is not now used at MLRS.

Equipment used: See Figure 1.

Description of setup: The etalon is positioned in the optical path ahead of the photomultiplier (Figure 2). It is used as a fixed and stable narrow-band filter by stabilizing the cavity spacing using the narrow scanning mode (Figure 3). For this technique the ramp amplitude is reduced until the etalon scans only a fraction of the half-width of the reference HeNe laser line (Figure 4) and both stabilization windows are set to span the whole ramp duration.

Mirror angle ø is adjusted to yield a maximum throughput of 532 nanometer. The detector position must be re-peaked for each angle adjustment. To fully utilize the finesse stabilization option, the reference laser beam must be made nearly as large as the etalon aperture by using expanding lenses. In the MLRS station, space is not available to install expanding lenses therefore, finesse correction circuits are not used. Since ranging passes are usually shorter than 60 minutes, it is reasonable to not use the finesse correction.

Since this etalon has a free spectral range of 14 Å, it will pass ≈1 Å of bandpass every 14 Å. Therefore it is necessary to use a fixed filter whose bandpass is less than 14 Å centered on the desired wavelength. In this setup a 10 Å filter was used which happens to be our standard filter (Figure 5).

The etalon is mounted so that it can be removed quickly or installed and aligned in less than 5 minutes. Throughput was determined by observing the photomultiplier signal with the etalon in position and also removed. Three different throughput tests were used:

1. Observing the raw photomultiplier signal,
2. Observing the feedback calibration signal during ranging, and
3. Observing the data during Lageos ranging.

The maximum etalon throughput observed was 0.5 units of signal. Many possible failure modes were studied (Figure 6) and eliminated. The etalon throughput is less than expected and required. This is probably due to the coatings favoring the reference laser instead of the ranging laser to assure a good finesse for the reference laser. The coatings range from 550 nm to 650 nm. Unfortunately, Burleigh does not offer a better coating choice.

Comments: The MLRS ranging system does not use the etalon and has resorted to replacing the 10Å filter with a 3Å filter during unfavorable light conditions. These are both multilayer interference-coated filters centered at 532 nanometer. The results have been much better than expected.

Recoating the etalon plates with a better range would probably enhance the throughput. Using a capacitive servo etalon would avoid this coating conflict entirely.

Acknowledgements: The above work was supported by the NASA Contracts NAS5-25948 and NASW-3296. The author would like to thank Ben Green for his helpful studying and suggestions and Bill Schemp for his informing discussions.

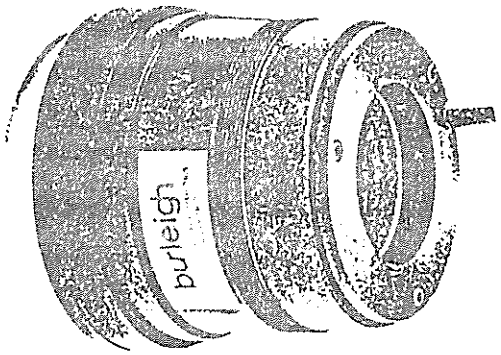

TL-38

TUNABLE
ETALON

65 to 75 mm

DAS-10 STABILIZATION SYSTEM

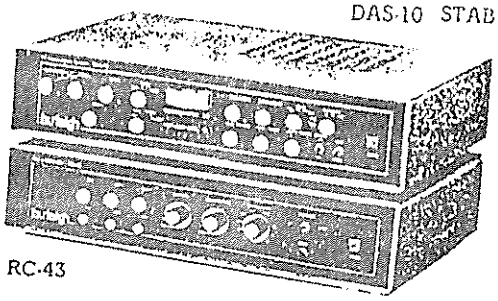

RC-43

RAMP GENERATOR

burleigh

Burleigh Instruments, Inc.
Burleigh Park
Fishers, NY 14453
(716) 924-9355
Telex 97-8379

Etalon Equipmen
Figure 1

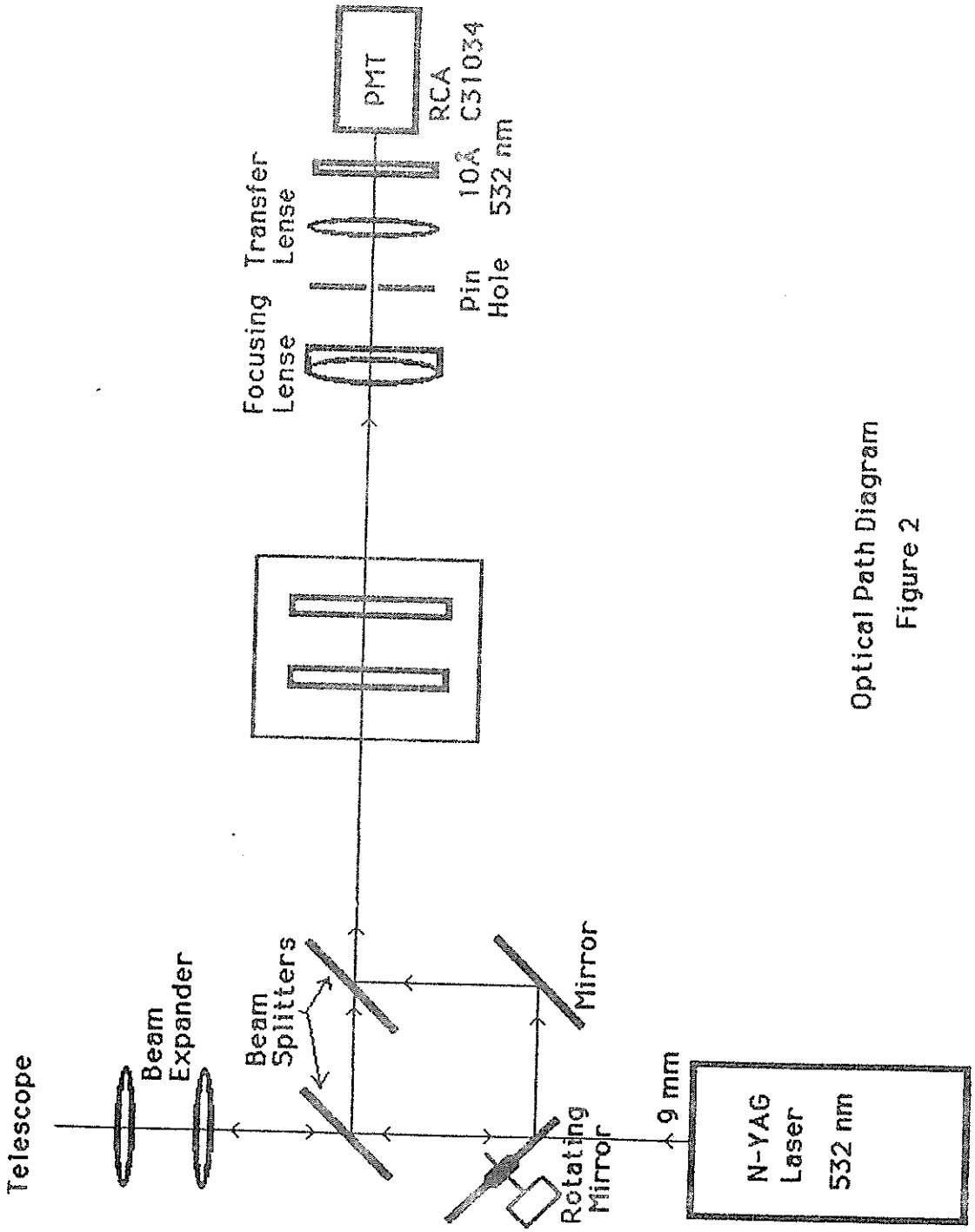

Optical Path Diagram
Figure 2

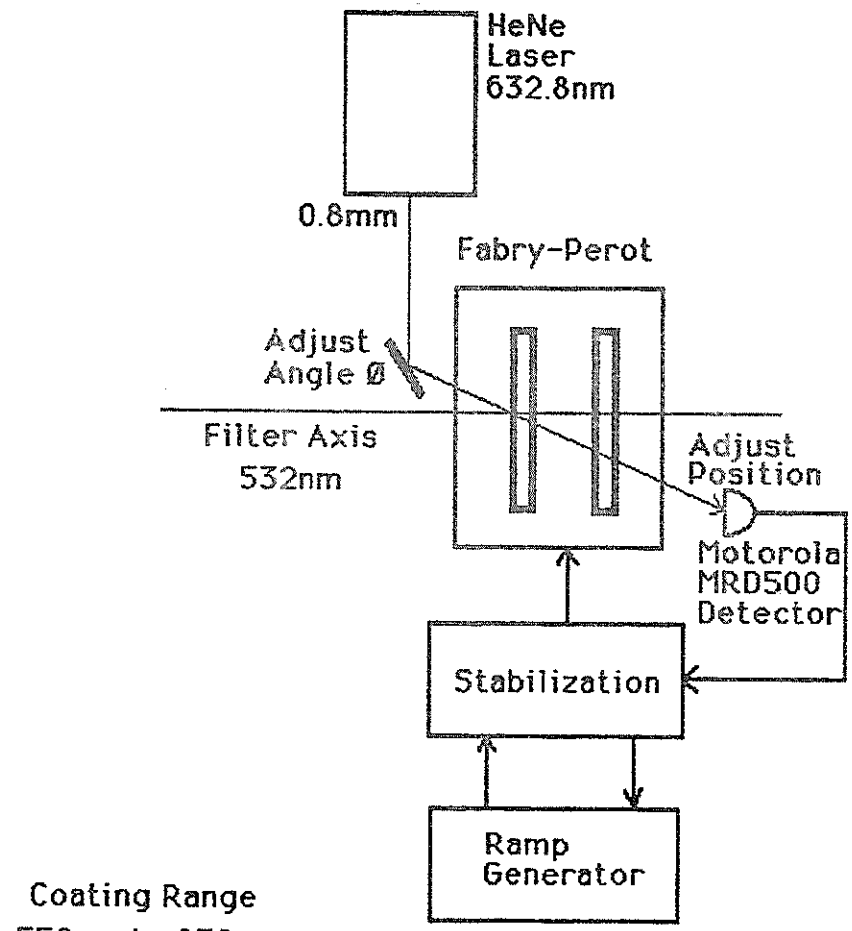

Narrow Filter Diagram

Figure 3

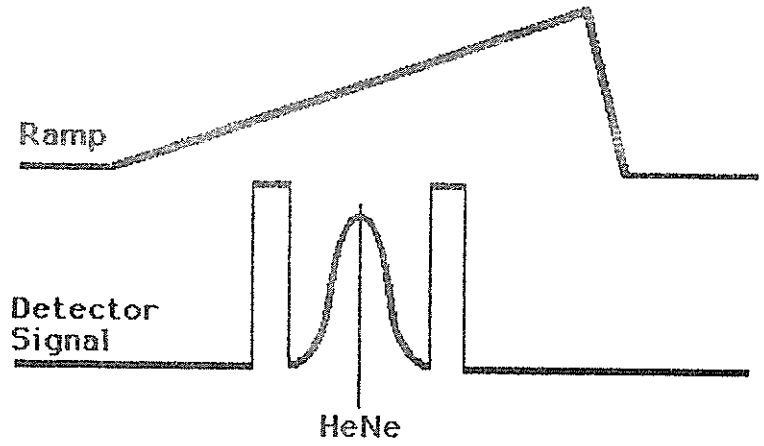

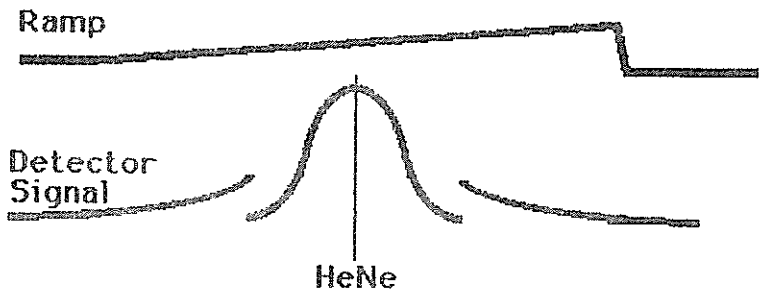

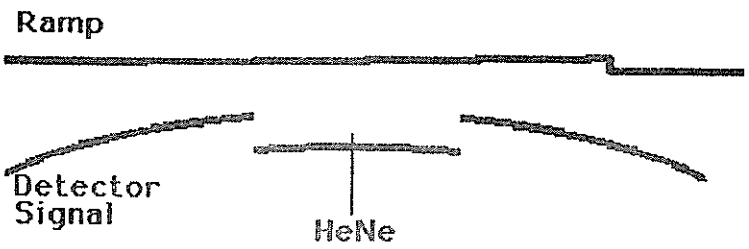

Ramp Amplitude Figure 4

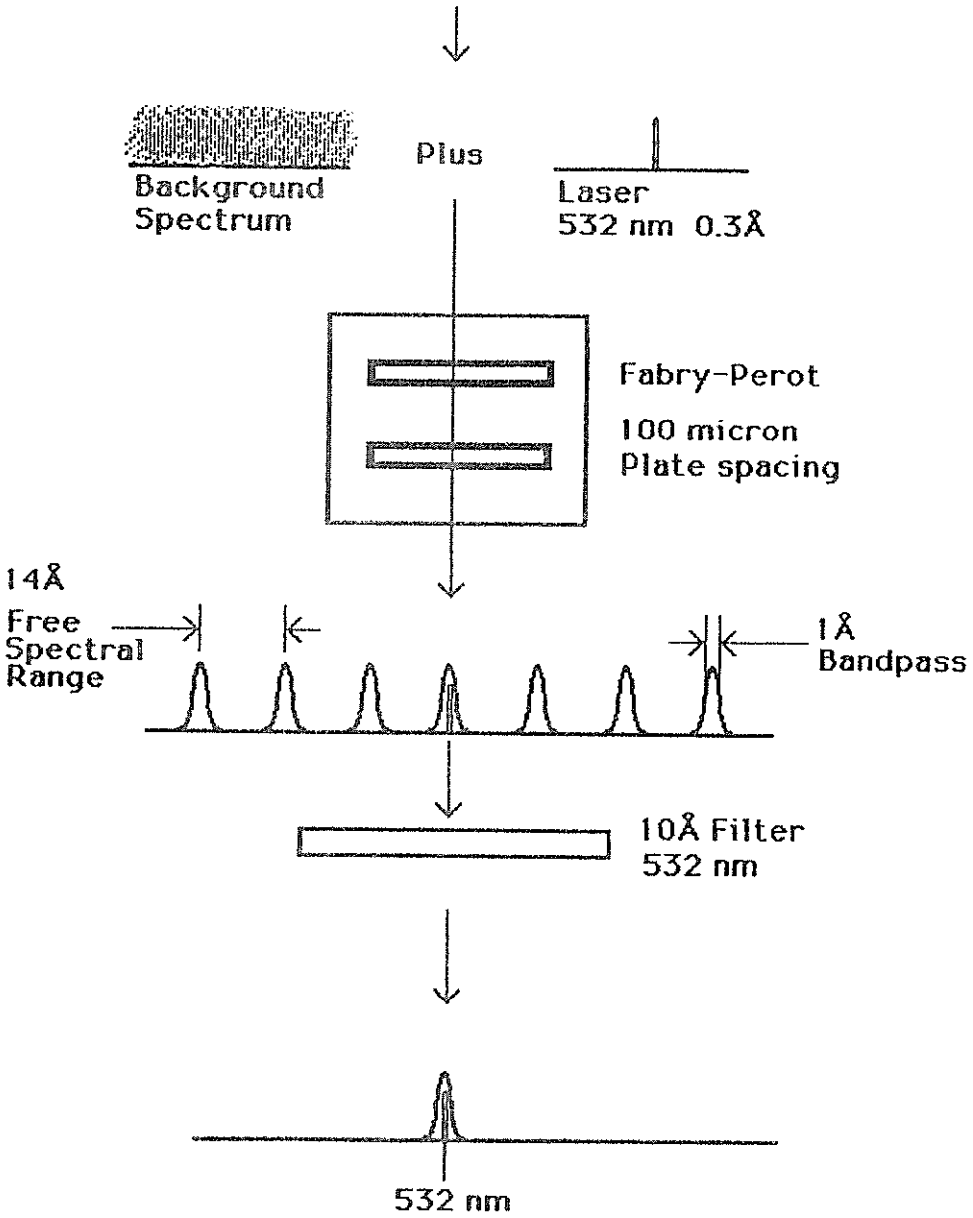

Etalon Bandpass Figure 5

Possible Throughput Failure Modes

1. Etalon damage
2. Ramp generator or Stabilizer malfunction
3. Controls set improperly
4. Mechanical alignment poor
5. Plates not parallel to incoming beam
6. Temperature changes affecting etalon
7. Vibrations affecting etalon
8. Detector poor
9. Detector not aligned
◇10. Plate coating improper
11. Plate spacing improper
12. Finesse poor
13. Incoming beam not collimated
14. Bandpass of laser greater than etalon
15. Reference laser output amplitude varying

Figure 6

IN PASS CALIBRATION DURING LASER RANGING OPERATION

P. Kloeckler, I. Bauersima
Astronomisches Institut
Sidlerstrasse 5 CH 3012 Bern

Telephone 31 65 85 91
Telex 32320

ABSTRACT

In order to avoid atmospheric refraction problems encountered with external targets, an internal calibration path was included in the Zimmerwald LRS. Light is picked up in front of the transmitting telescope, attenuated by diffuse reflection via two spheres plus a variable density filter, and fiber coupled to the receiver photomultiplier. The same discriminator/time digitizer - channel is used both for ranging and calibration. Selection of one calibration shot in n rangings is by range gate setting only. Pulse strength is also recorded. Thus a comprehensive record of internal range bias and its temporal variation is kept, and residual discriminator time walk can be corrected for.

1. CONCEPT

The convenience of in-pass, or feedback, calibration has been noted before (Silverberg, 1982). In fact, there is no compelling reason for external calibrations at all, save for residual range bias tests with terrestrial surveying methods.
In contrast to the TLRS method, we strictly wanted to use the same path and vernier time unit (TDC) both for calibration and ranging. Since the load on our minicomputer is heavy, we could not expect to read out the TDC during the time-of-flight to lower satellites. Thus, every n-th shot has to be sacrified for calibration. This is no great loss because the return probability is not much modified by this in the few photoelectron mode. The selection of ranging/calibration is then by range gate only. Pulse charge is also recorded.

2. PRESENT STATUS

Light is picked up in front of the transmitting telescope, attenuated by diffuse reflection via two spheres plus a variable density filter, and coupled into the receiving optics via light fibre. A chopper-wheel in front of the optics gates out atmospheric backscatter. This serves to reducing unnecessary loading of the photomultiplier as well as permitting pulse strenght recording with a gate time not compatible with spurious returns shortly after the calibration pulse*) (Fig. 1).
Two light paths can be realized for calibration:
a) via light fibre and b) via diffuse reflection onto the primary mirror (used for calibration of the light fibre delay).
The ranging electronics comprise the photomultiplier, amplifier, TDC and ADC and discriminator. A couple of coaxial relays permits switching to electronic calibration. There, a pulse generator - simulating the photomultiplier pulse - and a delay-line (0-64 ns) plus a variable attenuator permit isolation of discriminator and TDC parameters. Another pulse generator is controlled by the station frequency standard and supplies one start pulse and a 1 MHz pulse train for the stop-channel, if triggered by the computer. By range-gating, a TDC test can be performed for longer delays. Although systematics and jitter from the time standard are no longer measured (the same standard is fed to test generator and TDC), an upper limit of the timing jitter of the two TDC verniers (nonlinearity which maps into jitter) still can be judged with this method.
With this setup, the main receiver parameters could be investigated; in fact, with the picosecond laser as optical excitation source a nearly optimal test facility is available in situ. The only facility lacking for pulse analysis and detection strategy optimization is a fast pulse digitizer; here we have to be content with a TEKTRONIX 7834 model oscilloscope plus 7A19 vertical amps's with a combined

---

*) The chopper has not been used up to this date in order to have minimum receiver complexity.

band width/rise time of 400 MHz/.9 ns.
In addition, an external target in a distance of 1.4 km is now and then used for testing beam divergence, telescope pointing and for veryfying the calibration constant.

3. INVESTIGATIONS

Delay Calibration of Light Fibre

The fibre has a length of 211. cm. A first estimate with a speed of light of 18 cm/ns yields a delay of 11.7 ns. Comparing the geometries of the calibration paths (light fibre/direct) we arrive at the empirical formula

$$\Delta t_{LF} = \Delta t_{CAL_{LF}} - \Delta t_{CAL_{DIR}} + 9.16 \text{ ns} \quad (1)$$

On two different occasions, this formula yielded the value

$$\Delta t_{LF} = 11.92 \pm 0.01 \text{ ns} \quad (1a)$$

Reduction of Time of Flight to Geodetical Zero

For ranging, the empirical formula derived from geometry for the correction time-of flight is:

$$2R/c = \Delta t_{SAT} - [\Delta t_{CAL_{LF}} - \Delta t_{LF} + 1.80 \text{ ns}] \quad (2)$$

and with (1a)

$$2R/c = \Delta t_{SAT} - [\Delta t_{CAL_{LF}} - 10.12 \text{ ns}] \quad (3)$$

Calibration Constant vs. Time

The constants which have been applied to the quick look data for the period of May, 15 through August, 31, are tabulated in table C. Three groups of data can be distinguished: 75.1 ± .3 / 75.6 ± .4 / 76.3 ± .3, which are due to the selection of various delays in the constant fraction discriminator. These values are subject to final adjustments.
The procedure of establishing this constant for each pass was the following: In-pass calibration was performed after every 6th range. In post-processing, these values were visually screened. Calibrations from low elevations have been removed because of parasitic pulses from the dome. Then the mean was calculated and inserted for each range (Fig. 5). The reason for this procedure - which does not allow for temporal variations during the pass - was the

lack of pulse charge recordings for this period because of the missing light chopper. This fact means that in-pass calibration was prone to slight systematic errors if the operator did not carefully watch and adjust the variable attenuator. This, because the constant fraction discriminator's dynamic range - with the given amplifier - was not better than 1:10. Improvement are under way, but for the period reported, there would be the only alternative to correct visibly biased values with off-line calibrations of the same date.

Residual Time Walk of the Discriminator

A heavy time-slewing was found for pulse amplitudes below 100 mV (threshold at 30 mV). Appropriate amplifier gain and a threshold of 100 mV were then selected (Fig. 2). Residual time walk was still detectable (Fig. 3, 4) but was found to be sufficiently small for LAGEOS tracking, where seldom returns occured with more than $n = 8$ photoelectrons (Fig. 6). Problems arise with STARLETTE with $n > 60$; and with in-pass calibration runs if the beam attenuation is not closely controlled.

The modelling of the residual time walk is not easily done because of the lack of understanding it's cause. For this reason, leading edge discrimination still appears attractive because of it's bell-shaped response.

4. CONCLUSIONS

In-pass calibration has already proven to be a valuable asset to Zimmerwald LRS. Once the deficiencies of the present setup will be overcome, all calibration points will be corrected for the residual time walk. Then a comprehensive record of the stations internal range bias will be accumulated without the effort of cumbersome pre- and post-pass calibrations to an external target board.

REFERENCES

Silverberg, E.C., 1982 "The Feedback Calibration of the TLRS Ranging System" in Proc. of the 4th International Workshop held at the University of Texas in Austin, Texas, USA

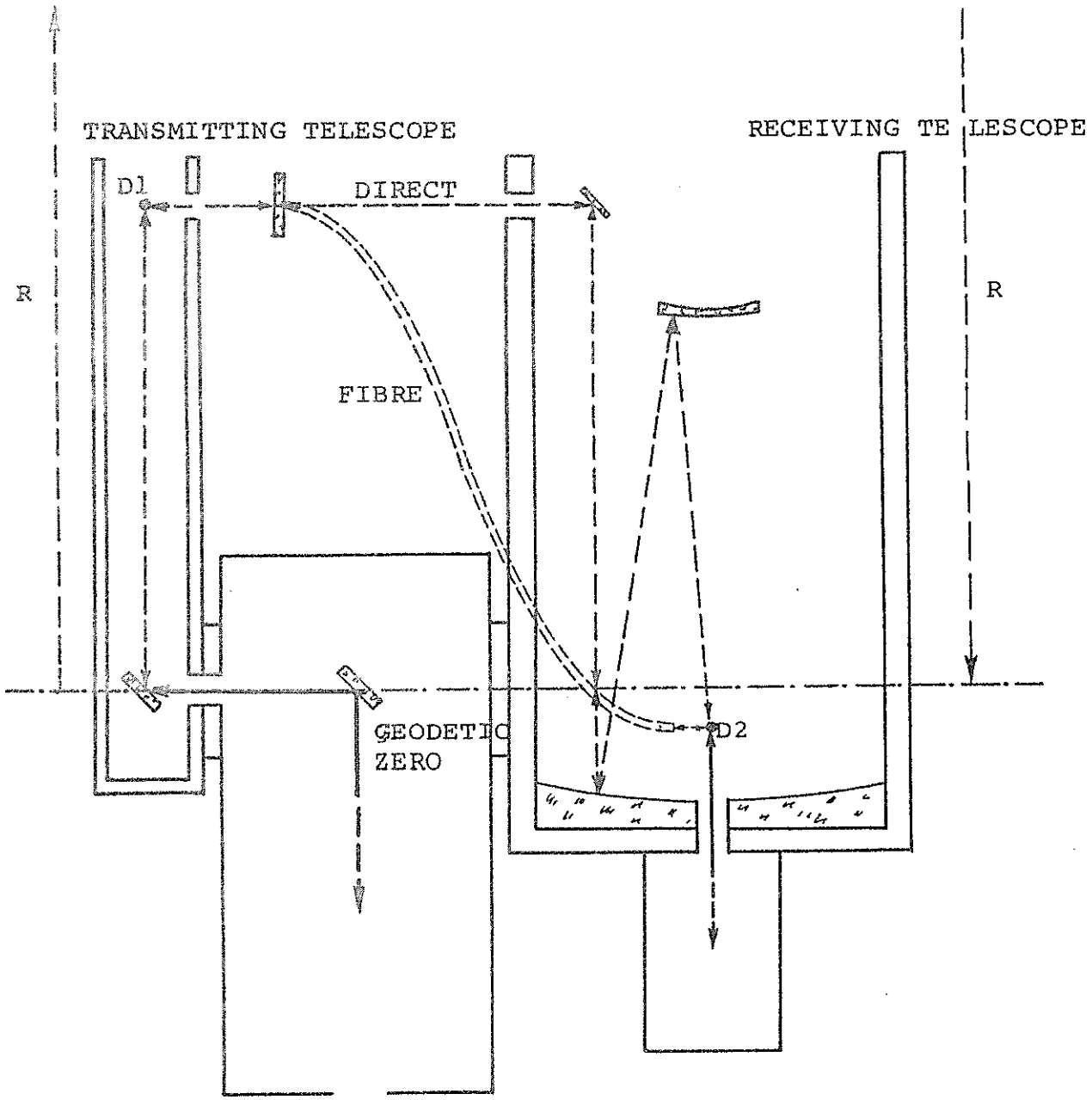

FIGURE 1 THE TWO CALIBRATION PATHS (DIRECT AND LIGHT FIBRE) OF THE ZIMMERWALD L R S.

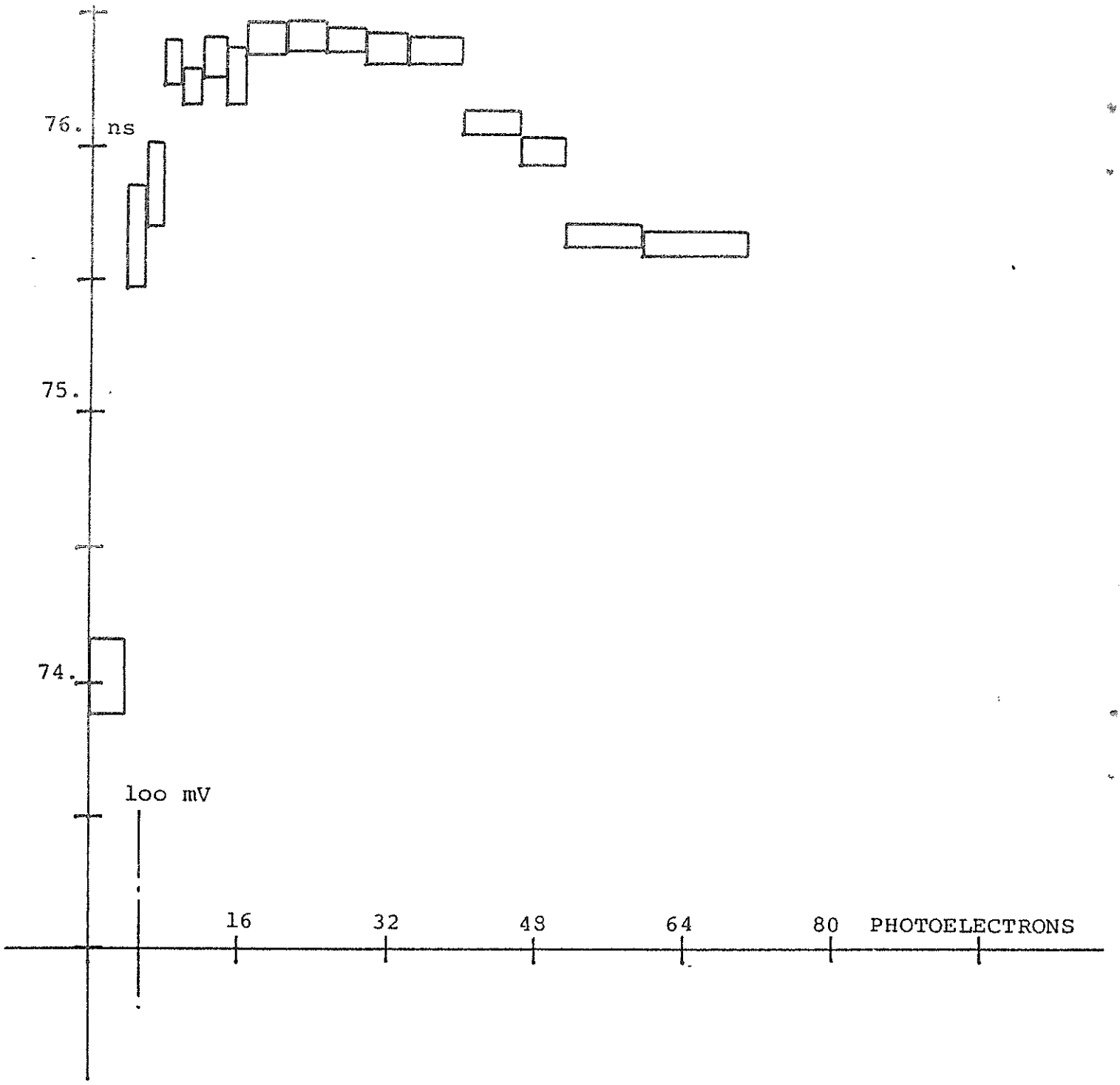

FIGURE 2 TIME SLEWING BELOW 100 mV SHOWS in IN THIS CALIBRATION DELAY VS. PULSE STRENGTH PLOT. ALSO VISIBLE IS TIME WALK STARTING AT 600 mV DUE TO AMP-LIFIER SATURATION

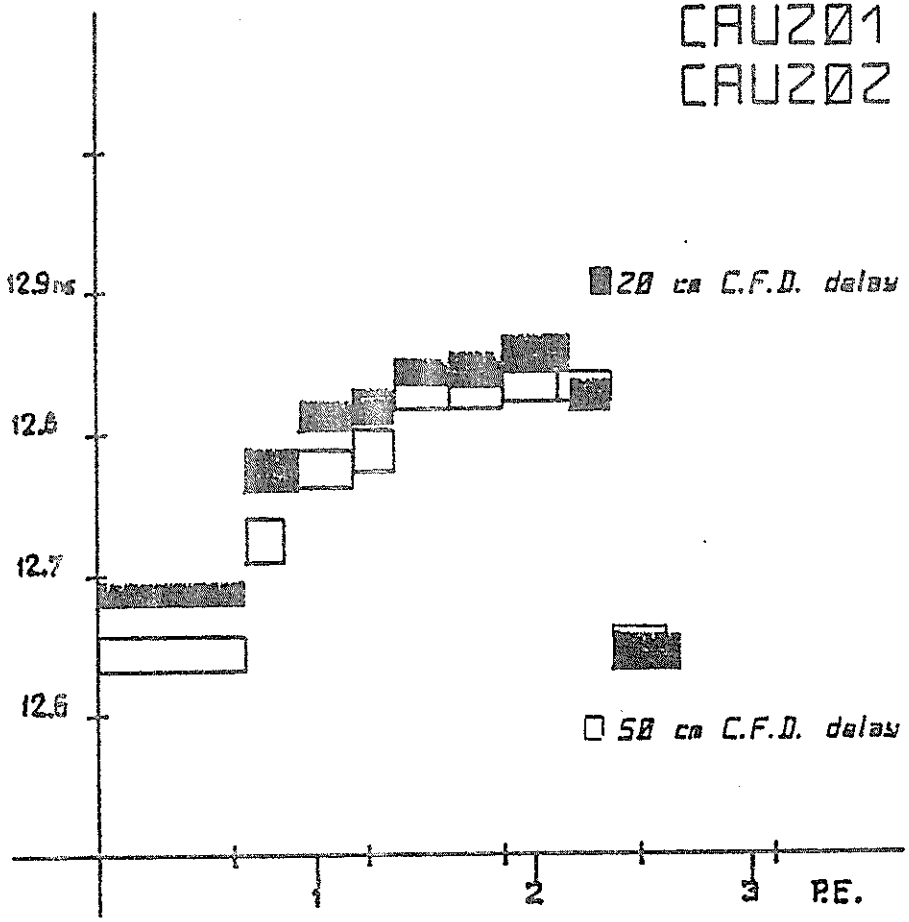

Fig.3 Residual time-walk of constant fraction discriminator vs. photoelectron equivalents. (Few photoelectron regime)

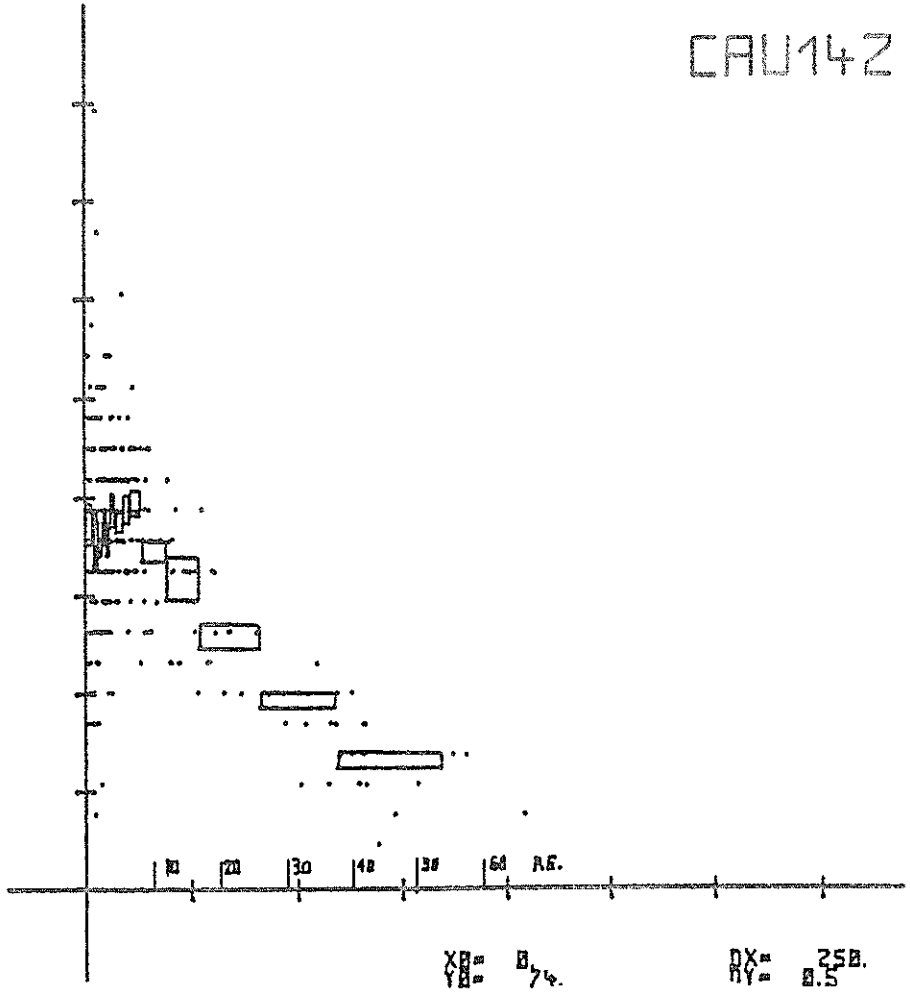

Fig.4 Residual time-walk, multiphotoelectron regime. Note degradation above 15 photoelectron equivalents!

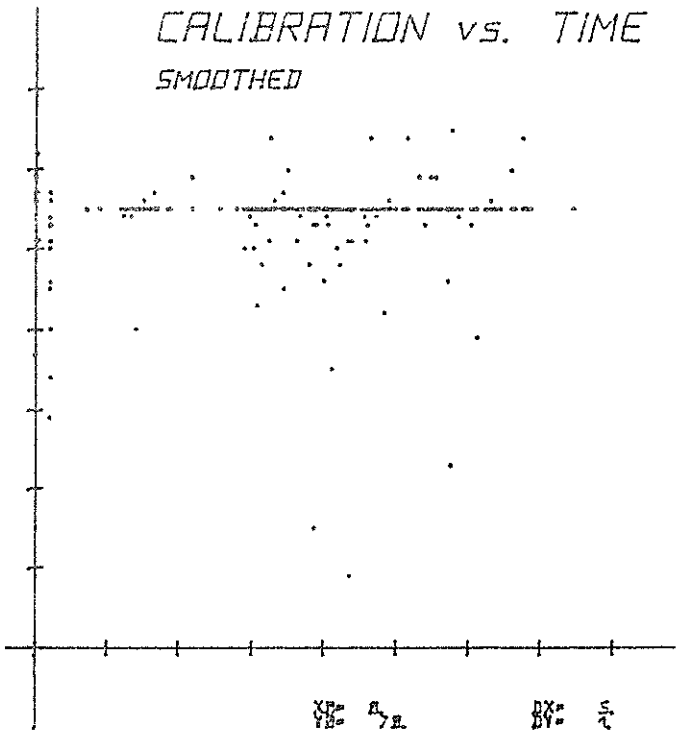

Fig.5 Result of in-pass calibration before and after screening

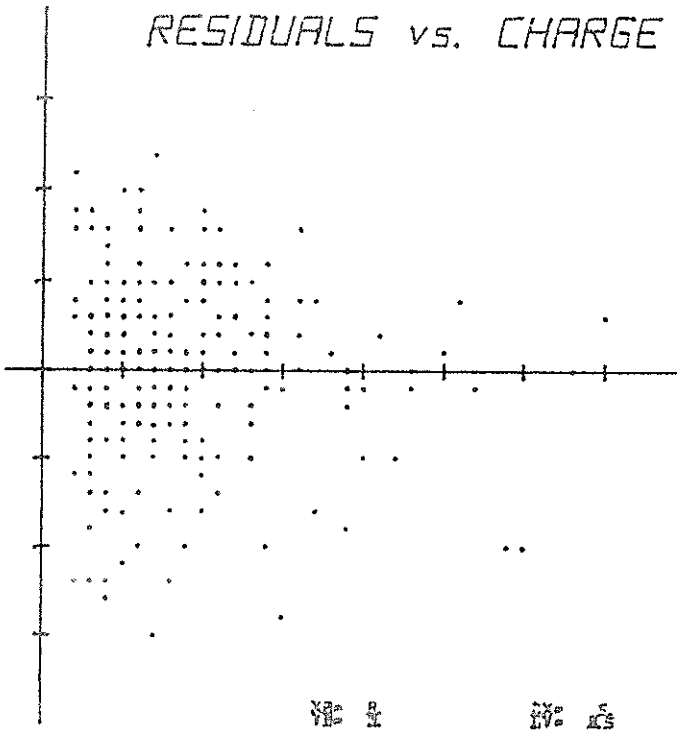

Fig.6 Residuals of LAGEOS-pass after off-line screening vs. return pulse strength.
vert.scale: 7.5 cm/division
hor. scale: 1.2 P.E./div.

LAGEOS	1984- 5-15	1:22	75.6
LAGEOS	1984- 6-16	22:44	74.9
LAGEOS	1984- 6-17	21:27	75.2
STARLETT	1984- 6-17	0:16	75.4
STARLETT	1984- 6-17	20:57	75.0
STARLETT	1984- 6-18	0:37	75.2
LAGEOS	1984- 6-18	0:50	75.2
STARLETT	1984- 6-17	22:47	75.0
STARLETT	1984- 6-18	21:16	75.7
STARLETT	1984- 6-19	0:56	75.4
STARLETT	1984- 6-19	21:36	74.8
LAGEOS	1984- 6-19	22:12	75.0
STARLETT	1984- 6-19	23:26	75.0
LAGEOS	1984- 6-20	1:37	75.0
STARLETT	1984- 6-20	23:46	74.8
LAGEOS	1984- 6-25	21: 8	75.0
STARLETT	1984- 6-25	21:44	75.0
STARLETT	1984- 6-26	22: 4	75.0
LAGEOS	1984- 6-26	23: 9	75.0
LAGEOS	1984- 6-27	21:52	75.0
STARLETT	1984- 6-27	22:25	75.0
LAGEOS	1984- 6-29	22:37	75.2
LAGEOS	1984- 7-17	0: 6	75.1
LAGEOS	1984- 7-17	22:43	75.0
LAGEOS	1984- 7-18	2:16	75.0
LAGEOS	1984- 7-19	23:28	74.9
LAGEOS	1984- 7-20	22: 9	74.8
BEACON-C	1984- 7-21	1:18	75.0
LAGEOS	1984- 7-21	1:39	74.9
LAGEOS	1984- 7-22	22:54	74.8
BEACON-C	1984- 7-22	23:55	74.5
LAGEOS	1984- 7-23	2:33	74.6
LAGEOS	1984- 7-27	23: 7	76.5
LAGEOS	1984- 7-29	20:32	76.1
BEACON-C	1984- 7-29	22:49	76.6
LAGEOS	1984- 7-29	23:59	76.3
LAGEOS	1984- 7-30	22:34	76.3
BEACON-C	1984- 7-30	22: 8	76.6
LAGEOS	1984- 7-31	2:13	76.3
LAGEOS	1984- 8- 2	22: 1	74.9
LAGEOS	1984- 8- 3	1:36	74.9
LAGEOS	1984- 8- 5	21:29	74.9
BEACON-C	1984- 8- 3	21:17	0.1
LAGEOS	1984- 8-14	23:16	75.5
STARLETT	1984- 8-15	1:53	75.9
LAGEOS	1984- 8-15	21:55	75.8
STARLETT	1984- 8-16	0:26	75.8
LAGEOS	1984- 8-16	1:33	75.8
STARLETT	1984- 8-16	2:13	75.6
LAGEOS	1984- 8-16	20:36	75.3
LAGEOS	1984- 8-17	0: 5	75.7
STARLETT	1984- 8-17	0:46	75.4
STARLETT	1984- 8-17	2:33	75.6
LAGEOS	1984- 8-17	22:41	75.9
STARLETT	1984- 8-18	1: 3	76.0
LAGEOS	1984- 8-19	23:36	75.6
STARLETT	1984- 8-20	3:31	75.8
LAGEOS	1984- 8-20	22: 8	75.6
LAGEOS	1984- 8-21	1:52	75.8
STARLETT	1984- 8-21	0:13	75.2
STARLETT	1984- 8-20	1:42	75.7
LAGEOS	1984- 8-21	20:49	75.4
LAGEOS	1984- 8-22	0:21	75.6
STARLETT	1984- 8-22	2:21	75.5
STARLETT	1984- 8-27	21: 2	75.5
LAGEOS	1984- 8-27	23:10	75.5
STARLETT	1984- 8-28	19:33	75.8
STARLETT	1984- 8-28	21:21	76.0
LAGEOS	1984- 8-28	21:48	75.8
STARLETT	1984- 8-29	19:52	75.8
LAGEOS	1984- 8-29	20:29	75.8
STARLETT	1984- 8-29	21:42	76.1
LAGEOS	1984- 8-30	0: 5	76.0
LAGEOS	1984- 8-30	22:35	75.9
STARLETT	1984- 8-31	20:30	75.9
LAGEOS	1984- 8-31	21:14	75.9
STARLETT	1984- 8-31	22:20	76.0
STARLETT	1984- 9- 1	0:14	75.8
LAGEOS	1984- 9- 1	0:53	75.9
LAGEOS	1984- 9- 1	19:58	75.7
LAGEOS	1984- 9- 1	23:24	75.6
STARLETT	1984- 9- 2	19:22	75.8
STARLETT	1984- 9- 2	21:10	75.9
STARLETT	1984- 9- 2	22:59	75.7
LAGEOS	1984- 9- 2	22: 3	75.8
LAGEOS	1984- 9- 3	20:43	75.6
STARLETT	1984- 9- 3	21:30	75.6

Table C In-pass calibration values obtained and submitted with the passes' quick-look selection. These values are subject to final adjustments.

REAL TIME FILTERING OF LASER RANGING OBSERVATIONS AT THE ZIMMERWALD SATELLITE OBSERVATORY

G. Beutler, W. Gurtner, M. Rothacher
Astronomical Institute
University of Berne
Sidlerstrasse 5 CH - 3012 Berne Switzerland

Telephone 31 65 85 91
Telex 32320

ABSTRACT

Since May 1984 a third generation Nd:YAG Laser system is fully operational at the Zimmerwald Satellite Observatory. In order to maximize the number of successful observations a real time data handling based on the Kalman-Filter technique was developed and implemented into the PDP 11/40 computer system of the observatory. Although many simplifications had to be accepted due to the limitations of our small computer system, the algorithm is capable of predicting the signal-travelling times for the next 20 to 40 seconds counted from the last successful observation with a precision typically better than 10 Nanoseconds (ns). These predictions are used to define in real time the range gate (time interval during which the signal detection is active). At present time the width of the range gate may be reduced from originally 2000 to 4000 ns to 200 to 400 ns after the first few returns of a pass, even if the quality of the predicted orbit is rather poor. So far the filter was used only for night time observations. It proved to (a) increase the number of successful measurements and to (b) produce in real time a relatively clean set of measurements for post-processing. These advantages will be even more pronounced for day time observations.

1. Introductory Remarks

The data filter now in use in our observatory is essentially the real time filter presented in {Beutler, 1983}. Since May 1984 this algorithm has been tested with real observations. As only minor changes of the 1983 filter version proved to be necessary, we restrict ourselves to a brief summary of the theoretical background and we put the emphasis on the performance of the filter in practice. The reader interested in mathematical details is referred to {Beutler, 1983}.

2. Statement of the Problem

During the pass of a satellite over the observatory we are measuring the travel times of Laser pulses from the observatory to the satellite back to the observatory. Certainly we detect more returning light pulses if we have a good a priori estimation of the light travel times at the epoch of the observation, because we are then in a position to reduce the range gate to a few hundred nanoseconds, which in turn reduces the number of spurious pulses. These light travelling times are functions of the geocentric position of the observatory and of the orbit of the satellite. If we had perfect station coordinates and perfect orbit predictions, the problem of setting the range gate would be very simple. Before the pass we would produce a table of theoretical light travelling times, and during the pass the range gate could be set according to this table. Unfortunately matters are not as simple as that. Certainly the position of our observatory is known with sufficient precision for this purpose. The same however is not true for the predicted satellite orbits. Therefore - if we want to have good estimates for the light travelling times in real time - we have to update the orbit during the pass of the satellite in real time. This, of course, is a typical Kalman Filter problem. It is even a somewhat simpler problem, because the underlying system equations are ordinary and not stochastic differential equations, the well known equations of motion of the satellite. But even then the

solution of this problem is out of scope for a small computer system. It was shown however in {Beutler, 1983} that the problem can be reduced to a manageable size (a) by using the perturbation equations instead of the original equations of motion and (b) by estimating only one osculating element, the perigee passing time T_0 in real time. With these simplifications the well known matrices of the Kalman Filter theory reduce to scalars. Moreover the celestial mechanics part of the problem, computation of the predicted orbit and its derivatives with respect to the element T_0, are computed off line before the satellite pass.

3. Outline of the Algorithm

The Zimmerwald Filter may be divided into two parts

(a) Initialization phase with $n_I \leq 14$ observations

(b) one filter-step for each subsequent observation

Initialization is a delicate problem in many applications. Here we have the additional problem of a relatively high percentage of parasitical pulses. The normal filter setup (assumption of a large a priori variance for the unknown element T_0) would therefore erroneously interpret many parasitical pulses as real, which would lead to a filter divergence from the very beginning.
Therefore we proceed as follows:

(1) We establish a series of $n_I \leq 14$ measurements with maximum repetition rate (5 Hz).

(2) We compute n_I independent estimates for the improvement of T_0

$$\Delta T_{0,k} = (\Delta t'_k - h(t_k))/\, C(t_k), k=1,2,..,n_I \quad (1a)$$

Where $\Delta t'_k$ is the observed signal travel time,
$h(t_k)$ is the predicted travel time
$C(t_k)$ is the partial derivative of $h(t_k)$ with respect to T_0

$(1)_1$

(3) We form the differences

$$d_{ik} = |\Delta T_{0,i} - \Delta T_{o,k}| \quad , \quad i,k=1,2,\ldots,n_I$$

(4) If $d_{ik} \leq \sigma_i / |C(t_i)|$ for at least n^* different d_{ik}, the initialization process is said to be successful. Otherwise the the whole process has to be repeated from point (1).

(1)$_2$

σ_i and n^* are program parameters. At present time we use the values

$$\sigma_i = \begin{matrix} 50 \text{ ns for Lageos} \\ 150 \text{ ns for Starlette} \end{matrix}$$

$$n^* = 2$$

(2)

The formulae to compute $h(t)$ and $C(t)$ in eqn. (1a) are rather complicated. Therefore a table of these quantities is computed off line before the satellite pass. During the pass $h(t_k)$, $C(t_k)$ are established by interpolation in this table. As the degree of the interpolating polynomial is only 3, the computation of $h(t_k)$ and $C(t_k)$ is <u>not</u> time consumptive.

If the initialization was successful, the subsequent filter steps have to be initialized as follows:

i_0 is the index of the first successful observation

$$\Delta T := \Delta T_{i_0}$$

$$Q := 1/C(t_{i_0})^2$$

$$E := 0$$

$$j := 1$$

(3)

The complete algorithm may then be represented by scheme (4).

THE ZIMMERWALD REAL TIME DATA HANDLING - VERSION 1984

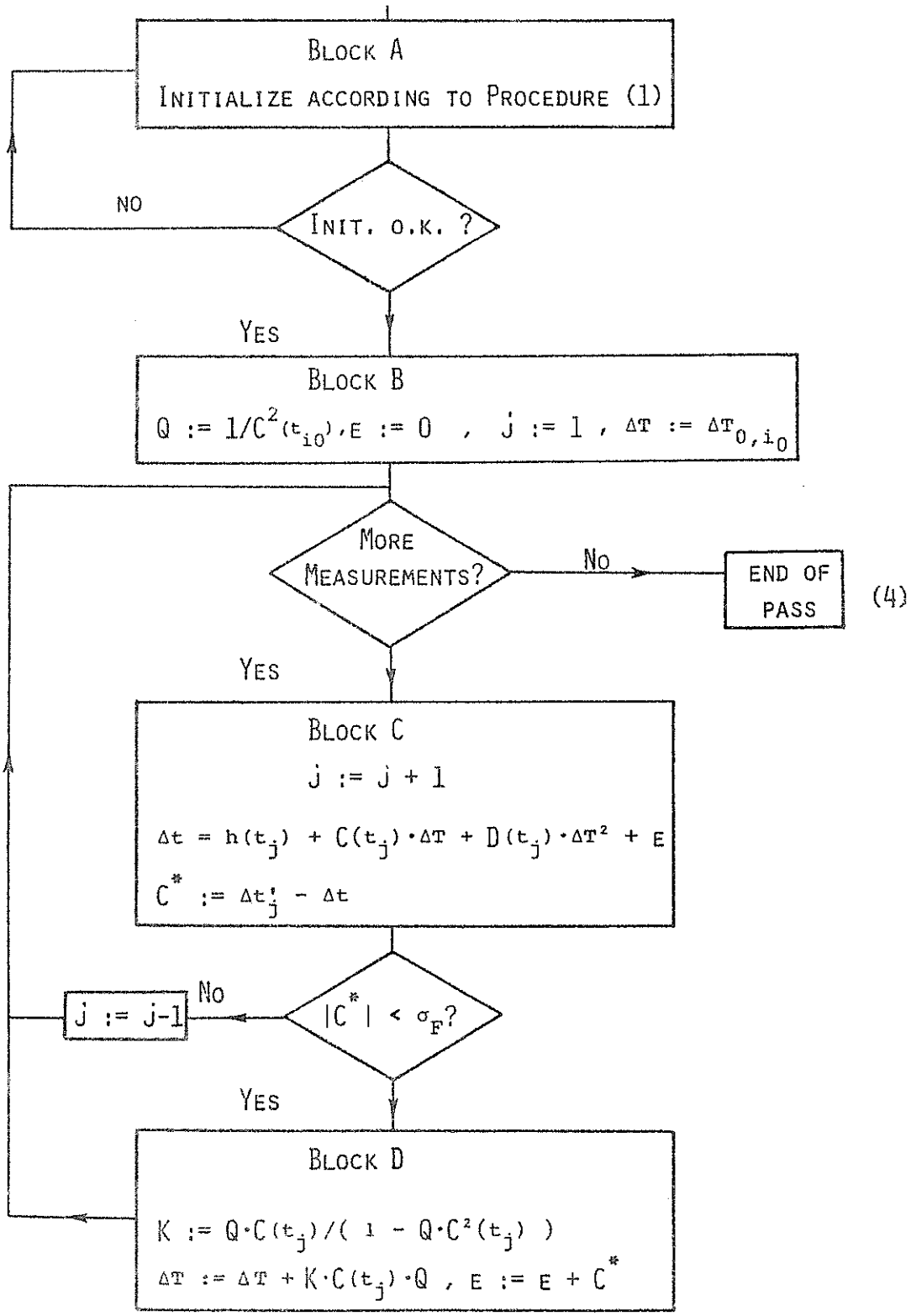

Some remarks concerning scheme (4)

- The prediction of the light travel times Δt in the above scheme differs in two points from the pure Kalman-formulation :
  (a) the quadratic term " $D(t_j) \cdot \Delta T^2$ " is taken into account, where the coefficient $D(t_j)$ is computed in the same way as the quantities $h(t_j)$, $C(t_j)$ in eqn. (1a).
  (b) A very simple empirical correction term E was introduced to prevent the filter from the well known effect of diverging. A full dicussion of this term may be found in {Beutler, 1983, section 5.4.2}.
- σ_F is an input parameter of the program. At present time we use

$$\sigma_F = \begin{cases} 15 \text{ ns} & \text{for Lageos} \\ 50 \text{ ns} & \text{for Starlette} \end{cases}$$

4. Results

Figures 4.1, 4.2 and 4.3 are included to illustrate the filter performance. The three figures refer to the same pass of the satellite Lageos (1984, September 1, 19^h56^m - 20^h29^m U.T.).

Figure 4.1 shows the predicted*) minus the observed light travel times for <u>all</u> measurements recorded (good and faulty). The effect of narrowing the range gate after the initial phase is clearly visible. Clearly the probability to detect the real echo is increased by a factor 5 (initially the range gate width was 2000 ns, after the initialization it could be reduced to 400 ns).

Figure 4.2 shows the residuals of all measurements accepted by the real time filter. The plot was produced by the off line data screening program (no such plots are produced in real time). The residuals therefore refer to an a posteriori optimized orbit. A similar Figure would result however, if we would display the differences "light travel times predicted by Kalman-

*) predicted without a filter, using only the predicted ephemeris

Filter minus observed travel times" for the observations accepted by the Filter algorithm (4). Figure 4.2 also shows that our real time filter produces a relatively clean data set in real time. That there still are some blunders left follows by comparing Figures 4.2 and 4.3 (Figure 4.3 shows the residuals of the measurements finally accepted by the automatic screening program).

So far the real time filter was used for 80 passes (44 of Lageos, 31 of Starlette and 5 of Beacon - C). Usually - as e.g. in the example given by Figures 4 - the real time filter accepts more measurements than the off-line data screening. The opposite may happen, if the operator looses the satellite during the pass and a re-initialization is invoked. Therefore we measure the filter performance by the percentage of wrong real-time decisions "hit yes or no".

Table 4.1

Satellite	Number of Passes	Percentage of wrong decisions
Lageos	44	5.7 %
Starlette	31	8.7 %
Beacon-c	5	3.9 %

5. Conclusions

A very efficient real time data data handling system was developed and tested in the Zimmerwald Satellite observatory. The main difficulty was the reduction of the problem to a manageable size. The first practical experiences are very encouraging.

Reference

Beutler, G. , 1983 "Digitale Filter und Schätzprozesse" , Mitteilung Nr. 11 der Satellitenbeobachtungsstation Zimmerwald, Druckerei der Universität Bern.

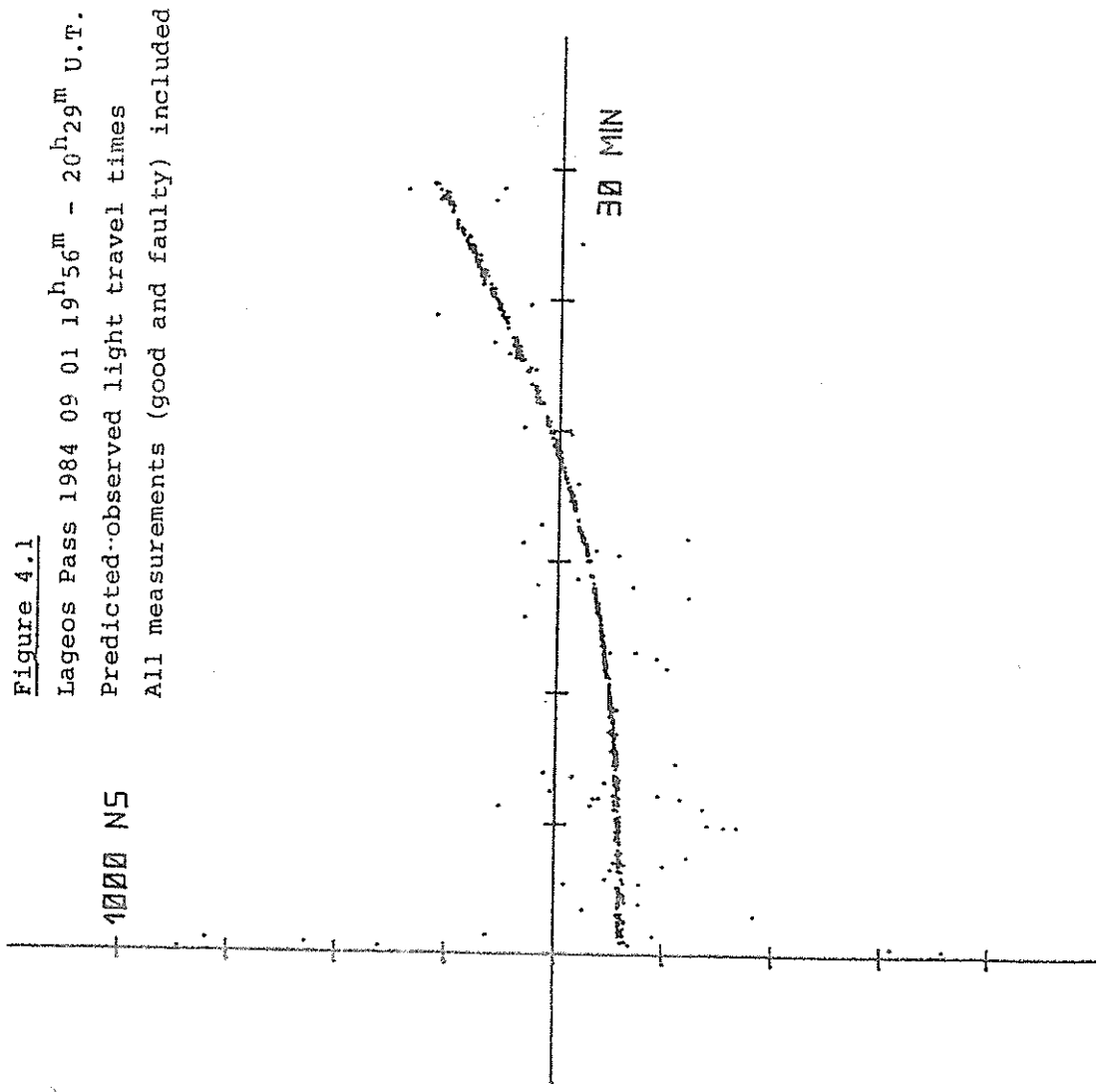

Figure 4.1

Lageos Pass 1984 09 01 19^h56^m - 20^h29^m U.T.

Predicted-observed light travel times

All measurements (good and faulty) included

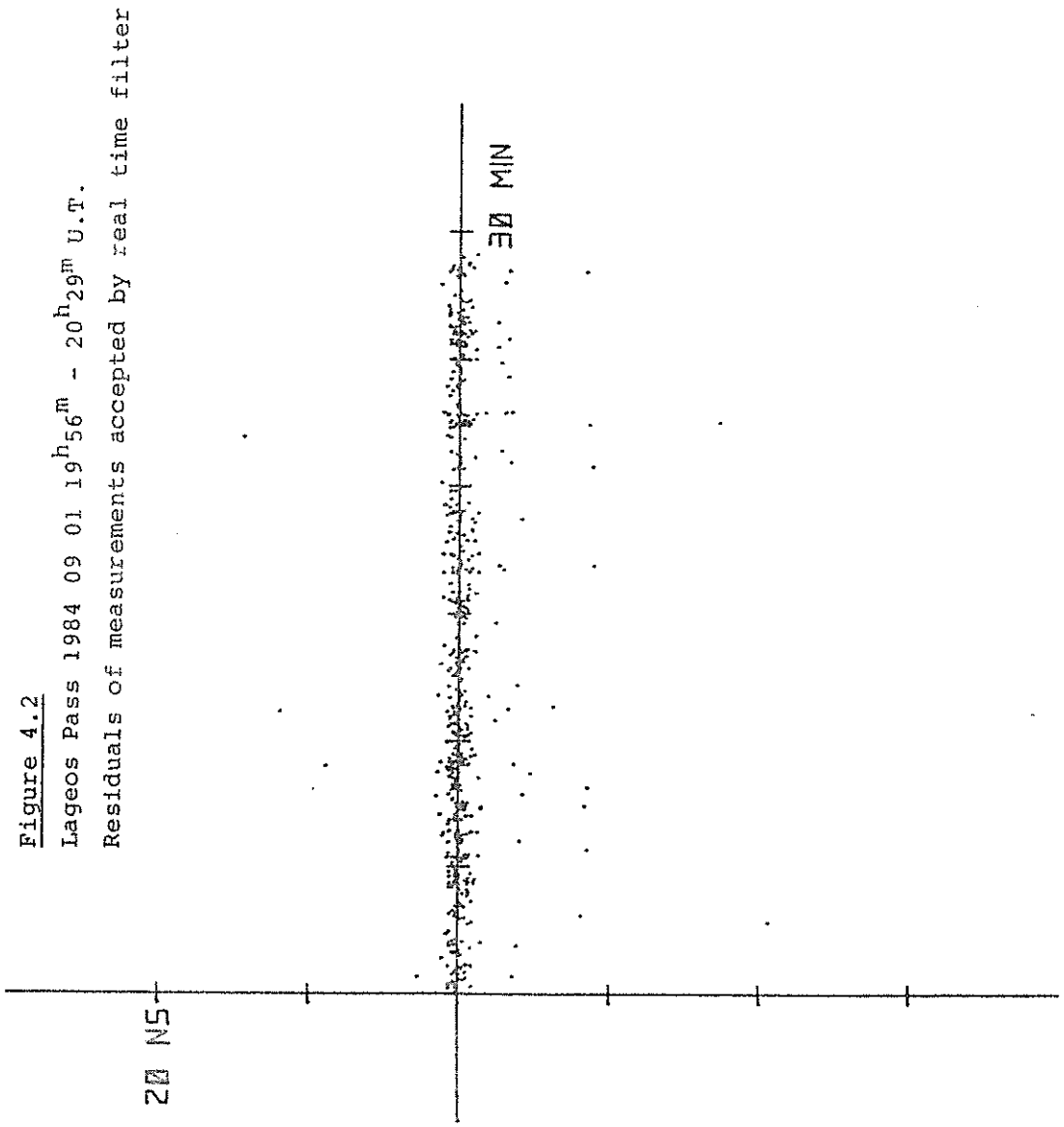

Figure 4.2

Lageos Pass 1984 09 01 19^h56^m - 20^h29^m U.T.

Residuals of measurements accepted by real time filter

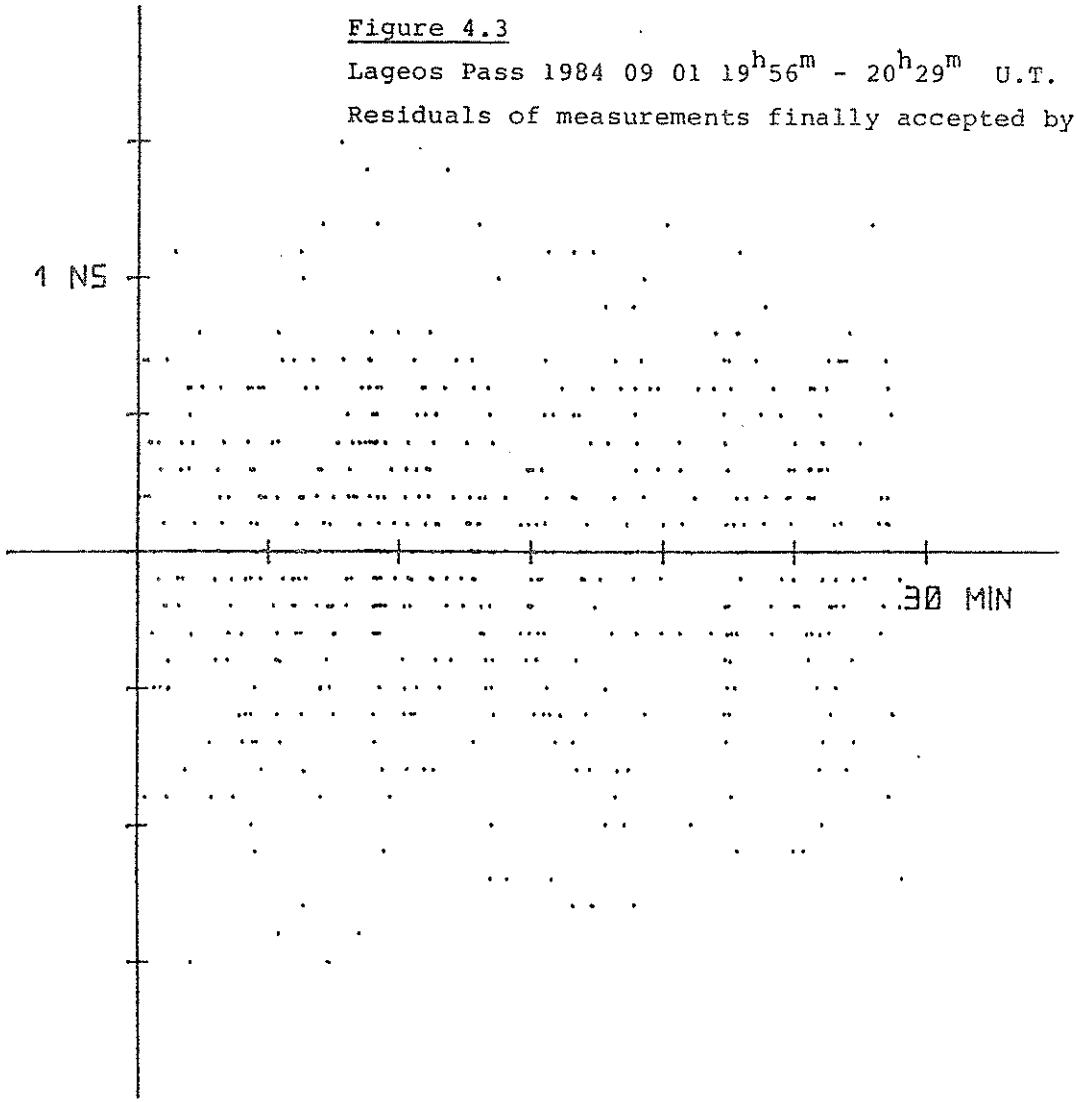

Figure 4.3

Lageos Pass 1984 09 01 19^h56^m - 20^h29^m U.T.

Residuals of measurements finally accepted by off-line screening

Statement of Problem

- Perfect a priori knowledge of light travelling times $\Delta t_i, i=1,2,\ldots$ allow
  - Reduction of range gate width, which
  - increases the number of successful observations

- Only source of incertainty in knowledge of Δt_i is the orbit of the satellite. Therefore we should Improve the orbit in real time using the Kalman-filter-theory.

- Main Contribution of the Zimmerwald Filter is the reduction of this Problem to a <u>manageable size</u> for small computers by
  - Use of perturbation equations instead of Newtonian Equations of Motion
  - Reduction of the number of unknowns from originally 6 to 1 (perigee-passing-time T_0)
- Consequence of these simplifications : All Matrices in Kalman-Theory are reduced to scalars, which speeds up on line computations essentially.
- Initialization : A special procedure related to the majority - voting in Doppler observations was developed: The first 10 - 14 observations are used to produce 10 - 14 independent estimates of T_0. If - within the expected variances of the measurements - 3 or more coincidences are found, the initialization process is said to be successful.

INTERKOSMOS LASER RADAR, VERSION MODE LOCKED TRAIN

K. Hamal, H. Jelinkova, A. Novotny, I. Prochazka
INTERKOSMOS
Faculty of Nuclear Science and Physical Engineering
Czech Technical University
Brehova 7, 115 19 Prague 1 Czechoslovakia

Telephone (2) 84 8840
Telex 121254

ABSTRACT

To obtain the system internal noise level below 10 cm at the INTERKOSMOS laser radar in Helwan, the picosecond laser was implemented. The Nd YAG oscillator/amplifier/SHG laser generates a mode locked train at 0.53 μm, most of the energy is contained in three pulses, the individual pulse duration is 70 psec. During the 1983 Merit Campaing, within 4 months, 100 low satellite passes and 31 Lageos passes have been ranged. When the mode locked substructure has been resolved for the received signal (about 50 % of passes), the RMS was 6-8 cm.

INTERKOSMOS LASER RADAR,VERSION MODE LOCKED TRAIN

The INTERKOSMOS 2.generation laser radar /1/ located at Helwan has been operating since December 1980. Satellite ranging data having RMS 20 cm, obtained during the preliminary MERIT campaign /September 1981/, using 5 ns ruby laser, showed acceptable consistency with other data /3,4/.

To obtain the RMS below 10 cm level we adopted a picosecond mode locked train laser /2/. Assuming the space available for the transmitter /two axe mount, moving transmitter/, we have chosen the mode locked train Nd:YAG oscillator/amplifier/ SHG laser system /5/. The oscillator is passively mode locked- the individual pulse length is 70 psec, the round trip time is 2nsec, most of the energy is concentrated in two or three pulses of the train.

The station has been upgraded to exploit the mode locked train /6/, the software package for the ranging data processing has been developed /7/.

The system block scheme is on Fig.1., the main parameters are summarized on the table 1.

To improve the mount positioning accuracy, the aiming errors model was implemented. The transmitted beam divergence is adjustable by means of a transmitting optics /from 0.2 to 3 mrad/. The receiver PMT is cooled to decrease its single PE dark count rate. The Start dezector /8/ was adopted to proceed the train of transmitted pulses. Two wideband preamplifiers and the constant fraction discriminator were implemented into the Stop channel to guarantee a low jitter on sigle PE level. The epoch timing counter resolution is 1 us. As the epoch reference, the Loran-C signal is used, the computerised comparison procedure of the station time base to the Loran signal was put into operation. The signal propagation delayes were calibrated by the flying Cs clock. The computer hardware/software control package was modified to accept the ranging reprates up to 5 pps, the on line graphics capability was implemented.

The indoor calibration experiment /9/ showed the ranging electronics interval noise 6 cm /RMS/.

During the 1983 MERIT campaign 100 low satellites and 30 Lageos passes have been ranged within four months. When the mode locked substructure has been resolved in the received signal /50% of passes/, the RMS 6-8 was achieved. The system stability /10/ /pre-post pass calibration difference/ is typicaly 2.5 cm. The average data rate is /1/ Lageos return every /30/ seconds.

TECHNICAL PARAMETERS OF THE INTERKOSMOS LASER RADAR IN HELWAN VERSION MODE LOCKED TRAIN

MOUNT	CONFIGURATION	AZIMUTH/ELEVATION
	TRACKING RATE	ZERO TO ONE DEG/SEC
	POINTING ACCURACY	30 ARCSEC
TRANSMITTER	LASER TYPE	Nd:YAG + SHG
	OPERATIONAL	MODE LOCKED TRAIN
	ENERGY	15 mJ/TRAIN
	PULSE LENGTH	70 PSEC
	ENVELOPE FWHM	4 NSEC /2-3 PULSES/
	REPRATE	2.5 PPS
	OUTPUT BEAM DIVERGENCE	ADJUSTABLE 0.2-2. mrad
RECEIVER	OPTICS	REFRACTOR, 0.4 METER
	BANDPASS FILTER	1 nm
	PHOTOMULTIPLIER	RCA 31034A,GATED,COOLED
RANGING ELECTRONICS	DISCRIMINATOR START	SPECIAL
	DISCRIMINATOR STOP	CONSTANT FRACTION
	FLYING TIME COUNTER	100 PSEC RESOLUTION
	TIME GATE	100 NSEC RESOLUTION
EPOCH TIMING	RESOLUTION	1 MICROSECOND
	FREQUENCY STANDARD	Cs BEAM FREQUENCY STD
	EPOCH REFERENCE	LORAN C,FLYING CLOCK
COMPUTER	CPU	FLOATING POINT
	MEMORY CAPACITY	64 KBYTES
	STORAGE MEDIUM	5 MBYTE DISC
	I/O FACILITIES	PAPER TAPE,PRINT
		GRAPHICS CAPABILITY
		HP CASSETTES, HP-IB
SOFTWARE	PREDICTION	0.2 ARCMIN ACCURACY
		ON SITE IMPROVEMENT
	CALIBRATION/TRACKING	COMPUTER CONTROLLED
	DATA PROCESSING	NOISE REJECTION
		ML TRAIN DATA ANALYSIS

Table 1.

L i t e r a t u r e

1/ K.Hamal,H.Jelinkova,A.Novotny,I.Prochazka,M.Cech,Interkosmos Second Generation Satellite Laser Radar,proceedings of the Fourth International workshop on Laser Ranging Instrumentation Texas,Austin,USA,published in Bonn,1982
2/ E.C.Silverberg, The Feedback Calibration of the TLRS Ranging System, in /1/, Vol II,p 331
3/ S.D.Tapley,B.E.Schutz,R.J.Eanes,A Critical Analysis of Satellite Laser Ranging Data, in /1/,Vol II,p 523
4/ J.H.Latimer J.M.Thorp,D.R.Hanlon,G.E.Gullahorn,A Review of Network Data Handling Procedures, in /1/, Vol I, p107
5/ H.Jelinkova, Mode Locked Train Laser Transmitter in this Proceedings
6/ I.Prochazka, Mode Locked Train Laser Ranging Data Processing, in this Proceedings
7/ A.Novotny,I.Prochazka, Upgrading the Computer Control of the Interkosmos Laser Ranging Station in Helwan, in this Proceedings
8/ M.Cech, Start Discriminator for the Mode Locked Train Laser Radar,in this Proceedings
9/ K.Hamal,I.Prochazka,J.Gaignebet, Mode Locked Train YAG Laser Calibration Experiment, in this Proceedings
10/ M.R.Pearlman,N.Lanham,J.Thorp, J.Wohn,SAO Calibration Techriques, in /1/, Vol.II,p 323

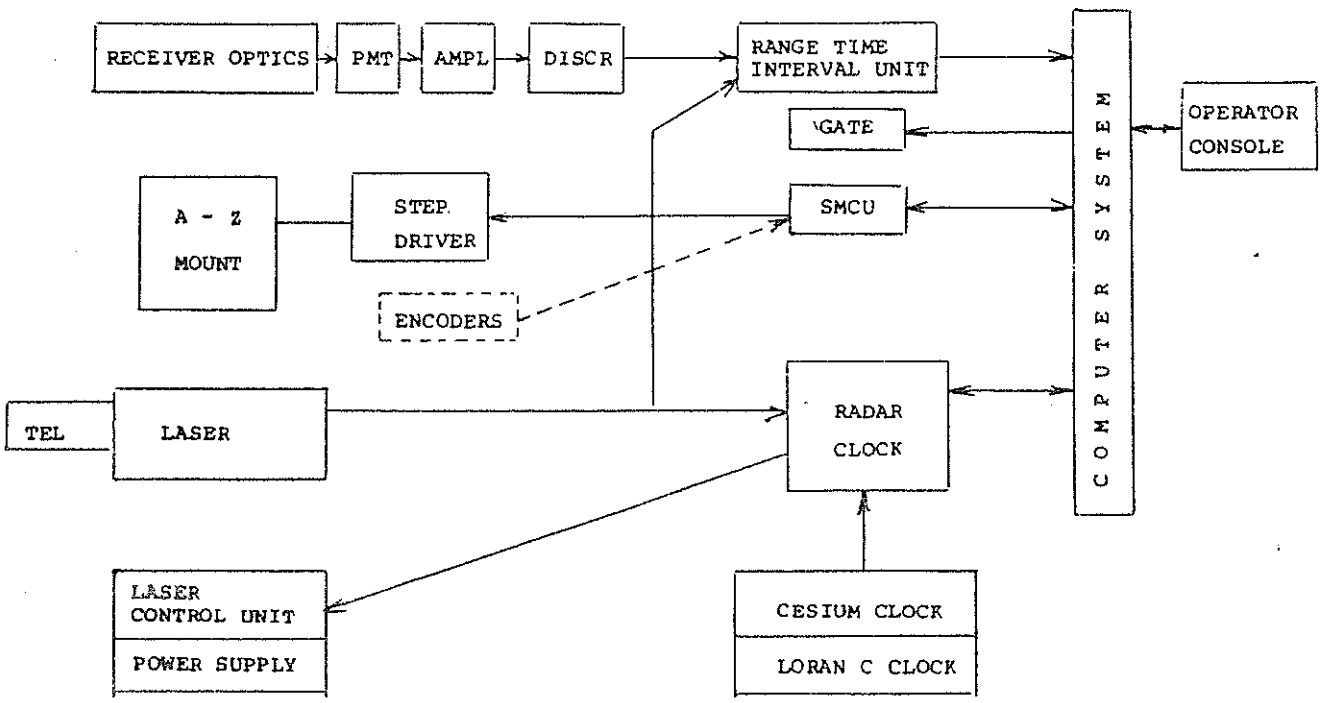

System block scheme

Fig. 1.

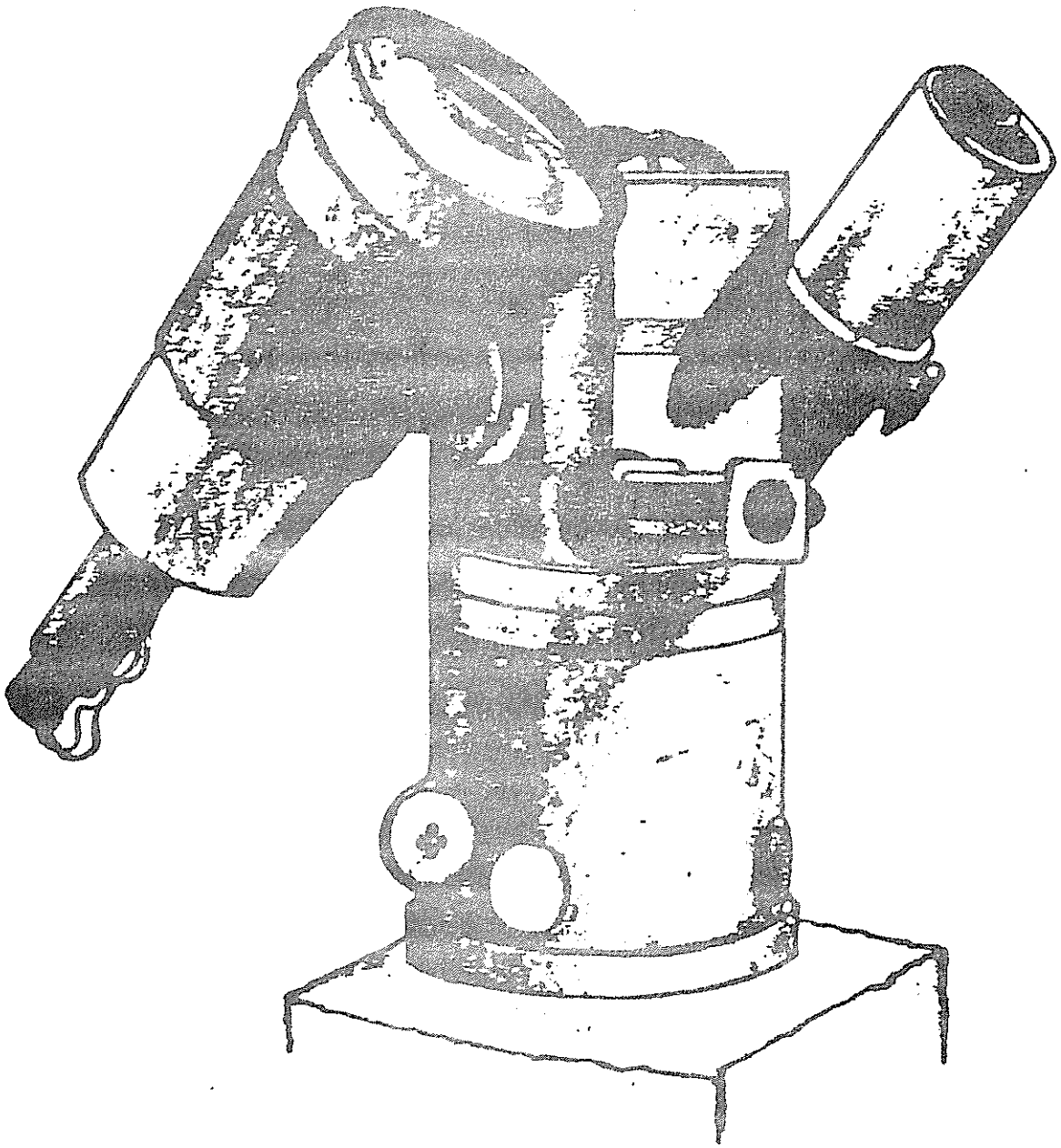

View of the mount/laser/receiver subsystem

START DISCRIMINATOR FOR MODE LOCKED TRAIN LASER RADAR

M. Cech
INTERKOSMOS
Faculty of Nuclear Science and Physical Engineering
Czech Technical University
Brehova 7, 115 19 Prague 1 Czechoslovakia

Telephone (2) 84 8840
Telex 121254

ABSTRACT

A problem of start detector is very topical in laser radar sation working with a train of pulses generating by mode locked Nd:YAG laser. This article deals with new developed start detector used in INTERKOSMOS laser radar station in Helwan, Egypt. A time resolution of the detector is better 150 ps.

START DISCRIMINATOR FOR MODE LOCKED TRAIN LASER RADAR

The start pulse for the time interval counter is generated by detecting a small part of laser beam in a start detector.

The described start detector consists of three part (fig. 1). In the first part, a silicon planar PIN photodiode HP4207 as detection element is used. The photodiode is connected to -150V bias to obtain very fast response.

The second part is a discriminator. The discriminator consists of tunnel diode (TD). The TD is connected as monostable multivibrator. The threshold of discrimination is set up by the level of the multivibrator.

The third part is amplifier, the output voltage from TD discriminator is 100-200 mV. The gain of the amplifier is approximately 20. The first stage is amplifier with common emitor (trans. T1) and second transistor is connected as current amplifier. The rise time is 4 ns and voltage output is 4V. The rise time is suitable for our application (uniform pulse).

The detector works as fixed threshold discriminator. This fact is not important because of rise time 200 ps and change of amplitude is 50% only. The theoretical error of the detector is 100ps only.

We have train of pulses - fig.2. (approx. 2-3 pulses). A problem is in defining the triggering pulse. The detector sends uniform trigger pulse, when the first laser pulse reaches threshold of discriminator. If we take as reference point the maximum pulse in train, it can be triggered from different pulses in respect to this point. The time of triggering is different but this time differes at resonator round trip time. (1.8 ns in our case).

Both stability and accuracy of the start detector were measured. The following measuring configuration was used: a laser pulse was divided into two parts. One part was detected by photodiode and entered to vertical amplifier of the Tektronics 7912AD oscilloscope. Second part of light pulse was processed by start detector. Output pulse from start detector externally triggered the oscilloscope.

Fig.2. shows the overlap of three pulses. Approximately 100 pictures were taken. These pictures were processed by computer. Two different parameters were studied.

The first parameter is the distance of reference point (the center

of maximum peak) from trigger pulse. We can see on the fig.3. that detector generates trigger pulse from the same peak in train in 85% cases, from second one 15% only. Distance between pulses there is 1.8ns.

Second parameter is a time resolution. Fig.4. was obtain by separating one pulse from fig.3. The time resolution of this detector is better then 150ps.

Conclusion

The start detector described in this article is very simple. The reference point obtained by the detector has the time resolution better 150ps. A one resonator round trip time (1.8ns) offset of the reference point is observed in 15% cases. The detector is used by investigation of mode locked lasers as triggering element of oscilloscopes, streak cameras, etc.

Literature:

1/ M.Jelinkova, in this proceedings

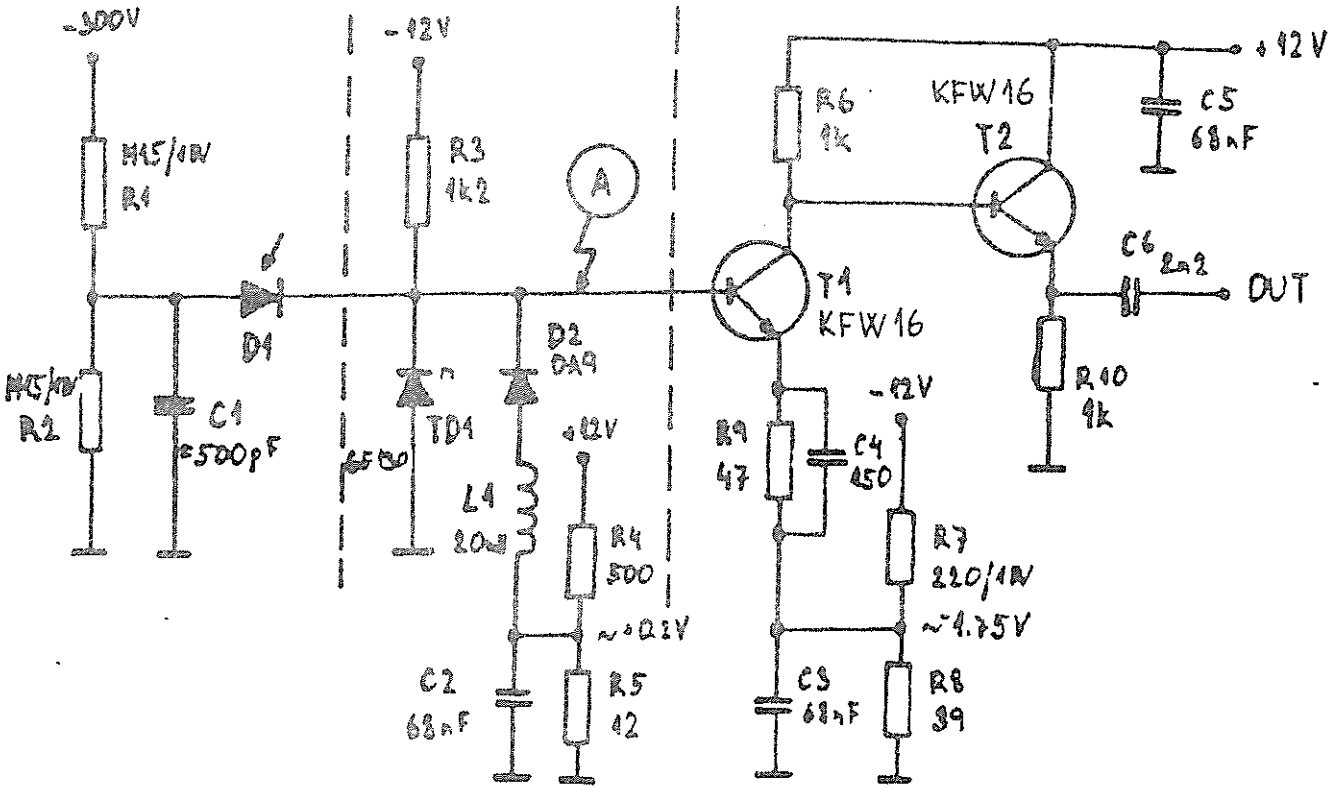

Fig.1.: Circuit diagram of the start detector

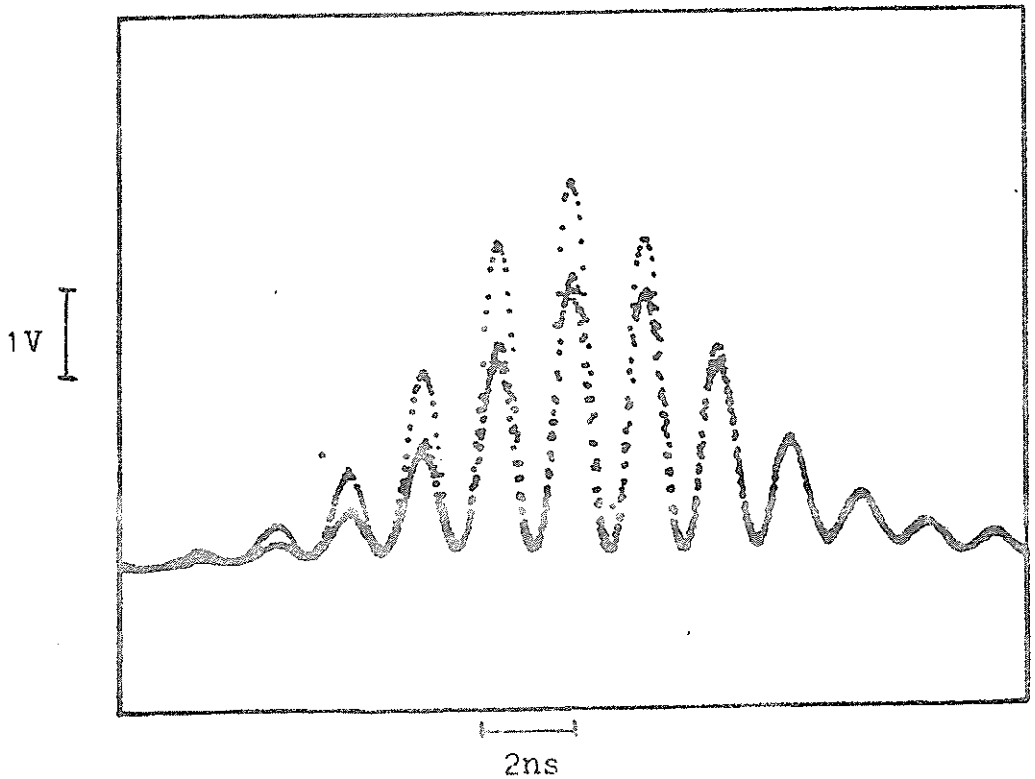

Fig.2.: The overlap of three pulses

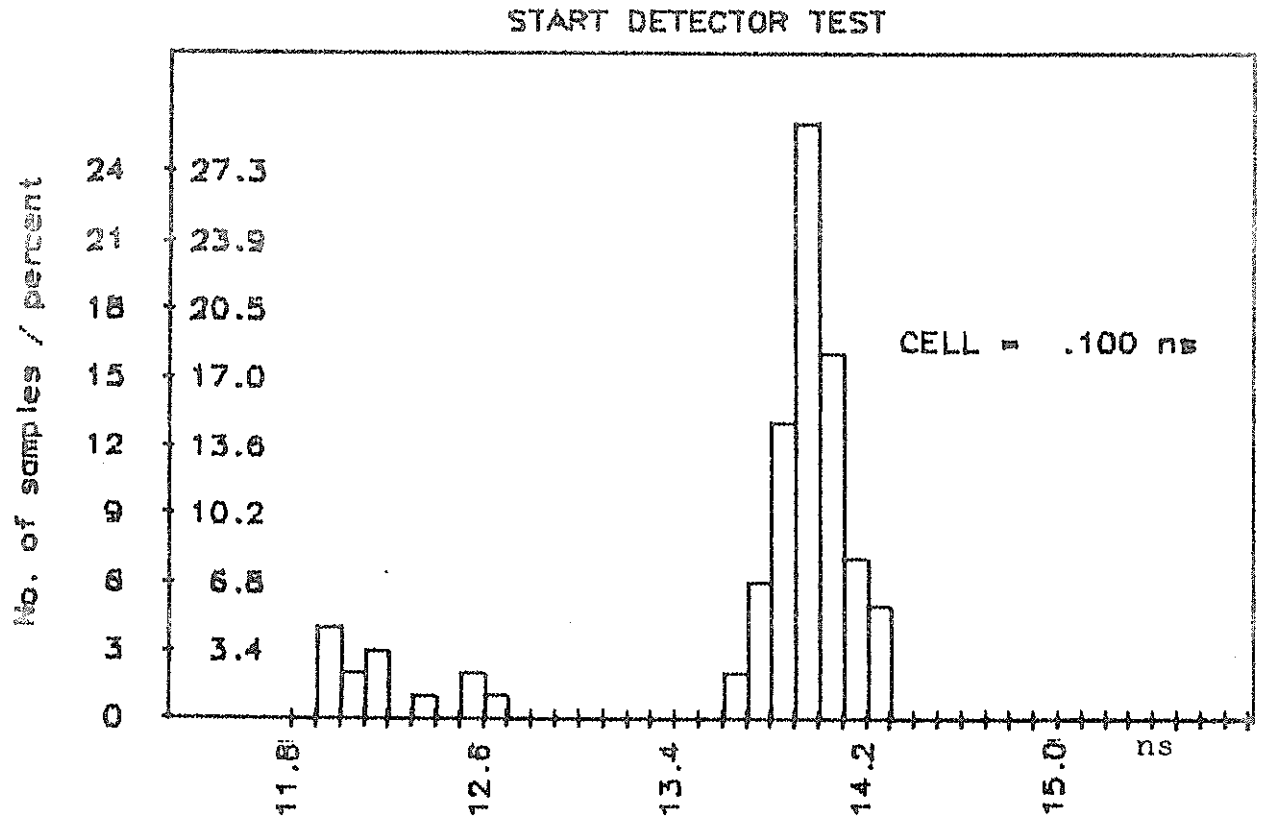

Fig.3.: The position of maximum peak from trigger

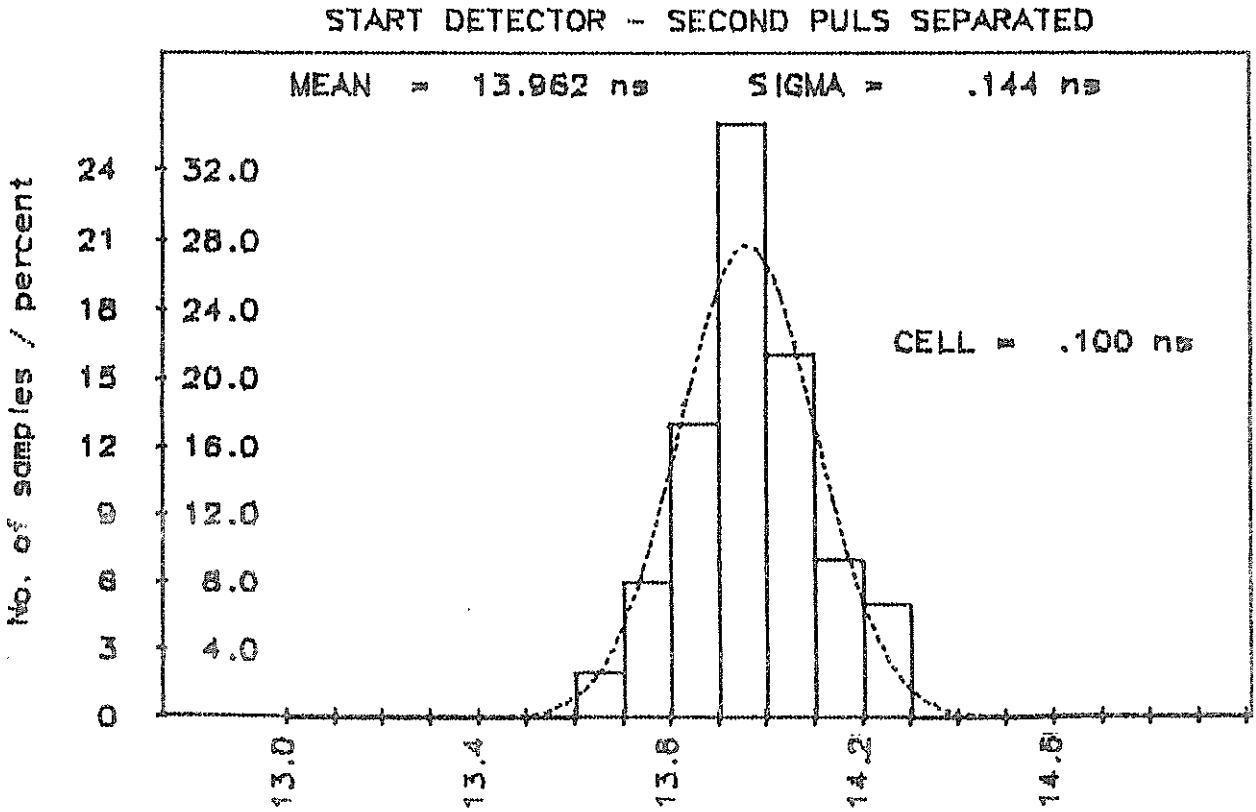

Fig.4.: The time resolution diagram

MODE LOCKED TRAIN LASER TRANSMITTER

J. Jelinkova
INTERKOSMOS
Faculty of Nuclear Science and Physical Engineering
Czech Technical University
Brehova 7, 115 19 Prague 1, Czechoslovakia

Telephone (2) 84 8840
Telex 121254

ABSTRACT

The passively mode locked frequency doubled Nd:YAG oscillator/amplifier/SHG laser radar transmitter is dercribed. It is generating a train of 2-3 pulses, the pulse duration is 77 psec, output energy in green is 20 mJ, the reprate 1-2.5 Hz. The stability of the output pulses was monitored and statistically treated using a computer. To analyse the laser beam structure, an on line diagnostic chain, giving a three dimensional graphic display of the output pattern, was implemented.

MODE LOCKED TRAIN LASER TRANSMITTER

1.0 INTRODUCTION

Considering satellite ranging, the length of the transmitted laser pulse is one of the main parameters, determining the accuracy of the measurements. To increase this accuracy, in the course of years, the pulse width of the transmitted light was shortened. Since 1973, when the Interkosmos laser radars have started to work, a total number of 30 laser transmitters have been put into the laboratory and field operation. Among the transmitters, there was a ruby Q-switched using either rotating mirror or Pockels cell generating the pulses from 13-25 nsec FWHM, PTM Q-switched (cavity dumped) ruby system having 6 nsec pulse width and constant gain pulse forming configuration varying in pulse width from 2-6 nsec /1/. In 1982 mode-locked Nd:YAG laser transmitter generating a train of pulses has been installed at the observatory Helwan in Egypt.

2.0 SYSTEM OF LASER TRANSMITTER

The laser system consists of TEMoo oscillator plus a single pass amplifier, followed by a frequency doubler. The specifications result from the demands of the accuracy in ranging and from the necessity of the system movability /2/. The technical parameters of this system are shown in Tab.1 and a schematic drawing in Fig.1.

Tab.1. TECHNICAL DATA OF THE LASER TRANSMITTER

Wavelength	530 nm	Output divergence	0.2 mrad
Pulse duration	77 psec	(Adjustable)	MIN
No.of pulses	2-3/train	Dimensions length	120 cm
Output energy	20 mJ/train	diameter	23 cm
Reprate	1-2.5 Hz	Power supply /5/	500 W
		(Average power)	

2.1 Laser Oscillator

The deterministic build up of passive mode locking in giant pulse lasers can be achieved by careful control of lasing modes between the first and the second threshold /3/. Stable stationary

pulse train solutions were found for passively mode locked systems with easily saturable active medium. The autors /4/ used the intraresonator telescope to improve the output pulse reproducibility of Nd:YAG system. In our system, the number of modes was reduced by the gain excess and by increasing the intermode frequency spacing via shortening the optical resonator length.

The configuration of the mode locked Nd:YAG oscillator, we employed, is shown in Fig.1. As the active medium, a 80 mm long, 6 mm in diameter, Nd:YAG crystal is used, one end is cut at angle 89° and second one is perpendicular to the axes. The crystal and the flashlamp are placed in the elliptical silver coated cavity. The optical resonator is formed by the high reflectivity (R=99%) dielectric mirror and the perpendicular surface of the Nd:YAG crystal (R=8%). Mode locking is accomplished using a saturable dye ML51 solved in dichlorethane /6/, innitial transmission T = 35%, thickness of the cell is 5 mm. The cell is at the Brewster angle near the 99% mirror. Using a 5 mm saturable dye cell the pulse duration was lengthened. Single mode operation is performed by the aperture (diam.1 mm) placed between YAG crystal and the saturable dye. The length of the resonator corresponds to 2 nsec round trip time. The shape and the reproducibility of the oscillator pulses are remembered in the section 3.

2.2 Amplifier, Doubler and Detection

In the amplifier, a 120 mm long, 6 mm in diameter, Nd:YAG crystal is used, both ends are cut at 2° and antireflection coated. The crystal is placed in the elliptical silver coated cavity and it is pumped by one linear Xe flashlamp. Both crystals, oscillator and amplifier one, and the flashlamps also are placed in a water cooled glass tubes. To isolate the oscillator from the amplifier, the saturable dye cell containing ML 51 disolved in dichlorethane is used. To extend 1 mm oscillator spot, the telescope 1:3 is placed between the oscillator and the amplifier head. For purpose of the laser radar, the generation of the second harmonic is needed. The KDP crystal, type II, is used behind the amplifier. The output pulse is monitored by a high speed photodiode. A sample of the output beam is sent to the start detector /7/. The output telescope changes divergence of the beam. A He-Ne laser is incorporated into the system for easy alignment of the oscillator/amplifier chain and the pointing services. The whole optical system is protected by a removable tight dust cover.

3.0 LASER PERFORMANCE

The experimental setup for measuring of the output pulse reproducibility and the beam structure is in Fig.3.

3.1 Pulse Shape

The typical pulse shape is shown in Fig.2. The train has 2-3 pulses, the pulse separation is 2 nsec and the individual pulse width is 77 psec.

3.2 Pulse Energy and Divergence

The oscillator pulse energy is about 7 mJ/train in infrared. After the amplification, 80 mJ output beam is entering to SHG crystal, the conversion efficiency is 25%, the output energy per train at 0.53 μm is 20 mJ.

The divergence of the system is 2 mrad. The output Galileo adjustable telescope allowes to achieve the output beam divergence up to 0.2 mrad, minimum.

3.3 The Output Pulse Reproducibility and Beam Structure

The shot-to-shot reproducibility and the stability of the output pulses are of the primary importance in satellite ranging. The irregularity of the pulse may impair the timing accuracy. Therefore, the detailed tests of the laser transmitter stability and pulse reproducibility were carried in the indoor experiment. The experimental setup is in Fig.3. The first part is for measuring the stability of the pulse width of the individual pulses and the signal to noise ratio, the second part is for pulse train stability test and third one for beam structure measurement.

The laser pulse was detected by PIN photodiode and Tektronix Tranzient Digitizer 7912AD. The bandwidth of the system was 500 MHz, effective resolution 20 psec. The measured raw data were transmitted via HP 85 to the master HP 21 MX-E computer, processed and stored on the magnetic disc. The laser was operating at 2.5 Hz and 100 from the 100 000 shots consequence were put to the memory and processed. The corresponding software package consists of the programs for data collection and storing, noise elimination, pulse characteristics determination, statistics and graphics /9,10/. The results are in Fig.4.

A part of the laser output pulse is sent to Hammamatsu streak camera system. For data recording and processing, HP 85 calculator was interfaced to the Hammamatsu system (Fig.2). The mean value of the individual pulse width from the 100 measurements is 77 psec, RMS is 10 psec.

The far field structure was studied in the focal plane of the positive lens. As the detector, the Fairchild CCD camera was used. The camera signal was digitized and stored in the Digital Image Memory Quantex with the resolution 256x256 cells 256 intensity levels each. The data from the memory were transmitted via HP-IB to the HP 21 MX-E computer and stored on the disc. The extensive software package /10/ for TV image processing is available in the "nearly on-line" mode. The beam profile etc. was available within seconds after the laser shot

on the monitor in the lab. The Fourier two dimensional transform of the far field structure was available within minutes.

The focal length of the positive lens used for far field image was 2.5 m. In Fig.5, there is the plot of the 3D projection of the far field beam structure of the oscillator (1.06 μm) (a) and the contours (b). The far field beam structure of the transmitter (osc/ampl/doubler) chain is in Fig.6. The output beam divergence is 2 mrad.

4.0 CONCLUSION

The system has been operating in Helwan observatory (Egypt) through the summer 1983 and 1984. The target and satellite ranging shows RMS bellow 10 cm /11/.

REFERENCES

/1/ H.Jelinkova, Proceedings of the Fourth International Workshop, Austin, USA, 1981

/2/ K.Hamal etal., in this Proceedings

/3/ C.P.Auschnitt, IEEE Journal of Quantum Electronics, QE-13,321,1977

/4/ A.N.Zherikhin, V.A.Kovalenko, Kvantovaja Elektronika 2, 377,1974

/5/ V.Kubecek, M.Klasna, FJFI Preprint Series No.83/203

/6/ K.Hamal, V.Hruskova, H.Jelinkova, FJFI Preprint Series No.83/204

/7/ M.Cech, In this Proceedings

/8/ I.Prochazka, FJFI Preprint Series No.83/188

/9/ K.Hamal,I.Prochazka,M.Cech,P.Valach,H.Jelinkova,A.Novotny, FJFI Preprint Series No.83/194

/10/ P.Valach, FJFI Preprint Series No.83/197

/11/ I.Prochazka, In this Proceedings

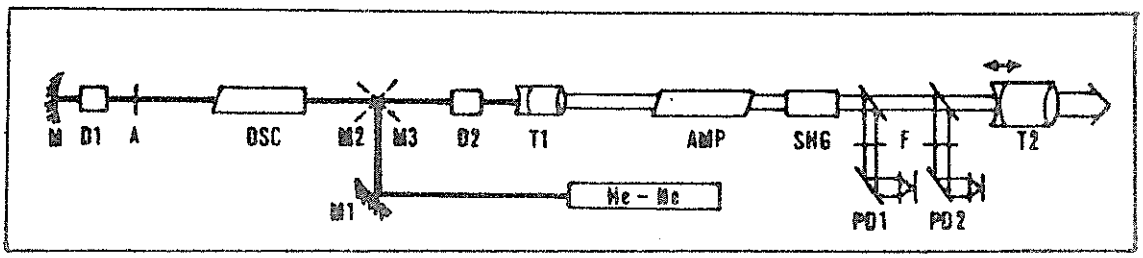

Fig.1. Block diagram of the optical lay-out of the Nd:YAG laser transmitter

M	End mirror	SHG	KDP Frequency doubler
D1	Dye cell	PD1	Monitor detector
A	Aperture	PD2	Start detector
OSC	Oscillator head	F	Neutral density filters
D2	Dye cell	T2	Output telescope
T1	Telescope	M1	Adjustable mirror
AMP	Amplifier head	M2,M3	Removable mirrors

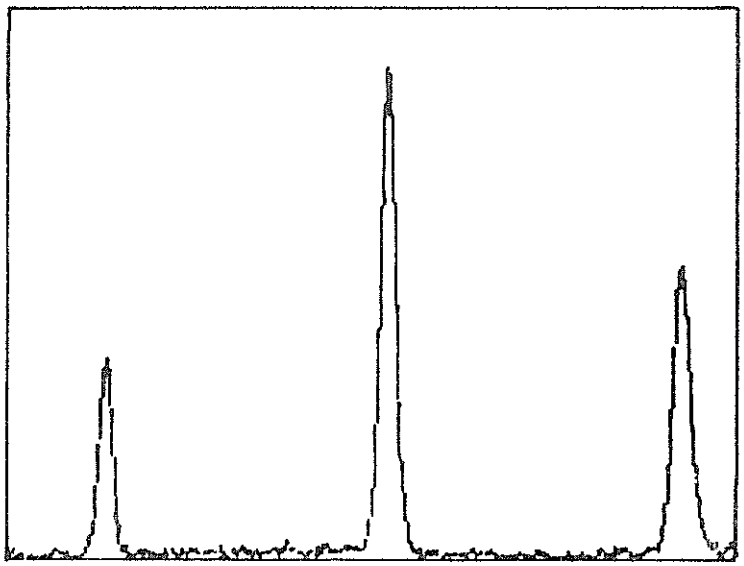

Fig.2. The transmitted pulse
Streak camera trace /5 nsec/screen/

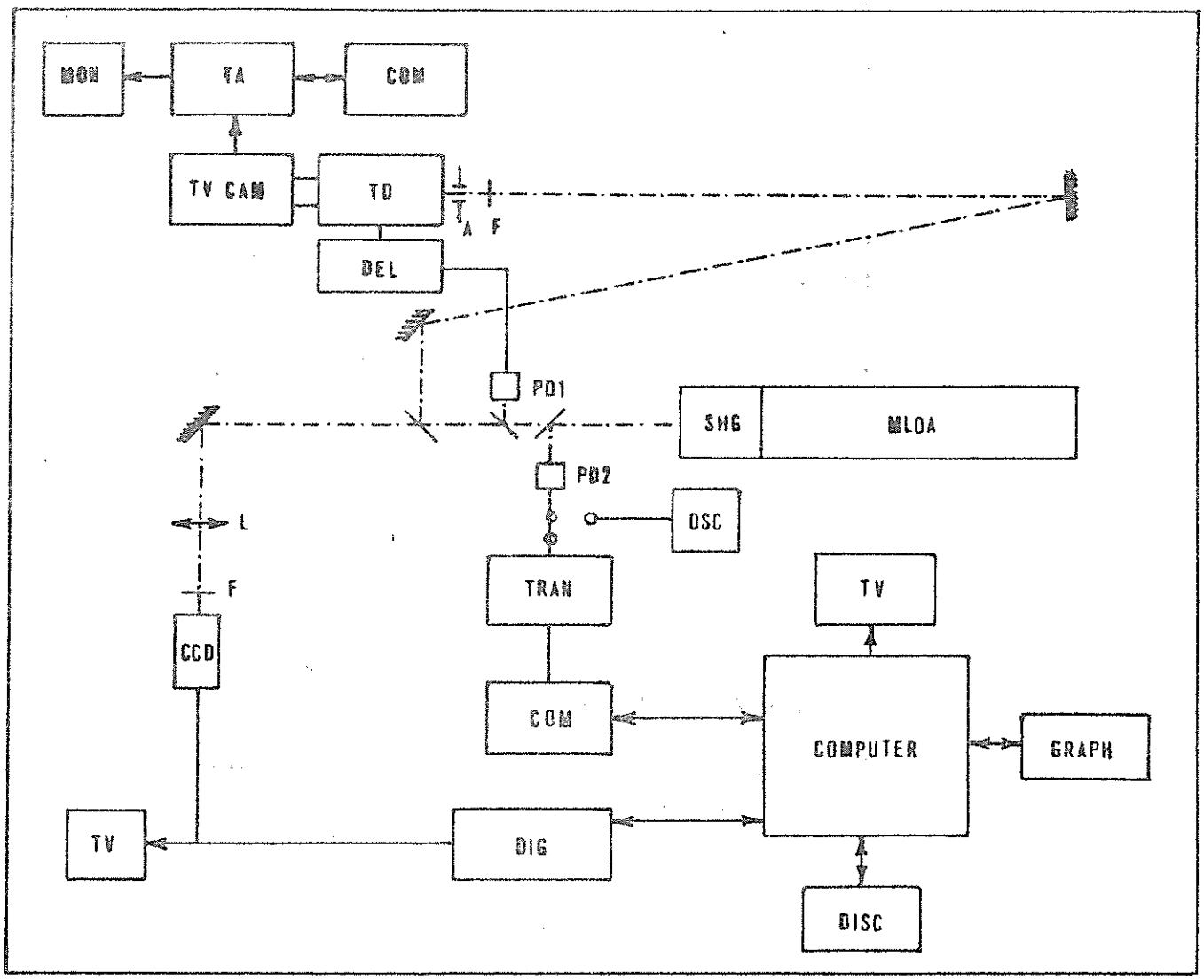

Fig.3. The experimental setup for measuring of the output pulse reproducibility and beam structure

MLOA - Mode locked osc/ampl system, SHG - Frequency doubler, PD1,PD2 - photodiode, TV CAM - SIT TV camera Hamamatsu C1000-12, DEL - Delay unit, TA - Temporal analyzer Hamamatsu C1098, MON - TV monitor, COM - Computer HP 85, F - Neutral density filter, A - Aperture, OSC - Oscilloscope Tektronix 7834, TRAN - Tranzient Digitizer TR 7912A, COMPUTER - HP 21 MX-E, DISC - 50 Mbyte disc, TV - TV monitor, GRAPH - Graphic display, L - Positive lens /f 2.5 m/, CCD - CCD TV camera Fairchild, DIG - Digital Image Memory Quantex, TD - Temporal disperser Hamamatsu C979

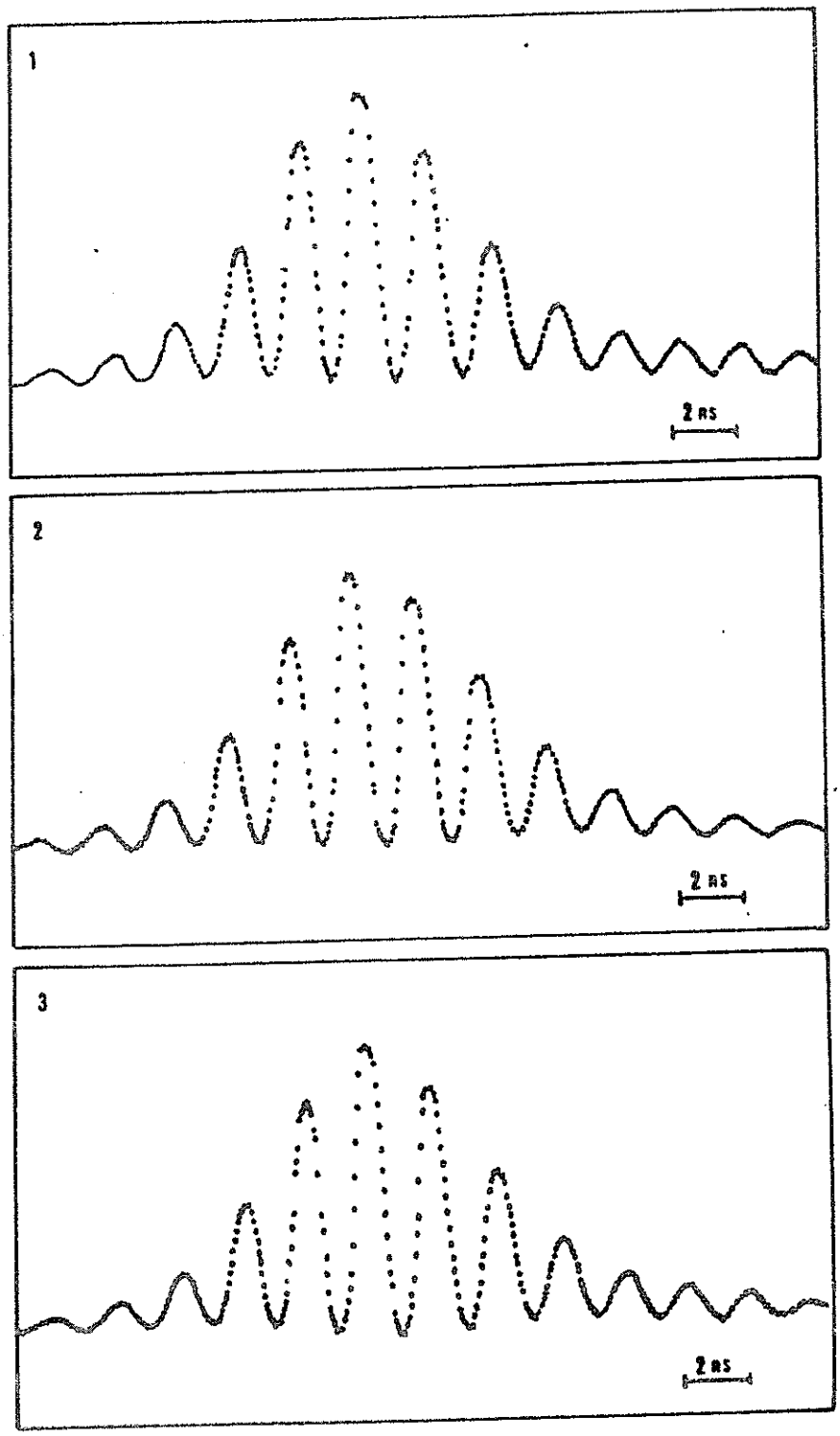

Fig.4. Output ML train long term stability
1 shot No.4000
2 shot No.20000
3 shot No.37000

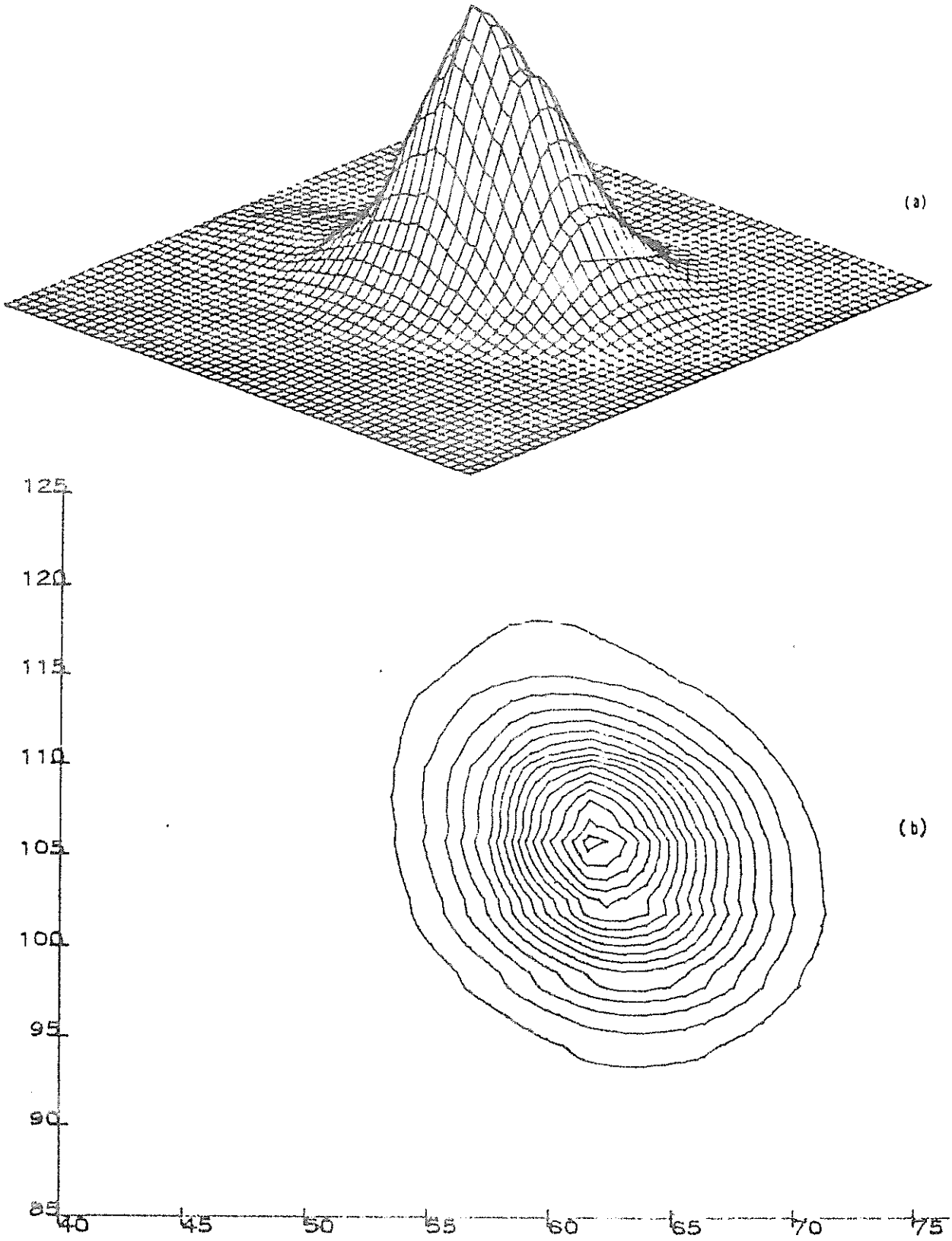

Fig.5. The plot of the 3D projection of the far field beam structure of the oscillator (1.06 μ) (a) the contours (b)

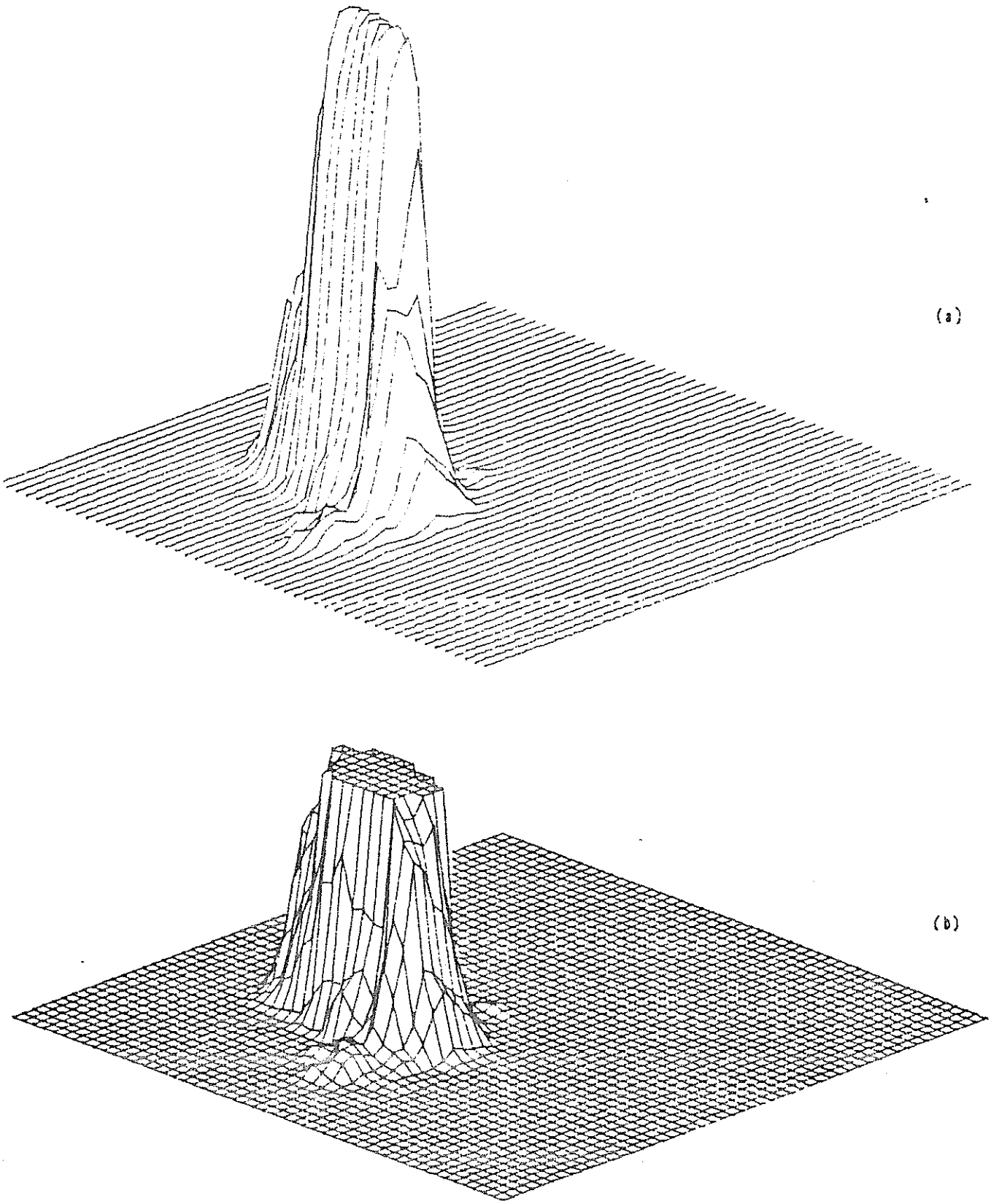

Fig.6. The far field beam structure of the transmitter (osc/ampl/doubler) chain (a) and the half amplitude cut (b)

PRESENT STATUS OF THE CERGA LLR OPERATION

C. Veillet
CERGA
Avenue Nicolas Copernic
06130 Grasse France

Telephone (93) 36 58 49
Telex 470865

ABSTRACT

The CERGA LLR station is now currently operating with a standard range accuracy smaller than 20 cm. The normal points are sent monthly to four scientific teams in France and USA, and are available for the interested people on request to the author.

PRESENT STATUS OF THE CERGA LLR OPERATION

The Figure 1 summarizes the main characteristics of the CERGA LLR operation. The station itself is located in Grasse (south of France) at an elevation of roughly 1300 meters. A 1.5-m reflector is used both for the emission and the reception. The ruby laser has a 3.5 ns pulse and can shoot the Moon every six seconds with a 3 J energy.

The first returns from the Moon have been observed in June 1981, but the first good normal points have been obtained in April 1982, after the solution of some problems with the events timer. Since then,the station has been given normal points (mainly on the Apollo XV reflector) as regularly as possible. The Figure 2 presents an histogram of the number of normal points obtained each month on Apollo XV. The main cause of a lack of results for some months (like February 1984) is the weather linked sometime to a low elevation of the Moon seen from CERGA. In July and August, where the weather is generally good on the French riviera, the nights are very often wet and foggy and the number of results is not as good as it could be expected in such a period.

The Figure 3 shows the distribution of the CERGA normal points with the age of the Moon. At the present time it is possible to obtain data on a reflector illuminated or not, but only during the night or at least after the sunset or before the sunrise. This limitation is not really due to the noise higher during the day than during the night. It is mainly due to the impossibility of pointing the reference craters with the daylight. It should be possible to receive echoes around the full moon. However a lack of results is apparent on the histogram at this phase. These nights have been ruled out from the observation schedule for a long time : the number of observers was not sufficient to cover 20 nights per lunar month. Low moon and bad weather prevented from getting data these last months around the full moon ...

The present laser used at CERGA is an old one. His pulse length prevents to obtain a very good accuracy. A request for money for a new laser and the related equipment will be pre-

sented once more to the french astronomical community in next October. During the waiting of such a change, two improvements are on hand.

The first one concerns the calibration. Made actually on an external target located on a mountain 8 km far from the reflector, it will be obtained as soon as possible on an internal way during the normal laser firings. Thus it will be possible to monitor both the calibration and the pulse length during the observations. The uncertainty on these parameters is the main error source of the CERGA data.

The second improvement concerns the pointing optics (mainly the TV camera) which contrast is too low to permit to point reference craters by daylight. The study of a new system will be made. If its implementation is easy, it would be possible to obtain very soon data in quite all the configurations (night or day on Earth and Moon).

After a reorganization of the LLR team in last November, some modifications have been made concerning the predictions and the analysis of the data. A prediction software has been installed on the main computer of the station. Every observer is thus able to prepare the predictions for the next nights using the last estimates of the Earth rotation parameters. The programm works with an extract of the JPL ephemeris (DE 121 and LLB 13) and gives direct residuals generally lower than 25 ns, giving very rapidly to the observer an insurance on the reality of the echoes.

The normal points are calculated by the LLR team on the CNES computer. It permits quick exchanges inside the station staff and a rapid solution of eventual problems. They are distributed to the interested people as soon as possible after the observations. After some problems of implementation, the software is now working quite well. Dr O. Calame receives directly the data in a file on the CNES computer. JPL and Austin University receive them through Mark III. Everybody else can get the CERGA normal points on request to the author and use them for his scientific work.

A great many people are contributing to the laser station at CERGA beside the author : J.F. Mangin, J.E. Chabaudie, C. Dumoulin, D. Feraudy, J.G. Langlois and J.M. Torre in the LLR team itself. In addition, we wish to thank some other CERGA members who work for one or two nights each month and permit thus to cover more than 20 nights per lunar month.

CERGA LLR

LOCATION

LONGITUDE 43° 45' N

LATITUDE 0h 27m E

ELEVATION 1300 m

1.5-m REFLECTOR for EMISSION and RECEPTION

3.5 nm RUBY LASER - 10 SHOTS PER MINUTE

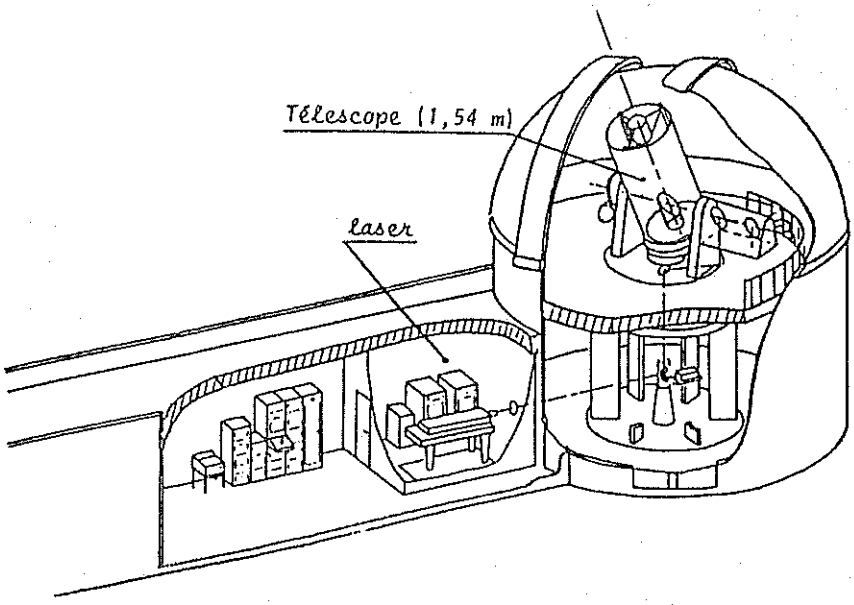

FIGURE 1

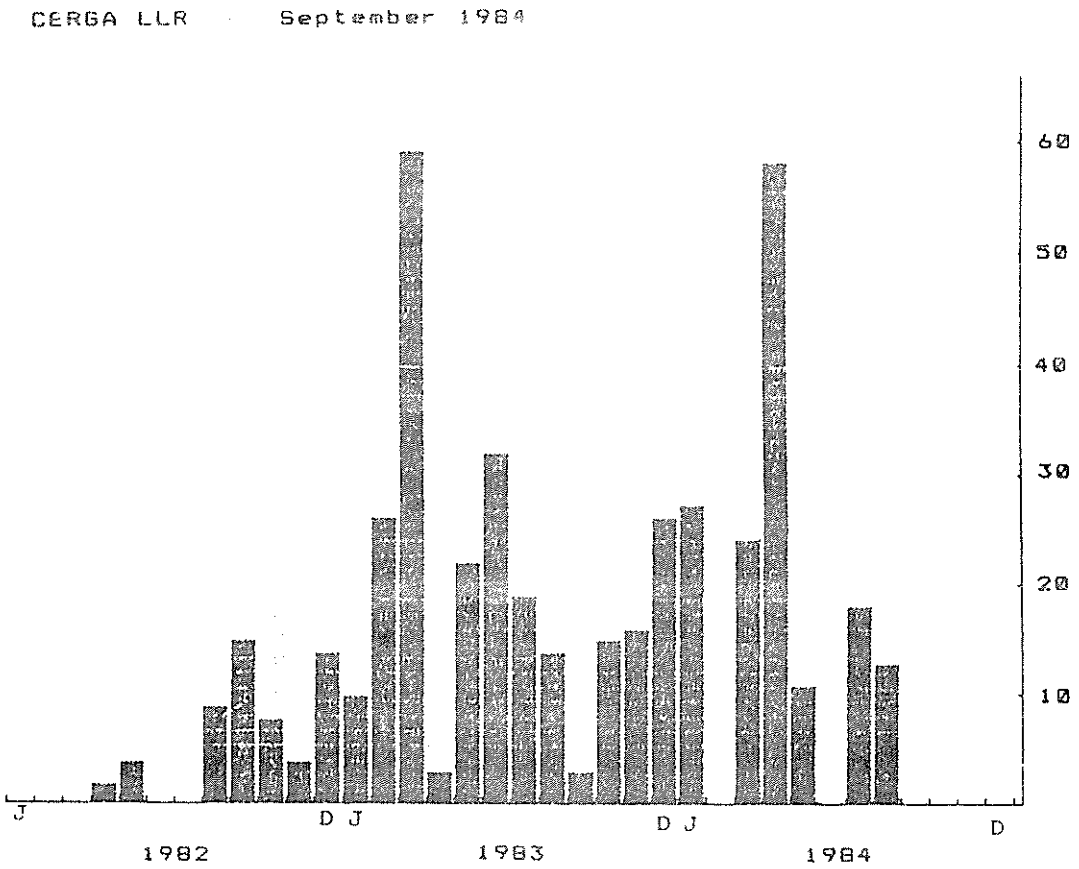

NUMBER OF NORMAL POINTS FOR EACH MONTH (1982-1984)

FIGURE 2

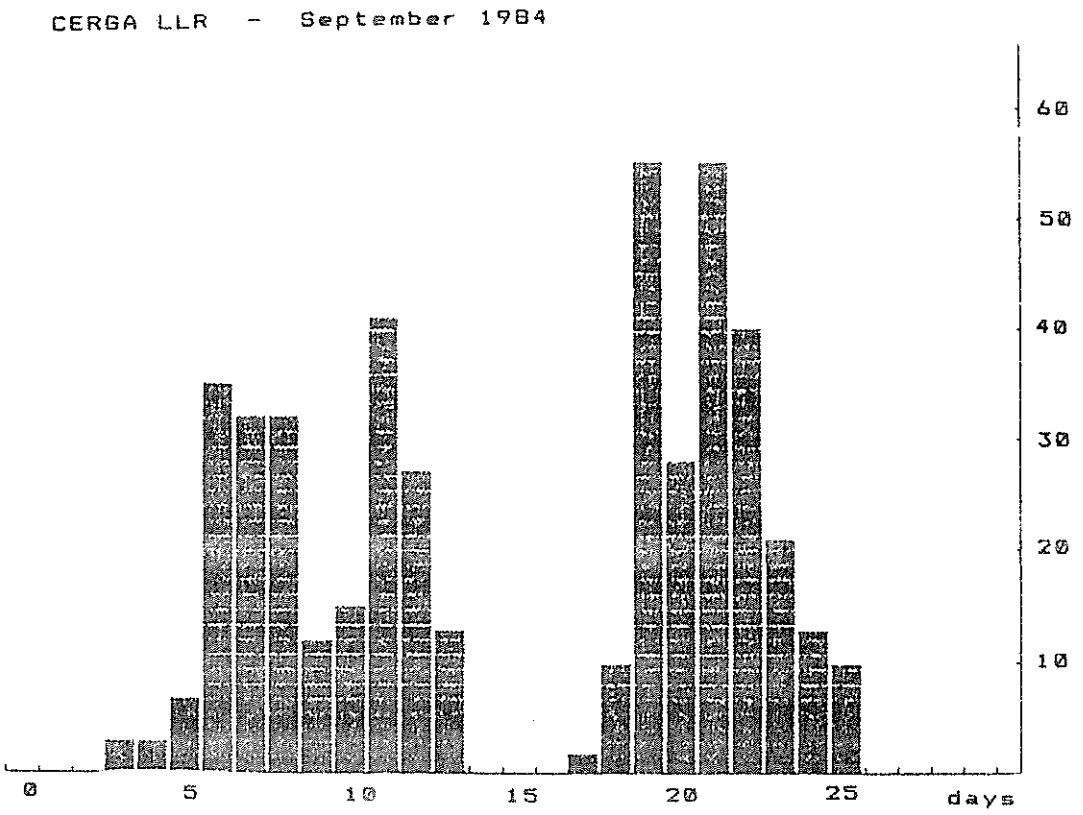

NUMBER OF NORMAL POINTS RELATIVE TO THE AGE OF THE MOON 1982-1984

FIGURE 3

SPECTRAL FILTERS FOR LASER RANGING

B.A. Greene
Division of National Mapping
PO Box 31
Belconnen ACT 2616 Australia

Telephone 062 525095
Telex 62230

H. Visser
Technisch Physische Dienst TNO-TH
Stiettjesweg 1 Delft Posthus 155 Holland

Telephone 78 72 12
Telex 38091

ABSTRACT

The available means of enhancing laser ranging system performance by means of spectral filters are reviewed. Multi-layer dielectric, Fabry -Perot, and Dispersive filters are described, with emphasis on the operational deficiencies and benefits of each filter type. Some projections for the future in spectral filtering for fully optimised system performance are given.

SPECTRAL FILTERS FOR LASER RANGING

1. Introduction

The need for enhancement of signal-to-noise ratio (SNR) in laser ranging systems by means of spectral filtering is continually increasing. For SLR systems the most severe requirements arise for mobile systems which have generally smaller lasers and less well defined coordinates than fixed stations. The combination of poor a priori station coordinates and prediction uncertainties mean that temporal and spatial filtering of the signal is limited, and only spectral filtering can be intensified to enhance SNR.

For LLR systems, it is usual to operate temporal, spatial, and spectral filtering at the design limits of the system, since signal levels are extremely low and noise can be very high (e.g. full moon or daylight ranging).

For laser ranging systems there are two principal parameters which characterise the system performance, signal and SNR. The goal is generally to maximise both, and various measures are taken to accomplish this in terms of varying or modifying system parameters. For example, doubling the laser power doubles signal and SNR, whilst doubling telescope aperture increases signal fourfold whilst not affecting SNR at all.

One of the most cost-effective ways in which most ranging systems can be upgraded is by improving the performance of the spectral filter. Halving the passband of the system spectral filter will double SNR. Doubling the filter throughput efficiency in the passband will double signal. Thus, for example, if an operational system could replace a 1.2A filter of 20% efficiency with a 0.6A filter with 40% efficiency, this would result in a doubling of signal and SNR - the same affect as doubling the laser power, at possibly far less expense.

Considerable emphasis on filter design and selection is also required in the design of minimal, portable, or eye-safe SLR systems.

This paper reviews the filter technology that is available to todays system designers, with the emphasis on operational characteristics. Three basic filter types are reviewed:

(a) Multi-Layer Dielectric Filters (MLDF)

(b) Fabery Perot Filters (FPF)

(c) Dispersion Filters (DF)

2. Multi Layer Dielectric Filters (MLDF)

The principles of operation of MLD filters are well documented in the literature, and widely known. The term MLDF is usually used in the context of laser ranging systems to refer to a composite device consisting of an all-dielectric filter, an induced transmission filter, and a broadband (glass) blocking filter.

The particularly useful features of MLDFs are:

1. Compactness

2. Ruggedness

3. Easy to temperature control or temperature tune

4. Relatively insensitive to incidence angle

5. Single passband only

These features represent why the MLDF is the basic and universal filter for laser ranging systems. It is only in the area of filter efficiency, or transmission, where high performance requirements are difficult to meet with MLDFs. Typical transmission efficiencies for fully blocked filters range from 60% at 10A bandwidth to 20% at 1A. Other filter types become superior in transmission for filter bandwidths below about 3A.

For filter bandwidths in excess of 3A, efficiencies of 50% (and higher) can be obtained for MLDFs. This value of throughput, together with the advantages listed above, make them the natural first choice for most laser ranging systems.

3. Fabery Perot Filters

MLDFs evolved several decades ago from classical Fabery perot filters (FPF). The family similarities remain in that both use interferometric principles to enhance or retard transmission. FPFs, however, use two mirrors separated by a distance which is very large compared to the wavelength of light, and for some applications this original configuration can be utilised to better effect than the MLDF.

In particular, high transmission efficiencies coupled with very narrow bandwidths may be realised. For example, a blocked FPF with 0.5A bandwidth may have 40-60% transmission at line centre - approximately double that realisable with an equivalent bandwidth MLDF. At first sight this looks extremely attractive, but there are many factors weighing against the operational application of FPFs.

The principal difficulties with FPFs arise in the following areas:

(a) Free Spectral Range (FSR) and blocking

(b) Bandwidth control

(c) Angular sensitivity

(d) Vibration sensitivity

(e) Temperature sensitivity

(f) Field-of-view (FOV) problems

(g) Alignment/Servo is highly specified

The Free Spectral Range (FSR) is the distance from one peak of transmission to another in the 'comb' response of the FPF. It is given by

$$FSR = \lambda^2/2d$$

where λ = centre (design) wavelength

d = plate separation

The finesse (F) of the filter is made up of a number of terms, but in practice is usually given by

$$F = \pi R^{\frac{1}{2}} /(1-R)$$

where R = reflectivity of FP mirrors

Bandwidth (BW) is given by

$$BW = FSR/F$$

If (typically) $\lambda = 532$ nm

$d = 0.1$ mm

$F = 28$

then $FSR = 14A$

$BW = 0.5A$

This represents a typical FPF design.

Now the overall efficiency of the FPF itself may be as high as 85% if the device is very precisely manufactured and aligned. However, because the passband recurs at a frequency given by the FSR, a blocking filter must be used to eliminate all but the desired passband. The blocking filter passband must be less than the FSR to avoid passing more than one passband. In the above example, a 10A MLD filter would be used, yielding an overall efficiency of around 50%.

FPFs are extremely sensitive to angle detuning, because the interferometric operation depends upon the path length travelled between mirrors to be an integral number of half wavelengths. It is simple to establish the angle sensitivity as

$$\Delta\lambda = \lambda_c \left(\frac{1}{\cos\theta} - 1\right)$$

or

$$\theta = \cos^{-1}\left(\lambda_c/(\lambda_c + \Delta\lambda)\right)$$

for $\lambda = 5320$ A

$\Delta\lambda = 0.1$ A

then $\theta = 1264$ arc sec.

If the filter is working at a X60 demagnification from the receiving telescope, then the centre wavelength of the filter will move 0.1A over a 21 arc second field of view. More significantly, the filter must be held stable to 21 arc minutes (1264 secs) in its holder if the centre frequency is not to move by more than 0.1A.

It is important to note also that spatial filtering must complement the FPF, since the filter only 'works' at normal incidence, and the passband simply moves (spectrally) with angle of incidence. That is, the system FOV is dictated by the FPF design.

Temperature effects can be the limiting factor in FPF implementation. Even INVAR stabilised mounts can 'walk' a filter line centre by up to 3A per °C. For a 0.5A filter, 0.5°C temperature control is totally unsatisfactory.

A recent development has been the active control, using PZT or similar drive, of the parallelism and spacing of the FP mirrors. Using a CW laser injected off-axis and directed to a detector, the FP tilt and spacing can be servo controlled for optimum performance. The off-axis alignment laser can be at any wavelength, but is often at 6328A as little power is required. A dither technique is used to lock the FPF to line centre of this laser, and the on-axis passband tuned to the desired wavelength by tuning the incidence angle of the alignment laser. This technique has been very successful in overcoming mount creep, temperature drift, and even some vibration-induced detuning of the FPF in tests at the Orroral Observatory. However, the hardware is complex and sensitive, and major efficiency improvements over MLDFs must be demonstrated before the major task of integrating FPFs should be undertaken.

The Orroral Observatory is extending its examination of FPF characteristics to determine the realisable peak transmission efficiency, the long term stability, and the (light) noise immunity of FPF servo systems.

4. Dispersive Filters

Both refraction and diffraction can be used as the dispersive mechanism for dispersive filters. Refractive-Dispersive Filters (RDFs) and Diffractive-Dispersive Filters (DDFs) are both common in a wide range of optical applications. It is only recently [1] that either has been used for laser ranging.

The principal of operation of these devices is extremely simple. The spectral dispersion of the incident radiation allows spatial isolation of narrow wavebands of interest by means of spatial filtering (pinholes, slits).

The significant features of DFs in general can be summarised as:

(a) temperature stable

(b) vibration/mechanical noise sensitive

(c) complex design and optical fabrication

(d) relatively high efficiencies possible

(e) widely and easily tuneable

(f) efficiency not bandwidth dependent

(g) bandwidth also tuneable

(h) bandwidth and field of view not independently adjustable

(i) precision alignment necessary

Apart from these general characteristics, each type of DF has specific advantages and disadvantages. DDFs have an unfortunate characteristic which causes temporal dispersion of the processed optical signal. Precision correction for this effect, due to the non-normal incidence of the input beam on the grating, is extremely difficult. Thus an additional ranging error is introduced. Further, the dispersive mechanism is not more efficient than 50-60%. Finally the coupling of bandwidth and FOV by the exit slit (spatial filter) results in impractically small FOV for very narrow bandwidths. A typical DDF [1] will give 3.5A per 60 arc sec FOV. Thus a 0.5A exit slit would give a maximum FOV of 9 arc seconds. Increasing the FOV is not possible without expanding the BW also, despite the fact that this is detrimental to system performance. The example given will give a BW of 2A for a FOV of 35 arc seconds and an efficiency of 50%, a performance level around which an excellent SLR may be built.

RDF characteristics do not include temporal dispersion of the signal, and efficiencies near 90% are feasible. The major limitation with RDF application is the practical limit to the size of dispersive prisms which can be constructed. This limits the degree of dispersion attainable, and filters for (typical) ranging configurations may be limited to 3A (min) by

this. However, it is unlikely that an RDF of less than 3A would be of general use, since the FOV for smaller bandwidths becomes unreasonably small.

5. Future Developments

Further development is likely to see incremental improvements in MLDF efficiency at all bandwidths.

The use of FPF technology should move gradually into the operational sector from the research environment.

A most promising long term development is the combination of FPF and DDF to form 0.5A filters with 75% throughput in the centre of the passband. This proposed design would use the DDF in its optimum role - as a high efficiency wide band filter. Thus the DDF would not limit the system FOV. If a DDF was used as (say) a 10A block for a 0.5A FPF with 14A free spectral range, an efficiency of 90% is possible, with a working FOV of an arc minute. This FOV can then be controlled independently of the spectral filtering process using a conventional lens/pinhole combination. This is not really necessary, since in the DDF/FPF combination, the DDF can be used as the spatial filter as its transmission efficiency will not vary as its FOV and bandwidth are tuned. Clearly a FOV corresponding to a DDF bandwidth greater than 14A cannot be selected, since the DDF is then not effectively blocking the FPF. Similarly, a FOV corresponding to a DDF bandwidth of less than 0.5A cannot be selected without reducing the effective bandwidth of the DDF/FPF combination. This lower limit of filter bandwidth is most likely to be fixed by the power spectrum of the laser. For a 100 ps laser, a filter of around 0.6A is needed to transmit the power spectrum. If a 0.6A FWHM filter is used, a large proportion of the signal from a 100 ps laser will be transmitted at an efficiency below the peak transmission of the filter.

For the example given above, if a FPF efficiency of 85% can be achieved routinely, then the spectral filter will operate at 75% efficiency for 0.5A bandwidth over a wide range of FOV. This is four times better than MLDF performance, and almost 1.5 times as good (efficient) as a MLDF blocked FPF.

Large systems, and particularly LLR systems will gain 300% to 50% improvements in data production over current capabilities at 0.5A.

EPOCH TIMING FOR LASER RANGING

B.A. Greene
Division of National Mapping
PO Box 31
Belconnen ACT 2616 Australia

Telephone 062 525095
Telex 62230

ABSTRACT

The well established advantages of epoch timing are reviewed in the light of recent and iminent developments in laser ranging hardware. The capability of asymetric Stop-Start time interval measurement techniques to meet the emerging demands for timing system precision, accuracy, and event rates is questioned. The ability of systems using epoch timing to adapt to the new technology and meet the highest performance specifications is emphasised.

EPOCH TIMING FOR LASER RANGING

1. Introduction

The advantages of epoch timing for laser ranging have been known for some time. Some of the earliest timing equipment specifically designed for laser ranging used epoch timing principles (e.g. the 'Maryland' event timer).

The principal advantages of epoch timing have been:

1. Measurement symmetry for START and STOP.

2. Capability to accommodate many shots in flight with a single instrument (i.e. multiple-stop capability).

3. Precise epochs are produced as well as range measurements.

Recent developments have highlighted these advantages as well as throwing light on some previously undetected advantages.

2. Epoch Timing Principles

A epoch timing system measures range by determining the epoch of the transmission and reception of the laser pulse, and obtaining the difference by subtraction.

An epoch timing system can be constructed from commercial electronics modules, since all that is required is a scaler/counter and a time interval unit (TIU). If the scaler and TIU are properly chosen, the epoch precision is the precision of the TIU. The specification for these 2 components are that the maximum count of the TIU must be greater than the period (1/f) at which the scaler is clocked. The scaler is simply latched by the event, which also starts the TIU, which is stopped by the same clock pulse which clocks (increments) the scaler. For example, the original (1974) Orroral LLR timing system consisted of a 10 MHz scaler, which, when latched, gave 100 ns precision epoch. The event which latched the scaler also started the 1ns precision TIU, which was stopped by a 100 KHz pulse train, giving a maximum count of 10 microseconds.

The epoch is given by

$$E = L + (c - t)$$

where L = epoch latched in scaler
c = maximum count of TIU
t = TIU measurement

In practice the epoch E is formed in a minicomputer which first truncates L to eliminate least significant digits which would overlap (c-t). If the STOP pulse train going to the TIU is not in phase with the latch clock pulse to better than the precision of the TIU, then additional adjustments need to be made to E.

The epoch E will be absolutely accurate only to the extent that the frequency standard which supplies the latch clock/TIU stop is absolutely accurate. If the clock rate is known, then the epoch accuracy can be upgraded in post-processing. The range measurements derived from these epochs will have a precision approximately equal to 1.4 times the epoch precision plus the frequency standard's error over the measurement interval.

The major difficulties in epoch timing systems are:

1. Overlapping of START and STOP events in TIU.

2. Perfect recombination of E and (c-t) to give precise epoch.

The overlapping of START and STOP events in the TIU will generally cause errors. Some systems employ two TIUs with one TIU having its STOP channel input frequency 180 degrees out of phase with the other, so that overlap can be avoided. This of course introduces more calibration complexity, but has been successful. An alternative is to make the TIU input pulses very short, and the maximum count very long, and accept overlaps. For example if the pulses were 4 ns wide and the max count 1000 ns, only 0.4% of measurements would be affected. Lengthening the max count also makes combining the TIU and scaler readings simpler, as more overlapping digits occur for longer counts, and the software algorithm for combining the two numbers into a single epoch is simpler.

3. Recent Developments

Laser ranging systems now routinely operate with a single-shot precision of 5 cm. Soon 2 cm single-shot precisions will be routine, based on new laser, receiver, and timing system technology. The precisions required by the new laser ranging systems may demand the adoption of epoch timing techniques.

An acceptable standard for ranging timing systems for the next 5 years is likely to be 30 ps (RMS) accuracy in range over 100 ms ranges, and 50 ps over lunar ranges. It is now relatively easy to acquire or even construct a TIU with 20-30 ps precision. However very few available designs will maintain this precision over more than a few microseconds. One exception, the HP5370 series TIU, limits the rate at which the laser can be fired to 5 Hz once the max count exceeds 50 ms.

Thus the newer technology in TIUs may be applicable only as the vernier, or as an add-on, to an existing measurement system. Since epoch timing scalers can easily run up to 100 MHz, giving a TIU max count requirement of 10 ns, minimal demands are placed on the TIU in this regard by epoch timing. That is, epoch timing systems are ideally suited to take advantage of high precision, short count TIUs.

An additional problem for conventional systems using direct time interval measurements to measure range arises from temperature drift of TIUs. It has recently been discovered that the HP5370B shows a measurement bias of 10 ps per degree Celsius. Other TIUs show similar biases. The error, which is systematic, does not depend on the length of count, and thus is removed entirely if the TIU is used as the vernier for an epoch timing system, since the error will occur in both epochs, and cancel out in the formulation of a time interval by subtraction.

The development of solid-state pumping for Nd:YAG lasers raises the possibility of significant improvements in laser efficiency, and may lead to higher repetition rate capabilities well beyond the present 10 Hz. At 200 Hz repetition rates, even the lower satellites will require multiple shots in flight. If recent developments in detector technology lead to 1 micron ranging systems, even higher rates could be required. Only epoch timing techniques can meet these event rate specifications. (The data acquisition and control specification is not considered here.)

Finally, new streak cameras are now available which allow 2-D scanning of the electron beam. If such a streak tube was to be integrated with a 2-D CCD array of large dimensions, then it is conceivable that it could be used as a picosecond precision vernier for an epoch timing system. If the 2-D scanning algorithm is correctly specified, it is possible to use a large proportion of the addressable space on the CCD to give an unambiguous, picosecond precision epoch readout over long periods (up to 10 ns, i.e. 10 ns maximum count). It seems unlikely that this ultra-high precision development will integrate naturally with timing systems other than epoch timing systems.